Recovery from the end-Triassic mass extinction in European shelf seas: body size changes in marine invertebrates and the role of temperature and anoxia

Jed William Atkinson

Submitted in accordance with the requirements of the degree of Doctor of Philosophy

The University of Leeds

Earth Surface Science Institute

School of Earth and Environment

August, 2019

The candidate confirms that the work submitted is his own, except where work which has formed part of jointly-authored publications has been included. The contribution of the candidate and the other authors to this work has been explicitly indicated below. The candidate confirms that appropriate credit has been given within the thesis where reference has been made to the work of others.

Contributions of the candidate and the other authors:

In all chapters the candidate (J.W. Atkinson) was the primary data gatherer and processor. All chapters were primarily written by the candidate with comments and suggested edits to the manuscripts provided by P.B. Wignall (all chapters) and T. Aze (Chapter 2). Contribution to data gathered for Chapter 2 was provided by J.D Morton and Chapter 4 by P.B. Wignall. Ammonite identifications and short related paragraph provided by K.N. Page also in Chapter 4.

Acknowledgements

A hearty thanks goes to all those who permitted me to take a hammer to a SSSI: Tom Sunderland, Bob Corns, Tom Charman, and Hugh Luttrell. Also thanks to all those museum staff who granted me access to their collections: Caroline Buttler, Lucy McCobb, Deborah Hutchinson, Jon Radley, Matt Williams, Sarah King, Stuart Ogilvy, Roger Osborne, Tim Burnhill and especially to Peter Hodges whose meticulous and extensive collections greatly improved my own work. Mike Simms and Mick Oates, thank you to you both for showing us field locations and additionally, Mick for allowing me to trawl through your collections. A thanks to temporary field assistants Karolina Zarzyczny and Ovye Yohanna and most crucially to long suffering field assistant and valued friend Jacob Morton – who I have lead off many ridiculous cliffs, made to carry twice his own body weight in stone and subjected to the aromas of rotting badger flesh – there could have been no better 'Watson' to have in the field at my side.

For technical help I wish to thank Duncan Hedges and Harri Wyn Williams. Everyone in the basement offices – past and present: Autumn Pugh, Tom Fletcher, James Witts, Luke Faggetter, Kathy Doyle, James Woodman, Andy Cooke, Sam Parsons, Connor O'Keeffe, Dot Drayton, Delia Cangelosi, Beth Allen, Adam Woodhouse, Andy Mair, Carl Spence-Jones and anyone I missed. Thank you to you all for making the time here so enjoyable.

Of course my deepest gratitude to my supervisors Tracy Aze, Rob Newton and most of all Paul Wignall – whose guidance and occasional company in the field has been quite capital. My Parents I thank for their support, especially to my Father to whom I owe a great mechanical debt. The Mustard King (Acey) and Doc Shaw (Alex) for keeping me insane whenever sanity threatened to take grasp, for keeping me in the wrong century and reminding me that in life *three is company, two is none.* And lastly an apology to the dear ladies in the reception who have, over the last four years, had a menagerie of the dead pass through their office in all manner of unsavoury conditions.

Abstract

Fossil communities in the wake of mass extinction are often characterised by small sized individuals, this is often ascribed to the Lilliput Effect (a transient body size reduction within a surviving species). During periods of biotic recovery body size should increase, this, and its relationship with other recovery parameters are seldom documented. In order to explore the relationships between size, diversity and environments bivalve taxonomic richness and body size are recorded from the latest Triassic and Lower Jurassic of the British Isles. This interval encompasses the end-Triassic mass extinction event and its subsequent recovery. During the post-extinction interval oxygen depleted marine waters are reported to have become widespread and allegedly delayed onset of biotic recovery.

During the Lower Jurassic three phases of size change are noted: an initial size increase from the extinction event through the Hettangian Stage (Lower Jurassic); a phase of size decrease characterises the next Stage, the Sinemurian; another phase of size increase then followed during the Pliensbachian Stage. These trends are reported for whole communities as well as among- and within-species. The latter is well exemplified by the dramatic size increase seen in *Plagiostoma giganteum* J. Sowerby which increases in size by 179% over the Hettangian. It is here proposed that within-species size increase in newly originating taxa following mass extinction be termed the Brobdingnag Effect, in honour of the giants in Gulliver's Travels.

Such patterns in body size act independent of other recovery metrics and appear unrelated to marine oxygenation which, for the Hettangian and lowermost Sinemurian, was oxic-dysoxic interspersed by comparably brief, localised bouts of anoxia. Temperature often exerts a control on the body size with creatures in cooler climates often being larger sized (i.e. Bergmann's Rule). Temperature appears unrelated to body size patterns in the Lower Jurassic, however there are gaps at critical intervals.

Table of contents

Acknowledgements ……..……**v**

Abstract ……..……**vii**

Table of contents……**ix**

List of tables……....**xv**

List of figures……**xvii**

Abbreviations……..……..**xxiii**

Chapter 1: Introduction……...**1**

1.1 Extinction losses……..……1

1.2 Extinction mechanism……..3

1.3 Biotic recovery from mass extinction……..……..6

1.4 Recovery from the end-Triassic mass extinctions……..9

1.5 Body size……..…..11

1.6 Aims……..…..15

1.7 Rationale for work……...…...16

1.8 Geological overview……...…16

1.8.1 The Rhaetian……...…17

1.8.2 The Hettangian……...…19

1.8.3 The Sinemurian……...…20

1.8.4 The Pliensbachian……....20

1.9 Thesis outline……..21

References……..……22

Chapter 2: Body size changes in bivalves of the family Limidae in the aftermath of the end-Triassic mass extinction: the Brobdingnag Effect……..…..**39**

2.1 Abstract……41

2.2 Introduction……..……..42

2.3 Geological setting……..……44

2.4 Materials and Methods……..……...47

2.4.1 Species studied……..……47

2.4.2 Sampling……..……...48

2.4.3 Growth lines……..…..54

2.5 Results……..……..55
2.5.1 Body size…….55
2.5.1.1 *Plagiostoma giganteum*……...……...55
2.5.1.2 *Plagiostoma punctatum*……...……....60
2.5.1.3 *Antiquilima succincta*……...…....63
2.5.1.4 *Pseudolimea pectinoides*……64
2.5.1.5 *Ctenostreon philocles*……...…...66
2.5.2 Growth patterns……..……67
2.5.3 Museum versus field collections……...……69
2.6 Discussion……..……71
2.6.1 Body size……..71
2.6.2 Growth patterns……..……72
2.6.3 Contemporary Early Jurassic size increase……...….73
2.6.4 Causes of body size and growth rate changes……73
2.6.4.1 Water depth and body size……..……..73
2.6.4.2 Oxygen availability……..……...74
2.6.4.3 Temperature and body size……76
2.6.4.4 Food availability……..……77
2.6.5 Lilliputians and Brobdingnagians……..78
2.7 Conclusions……...……....81
References……..…….82
Chapter 3: How quick was marine recovery after the end-Triassic mass extinction and what role did anoxia play?.....**93**
3.1 Abstract……95
3.2 Introduction……..……..96
3.3 Geological setting……..……98
3.4 Materials and methods……..……102
3.5 Results……..……104
3.5.1 Pyrite framboids……..……104
3.5.1.1 Lithological variability……..……104
3.5.1.2 Regional variability……..……112
3.5.1.3 Temporal variability……..……120
3.5.2 Faunas……..……121

3.5.2.1 Field collections……..……..121
3.5.2.2 Museum collections……..……...128
3.6 Discussion…….128
3.6.1 Recovery……..…….128
3.6.2 Duration of recovery……..……..134
3.6.3 Role of anoxia in recovery……135
3.7 Conclusions……...……...137
References……..138
Chapter 4: The Hettangian-Sinemurian strata of Redcar, Cleveland Basin, NE England: facies and palaeoecology……..**145**
4.1 Abstract……..……..147
4.2 Introduction……..……148
4.3 Geological setting…….149
4.4 Materials and methods……..…….151
4.5 Results……..……152
4.5.1 Sedimentology……..……...152
4.5.2 Fauna……..……..157
4.5.3 Framboid analysis…….166
4.6 Discussion…….167
4.7 Conclusions……..……...171
References……..172
Chapter 5: Body size trends and recovery amongst bivalves following the end-Triassic mass extinction……..……**175**
5.1 Abstract……..……..177
5.2 Introduction……..……178
5.3 Geological setting…….181
5.4 Materials and methods……..…….186
5.5 Results……..……190
5.5.1 All bivalves……...……..190
5.5.2 Basin trends……...……193
5.5.3 Trends within ecological groups……..…..196
5.5.4 Within lineage trends……198
5.6 Discussion…….216

5.6.1 Body size trends……216
5.6.1.1 Lilliputians……216
5.6.1.2 Brobdingnagians……217
5.6.1.3 Cope's Rule……218
5.6.1.4 No trends……219
5.6.1.5 Those that get smaller……219
5.6.1.6 *Gryphaea*……220
5.6.1.7 Bivalves' size changes across Europe and beyond……221
5.6.1.8 Size trends in other groups……222
5.6.2 Possible causes of size change……224
5.6.2.1 Sea level, sediments and size……224
5.6.2.2 Redox……226
5.6.2.3 Temperature……227
5.6.2.4 Food availability……228
5.6.3 Body size and biotic recovery……230
5.7 Conclusions……231
References……233
Chapter 6: Discussion……**243**
6.1 Recovery from the end-Triassic mass extinction: bivalve diversity……243
6.2 Lilliput versus Brobdingnag Effect……244
6.3 Sinemurian Small Episode……248
6.4 Size and recovery……249
6.5 Early Jurassic oxygenation……250
6.6 Comparison with other recovery intervals……252
References……255
Chapter 7: Conclusions and future work……**261**
7.1 Conclusions……261
7.2 Future work……264
References……266

Appendices

Appendix A: Figures from Chapter 2 rescaled to most recent Hettangian timescale……..……..267

Appendix B: Bivalve life modes……271

Appendix C: Species abundance counts and summary of framboid analysis per sample horizon……277

Appendix D: NMW collection list……..295

Appendix E: Compendium of bivalve body size data spanning the uppermost Triassic through the Lower Jurassic……...295

Appendix F: Diagnostic features to differentiate species of Lower Jurassic bivalves……...297

List of tables

Table 2.1. Details of field localities……..……..51

Table 2.2. Comparison between maximum GMBS (mm), per ammonite zone, of *Plagiostoma giganteum* and *Antiquilima succincta*…..……..64

Table 4.1 Bivalve ecologies encountered within the Redcar sequence, assigned from published literature……163

Table 4.2 Bivalve species richness per zone for four basins of the classic Blue Lias Formation compared to the Cleveland Basin……..….169

List of figures

Fig. 1.1. $\delta^{13}C_{org}$ curves for Triassic-Jurassic boundary sections……..4

Fig. 1.2 Schematic diagram of expected diversity during survival and recovery intervals…….. ……..…….7

Fig. 1.3 Species richness plots through the British Lower Jurassic from Hallam (1996). ……..……10

Fig. 1.4 Schematic diagrams of body size changes across extinction events after Twitchett (2007) ……13

Fig. 1.5 Schematic lithostratigraphy of studied sedimentary basins with ammonite zone scheme and geological stages……..……18

Fig. 2.1 Map depicting field locations..…….……49

Fig. 2.2 Measurement schematic of a left valve in Limidae……,……..……..53

Fig. 2.3 Size distribution histograms for *Plagiostoma giganteum* per time bin…56

Fig. 2.4 Time-binned variation in the size of *Plagiostoma giganteum* (top) and *Antiquilima succincta* (bottom)……..…….57

Fig. 2.5 Stratigraphically tied size variation of *P. giganteum* from Pinhay Bay (A) and Nash Point (B)……59

Fig. 2.6 Time-binned variation in the size of *Plagiostoma giganteum* per locality, (top). Variation in size between specimens measured from different oxygenation regimes inferred from host lithology (bottom)…….60

Fig. 2.7 Time-binned variation in the size of *Ctenostreon philocles* (top), *Pseudolimea pectinoides* (middle) and *Plagiostoma punctatum* (bottom)……..62

Fig. 2.8 Size distribution histograms for *Plagiostoma punctatum* per time bin with sufficient samples……..……..63

Fig. 2.9 Size distribution histograms for *Pseudolimea pectinoides* per ammonite zone……..…….65

Fig. 2.10 Time-binned variation in the size of *Pseudolimea pectinoides* per locality, (top). Variation in size between specimens from different oxygenation regimes inferred from host lithology……..66

Fig. 2.11 Growth rate plot for *Plagiostoma giganteum* ……....……...68

Fig. 2.12 Growth line densities with a three point moving average trend line showing cycles in a large *Plagiostoma giganteum* collected from the *bucklandi* Zone of Hock Cliff……..……69

Fig. 2.13 Variation in body size of *Plagiostoma giganteum* from museum collections (closed circles) and field observations (open circles)…….70

Fig. 3.1 Lithological correlation of members of the Blue Lias Formation, after Hodges (2000)……..……101

Fig. 3.2 Location map and palaeogeography of southwestern Britain, Early Jurassic islands indicated by shaded regions, modified from Martill *et al.* (2016)……..……102

Fig. 3.3 Example populations of pyrite framboids from an anoxic mudstone (Q39, top) and a dysoxic marl (NP15, bottom)……..105

Fig. 3.4 Mean framboid diameter (μm) against standard deviation of framboid diameters (Wilkin diagram), samples plotted according to lithology……106

Fig. 3.5 St. Audrie's Bay, Somerset. Box and whisker plots……107

Fig. 3.6 East Quantoxhead Somerset, sedimentary log modified from Bloos and Page (2002)……109

Fig. 3.7 Lavernock Point, Glamorgan. Sedimentary log modified from Simms (2004)……..……112

Fig. 3.8 Nash Point, Glamorgan……114

Fig. 3.9 Wilkin diagram, samples plotted according to geographic region…….117

Fig. 3.10 Pinhay Bay, Devon. Sedimentary log modified from Hesselbo and Jenkyns (1995)……..……119

Fig. 3.11 Wilkin diagram, samples plotted according to ammonite zone/time bin……120

Fig. 3.12 Species range chart and bivalve abundances for Glamorgan (Lavernock Point and Nash Point)……..……....122

Fig. 3.13 Species range chart for Somerset (St Audrie's Bay and East Quantoxhead)……..……..123

Fig. 3.14 Species range chart for Devon (Pinhay Bay)…….…124

Fig. 3.15 Compiled recovery metrics and oxygenation states for each of the three studied regions……..126

Fig. 4.1 UK location map showing Lower Jurassic outcrop and key sedimentary basins modified from Gründel *et al.* (2011)……..……..150

Fig. 4.2 Graphic log of Redcar Rocks including box and whisker plots of pyrite framboid results……..……...…154

Fig. 4.3 Photomicrographs of thin sections. A. Red 23, shell fragment rotated by burrowing. B. Red 28, example shell bed including *Gryphaea* shell with simple boring on the right. C. Red 6, example of biosparite. D. Red 24, phosphatic nodule featuring burrow mottling. E. Red 8, two nests of serpulid tubes……156

Fig. 4.4 *Gryphaea*-rich shell bed at outcrop. Hammer 30 cm long……..…157

Fig. 4.5 SEM images. A Red 11, abundant rice-shaped ankerite grains (pale grey). B Red 15, pyrite framboids surrounded by a cloud of dissociated pyrite microcrysts……..……...158

Fig. 4.6 Examples of fossils collected from Redcar. A Red 1, *Schlothemia* sp.; B Red 21, *Arnioceras* sp. encrusted by *Liostrea irregularis* (Münster); C Red 17, *Pleurotomaria cognata* Chapuis & Dewalque; D Red 2 photomicrograph of microgastropod in thin section; E Red 12 *Isocrinus psilonoti* (Quenstedt), partially articulated specimen with cirri, photographed *in situ;* F-I Red 15, *Cardinia listeri* (J. Sowerby) featuring a range of cirripede borings. J cross-section through part of *C. listeri* shell (I) showing potential *Simonizapfes*; K detail of *C. listeri* shell (I) with possible bryozoan borings; L *C. listeria* with growth defect dashed line projects normal shell outline, note altered growth line spacing towards damaged regions..……..160

Fig. 4.7 Species range chart and range through (RT) species richness for Redcar Rocks……..……165

Fig. 4.8 Mean framboid diameter (µm) against standard deviation of framboid diameters (Wilkin diagram) for Redcar…….....166

Fig 4.9 Average framboid diameter and standard deviation for three Blue Lias hosting basins in southwest Britain……..……..171

Fig. 5.1 Palaeogeography of the British Isles with Hettangian landmasses indicated by shaded regions and sedimentary basins……..…..……...182

Fig. 5.2 Schematic lithostratigraphy of studied sedimentary basins……..184

Fig. 5.3 Measurement schematic for a variety of bivalve morphologies……..188

Fig. 5.4 Time-binned geometric mean size plots for all Lower Jurassic bivalves. A, All bivalves measured per time bin, additionally bivalve species richness per time bin (grey triangles). B, size of newly arriving bivalve species per zone……..……..……192

Fig. 5. 5A-D Maximum GMBS of bivalves per time bin per basin/shelf…….....……195

Fig. 5.6 Maximum GMBS for bivalves per ecological guild……..……197

Fig. 5.7 Time-binned GMBS plot for A, *Pseudopecten equivalvis* and B, *Entolium lunare*……..……200

Fig. 5.8 Time-binned GMBS plot for *Chlamys valoniensis*…….……201

Fig. 5.9 Time-binned GMBS plot for A, species of *Camptonectes* and B, species of *Oxytoma*…..……..……...…203

Fig. 5.10 Time-binned GMBS plot for A, undifferentiated of species of *Liostrea* and B, *Atreta intusstriata*…..……...205

Fig. 5.11 Time-binned GMBS plot for species of *Modiolus*. A, *M. hillanus* and B, *M*. *minimus*……..……..……...207

Fig. 5.12 Time-binned GMBS plot for A, *Pteromya crowcombeia,* B, *Isocyprina ewaldi,* C, *Neocrassina gueuxii*…….209

Fig. 5.13 A, Time-binned GMBS plot for *Cardinia ovalis*. B, Primary growth line plot for *C. ovalis* specimens from the Penarth Group and Blue Lias/Waterloo Mudstone formations……..…….210

Fig. 5.14 A, Time-binned GMBS plot for *Mactromya cardioideum*. B, Growth line plot also for *M. cardioideum* specimens from the Blue Lias Formation and from Blockley Quarry, Severn Basin (Charmouth Mudstone Formation)……..…….211

Fig. 5.15 Time-binned GMBS plot for species of *Protocardia*……...213

Fig. 5.16 Time-binned GMBS plot for A, species of *Gresslya,* B, species of *Pleuromya,* and C, species of *Pholadomya.* D, Growth line plot for *Pholadomya glabra* from the Blue Lias Formation comparing specimens of the *angulata* and *bucklandi* zones……..……...215

Fig. 5.17 Temperature and sea level changes in relation to maximum GMBS of all bivalves and maximum log volume of ammonites……..……..223

Fig. 5.18 Maximum GMBS trends for the Bristol Channel Basin-Welsh Massif, Dorset and Central Somerset basins and oxygenation states for each of the three basins from Atkinson & Wignall (2019)……..…....227

Fig. 6.1 Schematic diagrams of body size changes across extinction events. A. The Lilliput Effect, *sensu* Urbanek; B. The Brobdingnag Effect. C. Cope's Rule; D. Brobdingnag Effect in concert with Cope's Rule……..….245

Abbreviations

BGS	British Geological Survey
BRLSI	Bath Royal Literary and Scientific Institute
BRSMG	Bristol City Museum and Art Gallery
CAMP	Central Atlantic Magmatic Province
CIE	Carbon isotope excursion
EMS	East Midlands Shelf
ETE	End-Triassic extinction
GMBS	Geometric mean body size
GSSP	Global boundary stratotype section and point
H	Height of valve
KPg	Cretaceous-Paleogene
K-S test	Kolmogorov-Smirnov test
kyr	Thousand years
L	Length of valve
LIP	Large igneous province
LV	Left valve
Ma	Million years ago
Myr	Million years
NMW	National Museum of Wales
PTME	Permo-Triassic mass extinction
PZE	Photic zone euxinia
RT	Range through
RV	Right valve
SEM	Scanning electron microscope

SSE	Sinemurian Small Episode
SSSI	Site of special scientific interest
TJB	Triassic-Jurassic boundary
TOC	Total organic carbon
UA	Umbonal angle
WARMS	Warwickshire Museum Services
WHITM	Whitby Museum
YORYM	Yorkshire Museum

Chapter 1: Introduction

The mass extinction that struck towards the end of the Rhaetian Stage (Late Triassic) ranks as third greatest in terms of ecological severity and fourth for diversity loss (Hallam 2002; McGhee *et al.* 2004). Causal mechanisms behind this event have been greatly debated; potential culprits have included sea level change, meteorite impacts and the consequences of massive continental flood basalt volcanism (e.g. Courtillot *et al.* 1996; Hallam & Wignall 1999; Olsen *et al.* 2002). There is now a consensus that the end-Triassic extinction (ETE) was linked to the continuing breakup of Pangaea and emplacement of the Central Atlantic Magmatic Province (CAMP, Marzoli *et al.* 1999, 2004; Pálfy 2003).

1.1 Extinction losses

The extinction severely affected both marine and terrestrial realms with notable losses on land including dicynodonts, cynodonts and crurotarsans such as phytosaurs and rauisuchians (Colbert 1958; Olsen *et al.* 1987). The late Rhaetian also bore witness to floristic turnover with gymnosperm forests of north-western Europe, Greenland and North America transiently replaced by fern dominated communities (Fisher & Dunay 1981; Whiteside *et al.* 2007; van de Schootbrugge *et al.* 2009; Steinthorsdottir *et al.* 2011; Mander *et al.* 2013). In the marine realm 46% of genera disappeared (Dunhill *et al.* 2018). Diverse Triassic marine reptile communities were severely depleted, losses include placodonts, nothosaurs, thalattosaurs and many ichthyosaurs resulting in a decline in

disparity: only “dolphin-shaped” parvipelvian ichthyosaurs survived (Thorne *et al.* 2011; Stubbs & Benton 2016).

Among marine invertebrates, losses were greatest among heavily calcified, immobile suspension feeding epifauna (Dunhill *et al.* 2018). Many reef dwelling species fall into this life mode and 96% of scleractinian species died (Flügel 2002), resulting in the loss of reef ecosystems (Stanley 1988; Wood 1999). Brachiopods also suffered losses, especially amongst the Spiriferida, with ~25% of families going extinct at this time (Ager 1987; Hallam 2002).

Through the Late Triassic the usually diverse and rapidly evolving conodonts and ammonoids were in decline, culminating in the late Rhaetian extinction of conodonts (Swift 1989, 1999). Ammonoids were almost lost at this point too, with the major suborder Ceratitina disappearing and only a few smooth, extremely evolute Phylloceratidae ammonites surviving into the Jurassic (Guex 1982; Guex *et al.* 2012). Radiolarians suffered severe losses with morphologically ornate Triassic taxa replaced by small, simple forms in the earliest Jurassic, in much the same fashion as seen amongst ammonoids (Guex 1992; Carter & Hori 2005; Kocsis *et al.* 2014).

Of particular relevance for this work is the fate of bivalves during the ETE. Overall around 30% of genera were lost (Hallam 2002). Locally, species-level losses were high with 71% of species extinct in Lombardy (Italy), 85% of bivalve species in the German and Austrian Northern Calcareous Alps, and 77% in Britain (McRoberts & Newton 1995; Wignall & Bond 2008). At a local to regional scale extinction losses appear to have most severe amongst infaunal species with European and some Asian sections recording losses of between 92 – 100% (Hallam 1981; McRoberts & Newton 1995; Hautmann *et al.* 2008a; Wignall & Bond 2008). In addition, no very large bivalve species survived the extinction –

with large taxa such as megalodontids, dicerocarditids and wallowaconchids dying out (Hallam 2002).

1.2 Extinction mechanisms

During the Phanerozoic large-scale mass extinction events have been closely associated with large igneous provinces (LIPs) (see Wignall 2001a; Bond & Wignall 2014). This is also the case for the ETE which has been linked to initial phases of rifting of the supercontinent Pangaea and resulting emplacement of the CAMP (e.g. Marzoli *et al.* 1999, 2004; Pálfy 2003). This province is amongst the largest of all Phanerozoic LIPs stretching from Greenland through North and South America and Africa, covering an area of up to $10x10^6$ km^2 (May 1971; Wilson 1997; Marzoli *et al.* 1999; Knight *et al.* 2004).

A commonly cited kill mechanism induced by LIPs is extreme warming brought about by volcanogenic CO_2 (see Bond & Grasby 2017 for a recent review). This has also been suggested for the ETE which is associated with a short, sharp negative carbon isotope excursion (CIE) of 2-4‰ magnitude, which is often referred to as the initial CIE (Hesselbo *et al.* 2002). The initial CIE has been noted in many boundary sections worldwide (Fig. 1.1) including Nevada (Guex *et al.* 2004), Spain (Gómez *et al.* 2007), Hungary (Pálfy *et al.* 2001), Austria (Morante & Hallam 1996; Kürschner *et al.* 2007) and Canada (Ward *et al.* 2001).

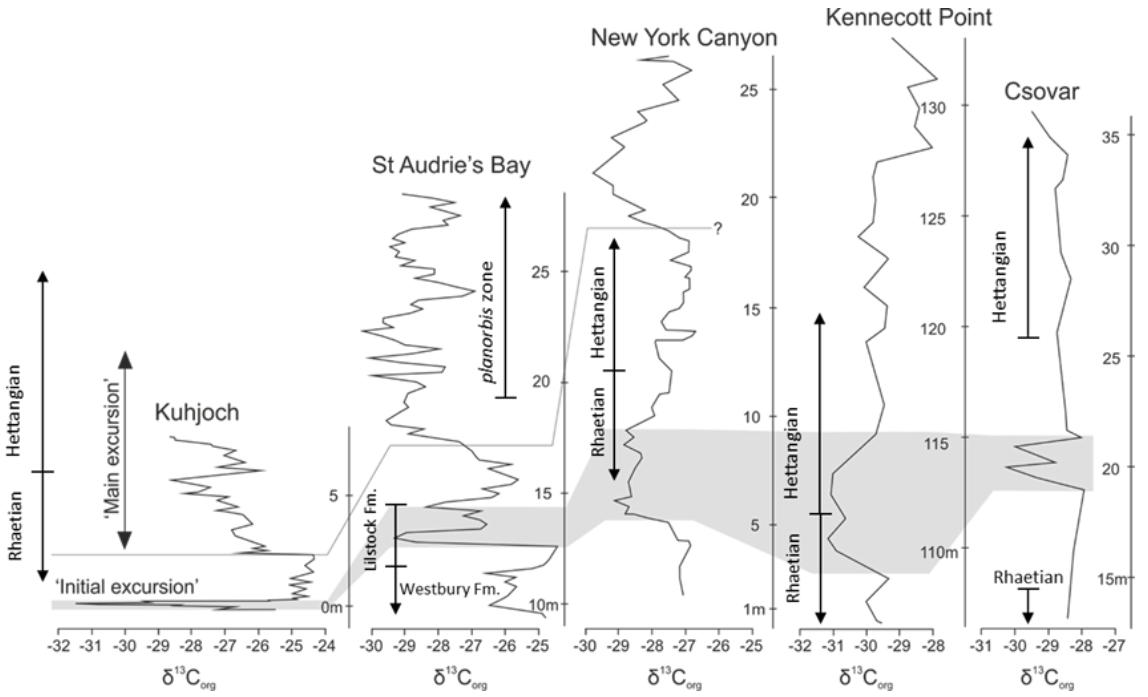

Fig. 1.1 $\delta^{13}C_{org}$ curves for Triassic-Jurassic boundary sections. Kuhjoch, Austria (Ruhl *et al.* 2009); St Audrie's Bay, Britain (Hesselbo *et al.* 2004); New York Canyon, Nevada (Bartolini *et al.* 2012); Kennecott Point, British Columbia (Williford *et al.* 2007); Csovar, Hungary (Pálfy *et al.* 2007). Boundary positions marked according to authors.

Using the magnitude of the negative CIE and outgassing rates of modern basaltic eruptions Beerling and Berner (2002) suggested volcanogenic CO_2 from CAMP was insufficient to satisfy the magnitude of the perturbation to the carbon cycle proposing additional ^{12}C was released to the atmosphere from methane hydrates. Other sources may have included baking of organic-rich sediments during intrusion of dykes and sills (Svensen *et al.* 2007).

Pre-extinction Rhaetian atmospheric CO_2 concentrations were calculated from fossil leaf stomatal densities to have been ~1000 ppm rising to 2000-2500 ppm across the extinction event resulting in a temperature increase of 2.5 - 5°C in an already hot world (McElwain *et al.* 1999; Steinthorsdottir *et al.* 2011).

During periods of elevated atmospheric CO_2 the oceans' dissolved CO_2 concentrations also increase, lowering pH and decreasing the carbonate saturation-state (Cyronak *et al.* 2015). This effect is known as ocean acidification and is popularly invoked as a mechanism for marine extinctions during the end-Triassic (Hautmann 2004, 2012; Hautmann *et al.* 2008a; Kiessling & Simpson 2011; Greene *et al.* 2012; Ikeda *et al.* 2015). However, evidence for this as a kill mechanism is disputable. Hautmann *et al*. (2008a) proposed that aragonitic bivalves were preferentially targeted during the ETE, but this has not been replicated by other studies and fails to explain the severity of losses amongst the non-calcareous radiolarians (Kiessling *et al.* 2007; Dunhill *et al.* 2018). An additional argument for extreme ocean acidification at the ETE is a purported gap in carbonate deposition (Hautmann *et al.* 2008a; Ritterbush *et al.* 2015), yet, some of the reported 'gaps' are attributable to regression and emergence, as evidenced by karstic surfaces or desiccation cracks (Hautmann 2004; Hesselbo *et al.* 2004; Wignall & Bond 2008).

Often associated with LIPs, warming and mass extinction is the spread of anoxic bottom waters (cf. Bond & Grasby 2017). Yet in spite of drastic warming at the ETE there is little to suggest that marine anoxia played a major role in the extinction itself with only localised oxygen depletion, indicated by a thin black shale coincident with the initial CIE in the Kujoch GSSP (Bonis *et al.* 2010; Lindström *et al.* 2017). Some regional development of oxygen restricted waters within the Panthalassa Ocean is seen in Canada (Wignall *et al.* 2007; Kasprak *et al.* 2015) whilst the ETE coincides with a time of the most oxygenated waters of the same ocean when sections in Japan are considered (Fujisaki *et al.* 2016).

An alternative kill mechanism related to LIPs that is often proposed but is usually difficult to assess is the effect of SO_2 (cf. Wignall 2001a).The short-term

formation of aerosols in the stratosphere produces transient cooling and darkening which has been suggested as the cause of a collapse in primary productivity and food webs at the ETE (Guex *et al.* 2004; Schaltegger *et al.* 2008; Schmidt *et al.* 2015). Effects of elevated atmospheric SO_2 are expressed best in the terrestrial realm where morphology and cuticle of fossil leaves show SO_2 related damage (Bacon *et al.* 2013; Steinthorsdottir *et al.* 2018). Additionally, the combination of this gas with rain water produces acid rain which likely contributed to floral turmoil in the late Rhaetian (van de Schootbrugge *et al.* 2009).

1.3 Biotic recovery from mass extinctions

Most research effort surrounding mass extinctions has focused on losses and extinction mechanisms, with relatively little study of the subsequent biotic recovery. Only the recoveries following the Permo-Triassic mass extinction (e.g. Schubert & Bottjer 1995; Rodland & Bottjer 2001; Payne *et al.* 2011; Chen & Benton 2012; Foster & Sebe 2017) and the Cretaceous-Paleogene extinction (e.g. Hansen 1988; Harries 1999; Peryt *et al.* 2002; Alegret 2007; Aberhan & Kiessling 2014; Leighton *et al.* 2017) have received major attention.

Several means by which recovery can be monitored exist, perhaps the simplest being to document extinction and origination rates. Under this scheme the post extinction interval can be divided into two sections, the “survival interval” and the “recovery interval” (Fig. 1.2; Kauffman & Erwin 1995). The first of these refers to the period immediately following the extinction horizon, when environmental conditions remain adverse and no net diversity increase occurs. Fossil assemblages characteristic of this phase are dominated by only a handful of opportunistic species (Schubert & Bottjer 1995; Harries *et al.* 1996). Such

species are morphologically conservative, small in stature with rapid growth, attain maturity at young age, show high juvenile mortality and occupy limited levels of ecological tiers - usually only shallow infaunal or epifaunal (Guex 1992; Harries *et al.* 1996).

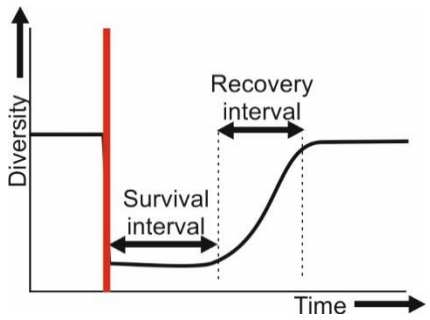

Fig. 1.2 Schematic diagram of expected diversity during survival and recovery intervals, red line indicates extinction event.

The recovery interval proper begins when origination rates exceed extinction rates. During this time habitats are restored, ecological niches repopulated, new specialised forms arise with increased morphological complexity, and taxonomic differentiation between habitats occurs (Harries *et al.* 1996; Guex 2001; Bambach *et al.* 2007).

Defining the point when recovery terminates can be problematic and seldom accurately placed owing to variable rates of recovery between different groups. Estimates of full recovery are often placed when pre-extinction taxonomic richness or a stable diversity has been attained. However, for some extinction events this does not occur before subsequent mass extinctions deplete biotas again (Song *et al.* 2018).

The recovery interval that has received the greatest attention is that following the Permo-Triassic mass extinction (PTME) (e.g. Twitchett 1999; Hofmann *et al.* 2011; Payne *et al.* 2011; Hautmann *et al.* 2015; Dai *et al.* 2018;

Foster *et al.* 2018a). Survival interval assemblages were dominated by the brachiopod *Lingula,* the bivalve *Claraia* and often prolific numbers of microgastropods (e.g. Schubert & Bottjer 1995; Fraiser *et al.* 2005; Zonneveld *et al.* 2007). The recovery is notable for its protracted nature, spanning the entirety of the early Triassic (some 4.7 Myr) with corals, sponges, echinoids, brachiopods and metazoan reef ecosystems only beginning to recover in the Middle Triassic, 7-10 Myr after the extinction (Stanley 1988; Flügel 1994, 2002; Foster *et al.* 2015; Foster & Sebe 2017). Here is a fine example of heterogeneity inherent with recovery because individual groups repopulated at different rates: foraminifera, conodonts and ammonoids were far faster than benthic groups to recover and were well on their way to regaining their former diversity levels within 1.5 Myr of the main extinction (Song *et al.* 2016; Dai *et al.* 2018).

Theories for the underlying cause of this extremely protracted recovery include the magnitude of the extinction (Harries 1999; Hautmann *et al.* 2015) and successive pulses of extinction (e.g. Twitchett *et al.* 2004; Zhang *et al.* 2015; Foster *et al.* 2017; Dai *et al.* 2018). A factor that perhaps is most pertinent was the continuation of adverse environmental conditions, with extreme temperatures and also persistence of widespread marine anoxia, including in shallow water regions, for much of the Lower Triassic (Hallam 1991; Wignall & Hallam 1992; Schubert & Bottjer 1995; Woods *et al.* 1999; Fraiser & Bottjer 2007; Tong *et al.* 2007; Meyer *et al.* 2008, 2011; Sun *et al.* 2012; Wignall *et al.* 2016; Foster *et al.* 2018b). Only once the severe oxygen depletion ameliorated did recovery begin (Hallam 1991; Twitchett 1999; Twitchett & Barras 2004; Foster *et al.* 2018b). The dampening effect of such severe oxygen restriction on recovery can be evidenced by comparing the pace of recovery in regions that show evidence for better aerated waters where recovery of benthic communities was perhaps as much as

5 Myr ahead of those areas where oxygen restriction persisted (Twitchett *et al.* 2004).

By way of contrast, the recovery interval following the Cretaceous-Paleogene (KPg) extinction was remarkably rapid. Benthic communities were dominated by low diversity, small, infaunal deposit-feeding or chemosymbiotic molluscs for some 300 kyr following the KPg (Hansen 1988; Hansen *et al.* 1993; Harries 1999; Aberhan *et al.* 2007; Alroy 2010; Aberhan & Kiessling 2015). The time necessary for molluscan diversity and ecological structure to return to pre-extinction state from 0.5 to 2.7 Myr of the event (Hansen 1988; Sessa *et al.* 2009; Aberhan & Kiessling 2014; Whittle *et al.* 2019).

1.4 Recovery from the end-Triassic extinction

The first studies dedicated to post-ETE recovery were by Hallam (1987, 1996). These entailed zone-by-zone species richness counts for major groups of marine fauna, predominantly from Europe (Fig. 1.3), that showed recovery occurred throughout the Hettangian (Lower Jurassic) with species richness only reaching a plateau during the subsequent Sinemurian Stage (approximately 2 Myr after the ETE using the chronology of Ruhl *et al.* (2010), however a recent reappraisal of the duration of the Hettangian suggests that the stage may have been far longer and so recovery may have taken as long as 4 Myr; Weedon *et al.* 2019). A further increase in diversity to a new, broadly stable level, occurs across the Sinemurian-Pliensbachian boundary, approximately 9 Myr after the ETE. Dunhill *et al*.'s (2018) global database analysis also showed that recovery of level-bottom communities was largely complete by the Sinemurian. As seen after the PTME, pelagic recovery was quicker and achieved within the Hettangian.

Both radiolarians and ammonites underwent a radiation in the early Hettangian (Guex *et al.* 2004), but reefal recovery was far slower, with no significant reefs known for 10 Myr after the extinction (Stanley 1988). Full reef recovery was not seen until the Middle Jurassic and it has been suggested that this was set back during the early Toarcian extinction event (Stanley 1988; Wood 1999; Dunhill *et al.* 2018).

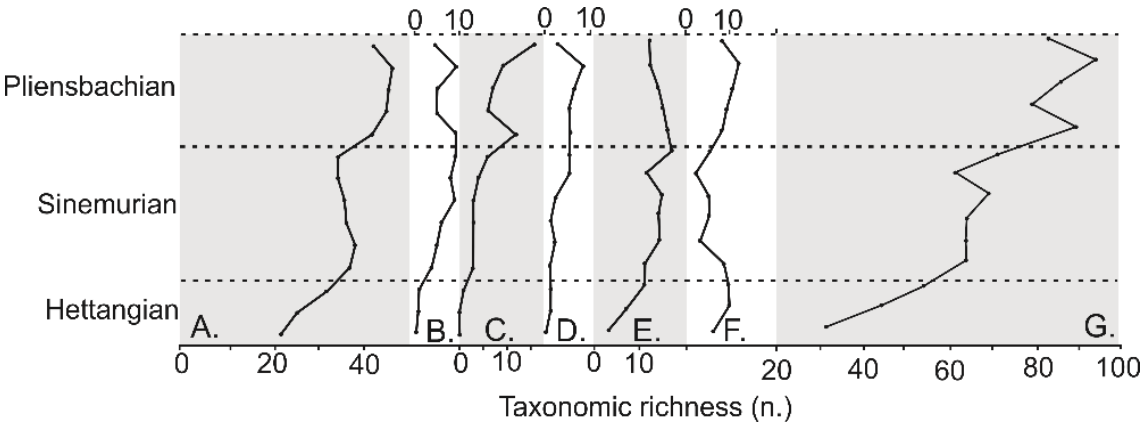

Fig. 1.3 Species richness plots through the British Lower Jurassic from Hallam (1996). A – bivalves; B – ammonite (generic richness); C – rhychonellid brachiopods; D – crinoids; E – foraminifera; F – ostracods; G – total. Vertical axis not scaled to time.

Studies conducted at finer temporal and geographic resolution indicate a shorter period of recovery within the Hettangian Stage. In the British Isles the survival interval is characterised by an abundance of the fossil oyster *Liostrea hisingeri* (Nilsson), lending these beds the name of the *Ostrea* beds (Richardson 1911). Similar high dominance communities are found in Austria at this time with *Cardinia*-dominated (McRoberts *et al.* 2012) and *Lobothyris*-dominated assemblages (Tomašových & Siblík 2007). However, post-extinction communities in Tibet (Hautmann *et al.* 2008b) were diverse and show no opportunist-dominated survival communities.

Following a ‘survival interval’ across key locations in southwest Britain Mander *et al*. (2008) and Pugh *et al*. (2014) report a sequential filling of ecological tiers and rising diversity. This may partly have been controlled by the transition from euryhaline to stenohaline faunas as fully marine conditions were established by transgression in the region (Hallam 1996). Pugh *et al.* (2014) suggested a latest Hettangian age (1.26-2.92 Myr) for completion of recovery based on the appearance of deep infaunal bivalves at this level. This trend occurred despite the wide extent of oxygen restricted marine waters in the European Seaway (Wignall & Hallam 1991; Richoz *et al.* 2012; van de Schootbrugge *et al.* 2013). It is claimed these conditions delayed benthic recovery (Hallam 1996; Clémence *et al.* 2010; Richoz *et al.* 2012; Jost *et al.* 2017; Luo *et al.* 2018); an idea supported by extremely rapid benthic recovery in Tibetan sections which lack evidence of dysoxia (Hautmann *et al.* 2008b).

1.5 Body size

Post mass extinction communities are typically dominated by individuals of small body size (e.g. Fraiser & Bottjer 2004; Sogot *et al.* 2014), as noted by Hallam (1960a, 1975) following the ETE, who noted that many marine mollusc species then increased in size in the Early Jurassic. Ammonites also increase their maximum shell size (Dommergues *et al.* 2002), although this is a phylogenetic size increase (Cope’s Rule) rather than an intraspecific one.

Hallam’s work did not consider molluscan body sizes prior to the extinction and so the size increase could be considered a manifestation of the Lilliput Effect. This term was coined by Urbanek (1993) who documented the effects of biotic crises on graptolite size. He found species that crossed the extinction event

exhibited a transient reduction in body size during the survival interval. The name Lilliput was given likening the diminutive size of organisms in the immediate post crisis interval to the tiny race of humans (Lilliputians) encountered in Jonathan Swift's novel – *Gulliver's Travels.*

The cause(s) of the Lilliput Effect are contentious (Twitchett 2007; Harries & Knorr 2009; Brayard *et al.* 2010; Metcalfe *et al.* 2011; Song *et al.* 2011; Sogot *et al.* 2014; Brom *et al.* 2015; Wiest *et al.* 2018; Chen *et al.* 2019). Often debate shifts away from explaining how and why a single species should exhibit a transient decrease of body size (as per the Lilliput Effect proper) and instead seeks to explain the prevalence of small species (not necessarily true Lilliputians) in the immediate aftermath of extinction intervals. There have been several explanations proposed to explain the latter observation (c.f. Payne 2005) including: preferential extinction of large taxa (Fig. 1.4A) or prevalence of communities dominated by small taxa. The latter may be achieved through increased abundances of miniature species (likely to have been opportunists) without an increase in their taxonomic richness or/and via preferential origination of small-sized species (Fig. 1.4B). In the strict sense the Lilliput Effect is a temporary within-species size reduction amongst surviving taxa, which return to pre-extinction body sizes during the recovery (Fig. 1.4C).

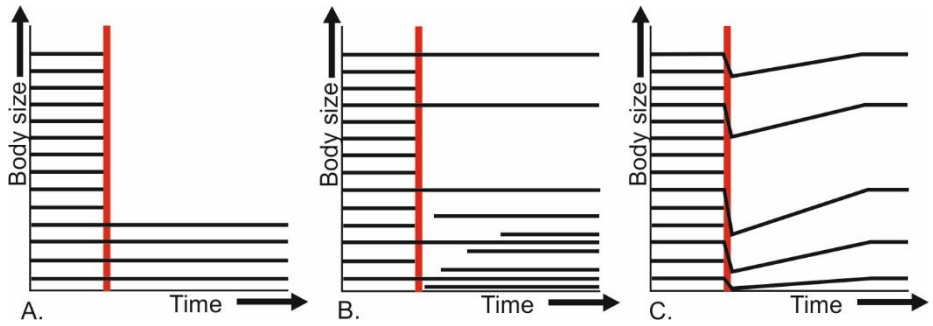

Fig. 1.4 Schematic diagrams of body size changes across extinction events (red line) after Twitchett (2007), Black lines represent theoretical species ranges.

As the Lilliput Effect produces a temporary decrease in body size it is likely a response to some environmental stress affecting growth or development rates. There are numerous possible stressors that could achieve such a condition, factors like: water temperature, salinity levels, dissolved oxygen content, and nutrient availability (Hallam 1965; His *et al.* 1989; Atkinson 1994; Wacker & von Elert 2008).

Marine environments exhibiting some degree of oxygen restriction often feature small sized invertebrates (Rhoads & Morse 1971; Richmond *et al.* 2006). Under low oxygen levels metabolic rates are reduced, and growth slowed (Richmond *et al.* 2006). Oxygen deficiency may work in tandem with absence of currents, which can be particularly detrimental to growth of suspension feeding organisms whose filtration rates scale with current speed, and the supply of food particles (Hallam 1965; Walne 1972). Food availability, nutritional quality and particle size are also known controls on body size and growth rates of organisms (Brown *et al.* 1997; von Elert *et al.* 2003; Wacker & von Elert 2003; Weiss *et al.* 2007).

Temperature of an organism's environment can have a profound effect on body size (McNab 1971; Geist 1987; James *et al.* 1995; van Der Have & De Jong

1996; van Voorhies 1996; Atkinson & Sibly 1997; Mousseau 1997; Roy & Martien 2001; Schmidt *et al.* 2004; Linse *et al.* 2006; Arendt 2011; Berke *et al.* 2013). Perhaps the most renowned temperature-related body size rule is Bergmann's Rule, this rule states that larger species of a taxon occur in cooler climates than smaller bodied relatives (Bergmann 1847; translated in James 1970). Bergmann's observations applied only for homeothermic animals, however this has since been applied to poikilotherms (McNab 1971; Partridge & Coyne 1997; Blackburn *et al.* 1999). Perhaps the largest issue with Bergmann's Rule, is that the original definition included a causal mechanism which revolved around conservation of heat energy in homeotherms (Bergmann 1847; translated in James 1970). Smaller animals have a higher surface area to volume ratio, heat loss will thus be proportionally greater than in a larger species. Smaller taxa thus expend a greater amount of metabolic energy to maintain a constant body temperature in cooler climates and so there is an advantage to being large. This explanation has since been refuted as the observed size body size increases are grossly insufficient to satisfy heat conservation calculations (Geist 1987). This mechanism also provides no explanation for why some poikilotherms exhibit a Bergmann's trend since their body temperature is dependent upon their surroundings (McNab 1971).

It is at this point that we consider the similar Temperature-Size Rule. This rule offers an alternative explanation for a Bergmann's size distribution whereby growth rates and development rates are affected unequally by temperature with the latter being more sensitive (Atkinson 1994; Atkinson & Sibly 1997). For example, under elevated temperatures both growth and development rates increase, the latter more so, thereby promoting sexual maturity at a younger age

and so smaller body size. Conversely in cooler conditions metabolic rates are lower, growth rates slower and longevity increased.

1.6 Aims

The primary aims of this project are to document the tempo and style of recovery amongst marine communities following the end-Triassic mass extinction within the British shelf seas and to examine the potential environmental and evolutionary controls on the trends. Recovery is documented through taxonomic richness, ecology and body size metrics, especially of bivalves which dominate benthic communities. Body size data has been collected for 145 species including five of the six bivalve species reported to increase in body size by Hallam (1960a). Only the body size trends of *Gryphaea* were not studied because these are well known (Hallam 1968, 1975; Johnson 1994; Jones & Gould 1999; Nori & Lathuiliére 2003). Collecting body size data from the breadth of bivalve diversity of the Lias, at the species level, allows assessment for how widespread body size increase was at that time as well as testing for trends within ecological groups, or specific regions. Growth line analyses are conducted to test whether any size trends are due to increased/decreased growth rates or longevity.

In addition marine redox is reconstructed because there is no record available over the entire span of the study/recovery interval. This is achieved through the use of pyrite framboid size distributions from samples that span the entire Hettangian and into the early Sinemurian. Changes in marine oxygenation and other environmental parameters, such as temperature, are compared against bivalve recovery, represented by both diversity and body size in order to investigate how such environmental factors impacted on recovery from the ETE.

1.7 Rationale for work

Body size is an important trait in any organism effecting its ecology, physiology and evolution (e.g. Jablonski 1996 Body size has been described to reset to diminutive forms in the immediate aftermath of mass extinction events but little is known on how body size trajectories are affected over long timescales (multimillion years). This work contributes to the understanding of recovery intervals, in a traditional sense of taxonomic richness but also through the little explored facet of body size.

The British Lias sections were chosen for this analysis because these stratigraphic successions are well-studied and have good age control from high resolution ammonite biostratigraphy. Additionally, the plethora of coastal and inland sites are easily accessed and well-exposed permitting detailed sampling. The study has focussed on bivalves, many of which have undergone recent taxonomic study (e.g. Hodges 2000, 2018), and have long stratigraphic ranges (Hallam 1976) allowing for detection of long term body size trends within species.

1.8 Geological overview

As this study's focus is on British Triassic-Jurassic boundary (TJB) and Lower Jurassic sections an overview of the stratigraphy is provided.

1.8.1 The Rhaetian

Rhaetian stratigraphy, represented by the Penarth Group (Fig. 1.5), is remarkably consistent across great swathes of the British Isles as Late Triassic sea level rise flooded a vast desert basin nestled within Pangaea at around 30-40°N, producing a quasimarine shallow sea punctuated by islands of Precambrian and Palaeozoic rock (Oates 1976; Hallam & El Shaarawy 1982; Simms *et al.* 2004).The Westbury Formation, at the base of the Penarth Group, mostly comprises dark, fossiliferous mudstone with occasional thin calcareous sandstones and tabular fibrous limestones known as 'beef' (Waters & Lawrence 1987; Gallois 2007). It is succeeded by the Lilstock Formation with its constituent Cotham and Langport members (Warrington *et al.* 1980). The Cotham Member contains the ETE, is 2-4m thick, formed of pale-green/cream, thinly bedded mudstones, siltstones and limestones (Hesselbo *et al.* 2004; Gallois 2007, 2009; Wignall & Bond 2008). The Cotham Member exhibits a widespread horizon of soft sediment deformation (Simms 2003, 2007; Lindström *et al.* 2015) that is penetrated by deep 'desiccation' cracks (Waters & Lawrence 1987; Hesselbo *et al.* 2004). Both the deformed bed and crack structures are postulated to have resulted from tectonic activity associated with the opening of the Central Atlantic (Hallam & Wignall 2004; Lindström *et al.* 2015).

The succeeding Langport Member is well exposed at Pinhay Bay, Devon where porcelaneous limestones form a striking white layer in the cliff up to 8 m thick (Hallam 1960b; Wignall 2001b; Gallois 2007). The Member is however abnormal in this location featuring an intraformational conglomerate possibly formed by seismically induced slumping (Wignall 2001b). In other regions of Britain, the Langport Member is typically a micritic mudstone, although in Northern Ireland this unit features shales with thin, occasionally hummocky,

sandstones (Simms & Jeram 2007). The upper surface of this member is marked by a period of sea level fall, capped by an exposure surface known as the 'Sun Beds' which feature truncated *Diplocraterion* burrows (Richardson 1911; Hallam 1960b).

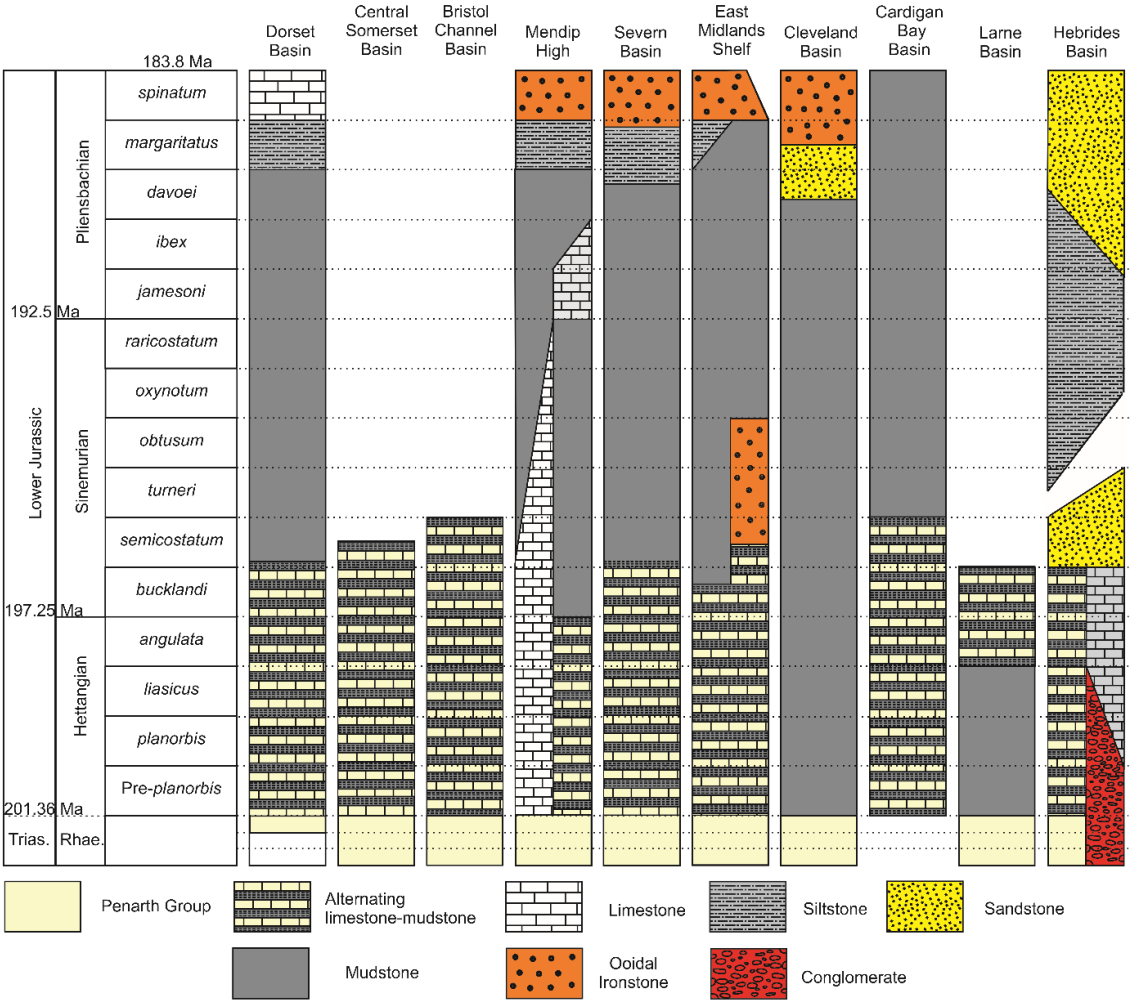

Fig. 1.5 Schematic lithostratigraphy of studied sedimentary basins with ammonite chronozone scheme and geological stages. Modified from Ivimey-Cook (1971); Simms et al. (2004); Simms & Jeram (2007). Stage boundary ages from Ruhl et al. (2016); Wotzlaw et al. (2014); Weedon et al. (2019).

1.8.2 The Hettangian

Placement of the TJB is defined by the lowest occurrence of the ammonite *Plioceras spelae* (Hillebrandt *et al.* 2013), although within Boreal provinces there is a distinct paucity of latest Triassic and earliest Jurassic ammonites until *P. erugatum,* which has been correlated with the uppermost *tilmanni* Zone (Lindström *et al.* 2017). Therefore placement of the TJB remains uncertain in Britain, although carbon isotope stratigraphy can assist. Traditionally the ammonite-barren interval above the Lilstock Formation but below the lowest occurrence of Jurassic ammonites, is referred to as the Pre-*planorbis* Beds.

All ammonite zonation schemes herein referred to for the British Lias follow Northwest European Province scheme reviewed in Page (2003). For the Hettangian three ammonite zones are recognised above the Pre-*planorbis* Beds. These are, in ascending order: *planorbis*, *liasicus* and *angulata* zones. These ammonite zones are, in many basins, represented lithologically by the Blue Lias Formation that consists of small-scale cycles of limestone-marl-shale (Fig. 1.5) (Hallam 1957a, b, 1960a, 1964; Cope *et al.* 1980; Weedon *et al.* 2018). The transition from the Langport Member to the Blue Lias signifies a rapid transgression heralding not only the development of fully marine conditions but also the spread of black shales (Wignall & Hallam 1991; Wignall 2001b). The classical Blue Lias development is considered to represent offshore deposition, around the Mendips of Somerset and in areas of Glamorgan these facies pass laterally into marginal facies, in Glamorgan this is the Sutton Stone and Southerndown Beds (Tawney 1865; Trueman 1922). The Sutton Stone is formed of conglomerates, grainstones and packstones (Sheppard 2002), whereas the succeeding Southerndown Beds are transitional between Sutton Stone and offshore Blue Lias (Trueman 1922).

Although Blue Lias facies are prevalent across much of the British Isles a notable exception includes the Cleveland Basin of north east England where the Redcar Mudstone Formation occurs (Fig. 1.5) - a fossiliferous mudstone and siltstone with subordinate shell beds and carbonate concretions (Powell 1984).

1.8.3 The Sinemurian

The Hettangian-Sinemurian boundary is marked by a change from schlotheimiid dominated ammonite assemblages to aretitids, specifically the first occurrence of *Metophiceras* (Bloos & Page 2002). The Sinemurian can be divided into six ammonite zones: *bucklandi*, *semicostatum*, *turneri*, *obtusum*, *oxynotum* and *raricostatum*. Initially, the Sinemurian continues in the same vein of the Hettangian with the *bucklandi* and lower part of the *semicostatum* zones seeing a continuation of the Blue Lias or Redcar Mudstone formations (Fig. 1.5). However, the Blue Lias fades out being replaced by mud dominated deposition primarily in the guise of the Charmouth Mudstone Formation across southern and central Britain (Fig. 1.5) (Cope *et al.* 1980; Cox *et al.* 1999).

1.8.4 The Pliensbachian

The base of the Pliensbachian is defined by the presence of the ammonite genus *Apoderoceras* and contains five ammonite zones: *jamesoni*, *ibex*, *davoei*, *margaritatus* and *spinatum* (Meister *et al.* 2004). The earliest Pliensbachian is, for most British basins, the same lithological formation as the latest Sinemurian (e.g. Charmouth Mudstone, Redcar Mudstone, Pabay Shale cf. Simms *et al.* 2004). The stage is characterised by an overall regression and so the stage

terminates with ferruginous ooid-bearing shallow water facies (e.g. Marlstone Rock, Cleveland Ironstone formations; Fig. 1.5).

1.9 Thesis outline

To assess recovery among marine communities following the end-Triassic mass extinction event this thesis is divided into a series of papers and chapters that consider body size changes, taxonomic richness and marine oxygenation during recovery. Chapter 2 provides a detailed account of *Plagiostoma giganteum* J. Sowerby, a species noted by Hallam to undergo an increase in its maximum size during the Hettangian and early Sinemurian. This chapter compares the size increase of *P. giganteum* to contemporaries of the same family, the Limidae and attempts to assess the driving mechanism behind the trends. Chapter 2 also introduces the Brobdingnag Effect. Chapter 3 addresses the issue of recovery among the bivalves, its duration and whether oxygen restriction acted to stall their recovery. This chapter focuses on the story within the Blue Lias Formation. Chapter 4 builds on the previous chapter by assessing recovery and reconstructing redox conditions in a non-Blue Lias setting. Chapter 5 returns to the concepts of Chapter 2 and the Brobdingnag Effect. This time expanding the study to encompasses all bivalves and across a greater length of time (Rhaetian to latest Pliensbachian). Size changes documented therein are compared to other indicators of recovery such as diversity and further discussion on potential drivers of body size changes is given. Chapter 6 draws together the results of the preceding chapters and compares the findings to other recovery intervals. Finally, Chapter 7 provides a summary of the key results as well as suggestions for further areas of study.

References

Aberhan, M. & Kiessling, W. 2014. Rebuilding biodiversity of Patagonian marine molluscs after the end-Cretaceous mass extinction. *PLoS ONE*, **9**, e102629, https://doi.org/10.1371/journal.pone.0102629.

Aberhan, M. & Kiessling, W. 2015. Persistent ecological shifts in marine molluscan assemblages across the end-Cretaceous mass extinction. *PNAS*, **112**, 7207–7212, https://doi.org/10.1073/pnas.1422248112.

Aberhan, M., Weidemeyer, S., Kiessling, W., Scasso, R.A. & Medina, F.A. 2007. Faunal evidence for reduced productivity and uncoordinated recovery in Southern Hemisphere Cretaceous-Paleogene boundary sections. *Geological Society, London, Special Publications*, **35**, 227–230, https://doi.org/10.1130/G23197A.1.

Ager, D. V. 1987. Why the rhynchonellid brachiopods survived and the spiriferids did not: a suggestion. *Palaeontology*, **30**, 853–857.

Alegret, L. 2007. Recovery of the deep-sea floor after the Cretaceous−Paleogene boundary event: The benthic foraminiferal record in the Basque – Cantabrian Basin and in south-eastern Spain. *Palaeogeography, Palaeoclimatology, Palaeoecology*, **255**, 181–194, https://doi.org/10.1016/j.palaeo.2007.02.047.

Alroy, J. 2010. Geographical, environmental and intrinsic biotic controls on Phanerozoic marine diversification. *Palaeontology*, **53**, 1211–1235, https://doi.org/10.1111/j.1475-4983.2010.01011.x.

Arendt, J.D. 2011. Size-fecuncity relationships, growth trajectories, and the Temperature-Size Rule for ectotherms. *Evolution*, **65**, 43–51, https://doi.org/10.1111/j.1558-5646.2010.01112.x.

Atkinson, D. 1994. Temperature and organism size—a biological law for ectotherms? *Advances in Ecological Research*, **25**, 1–58, https://doi.org/10.1016/S0065-2504(08)60212-3.

Atkinson, D. & Sibly, R.M. 1997. Why are organisms usually bigger in cold environments? Making sense of a life history puzzle. *Trends in Ecology & Evolution*, **12**, 235–239.

Bacon, K.L., Belcher, C.M., Haworth, M. & McElwain, J.C. 2013. Increased atmospheric SO_2 detected from changes in leaf physiognomy across the Triassic–Jurassic boundary interval of East Greenland. *PLoS ONE*, **8**, 1–12, https://doi.org/10.1371/journal.pone.0060614.

Bambach, R.K., Bush, A.M. & Erwin, D.H. 2007. Autecology and the filling of ecospace: key metazoan radiations. *Palaeontology*, **50**, 1–22.

Bartolini, A., Guex, J., Spangenberg, J.E., Schoene, B., Taylor, D., Schaltegger, U. & Atudorei, V. 2012. Disentangling the Hettangian carbon isotope record: Implications for the aftermath of the end-Triassic mass extinction. *Geochem. Geophys. Geosyst*, **13**, 1–11, https://doi.org/10.1029/2011GC003807.

Beerling, D.J. & Berner, R.A. 2002. Biogeochemical constraints on the Triassic-Jurassic boundary carbon cycle event. *Global Biogeochemical Cycles*, **16**,

1–13.

Bergmann, C. 1847. Ueber die Verhältnisse der Wärmeökonomie der Thiere zu ihrer Grösse. *Grottinger studien*, **3**, 595–708.

Berke, S.K., Jablonski, D., Krug, A.Z., Roy, K. & Tomašových, A. 2013. Beyond Bergmann's Rule: size–latitude relationships in marine bivalvia world-wide. *Global Ecology and Biogeography*, **22**, 173–183, https://doi.org/10.1111/j.1466-8238.2012.00775.x.

Blackburn, T.M., Gaston, K.J. & Loder, N. 1999. Geographic gradients in body size: a clarification of Bergmann's Rule. *Diversity and Distributions*, **5**, 165–174, https://doi.org/10.1046/j.1472-4642.1999.00046.x.

Bloos, G. & Page, K.N. 2002. Global stratotype section and point for base of the Sinemurian Stage (Lower Jurassic). *Episodes*, **25**, 22–28.

Bond, D.P.G. & Grasby, S.E. 2017. On the causes of mass extinctions. *Palaeogeography, Palaeoclimatology, Palaeoecology*, **478**, 3–29, https://doi.org/10.1016/j.palaeo.2016.11.005.

Bond, D.P.G. & Wignall, P.B. 2014. Large igneous provinces and mass extinctions: An update. *In*: Keller, G. & Kerr, A. C. (eds) *Volcanism, Impacts and Mass Extinctions: Causes And Effects*. The Geological Society of America, 29–55., https://doi.org/10.1130/2014.2505(02).

Bonis, N.R., Ruhl, M. & Kürschner, W.M. 2010. Climate change driven black shale deposition during the end-Triassic in the western Tethys. *Palaeogeography, Palaeoclimatology, Palaeoecology*, **290**, 151–159, https://doi.org/10.1016/j.palaeo.2009.06.016.

Brayard, A., Nützel, A., Stephen, D.A., Bylund, K.G., Jenks, J. & Bucher, H. 2010. Gastropod evidence against the Early Triassic Lilliput Effect. *Geology*, **38**, 147–150, https://doi.org/10.1130/g30553.1.

Brom, K.R., Salamon, M.A., Ferré, B., Brachaniec, T. & Szopa, K. 2015. The Lilliput Effect in crinoids at the end of the Oceanic Anoxic Event 2: a case study from Poland. *Journal of Paleontology*, **89**, 1076–1081.

Brown, M.R., Jeffrey, S.W., Volkman, J.K. & Dunstan, G.A. 1997. Nutritional properties of microalgae for mariculture. *Aquaculture*, **151**, 315–331.

Carter, E.S. & Hori, R.S. 2005. Global correlation of the radiolarian faunal change across the Triassic-Jurassic boundary. *Canadian Journal of Earth Science*, **42**, 777–790.

Chen, J., Song, H., He, W., Tong, J., Wang, F. & Wu, S. 2019. Size variation of brachiopods from the Late Permian through the Middle Triassic in South China: Evidence for the Lilliput Effect following the Permian-Triassic extinction. *Palaeogeography, Palaeoclimatology, Palaeoecology*, **519**, 248–257, https://doi.org/10.1016/j.palaeo.2018.07.013.

Chen, Z.-Q. & Benton, M.J. 2012. The timing and pattern of biotic recovery following the end-Permian mass extinction. *Nature Geoscience*, **5**, 375–383, https://doi.org/10.1038/ngeo1475.

Clémence, M.-E., Bartolini, A., Gardin, S., Paris, G., Beaumont, V. & Page, K.N. 2010. Early Hettangian benthic–planktonic coupling at Doniford (SW England): Palaeoenvironmental implications for the aftermath of the end-Triassic crisis. *Palaeogeography, Palaeoclimatology, Palaeoecology*, **295**,

102–115, https://doi.org/10.1016/j.palaeo.2010.05.021.

Colbert, E.H. 1958. Tetrapod extinctions at the end of the Triassic period. *Zoölogy*, **44**, 973–977.

Cope, J.C.W., Getty, T.A., Howarth, M.K., Morton, N. & Torrens, H.S. 1980. *A Correlation of the Jurassic Rocks in the British Isles Part One: Introduction and the Lower Jurassic*. Geological Scoiety of London Special Report, No. 14.

Courtillot, V.E., Jaeger, J.-J., Yang, Z., Féraud, G. & Hofmann, C. 1996. The influence of continental flood basalts on mass extinctions: Where do we stand? *The Cretaceous-Tertiary event and other catastrophes in Earth history*, **307**, 513–525, https://doi.org/10.1130/0-8137-2307-8.513.

Cox, B.M., Sumbler, M.G. & Ivimey-Cook, H.C. 1999. *A Formational Framework for the Lower Jurassic of England and Wales (Onshore Area)*. British Geological Survey Research Report, Np RR/99/01.

Cyronak, T., Schulz, K.G. & Jokiel, P.L. 2015. The Omega myth: what really drives lower calcification rates in an acidifying ocean. *ICES Jouranl of Marnie scienve*, https://doi.org/10.1093/icesjms/fsv075.

Dai, X., Song, H., et al. 2018. Rapid biotic rebound during the late Griesbachian indicates heterogeneous recovery patterns after the Permian-Triassic mass extinction. *Geological Society of America Bulletin*, **130**, 2015–2030, https://doi.org/10.1130/30/B31969.1.

Dommergues, J.-L., Montuire, S. & Neige, P. 2002. Size patterns through time: the case of the Early Jurassic ammonite radiation. *Paleobiology*, **28**, 423–434, https://doi.org/10.1666/0094-8373(2002)028<0423:SPTTTC>2.0.CO;2.

Dunhill, A.M., Foster, W.J., Sciberras, J. & Twitchett, R.J. 2018. Impact of the Late Triassic mass extinciton on functional diversity and composition of marine ecosystems. *Palaeontology*, **61**, 133–148, https://doi.org/10.1111/pala.12332.

Fisher, M.J. & Dunay, R.E. 1981. Palynology and the Triassic/Jurassic boundary. *Palaeobotany and Palynology*, **34**, 129–135.

Flügel, E. 1994. Pangean shelf carbonates: controls and paleoclimatic significance of the Permian and Triassic reefs. *In*: Klein, G. D. (ed.) *Pangea: Paleoclimate, Tectonics, and Sedimentation during Accretion, Zeneth and Break up of a Supercontinent*. Special Paper of the Geological Society of America, **288**, 247–266.

Flügel, E. 2002. Triassic Reef Patterns. *In*: Kiessling, W., Flügel, E. & Golonka, J. (eds) *Phanerozoic Reef Patterns*. Tulsa, SEPM, 391–463.

Foster, W.J. & Sebe, K. 2017. Recovery and diversification of marine communities following the late Permian mass extinction event in the western Palaeotethys. *Global and Planetary Change*, **155**, 165–177, https://doi.org/10.1016/j.gloplacha.2017.07.009.

Foster, W.J., Danise, S., Sedlacek, A., Price, G.D., Hips, K. & Twitchett, R.J. 2015. Environmental controls on the post-Permian recovery of benthic, tropical marine ecosystems in western Palaeotethys (Aggtelek Karst, Hungary). *Palaeogeography, Palaeoclimatology, Palaeoecology*, **440**, 374–

394, https://doi.org/10.1016/j.palaeo.2015.09.004.

Foster, W.J., Danise, S., Price, G.D. & Twitchett, R.J. 2017. Subsequent biotic crises delayed marine recovery following the late Permian mass extinction event in northern Italy. *PLoS ONE*, **12**, e0172321, https://doi.org/10.1371/journal.pone.0172321.

Foster, W.J., Danise, S., Price, G.D. & Twitchett, R.J. 2018a. Paleoecological analysis of benthic recovery after the Late Permian mass extinciton event in Eastern Lombardy, Italy. *Palaios*, **33**, 266–281.

Foster, W.J., Lehrmann, D.J., Yu, M., Ji, L. & Martindale, R.C. 2018b. Persistent environmental stress delayed the recovery of marine communities in the aftermath of the latest Permian mass extinction. *Paleoceanography and Paleoclimateology*, **33**, 338–353.

Fraiser, M.L. & Bottjer, D.J. 2004. The non-actualistic Early Triassic gastropod fauna: a case study of the Lower Triassic Sinbad Limestone Member. *Palaios*, **19**, 259–275.

Fraiser, M.L. & Bottjer, D.J. 2007. Elevated atmospheric CO_2 and the delayed biotic recovery from the end-Permian mass extinction. *Palaeogeography, Palaeoclimatology, Palaeoecology*, **252**, 164–175, https://doi.org/10.1016/j.palaeo.2006.11.041.

Fraiser, M.L., Twitchett, R.J. & Bottjer, D.J. 2005. Unique microgastropod biofacies in the Early Triassic: Indicator of long-term biotic stress and the pattern of biotic recovery after the end-Permian mass extinction. *Comptes Rendus Palevol*, **4**, 543–552, https://doi.org/10.1016/j.crpv.2005.04.006.

Fujisaki, W., Sawaki, Y., Yamamoto, S., Sato, T., Nishizawa, M., Windley, B.F. & Maruyama, S. 2016. Tracking the redox history and nitrogen cycle in the pelagic Panthalassic deep ocean in the Middle Triassic to Early Jurassic: Insights from redox-sensitive elements and nitrogen isotopes. *Palaeogeography, Palaeoclimatology, Palaeoecology*, **449**, 397–420, https://doi.org/10.1016/j.palaeo.2016.01.039.

Gallois, R.W. 2007. The stratigraphy of the Penarth Group (Late Triassic) of the east Devon coast. *Geoscience in South-West England*, **11**, 287–297.

Gallois, R.W. 2009. Lithostratigraphy of the Penarth Group (Late Triassic) of the Severn Estuary area. *Geoscience in South-West England*, **12**, 71–84.

Geist, V. 1987. Bergmann's Rule is invalid. *Canadian Journal of Zoology*, **65**, 1035–1038, https://doi.org/10.1139/z87-164.

Gómez, J.J., Goy, A. & Barrón, E. 2007. Events around the Triassic – Jurassic boundary in northern and eastern Spain: A review. *Palaeogeography, Palaeoclimatology, Palaeoecology*, **244**, 89–110, https://doi.org/10.1016/j.palaeo.2006.06.025.

Greene, S.E., Martindale, R.C., Ritterbush, K.A., Bottjer, D.J., Corsetti, F.A. & Berelson, W.M. 2012. Recognising ocean acidification in deep time : An evaluation of the evidence for acidification across the Triassic-Jurassic boundary. *Earth Science Reviews*, **113**, 72–93, https://doi.org/10.1016/j.earscirev.2012.03.009.

Guex, J. 1982. Relations entre le genre Psiloceras et les Phylloceratida au voisinage de la limite Trias- Jurassique. *Bulletin de la Société Vaudoise*

des Sciences Naturelles, **76**, 47–51.

Guex, J. 1992. Origine des sauts évolutifs chez les ammonites. *Bulletin de la Société Vaudoise des Sciences Naturelles*, **82**, 117–144, https://doi.org/10.5169/seals-280170.

Guex, J. 2001. Environmental stress and atavism in ammonoid evolution. *Eclogae Geologicae Helvetiae*, **94**, 321–328.

Guex, J., Bartolini, A., Atudorei, V. & Taylor, D. 2004. High-resolution ammonite and carbon isotope stratigraphy across the Triassic–Jurassic boundary at New York Canyon (Nevada). *Earth and Planetary Science Letters*, **225**, 29–41, https://doi.org/10.1016/j.epsl.2004.06.006.

Guex, J., Schoene, B., et al. 2012. Geochronological constraints on post-extinction recovery of the ammonoids and carbon cycle perturbations during the Early Jurassic. *Palaeogeography, Palaeoclimatology, Palaeoecology*, **346**–**347**, 1–11, https://doi.org/10.1016/j.palaeo.2012.04.030.

Hallam, A. 1957a. Primary origin of the limestone-shale rhythm in the British Lower Lias. *Geological Magazine*, **94**, 175–176.

Hallam, A. 1957b. The limestone-shale rhythm in the British Lower Lias. *Geological Magazine*, **94**, 512–514.

Hallam, A. 1960a. A sedimentary and faunal study of the Blue Lias of Dorset and Glamorgan. *Philosophical Transactions of the Royal Society of London B: Biological Sciences*, **243**, 1–44, https://doi.org/10.1098/rstb.1960.0003.

Hallam, A. 1960b. The White Lias of the Devon coast. *Proceedings of the Geologists' Association*, **71**, 47–60, https://doi.org/10.1016/S0016-7878(60)80031-4.

Hallam, A. 1964. Origin of the limestone-shale rhythm in the Blue Lias of England: a composite theory. *The Journal of Geology*, **72**, 157–169, https://doi.org/10.1086/626974.

Hallam, A. 1965. Environmental causes of stunting in living and fossil marine benthonic invertebrates. *Palaeontology*, **8**, 132–155.

Hallam, A. 1968. Morphology, palaeoecology and evolution of the genus Gryphaea in the British Lias. *Philosophical Transactions of the Royal Society of London B: Biological Sciences*, **254**, 91–128, https://doi.org/10.1098/rstb.1968.0014.

Hallam, A. 1975. Evolutionary size increase and longevity in Jurassic bivalves and ammonites. *Nature*, **258**, 493–496.

Hallam, A. 1976. Stratigraphic distribution and ecology of european Jurassic bivalves. *Lethaia*, **9**, 245–259.

Hallam, A. 1981. The end-Triassic bivalve extinction event. *Palaeogeography, Palaeoclimatology, Palaeoecology*, **35**, 1–44.

Hallam, A. 1987. Radiations and extinctions in relation to environmental change in the marine Lower Jurassic of Northwest Europe. *Paleobiology*, **13**, 152–168.

Hallam, A. 1991. Why was there a delayed radiation after the end-Palaeozoic extinction? *Historical Biology*, **5**, 257–262,

https://doi.org/https://doi.org/10.1080/10292389109380405.

Hallam, A. 1996. Recovery of the marine fauna in Europe after the end-Triassic and early Toarcian mass extinctions. *Geological Society, London, Special Publications*, **102**, 231–236, https://doi.org/10.1144/GSL.SP.1996.001.01.16.

Hallam, A. 2002. How catastrophic was the end-Triassic mass extinction? *Lethaia*, **35**, 147–157.

Hallam, A. & El Shaarawy, Z. 1982. Salinity reduction of the end-Triassic sea from the Alpine region into northwestern Europe. *Lethaia*, **15**, 169–178, https://doi.org/10.1111/j.1502-3931.1982.tb01136.x.

Hallam, A. & Wignall, P.B. 1999. Mass extinctions and sea-level changes. *Earth-Science Reviews*, **48**, 217–250, https://doi.org/10.1016/S0012-8252(99)00055-0.

Hallam, A. & Wignall, P.B. 2004. Discusion on sea-level change and facies development across potential Triassic-Jurassic boundary horizons, SW Britain. *Journal of the Geological Society*, **161**, 1053–1056.

Hansen, T.A. 1988. Early Tertiary radiation of marine molluscs and the long-term effects of the Cretaceous-Tertiary extinction. *Paleobiology*, **14**, 37–51.

Hansen, T.A., Upshaw, B., Kauffman, E.G. & Gose, W. 1993. Patterns of molluscan extinction and recovery across the Cretaceous-Tertiary boundary in east Texas; report on new outcrops. *Cretaceous Research*, **14**, 685–706.

Harries, P.J. 1999. Repopulations from Cretaceous mass extinctions: Environmental and/or evolutionary controls? *In*: Barrera, E. & Johnson, C. C. (eds) *Evolution of the Cretaceous Ocean-Climate System*. Boulder, Geological Society of America Special Papers, 345–364.

Harries, P.J. & Knorr, P.O. 2009. What does the 'Lilliput Effect' mean? *Palaeogeography, Palaeoclimatology, Palaeoecology*, **284**, 4–10, https://doi.org/10.1016/j.palaeo.2009.08.021.

Harries, P.J., Kauffman, E.G. & Hansen, T.A. 1996. Models for biotic survival following mass extinction. *In*: Hart, M. B. (ed.) *Biotic Recovery from Mass Extinction Eventsi*. Geological Society of London, Special Publication No. 102, 41–60., https://doi.org/10.1144/GSL.SP.1996.001.01.03.

Hautmann, M. 2004. Effect of end-Triassic CO2 maximum on carbonate sedimentation and marine mass extinction. *Facies*, **50**, 257–261, https://doi.org/10.1007/s10347-004-0020-y.

Hautmann, M. 2012. Extinction: end-Triassic mass extinction. *In*: *eLS*. Chichester, John Wiley & Sons, Ltd, 1–10., https://doi.org/10.1002/9780470015902.a0001655.pub3.

Hautmann, M., Benton, M.J. & Toma, A. 2008a. Catastrophic ocean acidification at the Triassic-Jurassic boundary. *N. Jb. Geol. Palaont. Abh*, **249**, 119–127, https://doi.org/10.1127/0077-7749/2008/0249-0119.

Hautmann, M., Stiller, F., Cai, H.W. & Sha, J.-G. 2008b. Extinction-recovery pattern of level-bottom faunas across the Triassic-Jurassic boundary in Tibet: implications for potential killing mechanisms. *Palaios*, **23**, 711–718, https://doi.org/10.2110/palo.2008.p08-005r.

Hautmann, M., Bagherpour, B., Brosse, M., Frisk, Å., Hofmann, R., Baud, A. & Nützel, A. 2015. Competition in slow motion: the unusual case of benthic marine communites in the wake of the end-Permian mass extinction. *Palaeontology*, **58**, 871–901, https://doi.org/10.1111/pala.12186.

Hesselbo, S.P., Robinson, S.A., Surlyk, F. & Piasecki, S. 2002. Terrestrial and marine extinction at the Triassic-Jurassic boundary synchronized with major carbon-cycle perturbation : A link to initiation of massive volcanism ? *Geology*, **30**, 251–254.

Hesselbo, S.P., Robinson, S.A. & Surlyk, F. 2004. Sea-level change and facies development across potential Triassic – Jurassic boundary horizons , SW Britain. *Journal of the Geological Society*, **161**, 365–379.

Hillebrandt, A. V, Krystyn, L., et al. 2013. The Global Stratotype Sections and Point (GSSP) for the base of the Jurassic system at Kuhjoch (Karwendel Mountains, Northern Calcareous Alps, Tyrol, Austria). *Episodes*, **36**, 162–198.

His, E., Robert, R. & Dinet, A. 1989. Combined effects of temperature and salinity on fed and starved larvae of the Mediterranean mussel Mytilus galloprovincialis and the Japanese oyster Crassostrea gigas. *Marine Biology*, **100**, 455–463.

Hodges, P. 2000. *The Early Jurassic Bivalvia from the Hettangian and Lower Sinemurian of South-West Britain Part 1*. London, Monograph of the Palaeontographical Society.

Hodges, P. 2018. *The Early Jurassic Bivalvia from the Hettangian and Lower Sinemurian of South-West Britain Part 2*. London, Monograph of the Palaeontographical Society, https://doi.org/10.1080/02693445.2017.11963960.

Hofmann, R., Goudemand, N., Wasmer, M., Bucher, H. & Hautmann, M. 2011. New trace fossil evidence for an early recovery signal in the aftermath of the end-Permian mass extinction. *Palaeogeography, Palaeoclimatology, Palaeoecology*, **310**, 216–226, https://doi.org/10.1016/j.palaeo.2011.07.014.

Ikeda, M., Hori, R.S., Okada, Y. & Nakada, R. 2015. Volcanism and deep-ocean acidification across the end-Triassic extinction event. *Palaeogeography, Palaeoclimatology, Palaeoecology*, **440**, 725–733, https://doi.org/10.1016/j.palaeo.2015.09.046.

Ivimey-Cook, H.C. 1971. Stratigraphical palaeontology of the Lower Jurassic of the Llanbedr (Mochras Farm) Borehole. *In*: Woodland, A. W. (ed.) *The Llanbedr (Mochras Farm) Borehole*. Institute of Geological Sciences Report No.71/18, 87–92.

Jablonski, D. 1996. Body size and macroevolution. *In*: Jablonski, D., Erwin, D. H. & Lipps, J. H. (eds) *Evolutionary Paleobiology*. Chicago, University of Chicago Press.

James, A.C., Azevedo, R.B.R. & Partridge, L. 1995. Cellular basis and developmental timing in a size cline of Drosophila melanogaster. *Genetics*, **140**, 659–666.

James, F.C. 1970. Geographic size variation in birds and its relationship to climate. *Ecology*, **51**, 365–390, https://doi.org/10.2307/1935374.

Johnson, A. 1994. Evolution of European Lower Jurassic Gryphaea (Gryphaea) and contemporaneous bivalves. *Historical Biology*, **7**, 167–186.

Jones, D.S. & Gould, S.J. 1999. Direct measurements of age in fossil Gryphaea: the solution to a classic problem in heterochrony. *Paleobiology*, **25**, 158–187.

Jost, A.B., Bachan, A., van de Schootbrugge, B., Lau, K. V, Weaver, K.L., Maher, K. & Payne, J.L. 2017. Uranium isotope evidence for an expansion of marine anoxia during the end-Triassic extinction. *Geochem. Geophys. Geosyst*, **18**, 3093–3108, https://doi.org/10.1002/2017GC006941.

Kasprak, A.H., Sepúlveda, J., et al. 2015. Episodic photic zone euxinia in the northeastern Panthalassic Ocean during the end-Triassic extinction. *Geology*, **43**, 307–310, https://doi.org/10.1130/G36371.1.

Kauffman, E.G. & Erwin, D.H. 1995. Surviving mass extinctions. *Geotimes*, **14**, 14–17.

Kiessling, W. & Simpson, C. 2011. On the potential for ocean acidification to be a general cause of ancient reef crises. *Global Change Biology*, **17**, 56–67, https://doi.org/10.1111/j.1365-2486.2010.02204.x.

Kiessling, W., Aberhan, M., Brenneis, B. & Wagner, P.J. 2007. Extinction trajectories of benthic organisms across the Triassic – Jurassic boundary. *Palaeogeography, Palaeoclimatology, Palaeoecology*, **244**, 201–222, https://doi.org/10.1016/j.palaeo.2006.06.029.

Knight, K.B., Nomade, S., Renne, P.R., Marzoli, A., Bertrand, H. & Youbi, N. 2004. The Central Atlantic Magmatic Province at the Triassic – Jurassic boundary: paleomagnetic and ^{40}Ar /^{39}Ar evidence from Morocco for brief, episodic volcanism. *Earth and Planetary Science Letters*, **228**, 143–160, https://doi.org/10.1016/j.epsl.2004.09.022.

Kocsis, Á.T., Kiessling, W. & Pálfy, J. 2014. Radiolarian biodiversity dynamics through the Triassic and Jurassic: implications for proximate causes of the end-Triassic mass extinction. *Paleobiology*, **40**, 625–639, https://doi.org/10.1666/14007.

Kürschner, W.M., Bonis, N.R. & Krystyn, L. 2007. Carbon isotope stratigraphy and palynostratigraphy of the Triassic-Jurassic transition in the Tiefengraben section - Northern Calcareous Alps (Austria). *Palaeogeography, Palaeoclimatology, Palaeoecology*, **244**, 257–280.

Leighton, A.D., Hart, M.B., Smart, C.W., Leng, M.J. & Hampton, M. 2017. Timing recovery after the Cretaceous/Paleogene boundary: edvidence from the Brazos River, Texas, USA. *Journal of Foraminiferal Research*, **47**, 229–238.

Lindström, S., Pedersen, G.K., et al. 2015. Intense and widespread seismicity during the end-Triassic mass extinction due to emplacement of a large igneous province. *Geology*, **43**, 387–391, https://doi.org/10.1130/G36444.1.

Lindström, S., van de Schootbrugge, B., et al. 2017. A new correlation of Triassic–Jurassic boundary successions in NW Europe, Nevada and Peru, and the Central Atlantic Magmatic Province: A time-line for the end-Triassic mass extinction. *Palaeogeography, Palaeoclimatology, Palaeoecology*, **478**, 80–102, https://doi.org/10.1016/j.palaeo.2016.12.025.

Linse, K., Barnes, D.K.A. & Enderlein, P. 2006. Body size and growth of benthic invertebrates along an Antarctic latitudinal gradient. *Deep Sea Research Part II: Topical Studies in Oceanography*, **53**, 921–931, https://doi.org/10.1016/j.dsr2.2006.03.006.

Luo, G., Richoz, S., van de Schootbrugge, B., Algeo, T.J., Xie, S., Ono, S. & Summons, R.E. 2018. Multiple sulfur-isotopic evidence for a shallowly stratified ocean following the Triassic-Jurassic boundary mass extinction. *Geochimica et Cosmochimica Acta*, **231**, 73–87, https://doi.org/10.1016/j.gca.2018.04.015.

Mander, L., Twitchett, R.J. & Benton, M.J. 2008. Palaeoecology of the Late Triassic extinction event in the SW UK. *Journal of the Geological Society*, **165**, 319–332, https://doi.org/10.1144/0016-76492007-029.

Mander, L., Kürschner, W.M. & McElwain, J.C. 2013. Palynostratigraphy and vegetation history of the Triassic – Jurassic transition in East Greenland. *Journal of the Geological Society, London*, **170**, 37–46, https://doi.org/10.1144/jgs2012-018.

Marzoli, A., Renne, P.R., Piccirillo, E.M., Ernesto, M., Bellieni, G. & De Min, A. 1999. Extensive 200-Million-Year-Old Continental Flood Basalts of the Central Atlantic Magmatic Province. *Science*, **284**, 616–618, https://doi.org/10.1126/science.284.5414.616.

Marzoli, A., Herve, B., et al. 2004. Synchrony of the Central Atlantic Magmatic Province and the Triassic-Jurassic boundary climatic and biotic crisis. *Geology*, **32**, 973–976, https://doi.org/10.1130/G20652.1.

May, P.R. 1971. Pattern of Triassic-Jurassic diabase dikes around the North Atlantic in the context of predrift position of the continents. *Geological Society of America Bulletin*, **82**, 1285–1291.

McElwain, J.C., Beerling, D.J. & Woodward, F.I. 1999. Fossil plants and global warming at the Triassic-Jurassic boundary. *Science*, **285**, 1386–1391.

McGhee, G.R., Sheehan, P.M., Bottjer, D.J. & Droser, M.L. 2004. Ecological ranking of Phanerozoic biodiversity crises: ecological and taxonomic severities are decoupled. *Palaeogeography, Palaeoclimatology, Palaeoecology*, **211**, 289–297.

McNab, B.K. 1971. On the ecological significance of Bergmann's Rule. *Ecology*, **52**, 845–854, https://doi.org/10.2307/1936032.

McRoberts, C.A. & Newton, C.R. 1995. Selective extinction among end-Triassic European bivalves. *Geology*, **23**, 102–104.

McRoberts, C.A., Krystyn, L. & Hautmann, M. 2012. Macrofaunal response to the end-Triassic mass extinction in the west-Tethyan Kössen Basin, Austria. *Palaios*, **27**, 607–616, https://doi.org/10.2110/palo.2012.p12-043r.

Meister, C., Aberhan, M., et al. 2004. The Global Boundary Stratotype Section and Point (GSSP) for the base of the Pliensbachian Stage (Lower Jurassic), Wine Haven , Yorkshire , UK. *Episodes*, **29**, 93–106.

Metcalfe, B., Twitchett, R.J. & Price-Lloyd, N. 2011. Changes in size and growth rate of 'Lilliput' animals in the earliest Triassic. *Palaeogeography, Palaeoclimatology, Palaeoecology*, **308**, 171–180, https://doi.org/10.1016/j.palaeo.2010.09.011.

Meyer, K.M., Kump, L.R. & Ridgwell, A. 2008. Biogeochemical controls on photic-zone euxinia during the end-Permian mass extinction. *Geology*, **36**, 747–750, https://doi.org/10.1130/G24618A.1.

Meyer, K.M., Yu, M., Jost, A.B., Kelley, B.M. & Payne, J.L. 2011. $\delta^{13}C$ evidence that high primary productivity delayed recovery from end-Permian mass extinction. *Earth and Planetary Science Letters*, **302**, 378–384, https://doi.org/10.1016/j.epsl.2010.12.033.

Morante, R. & Hallam, A. 1996. Organic carbon isotopic record across the Triassic–Jurassic boundary in Austria and its bearing on the cause of the mass extinction. *Geology*, **24**, 391–394.

Mousseau, T.A. 1997. Ectotherms follow the converse to Bergmann's Rule. *Evolution*, **51**, 630–632, https://doi.org/10.2307/2411138.

Nori, L. & Lathuiliére, B. 2003. Form and environment of Gryphaea arcuata. *Lethaia*, **36**, 83–96, https://doi.org/10.1080/00241160310003081.

Oates, M.J. 1976. *The Lower Lias of Western Scotland*. Unpublished Ph.D thesis, University of London, London.

Olsen, P.E., Shubin, N.H. & Anders, M.H. 1987. New Early Jurassic tetrapod assemblage constrain Triassic-Jurassic tetrapod extinction event. *Science*, **237**, 1025–1029, https://doi.org/10.1126/science.3616622.

Olsen, P.E., Kent, D. V, Sues, H., Koeberl, C. & Huber, H. 2002. Ascent of dinosaurs linked to an iridium anomaly at the Triassic-Jurassic boundary. *Science*, **296**, 1305–1307.

Page, K.N. 2003. The Lower Jurassic of Europe: its subdivision and correlation. *Geological Survey of Denmark and Greenland Bulletin*, **1**, 23–59.

Pálfy, J. 2003. Volcanism of the Central Atlantic Magmatic Province as a potential driving force in the end-Triassic mass extinction. *The Central Atlantic Magmatic Province: Insights from Fragments of Pangea, Geophysical Monograph **136***, 255–267.

Pálfy, J., Hass, D.A., Hetényi, M., Orchard, M. & Veto, I. 2001. Carbon isotope anomaly and other geochemical changes at the Triassic-Jurassic boundary from a marine section in Hungary. *Geology*, **29**, 1047–1050.

Pálfy, J., Demény, A., et al. 2007. Triassic – Jurassic boundary events inferred from integrated stratigraphy of the Csővár section, Hungary. *Palaeogeography, Palaeoclimatology, Palaeoecology*, **244**, 11–33, https://doi.org/10.1016/j.palaeo.2006.06.021.

Partridge, L. & Coyne, J.A. 1997. Bergmann's Rule in ectotherms: is it adaptive? *Evolution*, **51**, 632–635, https://doi.org/10.2307/2411139.

Payne, J.L. 2005. Evolutionary dynamics of gastropod size across the end-Permian extinction and through the Triassic recovery interval. *Paleobiology*, **31**, 269–290.

Payne, J.L., Summers, M., Rego, B.L., Altiner, D., Wei, J., Yu, M. & Lehrmann, D.J. 2011. Early and Middle Triassic trends in diversity, evenness, and size of foraminifers on a carbonate platform in south China: implications for tempo and mode of biotic recovery from the end-Permian mass extinction. *Paleobiology*, **37**, 409–425.

Peryt, D., Alegret, L. & Molina, E. 2002. The Cretaceous/Palaeogene (K/P) boundary at Aïn Settara, Tunisia: restructuring of benthic foraminiferal assemblages. *Terra Nova*, **14**, 101–107.

Powell, J.H. 1984. Lithostratigraphical nomenclature of the Lias Group in the Yorkshire Basin. *Proceedings of the Yorkshire Geological Society*, **45**, 51–57.

Pugh, A.C., Danise, S., Brown, J.R. & Twitchett, R.J. 2014. Benthic ecosystem dynamics following the Late Triassic mass extinction event : Palaeoecology of the Blue Lias Formation, Lyme Regis, UK. *Proceedings of the Ussher Society*, **13**, 255–266.

Rhoads, D.C. & Morse, J.W. 1971. Evolutionary and ecologic significance of oxygen-deficient marine basins. *Lethaia*, **4**, 413–428.

Richardson, L. 1911. The Rhaetic and contiguous deposits of west, mid part of east Somerset. *Proceedings of the Geologists' Association, London*, **67**, 1–74.

Richmond, C., Marcus, N.H., Sedlacek, C., Miller, G.A. & Oppert, C. 2006. Hypoxia and seasonal temperature: Short-term effects and long-term implications for Acartia tonsa dana. *Journal of Experimental Marine Biology and Ecology*, **328**, 177–196, https://doi.org/10.1016/j.jembe.2005.07.004.

Richoz, S., van de Schootbrugge, B., et al. 2012. Hydrogen sulphide poisoning of shallow seas following the end-Triassic extinction. *Nature Geoscience*, **5**, 662–667, https://doi.org/10.1038/ngeo1539.

Ritterbush, K.A., Ibarra, Y., et al. 2015. Marine ecological state-shifts folloing the Triassic-Jurassic mass extinction. *In*: Polly, D., Head, J. J. & Fox, D. L. (eds) *Earth-Life Transitions: Paleobiology in the Context of Earth System Evolution*. The Paleontological Society, 121–136.

Rodland, D.L. & Bottjer, D.J. 2001. Biotic recovery from the end-Permian mass extinction: behavior of the inarticulate brachiopod Lingula as a disaster taxon. *SEPM Society for Sedimentary Geology*, **16**, 95–101.

Roy, K. & Martien, K.K. 2001. Latitudinal distribution of body size in north-eastern Pacific marine bivalves. *Journal of Biogeography*, **28**, 485–493, https://doi.org/10.1046/j.1365-2699.2001.00561.x.

Ruhl, M., Kürschner, W.M. & Krystyn, L. 2009. Triassic-Jurassic organic carbon isotope stratigraphy of key sections in the western Tethys realm (Austria). *Earth and Planetary Science Letters*, **281**, 169–187, https://doi.org/10.1016/j.epsl.2009.02.020.

Ruhl, M., Deenen, M.H.L., Abels, H.A., Bonis, N.R., Krijgsman, W. & Kürschner, W.M. 2010. Astronomical constraints on the duration of the Early Jurassic Hettangian stage and recovery rates following the end-Triassic mass extinction (St Audrie's Bay / East Quantoxhead, UK). *Earth and Planetary Science Letters*, **295**, 262–276, https://doi.org/10.1016/j.epsl.2010.04.008.

Ruhl, M., Hesselbo, S.P., et al. 2016. Astronomical constraints on the duration of the Early Jurassic Pliensbachian Stage and global climatic fluctuations. *Earth and Planetary Science Letters*, **455**, 149–165, https://doi.org/10.1016/j.epsl.2016.08.038.

Schaltegger, U., Guex, J., Bartolini, A., Schoene, B. & Ovtcharova, M. 2008.

Precise U–Pb age constraints for end-Triassic mass extinction, its correlation to volcanism and Hettangian post-extinction recovery. *Earth and Planetary Science Letters*, **267**, 266–275, https://doi.org/10.1016/j.epsl.2007.11.031.

Schmidt, A., Skeffington, R.A., et al. 2015. Selective environmental stress from sulphur emitted by continental flood basalt eruptions. *Nature Geoscience*, 1–8, https://doi.org/10.1038/NGEO2588.

Schmidt, D.N., Thierstein, H.R. & Bollmann, J. 2004. The evolutionary history of size variation of planktic foraminiferal assemblages in the Cenozoic. *Palaeogeography, Palaeoclimatology, Palaeoecology*, **212**, 159–180, https://doi.org/http://dx.doi.org/10.1016/j.palaeo.2004.06.002.

Schubert, J.K. & Bottjer, D.J. 1995. Aftermath of the Permian-Triassic mass extinction event: Paleoecology of Lower Triassic carbonates in the western USA. *Palaeogeography, Palaeoclimatology, Palaeoecology*, **116**, 1–39.

Sessa, J.A., Patzkowsky, M.E. & Bralower, T.J. 2009. The impact of lithification on the diversity, size distribution, and recovery dynamics of marine invertebrate assemblages. *Geology*, **37**, 115–118, https://doi.org/10.1130/G25286A.1.

Sheppard, T.H. 2002. Stylolite development at sites of primary and diagenetic fabric contrast within the Sutton Stone (Lower Lias), Ogmore-by-Sea, Glamorgan, UK. *Proceedings of the Geologists' Association*, **113**, 97–109, https://doi.org/10.1016/S0016-7878(02)80013-X.

Simms, M.J. 2003. Uniquely extensive seismite from the latest Triassic of the United Kingdom: Evidence for bolide impact ? *Geology*, **31**, 557–560.

Simms, M.J. 2007. Uniquely extensive soft-sediment deformation in the Rhaetian of the UK: Evidence for earthquake or impact. *Palaeogeography, Palaeoclimatology, Palaeoecology*, **244**, 407–423.

Simms, M.J., Chidlaw, N., Morton, N. & Page, K.N. 2004. *British Lower Jurassic Stratigraphy*. Peterborough, Geological Conservation Review Series, No. 30, Joint Nature Conservation Committee.

Simms, M.J. & Jeram, A. 2007. Waterloo Bay, Larne, Northern Ireland: a candidate Global Stratotype Section and Point for the base of the Hettangian Stage and Jurassic System. *ISJS Newsletter*, **34**, 50–68.

Sogot, C.E., Harper, E.M. & Taylor, P.D. 2014. The Lilliput Effect in colonial organisms: Cheilostome bryozoans at the Cretaceous-Paleogene mass extinction. *PLoS ONE*, **9**, e87048.

Song, H., Tong, J. & Chen, Z.-Q. 2011. Evolutionary dynamics of the Permian – Triassic foraminifer size : evidence for Lilliput Effect in the end-Permian mass extinction and its aftermath. *Palaeogeography, Palaeoclimatology, Palaeoecology*, **308**, 98–110, https://doi.org/10.1016/j.palaeo.2010.10.036.

Song, H., Tong, J., et al. 2016. Early Triassic disaster and opportunistic foraminifers in South China. *Geol. Mag.*, **153**, 298–315, https://doi.org/10.1017/S0016756815000497.

Song, H., Wignall, P.B. & Dunhill, A.M. 2018. Decoupled taxonomic and ecological recoveries from the Permo-Triassic extinction. *Science Advances*, **4**, 1–7, https://doi.org/10.1126/sciadv.aat5091.

Stanley, G.D. 1988. The history of early Mesozoic reef communities: a three-step process. *SEPM Society for Sedimentary Geology*, **3**, 170–183.

Steinthorsdottir, M., Jeram, A.J. & McElwain, J.C. 2011. Extremely elevated CO_2 concentrations at the Triassic/Jurassic boundary. *Palaeogeography, Palaeoclimatology, Palaeoecology*, **308**, 418–432, https://doi.org/10.1016/j.palaeo.2011.05.050.

Steinthorsdottir, M., Elliot-Kingston, C. & Bacon, K.L. 2018. Cuticle surfaces of fossil plants as a potential proxy for volcanic SO_2 emissions: observations from the Triassic–Jurassic transition of East Greenland. *Palaeobiodiversity and Palaeoenvironments*, **98**, 49–69, https://doi.org/10.1007/s12549-017-0297-9.

Stubbs, T.L. & Benton, M.J. 2016. Ecomorphological diversifications of Mesozoic marine reptiles: the roles of ecological opportunity and extinction. *Paleobiology*, **42**, 547–573, https://doi.org/10.1017/pab.2016.15.

Sun, Y., Joachimski, M.M., et al. 2012. Lethally Hot Temperatures During the Early Triassic Greenhouse. *Science*, **338**, 366–370.

Svensen, H., Planke, S., Chevallier, L., Malthe-Sørenssen, A., Corfu, F. & Jamtveit, B. 2007. Hydrothermal venting of greenhouse gasses triggering Early Jurassic global warming. *Earth and Planetary Science Letters*, **256**, 554–566.

Swift, A. 1989. First records of conodonts from the Late Triassic of Britain. *Palaeontology*, **32**, 325–333.

Swift, A. 1999. Conodonts. *In*: Swift, A. & Martill, D. M. (eds) *Fossils of the Rhaetian Penarth Group*. London, The Palaeontological Association, 183–190.

Tawney, E.B. 1865. On the western limit of the Rhaetic beds in South Wales and on the position of the Sutton Stone. *Quarterly journal of the Geological Society of London*, **22**, 68–93.

Thorne, P.M., Ruta, M. & Benton, M.J. 2011. Resetting the evolution of marine reptiles at the Triassic-Jurassic boundary. *PNAS*, **108**, 8339–8344, https://doi.org/10.1073/pnas.1018959108.

Tomašových, A. & Siblík, M. 2007. Evaluating compositional turnover of brachiopod communities during the end-Triassic mass extinction (Northern Calcareous Alps): Removal of dominant groups, recovery and community reassembly. *Palaeogeography, Palaeoclimatology, Palaeoecology*, **244**, 170–200, https://doi.org/10.1016/j.palaeo.2006.06.028.

Tong, J., Zhang, S., Zuo, J. & Xiong, X. 2007. Events during Early Triassic recovery from the end-Permian extinction. *Global and Planetary Change*, **55**, 66–80.

Trueman, A.E. 1922. The Liassic rocks of Glamorgan. *Proceedings of the Geologists' Association*, **33**, 245–284, https://doi.org/10.1016/S0016-7878(22)80027-4.

Twitchett, R.J. 1999. Palaeoenvironments and faunal recovery after the end-Permian mass extinction. *Palaeogeography, Palaeoclimatology, Palaeoecology*, **154**, 27–37.

Twitchett, R.J. 2007. The Lilliput Effect in the aftermath of the end-Permian

extinction event. *Palaeogeography, Palaeoclimatology, Palaeoecology*, **252**, 132–144, https://doi.org/10.1016/j.palaeo.2006.11.038.

Twitchett, R.J. & Barras, C.G. 2004. Trace fossils in the aftermath of mass extinction events. *Geological Society, London, Special Publications*, **228**, 397–418, https://doi.org/10.1144/gsl.sp.2004.228.01.18.

Twitchett, R.J., Krystyn, L., Baud, A., Wheeley, J.R. & Richoz, S. 2004. Rapid marine recovery after the end-Permian mass-extinction event in the absence of marine anoxia. *Geology*, **32**, 805–808, https://doi.org/10.1130/G20585.1.

Urbanek, A. 1993. Biotic crises in the history of Upper Silurian graptoloids: A Palaeobiological model. *Historical Biology*, **7**, 29–50, https://doi.org/10.1080/10292389309380442.

van de Schootbrugge, B., Quan, T.M., et al. 2009. Floral changes across the Triassic/Jurassic boundary linked to flood basalt volcanism. *Nature Geoscience*, **2**, 589–594, https://doi.org/10.1038/ngeo577.

van de Schootbrugge, B., Bachan, A., Suan, G., Richoz, S. & Payne, J.L. 2013. Microbes, mud and methane: cause and consquence of recurrent Early Jurassic anoxia following the end-Triassic mass extinction. *Palaeontology*, **56**, 685–709, https://doi.org/10.1111/pala.12034.

van Der Have, T.M. & De Jong, G. 1996. Adult size in ectotherms: Temperature effects in growth and differentiation. *Journal of Theoretical Biology*, **183**, 3329–3340.

van Voorhies, W.A. 1996. Bergmann size clines: A simple explanation for their occurrence in ectotherms. *Evolution*, **50**, 1259–1264, https://doi.org/10.2307/2410666.

von Elert, E., Martin-creuzburg, D. & Le Coz, J.R. 2003. Absence of sterols constrains carbon transfer between cyanobacteria and a freshwater herbivore (Daphnia galeata). *Proceedings of the Royal Society of London B*, **270**, 1209–1214, https://doi.org/10.1098/rspb.2003.2357.

Wacker, A. & von Elert, E. 2003. Food quality controls reproduction of the zebra mussel (Dreissena polymorpha). *Ecophysiology*, **135**, 332–338, https://doi.org/10.1007/s00442-003-1208-5.

Wacker, A. & von Elert, E. 2008. Body size and food thresholds for zero growth in Dressena polymorpha: a mechanism underlying intraspecific competition. *Freshwater Biology*, **53**, 2356–2363.

Walne, P.R. 1972. The influence of current speed, body size and water temperature on the filtration rate of five species of bivalves. *Journal of the Marine Biological Association of the United Kingdom*, **52**, 345–374, https://doi.org/doi:10.1017/S0025315400018737.

Ward, P.D., Haggart, J.W., Carter, E.S., Wilbur, D., Tipper, H.W. & Evans, T. 2001. Sudden productivity collapse associated with the Triassic-Jurassic boundary mass extinction. *Science*, **292**, 1148–1152.

Warrington, G., Audley-Charles, M.G., et al. 1980. *A Correlation of Triassic Rocks in the British Isles*. Geological Scoiety of London Special Report, No. 13.

Waters, R.A. & Lawrence, D.J.D. 1987. *Geology of the South Wales Coalfield,*

Part III, the Country around Cardiff. London, Memoirs of the Geological Survey, England and Wales. HMSO.

Weedon, G.P., Jenkyns, H.C. & Page, K.N. 2018. Combined sea-level and climate controls on limestone formation, hiatuses and ammonite preservation in the Blue Lias Formation, South Britain (uppermost Triassic–Lower Jurassic). *Geolgical Magazine*, **155**, 1117–1149, https://doi.org/10.1017/S001675681600128X.

Weedon, G.P., Page, K.N. & Jenkyns, H.C. 2019. Cyclostratigraphy, stratigraphic gaps and the duration of the Hettangian Stage (Jurassic): insights from the Blue Lias Formation of southern Britain. *Geological Magazine*, **156**, 1469–1509, https://doi.org/10.1017/S0016756818000808.

Weiss, M.B., Curran, P.B., Peterson, B.J. & Gobler, C.J. 2007. The influence of plankton composition and water quality on hard clam (Mercenaria mercenaria) populations across Long Island's south shore lagoon estuaries (New York, USA). *Journal of Experimental Marine Biology and Ecology*, **345**, 12–25.

Whiteside, J.H., Olsen, P.E., Kent, D. V, Fowell, S.J. & Et-touhami, M. 2007. Synchrony between the Central Atlantic magmatic province and the Triassic – Jurassic mass-extinction event ? *Palaeogeography, Palaeoclimatology, Palaeoecology*, **244**, 345–367, https://doi.org/10.1016/j.palaeo.2006.06.035.

Whittle, R.J., Witts, J.D., Bowman, V.C., Crame, J.A., Francis, J.E. & Ineson, J. 2019. Nature and timing of biotic recovery in Antarctic benthic marine ecosystems following the Cretaceous-Palaeogene mass extinction. *Palaeontology*, https://doi.org/10.1111/pala.12434.

Wiest, L.A., Lukens, W.E., Peppe, D.J., Driese, S.G. & Tubbs, J. 2018. Terrestrial evidence for the Lilliput Effect across the Cretaceous-Paleogene (K-Pg) boundary. *Palaeogeography, Palaeoclimatology, Palaeoecology*, **491**, 161–169, https://doi.org/10.1016/j.palaeo.2017.12.005.

Wignall, P.B. 2001a. Large igneous provinces and mass extinctions. *Earth-Science Reviews*, **53**, 1–33, https://doi.org/10.1016/S0012-8252(00)00037-4.

Wignall, P.B. 2001b. Sedimentology of the Triassic-Jurassic boundary beds in Pinhay Bay (Devon, SW England). *Proceedings of the Geologists' Association*, **112**, 349–360, https://doi.org/10.1016/S0016-7878(01)80014-6.

Wignall, P.B. & Bond, D.P.G. 2008. The end-Triassic and Early Jurassic mass extinction records in the British Isles. *Proceedings of the Geologists' Association*, **119**, 73–84, https://doi.org/10.1016/S0016-7878(08)80259-3.

Wignall, P.B. & Hallam, A. 1991. Biofacies, stratigraphic distribution and depositional models of British onshore Jurassic black shales. *Geoogical Society Special Publications*, **58**, 291–309.

Wignall, P.B. & Hallam, A. 1992. Anoxia as a cause of the Permian/Triassic mass extinciton: facies evidence from northern Italy and the western United States. *Palaeogeography, Palaeoclimatology, Palaeoecology*, **93**, 21–46.

Wignall, P.B., Zonneveld, J.-P., Newton, R.J., Amor, K., Sephton, M.A. & Hartley, S. 2007. The end Triassic mass extinction record of Williston Lake,

British Columbia. *Palaeogeography, Palaeoclimatology, Palaeoecology*, **253**, 385–406, https://doi.org/10.1016/j.palaeo.2007.06.020.

Wignall, P.B., Bond, D.P.G., Sun, Y., Grasby, S.E., Beauchamp, B., Joachimski, M.M. & Blomeier, Dierk, P.G. 2016. Ultra-shallow-marine anoxia in an Early Triassic shallow-marine clastic ramp (Spitsbergen) and the suppression of benthic radiation. *Geol. Mag.*, **153**, 316–331, https://doi.org/10.1017/S0016756815000588.

Williford, K.H., Ward, P.D., Garrison, G.H. & Buick, R. 2007. An extended organic carbon-isotope record across the Triassic-Jurassic boundary in the Queen Charlotte Islands, British Columbia, Canada. *Palaeogeography, Palaeoclimatology, Palaeoecology*, **244**, 290–296, https://doi.org/10.1016/j.palaeo.2006.06.032.

Wilson, M. 1997. Thermal evolution of the Central Atlantic passive margins: continental break-up above a Mesozoic super-plume. *Journal of the Geological Society, London*, **154**, 491–495.

Wood, R. 1999. *Reef Evolution*. New York, Oxford University Press.

Woods, A., Bottjer, D.J., Mutti, M. & Morrison, J. 1999. Lower Triassic large sea-floor carbonate cements: Their origin and a mechanism for the prolonged biotic recovery from the end-Permian mass extinction. *Geology*, **27**, 645–648.

Wotzlaw, J., Guex, J., et al. 2014. Towards accurate numerical calibration of the Late Triassic: High-precision U-Pb geochronology constraints on the duration of the Rhaetian. *Geology*, **42**, 571-574, https://doi.org/10.1130/G35612.1.

Zhang, L., Zhao, L., Chen, Z.-Q., Algeo, T.J., Li, Y. & Cao, L. 2015. Amelioration of marine environments at the Smithian–Spathian boundary, Early Triassic. *Biogeosciences*, **12**, 1597–1613, https://doi.org/10.5194/bg-12-1597-2015.

Zonneveld, J., Beatty, T.W. & Pemberton, S.G. 2007. Lingulide brachiopods and the trace fossil Lingulichnus from the Triassic of western Canada: Implications for faunal recovery after the end-Permian mass extinction. *Palaios*, **22**, 74–97, https://doi.org/10.2110/palo.2005.p05-103r.

Chapter 2: Body size changes in bivalves of the family Limidae in the aftermath of the end-Triassic mass extinction: the Brobdingnag Effect

Published in Palaeontology

Atkinson, J.W., Wignall, P.B., Morton, J.D. & Aze, T. 2019. Body size changes in bivalves of the family Limidae in the aftermath of the end-Triassic mass extinction: the Brobdingnag Effect. *Palaeontology*, **62**, 561-582, https://doi.org/10.1111/pala.12415.

N.B. Following the acceptance of this manuscript for publication the duration of the Hettangian was reassessed as such Chapter 2 utilises the shorter Hettangian duration, whereas all subsequent chapters use the most recent longer duration. For updated figures, comparable to all subsequent ones see Appendix A.

Body size changes in bivalves of the family Limidae in the aftermath of the end-Triassic mass extinction: the Brobdingnag Effect

Jed W. Atkinson[1], Paul B. Wignall[1], Jacob D. Morton[2], and Tracy Aze[1]

[1]School of Earth and Environment, University of Leeds, Leeds, LS2 9JT, UK: gy12jwa@leeds.ac.uk

[2] School of Earth Sciences, University of Bristol, Bristol, BS8 1RJ, UK

2.1 Abstract

Reduced body size of organisms following mass extinctions are well-known and often ascribed to the Lilliput Effect. This phenomenon is expressed as a temporary body size reduction within surviving species. Despite its wide usage the term is often loosely applied to any small post-extinction taxa. Here the size of bivalves of the family Limidae (Rafineque) prior to – and in the aftermath of – the end-Triassic mass extinction event are assessed. Of the species studied only one occurs prior to the extinction event, though is too scarce to test for the Lilliput Effect. Instead, newly evolved species originate at small body sizes and undergo a within-species size increase, most dramatically demonstrated by *Plagiostoma giganteum* Sowerby which, over two million years, increases in size by 179%. This trend is seen in both field and museum collections. We term this within-species size increase of newly originated species in the aftermath of mass extinction, the Brobdingnag Effect, after the giants that were contemporary with the Lilliputians in Swift's *Gulliver's Travels*. The size increase results from greater

longevity and faster growth rates. The cause of the effect is unclear, although likely relates to improved environmental conditions. Oxygen-poor conditions in the Early Jurassic are associated with populations of smaller body size caused by elevated juvenile mortality but these are local/regional effects that do not alter the long-term, size increase. Although temperature-size relationships exist for many organisms (Temperature-Size Rule and Bergmann's Rule), the importance of this is unclear here because of a poorly known Early Jurassic temperature record.

Key words: Body size, End-Triassic mass extinction, Lilliput Effect, Early Jurassic, Brobdingnag Effect.

2.2 Introduction

Intervals of biotic recovery, following mass extinctions, are important for the evolution of life, as new species adapt and evolve to refill ecological vacancies. Several models for biotic recovery have been proposed. Kauffmann and Erwin (1995) simply divided post extinction times into two phases: the survival interval and the recovery interval. This was later expanded by Twitchett (2006) into a four-phase process that is defined by changes in ecological tiering, species richness, evenness, bioturbation and – of relevance to this study – body size. This last factor was initially highlighted by Urbanek (1993) who documented the effects of biotic crises on the size of graptolites. He found that surviving species (those that crossed the extinction event) exhibited a reduced body size during the initial recovery phase, and later increased in size to return to "normal" pre-event body sizes; a phenomenon he termed the Lilliput Effect. Urbanek's original definition was applied at the species level, however subsequent workers

have loosely applied this term to a range of higher taxonomic ranks (Harries and Knorr 2009; McGowan *et al.* 2009; Huang *et al.* 2010; Sogot *et al.* 2014; Chu *et al.* 2015).

The Hettangian and Sinemurian (Early Jurassic) intervals record the recovery from the end-Triassic mass extinction (Hallam 1960, 1996; Mander *et al.* 2008; Pugh *et al.* 2014). Based on ecological tiering and trace fossil diversity, biotic recovery was considered to have been completed by the *angulata* ammonite zone, approximately 1.1 million years (Myr) after the extinction (Twitchett & Barras 2004; Barras & Twitchett 2007; Ruhl *et al.* 2010; Pugh *et al.* 2014). Hallam (1960) recorded an increase in the maximum dimensions of six bivalve species during the Hettangian and lower Sinemurian and similar trends have been noted for other bivalves and other groups at this time (Hallam 1975; 1978; 1998; Johnson 1994; Dommergues *et al*. 2002; Barras & Twitchett 2007). However, this is not an example of the size increase seen in Lilliput faunas returning to pre-event sizes because the species concerned were not present before the extinction event, but instead originated as small-bodied animals during the recovery. A major issue with many studies on body size changes has been a lack of species level data, with most work usually conducted at the generic level (Hallam 1975; Dommergues *et al.* 2002; Hautmann 2004) or on whole fossil assemblages regardless of their taxonomy (e.g. Mander *et al.* 2008). Such data provide little information on the mechanisms of size change and fails to distinguish intra-species size increase from manifestations of Cope's Rule where evolutionary size increase occurs in a lineage (Cope 1887; Rensch 1948; Alroy 1998). An increase of average body size of a population can also record improving environments and decrease of juvenile mortality within a species or a record of changes in taxonomic composition as environments ameliorated.

Body size is a key factor in organisms because it influences ecology, physiology and evolution (e.g. Jablonski 1996). Understanding the nature and causes of body size change may reveal how animals are likely to respond to future stresses. This study aims to investigate the reported body size changes in bivalves of the British Isles during the latest Rhaetian, Hettangian and Sinemurian by considering five species of epibyssate bivalve of the family Limidae (Rafinesque): *Plagiostoma giganteum* Sowerby, *Plagiostoma punctatum* Sowerby, *Antiquilima succincta* (Schlotheim), (Terquem), *Pseudolimea pectinoides* (Sowerby) and *Ctenostreon philocles* (d'Orbigny), with each dealt with independently to ensure taxonomic consistency. The driving mechanisms for body size change and their significance for recovery from mass extinction are discussed.

2.3 Geological setting

The upper Rhaetian of Britain consists of the Penarth Group (and its constituent Westbury and Lilstock formations). The Westbury Formation is dominated by dark mudstone beds with thin, rippled sandy horizons and densely packed shell beds (Gallois 2007). The succeeding Lilstock Formation consists of the Cotham and Langport members. The Cotham Member is generally 2-4 m thick and formed of mudstone, siltstone and rippled, fine sandstone beds that often show an intensely deformed bed up to 2 m thick (Simms 2003). This is dissected by deep fissures, often interpreted as desiccation cracks that can attain depths of up to 1 m (Waters & Lawrence 1987). The end-Triassic mass extinction horizon occurred near the base of this unit and was followed by the 'initial'

negative carbon isotope excursion just above the crack level (Wignall & Bond 2008 and references therein).

The Langport Member exhibits the greatest lateral variation of the Rhaetian strata. In Pinhay Bay, Devon, the unit consists of micritic mudstone, giving a striking white appearance in the cliffs (hence the unit has also been known as the White Lias (Smith 1797)) and is capped by an exposure surface known as the Sun Beds (Richardson 1911). In places this bed has been cut-out and replaced by an impersistent, intraformational conglomerate (Wignall 2001). In Somerset the Langport Member, which is much thinner than along the Devonshire coast, lacks a conglomerate, instead a shaley unit termed the 'Watchet Beds' is developed in the upper part (Richardson 1911; Gallois 2009). On the Glamorgan coastline this Member is again a micritic mudstone, whilst in County Antrim this unit is characterised by shales with thin, occasionally hummocky, sandstones.

For much of the Penarth Group deposition occurred within a shallow epicontinental sea with variable connectivity to the Tethys in the south (Swift 1999). Abnormal salinity is suggested by the lack of stenohaline taxa such as ammonoids and brachiopods throughout much of the group (Hallam & El Shaarawy 1982). The presence of the ostracod *Darwinula* and the conchostracan *Euestheria* within the Cotham Member suggests brackish waters (Boomer *et al.* 1999; Morton *et al.* 2017). However, normal marine taxa such as echinoids and the ostracods *Ogmoconchella* and *Eucytherura* are present in the succeeding Langport Member (Boomer *et al*. 1999; Swift 1999).

Across southwest England and Wales the Penarth Group is overlain by the Blue Lias Formation, the base of which is marked by a black shale termed the 'Paper Shale' (Richardson 1911). The Formation consists of a rhythmic

sequence of alternating limestones, marls, mudstones and dark shales thought to reflect seafloor oxygen fluctuations that were likely orbitally controlled (Weedon 1986; Bottrell & Raiswell 1989; Moghadam & Paul 2000; Wignall 2001; Clémence *et al.* 2010; Ruhl *et al.* 2010). In the Larne Basin typical offshore Blue Lias-type facies were not developed, instead the Lilstock Formation was followed by the Waterloo Mudstone Formation: a succession of pale mudstones and thin silty beds, with thin limestone beds from the upper *planorbis* Zone onwards (Simms & Jeram 2007). Also, within the Cleveland Basin the Hettangian and basal Sinemurian are represented by the Calcareous Shale Member of the Redcar Mudstone Formation, this consists of interbedded mudstones and shales with limestone beds rich in the oyster *Gryphaea* (Powell 2010). The lower Sinemurian of the East Midlands Shelf is represented by the Frodingham Ironstone Member of the Scunthorpe Mudstone Formation, the sequence here is much condensed and formed of ferruginous sandstones with chamosite ooids (Simms & Page 2004). Returning to the southwest, the Blue Lias Formation is followed by the Charmouth Mudstone Formation, which in its lower part consists of the Shales-with-Beef and basal-most Black Ven Marls. These are distinct from the underlying Blue Lias Formation because of the greater dominance of mudstones and organic-rich shales (Gallois 2008). The Blue Lias and Charmouth Mudstone formations were deposited under fully marine conditions, with the Blue Lias representing an interval of transgression, during which the deepest waters were attained during the lowermost Sinemurian (*bucklandi* Zone) (Hallam 1981; Sheppard 2006; Sheppard *et al.* 2006). Localities on the Glamorgan coast were deposited much closer to a palaeo-shoreline than those across the Bristol Channel on the Somerset coast (Wobber 1965; Johnson & McKerrow 1995).

Despite local variations, correlation between sections is afforded by a well-constrained ammonite biostratigraphy (Bloos & Page 2002; Page 2002) except for the lowermost, ammonite-free Blue Lias. This level is known as the Pre-*planorbis* Beds, and is thought to be equivalent to the basal Jurassic *tilmanni* Zone (Page 2010). This is followed by the *planorbis, liasicus* and *angulata* zones of the Hettangian Stage and the *bucklandi, semicostatum* and *turneri* zones of the lowermost Sinemurian Stage.

2.4 Materials and methods

2.4.1 Species studied

The genus *Plagiostoma* has an obliquely ovate shell with length exceeding the height and is of a moderate to strong inflation. Umbones are placed posterior to the middle line and an anterior umbonal ridge is well-defined. The ligament pit is broad and the lunule excavated. The genus is edentulous or bears up to two broad, longitudinal teeth (Cox *et al.* 1969). Of the two species studied here, *Plagiostoma punctatum* is distinguished from *Plagiostoma giganteum* by the presence of approximately 100 fine radial ribs across the body of the shell and on the posterior auricle (Aberhan 1994). On abraded specimens the intersection between radial ribs and commarginal striae are rendered as punctae in the interspaces (Hodges 1987). *P. giganteum* features radial striae confined to the anterior and posterior regions of the shell, although they can be weakly developed on the centre of the valve in some specimens. Both species show a broad, flat antero-dorsal margin suggesting an epibyssate life mode and the frequent encrustation by epibionts, especially of larger specimens, further suggests an epifaunal life site.

Pseudolimea pectinoides bears an equivalved, subovate to orbicular, slightly oblique shell. The beaks are positioned centrally and are salient above the hinge line with small auricles (Cox *et al.* 1969).The shell is ornamented by 15-20 obtuse, striated, sharp radial ribs; these may appear rounded in cross section on abraded specimens. Interspace ribs are variable in nature and can appear as sharp crests or thin rounded threads; these secondary ribs extend over the auricles (Hodges 1987; Aberhan 1994). Cox (1944) remarked how *Pseudolimea hettangiensis* was often confused with *P. pectinoides*. Further to this Cox (1944) synonymized *P. hettangiensis* and *Pseudolimea eryx*, which in turn Peter Hodges (pers. comm. 2018) considers this to be a synonym of *P. pectinoides*.

Antiquilima succincta is obliquely subovate in outline, and only moderately inflated (Cox *et al.* 1969; Aberhan *et al.* 2011). The shell bears 30-56 primary ribs with numerous secondary ribs occupying the interspaces (Hodges 1987).

Ctenostreon philocles is distinguished by a thickened, suborbicular shell that may have a moderately irregular outline and is typically compressed. The auricles are large although the anterior auricle is usually the smaller. The surface of the shell is adorned by approximately ten rounded radial ribs that bear spines or tubercles and has broad interspaces (Hodges 1987).

2.4.2 Sampling

In order to document body size changes of the aforementioned bivalves across the end-Triassic extinction and throughout the Lower Lias, field collections were made from coastal locations in Somerset, Devon, Dorset, North Yorkshire, South Wales and County Antrim, a river cliff section in Gloucestershire, a quarry in North Lincolnshire and material retrieved from the Mochras borehole housed

in the British Geological Survey (BGS), Keyworth, Nottingham (Fig. 2.1). These sections represent a range of depositional settings within the epicontinental sea that covered much of the British Isles in the Early Jurassic (Table 2.1). Sample horizons were distributed at 1-2 m vertical intervals, where exposure permitted. Stratigraphic height of sampled horizons was determined using published sedimentary logs (e.g. Hesselbo and Jenkyns 1995; Bloos and Page 2002; Simms 2004*a*,*b*). If no sedimentary log of sufficient resolution was available, then the section was logged either from the foreshore directly or from the corresponding cliff section and dated using ammonites.

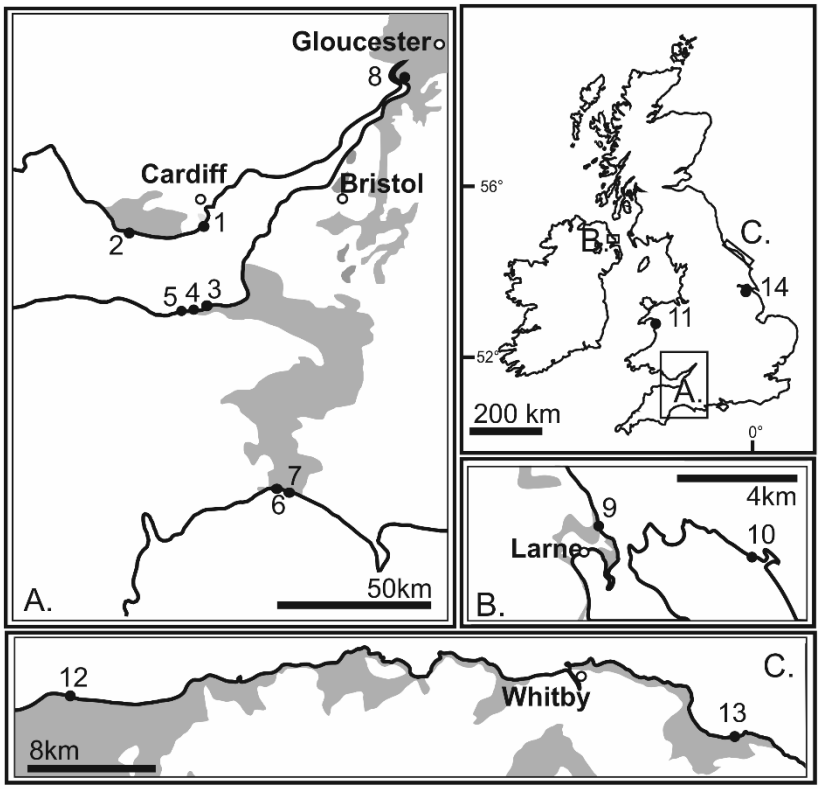

Fig. 2.1 Map depicting field locations (closed circles), see Table 2.1 for details, shaded regions depicting Rhaetian and Early Jurassic outcrops. Maps modified from Mander *et al.* (2008) and Powell (2010).

For mudstones, shales and marls, fossils were measured and collected from freshly split surfaces by use of hammer and chisel from approximately equal volumes of rock. For the harder limestone beds, which could not easily be split, fossils were measured *in situ* from upper bedding surfaces. Samples from Hock Cliff were collected from loose blocks at the foot of the river cliff, as the section spans only a single ammonite zone these could be ascribed to the *bucklandi* Zone (Simms & Chidlaw 2004). Where bedding was exposed in ledges on river banks sampling could be undertaken *in situ* following the above described methods.

Table 2.1 Details of field localities. Formation abbreviations: W = Westbury, BL = Blue Lias, L = Lilstock, CM = Charmouth Mudstone, WM = Waterloo Mudstone, RM = Redcar Mudstone, SM = Scunthorpe Mudstone.

Location	Grid ref.	Section type	Basin	Formations	Zones studied	Depositional setting (Exc. Penarth Grp)
1. Lavernock Point, Glamorgan	ST 188 682 – ST 183 679	Coastal	Bristol Channel	W-BL	Pre-*planorbis*-*liasicus*	Near basin margin becoming distal shelf
2. Nash Point, Glamorgan	SS 911 692 – SS 921 679	Coastal	Bristol Channel	BL	*angulata*-*bucklandi*	Distal shelf
3. Lilstock, Somerset	ST 178 453	Coastal	Bristol Channel	W-BL	Pre-*planorbis*-*liasicus*	Basinal, offshore, mud-dominated
4. East Quantoxhead, Somerset	ST 134 442 – ST 142 444	Coastal	Bristol Channel	BL	*angulata*-*bucklandi*	Basinal, offshore, mud-dominated
5. St Audrie's Bay, Somerset	ST 103 434 – ST 099 433	Coastal	Bristol Channel	W–BL	Pre-*planorbis*-*liasicus*	Basinal, offshore, mud-dominated
6. Pinhay Bay, Devon	SY 317 907 – SY 333 914	Coastal	Wessex	L–BL	Pre-*planorbis–bucklandi*	Mud-dominated middle shelf
7. Charmouth, Dorset	SY 352 929 – SY 370 929	Coastal	Wessex	CM	*semicostatum–turneri*	Basinal, mud-dominated
8. Hock Cliff, Gloucestershire	SO 725 093	River cliff	Severn	BL	*bucklandi*	Mud-dominated middle shelf
9. Waterloo Bay, Co. Antrim	NW 558 582	Coastal	Larne	W–WM	Pre-*planorbis planorbis*, *angulata*	Nearshore, silt-dominated
10. Portmuck Harbour, Co. Antrim	NW 558 582	Coastal	Larne	WM	*planorbis*	Nearshore, silt-dominated
11. Mochras, North Wales	SH 553 259	Drill core	Cardigan Bay	-	Pre-*planorbis–turneri*	Mud-dominated inner shelf
12. Redcar, North Yorkshire	NZ 613 253	Coastal	Cleveland	RM	*angulata–bucklandi*	Mud-dominated shelf
13. Robin Hood's Bay, North Yorkshire	NZ 971 028	Coastal	Cleveland	RM	*semicostatum–turneri*	Silt-dominated shelf
14. Conesby Quarry, North Lincolnshire	SE 889 145	Quarry	East Midlands Shelf	SM	*semicostatum*	Wave-dominated shelf

Body size data were bolstered by measurements from material previously collected housed in the School of Earth and Environment, University of Leeds, and additional specimens were donated by Michael Simms. Specimens housed in collections from the following Museums were also incorporated: National Museum of Wales, Cardiff (NMW); Warwickshire Museum, Warwick (WARMS); Bristol City Museum and Art Gallery, Bristol (BRSMG); Yorkshire Museum, York (YORYM); Whitby Museum, Whitby (WHITM); Bath Royal Literary and Scientific Institute, Bath (BRLSI).

For each specimen height (H) and length (L) of the valves were measured (Fig. 2.2) using a pair of digital callipers with a measurement error of +/-0.02 mm. These parameters were used to calculate geometric mean body size (GMBS): $GMBS = \sqrt{(\mathrm{H} \times \mathrm{L})}$. For incomplete specimens the missing value was calculated based on H:L ratios of coeval, complete specimens. GMBS was selected for size analysis over single linear measurements as it provides a better representation of a specimen's overall size, is easily obtained and correlates well with other, more complex, body size measurements (Kosnik *et al.* 2006).

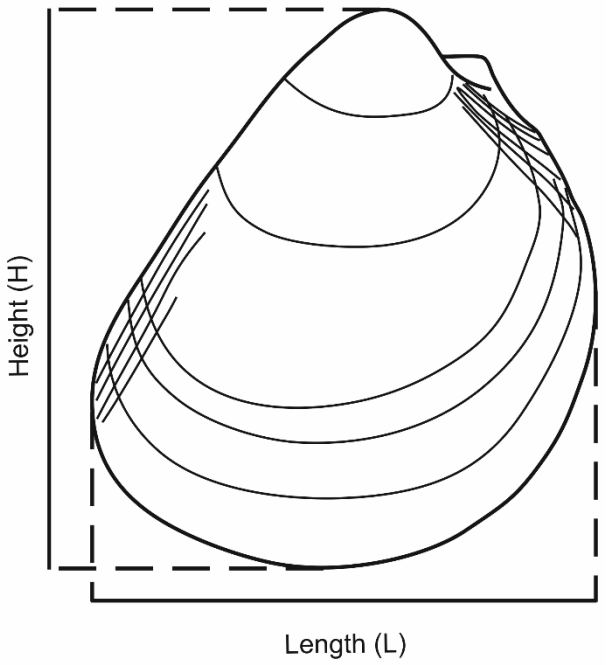

Fig. 2.2 Measurement schematic of a left valve in Limidae.

Size data were placed into time bins; ammonite zones were selected for this because they provide a high-resolution age model and allow museum specimens, with sufficient context, to be included with field observations. Durations of ammonite zones (including Pre-*planorbis* Beds) are from Ruhl *et al.* (2010). For the Rhaetian, which lacks ammonites, the Langport Member, Cotham Member and Westbury Formation are used as time bins, the durations of which are uncertain. Additionally, owing to small samples sizes, data from the *semicostatum* and *turneri* zones are here combined.

Size distribution histograms are produced for each time bin as well as mean GMBS along with error bars depicting a 95% confidence interval, allowing the population size ranges to be represented. Maximum body size is also shown. This is calculated as the mean of the largest 10% of the population in order to reduce the effects of abnormally large outliers (Johnson 1994). To test for

statistical significance of size changes between time bins a Kolmogorov-Smirnov test (K-S test) was performed, *p*-values are quoted with a 95% significance threshold ($p < 0.05$). These analyses were carried out using PAST 3.12 statistical software (Hammer *et al.* 2001). All other analyses were carried out using Microsoft Office Excel 2013.

To test for the effects of oxygen availability on body size, specimens were divided according to their host lithology. As the sedimentary rhythms in the Blue Lias Formation are thought to represent cycles in sea-floor oxygenation, the bioturbated limestones are considered the most oxic (this category also includes the Blue Lias marginal facies – the Sutton Stone), followed by pale marl/mudstone and dark, laminated mudstone in order of decreasing oxygen availability. Size variability between locations was also assessed.

2.4.3 Growth lines

In order to assess changes in growth rate, spacing of growth lines was measured from well-preserved specimens using a series of overlapping, high resolution images. When compiled these give a detailed transect from the umbo to the ventral margin of the valve. Two styles of plots were produced with these data, the first plots valve height against number of growth lines, the gradient of the resulting line is taken as an indication of growth rate, and allows for statistical comparison between populations. The second plots growth line separation (mm) against growth line number. In some specimens this reveals cycles in growth line density.

External growth lines were selected over more reliable internal growth increments (Lutz & Rhoads 1980) as all of the fossils within this study are formed

of recrystallized calcite or have been silicified and so lack original internal shell structures. This method is generally used in palaeontological studies (Craig & Hallam 1963; Wignall 1990; Morten & Twitchett 2009; Metcalfe *et al.* 2011) despite incurring potential errors introduced by abrasion, particularly around the umbones, and underestimation of growth lines at the clustered margins of older individuals and incorporation of disturbance lines (Craig & Hallam 1963).

2.5 Results

2.5.1 Body size

2.5.1.1 *Plagiostoma giganteum*

A total of 520 specimens (including 88 museum specimens) of *Plagiostoma giganteum* were recorded from within six time bins (Pre-*planorbis* Beds – *semicostatum-turneri* zones). Each of these size distribution histograms for *P. giganteum* bears a slight bimodality (Fig. 2.3), with the *angulata* and *bucklandi* zones showing a possible third peak. All show a slight skew towards larger individuals except for the *semicostatum-turneri* zones data that show a high proportion of small specimens (< 40 mm in size). *P. giganteum* showed an increase in mean and maximum GMBS from its first common occurrence in the *planorbis* Zone through until the *bucklandi* Zone (Fig. 2.4). From the *planorbis* to *liasicus* Zone mean GMBS increased by 15.6% (p = 0.02). The greatest relative size increase occurred between the *liasicus* and *angulata* zones (76.2% increase in GMBS, p= 3.95 x 10^{-21}). Mean body size continued to increase into the *bucklandi* Zone, however at a lessened rate (34.2% GMBS increase, p = 1.72 x 10^{-12}). Altogether from the *planorbis* Zone to the *bucklandi* Zone this species increased in size by 179%. Following the *bucklandi* Zone, there were fewer

occurrences of *P. giganteum,* and mean body size decreased by 74% (p = 2.78 x 10^{-17}) into the *semicostatum-turneri* zones. Thus, *P. giganteum* at this level decrease to a size smaller than that seen in their earliest occurrence in the pre-*planorbis* beds even though the maximum GMBS remained high (around the size recorded from the *angulata* Zone). Bed-by-bed sampling in Pinhay Bay from the *planorbis* to *bucklandi* Zone showed an increasing body size trend that matches that of the time-binned approach over the same interval (Fig. 2.5). The same was undertaken at Nash Point, despite the section only spanning the *angulata* and *bucklandi* zones, a trend towards a larger GMBS up-section was still seen. Throughout the studied interval minimum body size remained fairly constant around 10 mm, whereas both the mean and maximum GMBS increased up to the *bucklandi* Zone resulting in an increased size variance of *P. giganteum* populations.

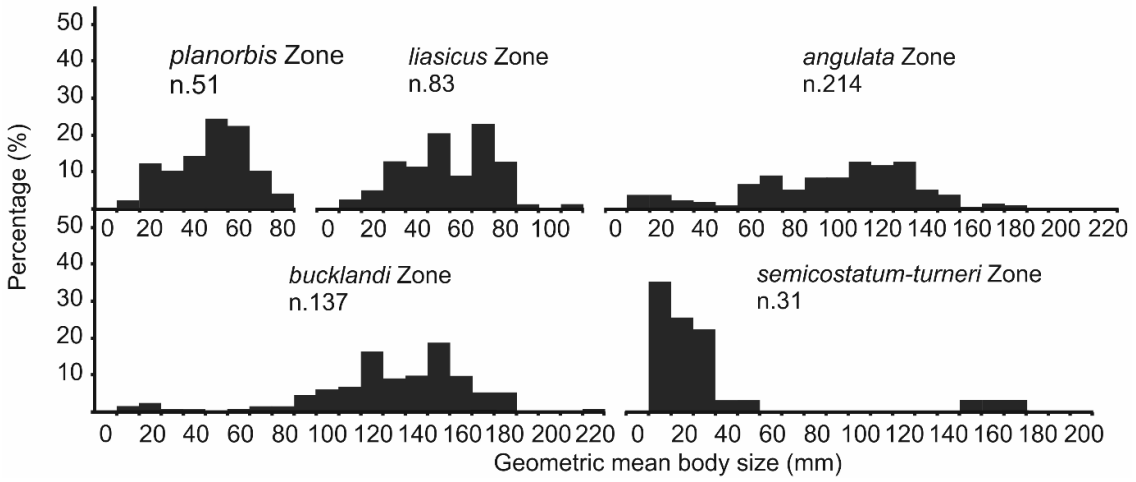

Fig. 2.3 Size distribution histograms for *Plagiostoma giganteum* per time bin.

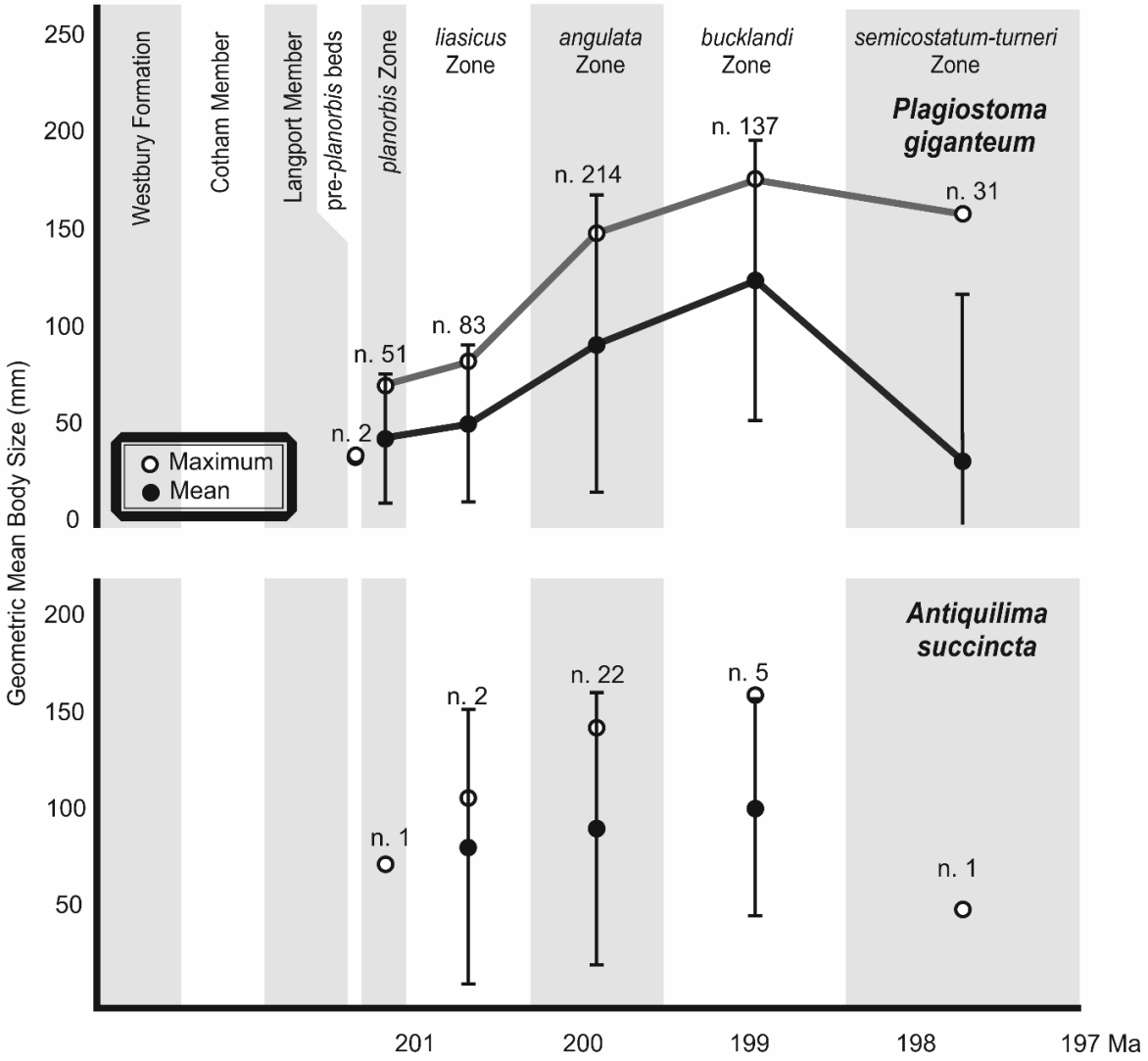

Fig. 2.4 Time-binned variation in the size of *Plagiostoma giganteum* (top) and *Antiquilima succincta* (bottom). Lines connect successive time bins with >10 specimens. Error bars depict 95% confidence intervals. Sample size quoted per time bin.

Due to large samples sizes from the *angulata* Zone it is possible to test for body size differences between sampled locations (Fig. 2.6). *P. giganteum* specimens from Pinhay Bay and Nash Point were statistically indistinct of one another (p = 0.27), whilst those from East Quantoxhead were typically smaller (p = 0.01 and 2.00×10^{-3}, when compared to Nash Point and Pinhay Bay respectively). Testing for a link between body size and oxygenation shows that *P. giganteum* was typically larger (and more abundant) in better oxygenated settings when compared with specimens measured from dysoxic settings of the same time bin. Nonetheless, the temporal body size increase occurs within individuals from the same oxygenation regimes (Fig. 2.6).

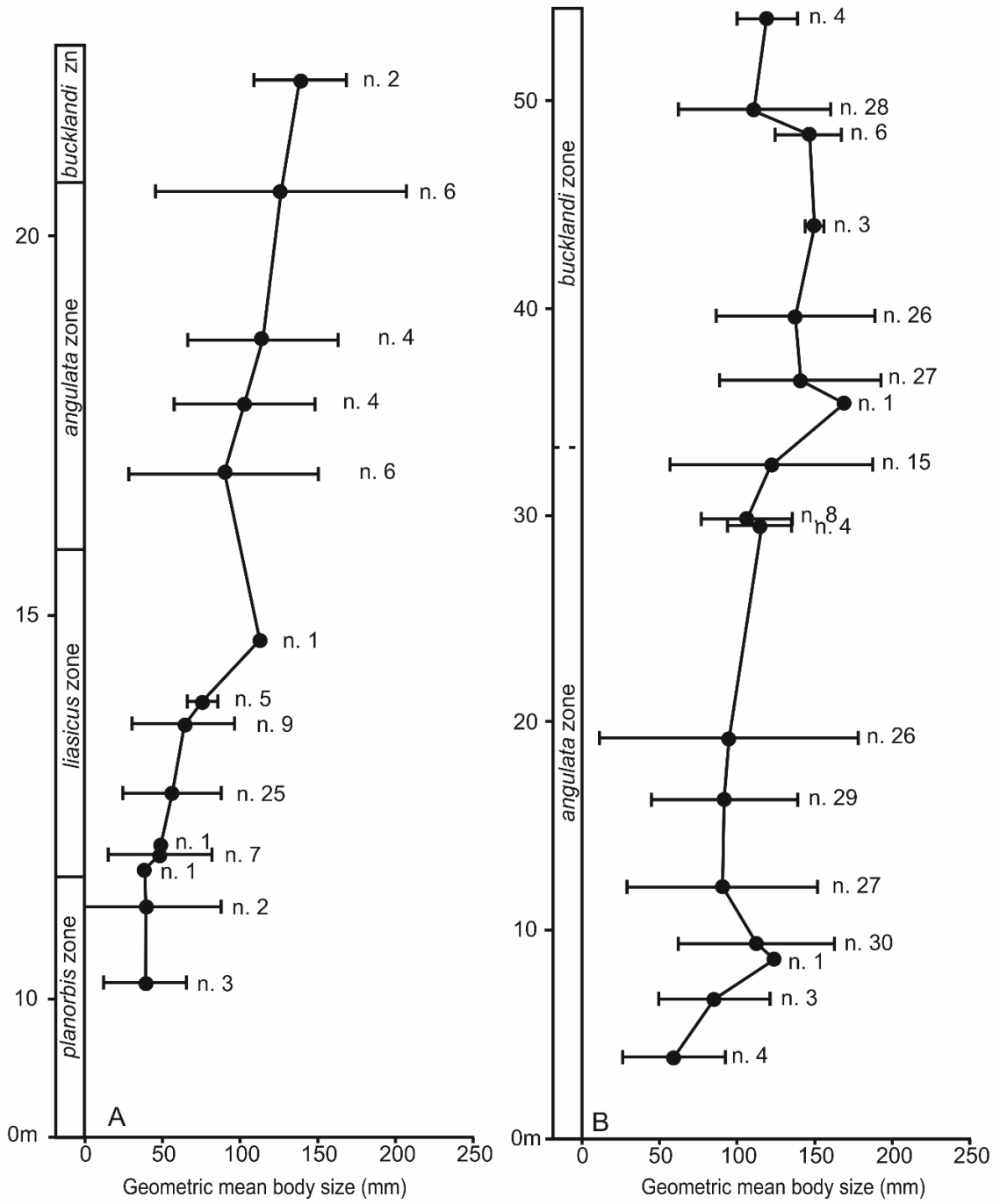

Fig. 2.5. Stratigraphically tied size variation of *P. giganteum* from Pinhay Bay (A) and Nash Point (B). Error bars depict 95% confidence intervals. Note different vertical scales.

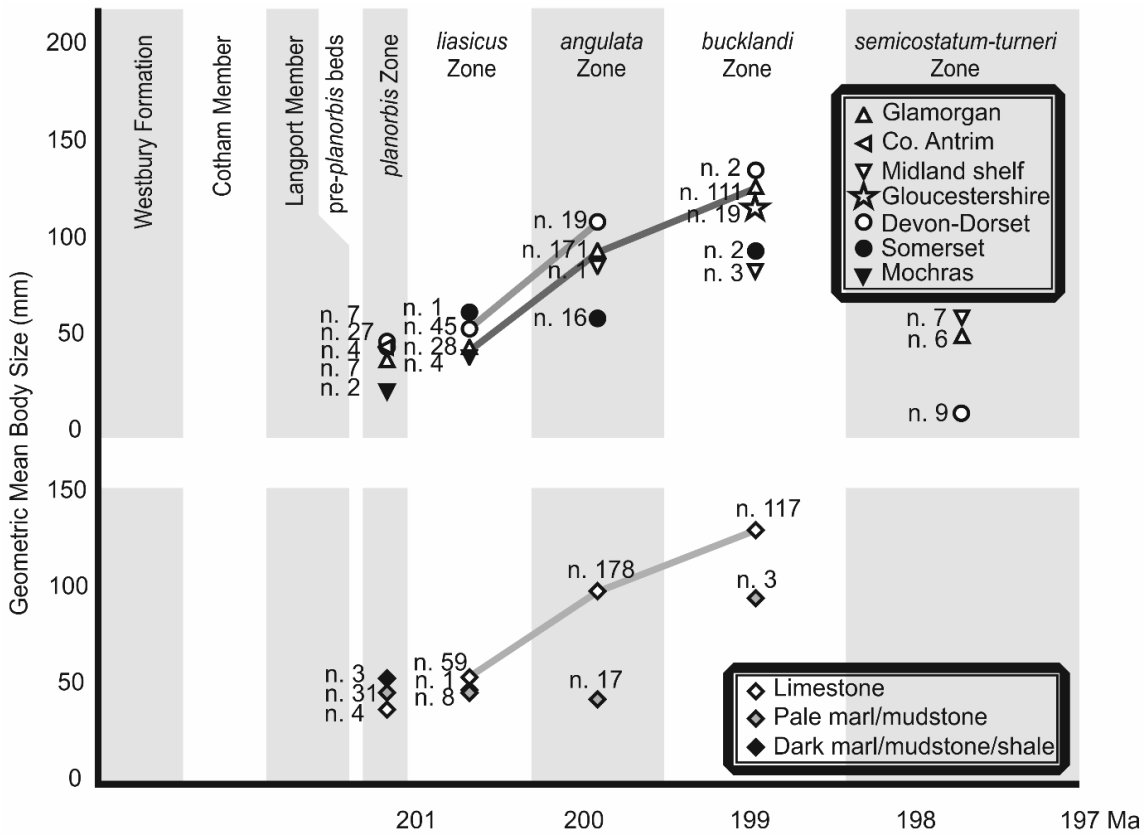

Fig. 2.6 Time-binned variation in the size of *Plagiostoma giganteum* per locality, (top). Variation in size between specimens measured from different oxygenation regimes inferred from host lithology (bottom), see methods for details. Lines connect successive time bins with >10 specimens. Sample size quoted per time bin.

2.5.1.2 *Plagiostoma punctatum*

This species appeared stratigraphically earlier than *Plagiostoma giganteum*, with a single specimen found in the Westbury Formation. *P. punctatum* was fairly abundant within the Langport Member (n = 27) though less common in the overlying formations with a total of 101 specimens from the six time bins (Fig 2.7). Of the eight time bins *P. punctatum* was recorded from, the Westbury Formation, Pre-*planorbis* Beds, *planorbis*, *liasicus* and *angulata* zones

bore too fewer specimens to produce a meaningful histogram. The sample from the Langport Member showed a size distribution with a peak at 30 mm (Fig. 2.8). For the *bucklandi* and *semicostatum-turneri* zones the peak had shifted towards smaller individuals with GMBS of 10-20 mm (Fig. 2.8). Using the time bins with a minimum of ten specimens it is possible to see an increase in mean body size from the Langport Member to the *planorbis* Zone of 92.92% (p = 1.67 x 10^{-05}). This was followed by a decline in mean GMBS from the *planorbis* to the *bucklandi* Zone of 63.9% (p = 8.20 x 10^{-05}) (Fig. 2.7). Maximum GMBS followed the same trend as the mean. This declining trend persisted into the *semicostatum-turneri* zones with a further 25% decline in mean GMBS from the *bucklandi* Zone (p = 8.13 x 10^{-04}). An additional 15 specimens were measured from BRLSI, one from YORYM and another previously collected specimen housed in the University of Leeds, these were recorded as being “Middle Lias” in age. Those from BRLSI were all collected in one location from Illminster, England. These additional specimens had a mean GMBS of 30.35 mm, a comparable value to those of the Langport Member.

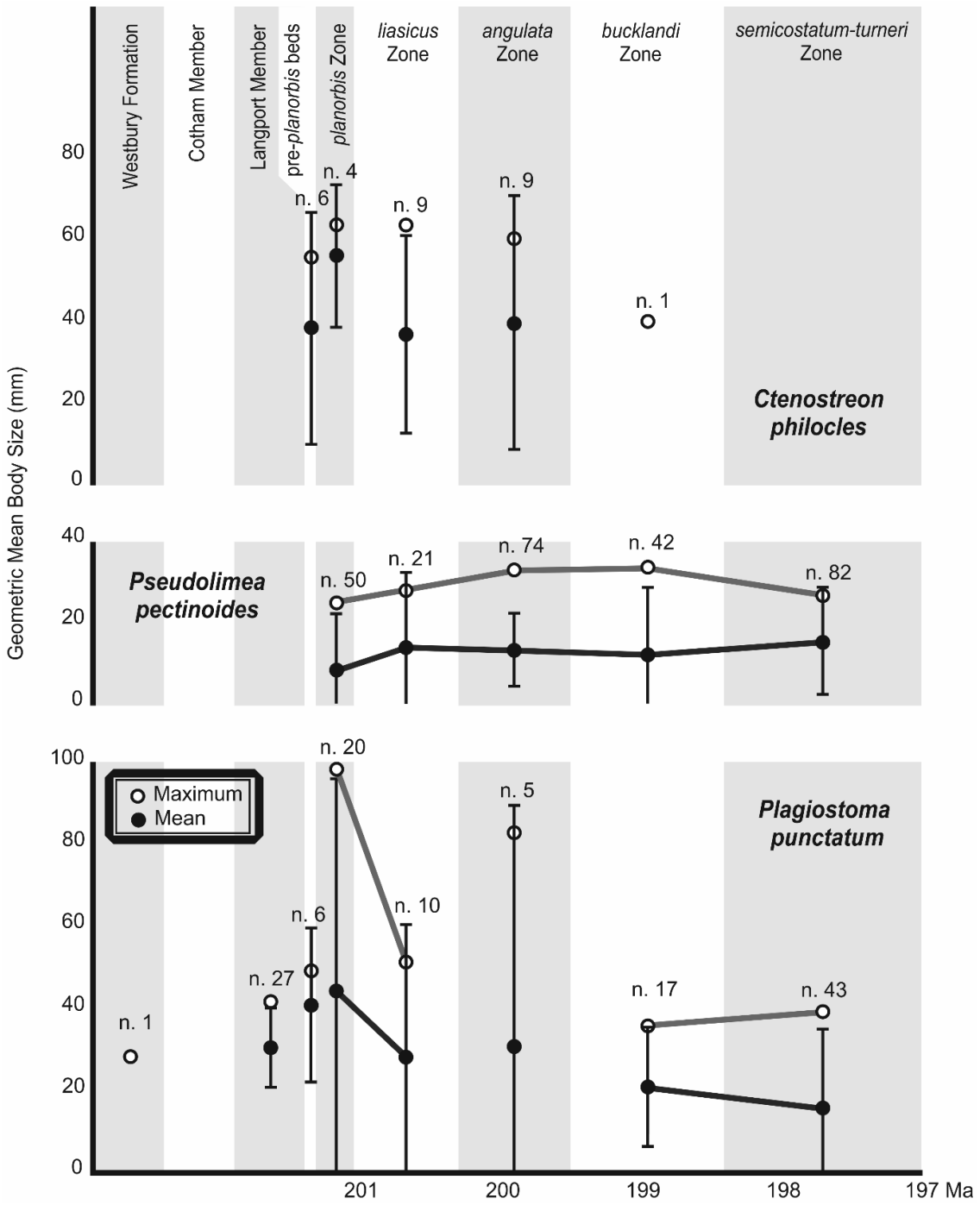

Fig. 2.7 Time-binned variation in the size of *Ctenostreon philocles* (top), *Pseudolimea pectinoides* (middle) and *Plagiostoma punctatum* (bottom). Lines connect successive time bins with >10 specimens. Error bars depict 95% confidence intervals. Sample size quoted per time bin.

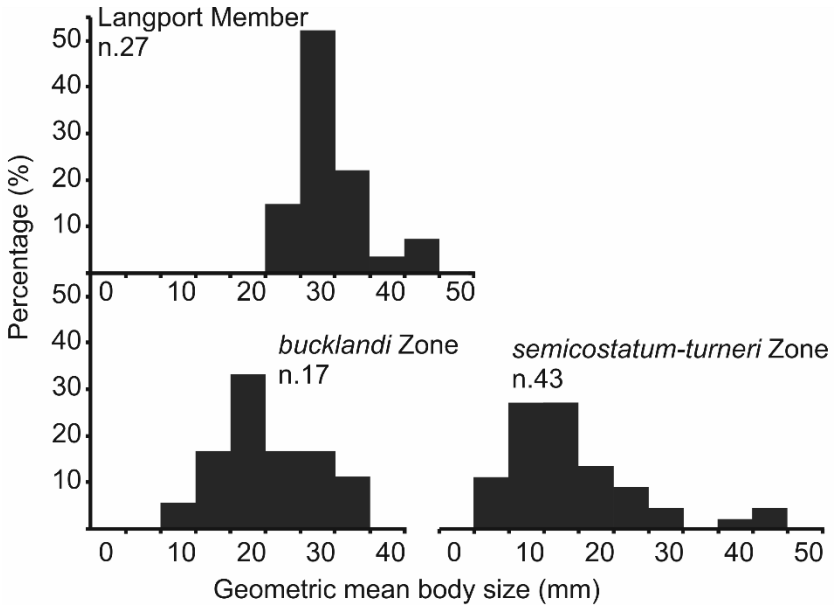

Fig. 2.8 Size distribution histograms for *Plagiostoma punctatum* per time bin with sufficient samples.

2.5.1.3 *Antiquilima succincta*

A total of 31 specimens of *A*. *succincta* were assessed for this study, with this species being most abundantly recorded from the *angulata* Zone of Glamorgan. The largest specimen measured H 162.76 mm, L 161.93 mm, collected from Southam Cement Quarry, Warwickshire (WARMS G.13092). Both maximum and mean size show an increasing size trend for this species (Fig. 2.4). Mean size increased by 39% from the *planorbis* to the *bucklandi* Zone, although sample size is rather small. Maximum size increased by 117% over the same interval (*planorbis* to *bucklandi* Zone). This then decreased by 68% from the *bucklandi* to the *semicostatum-turneri* zones. The absolute values of maximum size for *A. succincta* were akin to, and occasionally larger than, that of *P. giganteum* (Table 2.2).

Ammonite zone	*Plagiostoma giganteum*	*Antiquilima succincta*
semicostatum-turneri	173.60	52.45
bucklandi	179.97	162.34
angulata	152.75	145.67
liasicus	86.65	109.77
planorbis	74.20	74.83

Table 2.2 Comparison between maximum GMBS (mm), per ammonite zone, of *Plagiostoma giganteum* and *Antiquilima succincta*.

2.5.1.4 *Pseudolimea pectinoides*

A total of 269 specimens from five ammonite zones (*planorbis to semicostatum-turneri*) were measured. These revealed a mean size increase of 65% from the *planorbis* to *liasicus* Zone (p =0.03), thereafter mean GMBS remained fairly constant fluctuating slightly around 14 mm. After the *liasicus* Zone the only statistically significant size change occurred between the *bucklandi* and the *semicostatum-turneri* zones (29%, $p = 1.45 \times 10^{-03}$). Maximum size portrays a different trend, initially the *planorbis-liasicus* zone size increase was mirrored in the maximum size, however this trajectory continued (Fig. 2.7). Maximum GMBS shows a rise from the *planorbis* to the *bucklandi* Zone of 36% relative to the maximum during the *planorbis* Zone ($p = 3.2 \times 10^{-3}$). This size increase occurred over the same interval as that observed in *Plagiostoma giganteum* and

Antiquilima succincta, albeit at a lesser magnitude. For all time bins, size distribution histograms show a skew in favour of smaller individuals (Fig. 2.9).

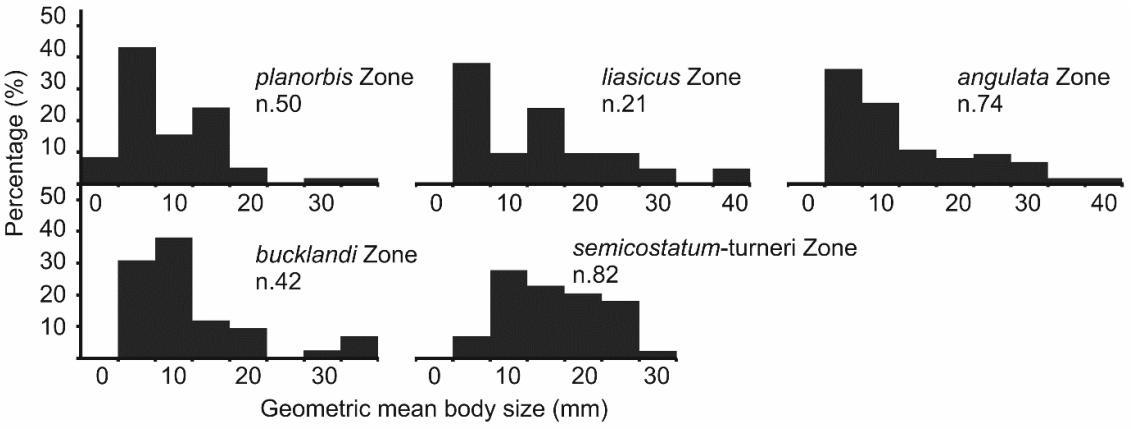

Fig. 2.9 Size distribution histograms for *Pseudolimea pectinoides* per ammonite zone.

As *P. pectinoides* was found in a range of localities, geographic variation of body size was tested. Although few locations had data from multiple time bins (Fig. 2.10) a few generalisations can be made: specimens from South Wales and in the region of the Radstock and East Midlands shelves were typically larger, with the smaller specimens coming from the Cardigan Bay Basin and Co. Antrim. Further to this, as with *P. giganteum,* size differences between oxygenation regimes were also considered. This was undertaken for field observations and five samples from the marginal facies of South Wales (housed in the NMW). For all but the *liasicus* Zone the largest individuals were collected from the more aerated environments, specimens collected from sediments representing intervals of oxygen-restriction typically have GMBS around 5 mm smaller (p = 0.02; Fig. 2.10). The increase in body size from the *planorbis* to the *liasicus* Zone is still recorded when comparing samples from individual oxygen regimes.

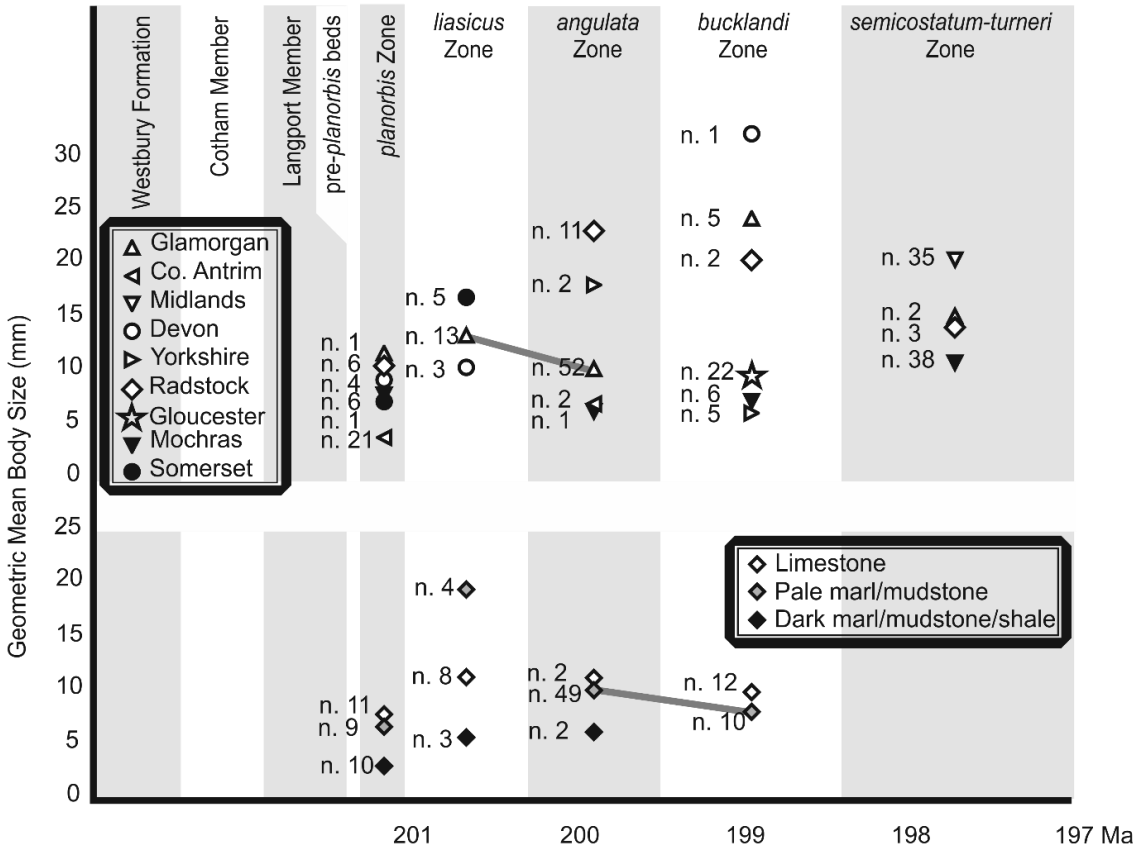

Fig. 2.10. **Time-binned variation in the size of *Pseudolimea pectinoides* per locality, (top). Variation in size between specimens from different oxygenation regimes inferred from host lithology (bottom), see methods for details. Lines connect successive time bins with >10 specimens. Sample size quoted per time bin.**

2.5.1.5 *Ctenostreon philocles*

Only 29 specimens of *Ctenostreon philocles* were measured from the Pre-*planorbis* Beds to *bucklandi* Zone. Although always scarce, this species was predominantly recorded from South Wales with a high proportion of the *liasicus* Zone specimens coming from the Sutton Stone marginal marine facies. The few specimens show only a modest maximum size increase of 15% from the Pre-*planorbis* Beds to the *planorbis* Zone but then remained stable between 60-64mm

(Fig. 2.7). Mean size was equally as unvarying. The sharp increase in the *planorbis* Zone only, was not accompanied by an increased maximum size, suggesting that the *planorbis* spike was caused by an absence of small individuals. During all other time bins mean size remained around 37-41 mm. Size differences between the *liasicus* and *angulata* Zone populations were indistinct (p = 0.25) despite being from different facies (the *angulata* Zone was from typical Blue Lias offshore facies, whilst the *liasicus Z*one data come from marginal facies).

2.5.2 Growth patterns

Growth line analyses were undertaken only for *Plagiostoma giganteum* due to a paucity of suitably preserved material for the other species. In addition, due to the small number of suitable samples, the *angulata* and *bucklandi* zones are combined for this analysis. Specimens collected from the *planorbis* Zone had an average of 366 growth lines, this value decreased during the *liasicus* Zone with only 226 lines typically, before returning to higher values (averaging 456 growth lines) during the *angulata-bucklandi* zones. Growth rate increased from the *planorbis* to *angulata-bucklandi* zone (Fig. 2.11), with a significant change from a mean gradient of 0.13 to 0.29 (p = 0.02) and was accompanied by an increased variability of gradients. Of the specimens from the *semicostatum-turneri* zones only one specimen was sufficiently preserved to conduct a formal growth line analyses, this had GMBS of 9.28 mm, and few, well-spaced growth lines, suggesting that this was a juvenile. *In situ* inspection of growth lines of specimens from the Charmouth Mudstone Formation confirm this. Plotting growth line density revealed distinct patterns in a small number of specimens with up to

four periods of high and low densities (e.g. from Hock Cliff; Fig. 2.12). However, this growth line cyclicity was not captured in every *P. giganteum* specimen and, with the exception of a single *planorbis* Zone specimen (NMW 20.362.G18), was only encountered in the *bucklandi* Zone.

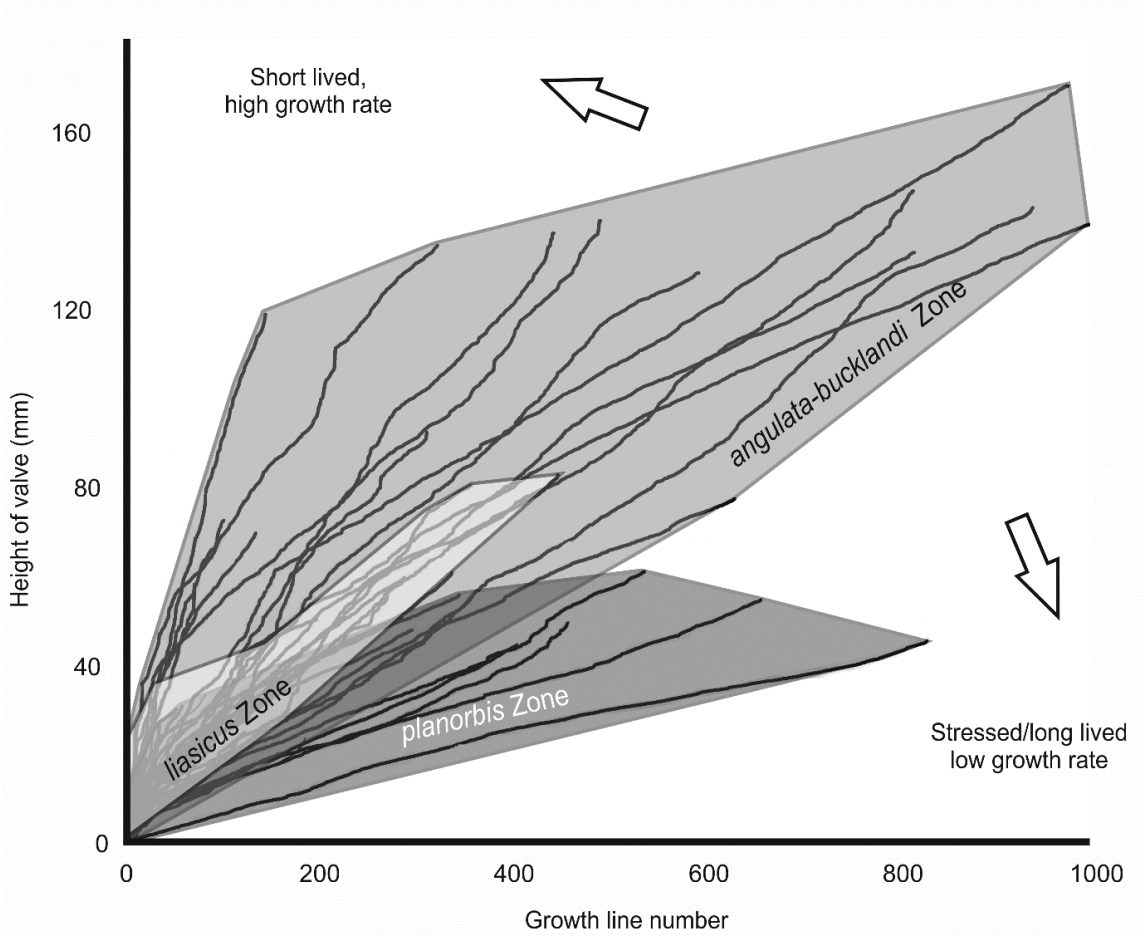

Fig. 2.11 Growth rate plot for *Plagiostoma giganteum*. Individual lines depict growth trajectories of single specimens. Shaded regions define spread of data per time bin.

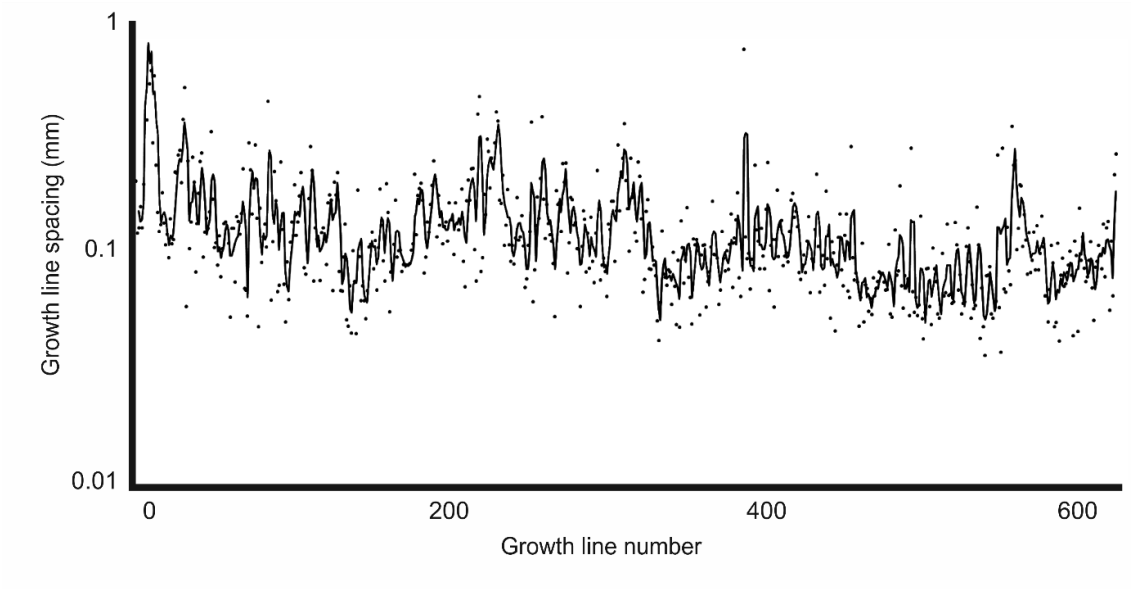

Fig. 2.12 Growth line densities with a three point moving average trend line showing cycles in a large *Plagiostoma giganteum* collected from the *bucklandi* Zone of Hock Cliff.

2.5.3 Museum versus field collections

In order to test for bias towards different size classes in museum specimens compared to those collected and measured directly from the field the two data sets were plotted separately. This evaluation was undertaken for *Plagiostoma giganteum*, owing to the larger available sample sizes. For *P. giganteum* the two collection methods show the same overall trend, with body size increasing towards the *bucklandi* Zone (Fig. 2.13). For the Pre-*planorbis* Beds there were only two specimens (one museum and one field) and so little can be said, beyond noting that they were around the same size. For the *planorbis* Zone, museum specimens contribute 24% of the data to the time bin. Specimens of this Zone collected from the field had a larger mean GMBS than

their museum counterparts, although this difference is on the threshold of 95% significance (p = 0.05). For the *liasicus* Zone 30% of specimens are from museum collections, and the two collections give indistinguishable mean GMBS values. For the *angulata* and *bucklandi* zones the percentage contributed from museums decreases with only 9% and 13% of the data, for both of these time bins the data produced from the two collection styles are again indistinct (p > 0.05). The reversal of the size trajectory in the *semicostatum-turneri* zones was also recorded by museum specimens.

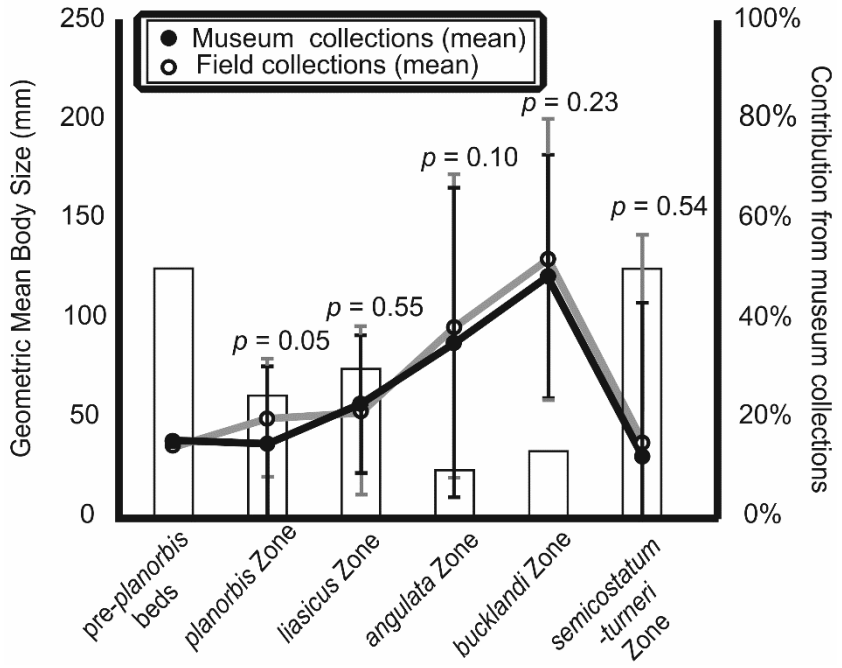

Fig. 2.13 Variation in body size of *Plagiostoma giganteum* from museum collections (closed circles) and field observations (open circles). K-S test *p* values quoted for difference between museum collection and field sample. Error bars depict 95% confidence intervals. White bars show percentage of the time-binned sample that is comprised of museum specimens.

2.6 Discussion

2.6.1 Body size

Hallam's original (1960) finding of size increase of the largest *Plagiostoma giganteum* in the first four ammonite zones of the Jurassic is replicated here. He subsequently expanded his study to include the entire Jurassic and showed that *P. giganteum*'s increase in maximum size continued into the Pliensbachian, though at a declining rate (Hallam 1975, 1998) before going extinct in the Toarcian. Size data presented here suggests this size increase was not sustained as previously reported, because the maximum body size plateaus out after a *bucklandi* Zone peak. The only other species shared between this study and those works of Hallam (1960, 1975, 1998) is *Pseudolimea pectinoides* (*Pseudolimea hettangiensis* in Hallam (1960)). Although the absolute values differ, the increased body size between the *planorbis* and *angulata* Zone reported by Hallam (1960) is confirmed in both the mean and maximum size data of this study. Our data then show mean size remained between approximately 12-14 mm from the *liasicus* Zone onwards, slightly rising in the *semicostatum-turneri* zones, whilst maximum size continued to increase into the *bucklandi* Zone before reducing in the *semicostatum-turneri* zones; the same pattern observed in *P. giganteum*. Data for *Antiquilima succincta* shows that it should be added to the list of Early Jurassic molluscs that exhibited a within-species size increase. In contrast, there is no persistent size trend for *Ctenostreon philocles,* whilst *Plagiostoma punctatum* initially increases and then shows a sustained reduction in body size during the Lower Lias. Limidae size increase in the Early Jurassic is therefore impressive amongst some species but is not uniformly developed throughout the family.

2.6.2 Growth patterns

Specimens of *Plagiostoma giganteum* from the *angulata-bucklandi* zone achieved a larger size compared to earlier individuals for comparatively fewer growth lines. As specimens were selected for their quality of preservation, and there were no variations in the style of preservation, it is likely that this is a true biological signal. Assuming that each growth line represents the same unit of time for all specimens, then *P. giganteum* achieved an increased size through improved growth rates. These findings are consistent with those reported for *Lingula* sp. (Metcalfe *et al.* 2011) and *Pseudomytiloides dubius* (Morten & Twitchett 2009) in the wake of the Permo-Triassic and early Toarcian mass extinction events respectively; diminutive forms display a greater density of growth lines compared to larger, later forms. A similar finding has also been reported for *Pholadomya ambigua, Cardinia concinna* (Hallam 1963) and species of *Gryphaea* (Johnson 1994) in the Early Jurassic.

The high growth line counts during the *planorbis* Zone may reflect the addition of disturbance rings formed during intervals of environmental stress or spawning (Craig & Hallam 1963; Lutz 1976; Lutz & Rhoads 1980). Therefore the populations of smaller body size and higher densities of growth lines may be stunted forms indicating growth under a highly stressed environment (Metcalfe *et al.* 2011). Specimens of *P. giganteum* from the *bucklandi* Zone of Hock Cliff, record clear cycles of expanded and contracted growth, this may indicate that these specimens lived in a stable, low stress environment and therefore have fewer disturbance rings masking a regular growth pattern, which may be annual. The greater number of growth lines on the largest individuals from the *angulata-*

bucklandi zone may therefore reflect increased longevity, and so the gigantism was achieved through both greater growth rates and a longer life span.

2.6.3 Contemporary Early Jurassic size increases

Early Jurassic size changes were not restricted to the Limidae, Hallam (1960, 1975) reported size increases for three epifaunal, two semi-infaunal and two infaunal suspension feeding bivalve species and for the nautiloid *Cenoceras striatus*. For *Liostrea irregularis and Cardinia concinna* this size increase persisted until the Pliensbachian. A similar case was noted for the pectinid *Chlamys textoria* with a size increase persisting through until Pliensbachian stage (Nürnberg *et al.* 2012). During the same interval that *Plagiostoma giganteum* increases in size (*planorbis* to *bucklandi* Zone) there is a marked increase in the size of ammonites. However, this was a rapidly evolving group and the size increase occurs amongst successive species; this is a good example of Cope's Rule (Hallam 1960; Dommergues *et al.* 2002). In contrast, the trends shown here occur within species and is not an evolutionary trend but an ecophenotypic response.

2.6.4 Causes of body size and growth rate changes

2.6.4.1 Water depth and body size

Water depth is thought to exert a control over body size due to variation of factors such as availability of food and oxygen (Shirayama 1983; Peck & Harper 2010; Shi *et al.* 2016). Several studies have shown that body size can decrease with depth (e.g. Attrill *et al.* 1990; Olabarria and Thurston 2003; Kaariainen and Bett 2006; Shi *et al.* 2016). This was shown by the *Plagiostoma giganteum* data

with the populations in the offshore East Quantoxhead location having a smaller mean body size than the contemporaneous specimens from the shallower Nash Point and Pinhay Bay sites. For *Pseudolimea pectinoides* the same pattern was not as clear although the largest individuals were recorded as being from the comparatively shallow shelf settings. Despite these observations, water depth does not explain the temporal pattern of body size increase in *P. giganteum* in the Blue Lias Formation because it was deposited during an overall deepening trend (Hallam 1981; Sheppard 2006; Sheppard *et al.* 2006). The initially small size of *Plagiostoma punctatum* in the Langport Member may relate to the reported unusual salinity at this level (Hallam 1965; Hallam & El Shaarawy 1982), but this is unlikely to be an influencing factor for the other species because they first appear above the Langport Member.

2.6.4.2 Oxygen availability

Oxygen restriction is generally regarded as a cause of reduced body size in marine invertebrates (Rhoads & Morse 1971; Richmond *et al.* 2006). Under low oxygen levels metabolic rates are reduced, and growth slowed (Richmond *et al.* 2006). Anoxic and euxinic conditions did develop intermittently during the lowermost Jurassic in our study area and are manifest as black shales and laminated limestones (Hallam 1987; Wignall and Hallam 1991; Wignall 2001; Richoz *et al.* 2012). These facies are best developed in the earliest Jurassic and typically become less frequent in the *angulata* and *bucklandi* zones, suggesting overall improved benthic oxygenation (Wignall & Hallam 1991). This trend occurred in tandem with the increased body size seen in the Limidae species. Greater oxygen restriction in the more offshore/deeper sections seen in the upper

Hettangian and Sinemurian of north Somerset may explain the smaller size of *P. giganteum* from that section.

The larger mean body sizes of both *Plagiostoma giganteum* and *Pseudolimea pectinoides* were found in bioturbated limestone and pale marls compared to the darker lithologies. Furthermore, *P. giganteum* is only common in the bioturbated limestones of the Blue Lias Formation further indicating its preference for better oxygenated conditions. These observations clearly indicate a link between body size and oxygen but they fail to account for the long-term trend of size increase because *P. giganteum* exhibits within-lithology (and therefore oxygen regime) size increase over the first 2 million years of the Jurassic.

The trend of size increase for the species of *Plagiostoma giganteum* and *Antiquilima succincta* was reversed in the *semicostatum-turneri* zones. Most of the data for this interval comes from the Charmouth Mudstone Formation of the Wessex Basin. The lower two members of this unit (Shales-with-Beef and Black Ven Marl members) are dominated by black shales with benthos restricted to thin discrete beds that likely record brief oxygenated intervals superimposed on a background of intense anoxia (Wignall & Hallam 1991). Inspection of valves revealed a low number of widely spaced growth lines indicating the small specimens were juveniles and not stunted adults. This is corroborated by the size-frequency histograms that show a left-skewed distribution (Fig. 2.3). The small sizes of individuals in the *semicostatum-turneri* zones is thus not comparable to the small sized specimens of the *planorbis* Zone but instead a local response to harsh conditions. This is corroborated by the continued presence of large, contemporary individuals of *P. giganteum* from the Bristol Channel Basin and from the East Midland Shelf which attain sizes as great as

170 mm. The same is true for specimens of *Pseudolimea pectinoides*. Thus, the size increase trend was locally reversed by regional anoxia but without affecting the overall trajectory.

2.6.4.3 Temperature and body size

The relationship between temperature and body size has been extensively studied for a wide range of organisms (McNab 1971; Geist 1987; James *et al.* 1995; van Der Have & De Jong 1996; van Voorhies 1996; Atkinson & Sibly 1997; Mousseau 1997; Roy & Martien 2001; Schmidt *et al.* 2004; Linse *et al.* 2006; Arendt 2011; Berke *et al.* 2013). Perhaps the most renowned temperature-related size rule is Bergmann's Rule (Bergmann 1847; translated in James 1970) whereby an organism's body size increases with latitude. Although Bergmann's Rule specifically refers to geographic body size distribution, it is thought to relate to the Temperature-Size Rule which relates solely to the effects of temperature on growth and final adult body size (Atkinson 1994; van Der Have & De Jong 1996; Atkinson & Sibly 1997). Generally growth and development rates increase with temperature thereby shortening the time taken to reach maturity and producing a small adult (Atkinson 1994; Kingsolver & Huey 2008; Chown & Gaston 2010).

The role of temperature in the size increase of the Early Jurassic Limidae is difficult to evaluate because of a poorly constrained temperature record. The end-Triassic mass extinction interval is thought to have been a period of intense warming, with fossil leaf stomatal indices suggesting a temperature increase of around 3-4°C (McElwain *et al.* 1999). The subsequent climatic cooling is not well constrained although it may have occurred during the *planorbis* Zone (McElwain

et al. 1999; Bonis 2010; Mander *et al.* 2013). Study of British sections instead suggests a warming trending (derived from oxygen isotope ratios of *Liostrea* shells), from <7-14°C in the Langport Member to 12-22°C in the *planorbis* Zone (van de Schootbrugge *et al.* 2007; Korte *et al.* 2009; Clémence *et al.* 2010). However, the salinity of the Langport Member is unlikely to have been normal marine (Hesselbo & Jenkyns 1995; Wignall 2001; Radley *et al.* 2008), making evaluation of the isotope record difficult. Clay composition provides an indirect indicator of palaeoclimate with high kaolinite/illite ratios thought to indicate wetter and possibly warmer climatic episodes (Deconinck *et al.* 2003). If so, data from SW England suggests the *planorbis* and upper *bucklandi* zones may have been warm and humid intervals with the *liasicus* and *angulata* zones being cooler and drier (Deconinck *et al.* 2003). The clay mineral changes (and the oxygen isotope data) do not appear to relate to the long-term size increase of the Limidae and therefore suggest that the trend is not an example of the Temperature-Size Rule. However, there is a clear need for a more reliable palaeotemperature curve for Early Jurassic time to better assess any size-temperature link.

2.6.4.4 Food availability

Changes to primary productivity can influence body size and growth rate of organisms higher in the food chain (Hallam 1965; Epifanio 1979; Wacker & von Elert 2008; He *et al.* 2010; Brom *et al.* 2015) and may have played a role in the initially small size of bivalves after the end-Triassic mass extinction. A productivity crash has been postulated for this crisis (Ward *et al.* 2004; Bottini *et al.* 2016) resulting in unusual Early Jurassic marine primary productivity with larger red algae (dinoflagellates) replaced by smaller green algae: prasinophytes and acritarchs (van de Schootbrugge *et al.* 2007) and occasionally cyanobacteria

(Jaraula *et al.* 2013). Such communities prevailed during Pre-*planorbis* to lower *planorbis* Zone interval only (van de Schootbrugge *et al.* 2007; Clémence *et al.* 2010; Paris *et al.* 2010) and may account for the small body size of bivalves (relative to later during the recovery). The smaller size of acritarchs and prasinophytes (relative to the dinoflagellates) could cause reduced efficiency of filtration in suspension-feeding bivalves (Weiss *et al.* 2007; van de Schootbrugge & Gollner 2013). Whilst prasinophytes and cyanobacteria lack essential long-chained polyunsaturated fatty acids that are required for growth (Brown *et al.* 1997; von Elert *et al.* 2003): both factors could reduce growth rates. However, such notions are speculative and difficult to disentangle from other co-occurring stresses.

2.6.5 Lilliputians and Brobdingnagians

The Lilliput Effect is defined as a temporary reduction in body size of a surviving species after a biotic crisis (Urbanek 1993), and is not applicable to the small-sized individuals of *Plagiostoma giganteum, Antiquilima succincta* and *Pseudolimea pectinoides* seen in the aftermath of the end-Triassic mass extinction, because these species are first recorded at this time. Their trend is one of within-species size increase following first appearance. We propose to name this as the Brobdingnag Effect (after the land inhabited by giant humans in Swift's *Gulliver's Travels*). We do not view this as a manifestation of Cope's Rule which involves the evolution of progressively larger species which includes an accompanying morphological change (Rensch 1948). Were this change in body size to be viewed as Cope's Rule with species succession occurring as an anagenetic change we would be required to erect a new species name for the larger bivalves in the *angulata* and *bucklandi* zones. As size alone distinguishes

the younger populations with no other morphological change we feel this to be inappropriate.

For the Limidae examples, the size increase is caused by increased growth rates and greater longevity of individuals suggesting improving benthic conditions were responsible. These could include improved oxygenation, because populations of smaller body size (caused by higher juvenile mortality) are found in areas experiencing frequent anoxic conditions. There may be a temperature-size relationship but this is difficult to judge without a reliable palaeotemperature curve. However, the cause of the overall, long-term trend (spread over 2 million years) is unclear as not all species show a dramatic size.

Both the Lilliput and Brobdingnag Effects relate to the observation that small species commonly dominate in the immediate aftermath of extinction intervals. There have been several explanations for the former effect. Payne (2005) suggested four models that could have produced assemblages of small gastropods in the aftermath of the Permo-Triassic mass extinction (although he did not explicitly call any of these alternatives the Lilliput Effect): 1) *size-biased extinctions* (preferential extinction of large taxa); 2) *changed relative abundances* (increased relative abundances and dominance of small taxa thereby lowering the mean size of an assemblage); 3) *size change within-lineages* (evolutionary trend towards smaller species via anagenesis); 4) *size-biased originations* (origination of new species in the aftermath of the extinction that were preferentially small). Twitchett (2007) later considered model 3 to be the Lilliput Effect (although this does not fit the original definition which was a within-species size decrease). As Harries and Knorr (2009) noted, model 3 is an example of the concept of dwarfing, as defined in Marshall and Corruccini (1978), although

frequently it also involves speciation. We ascribe Payne's model 4 to the Brobdingnag Effect with the modification that species increase in size following their appearance.

The term "Lilliput Effect" has been widely used but often applied at a higher taxonomic rank than species and so we suspect that many, perhaps the majority of examples, are in fact manifestations of the Brobdingnag Effect. Many studies of the supposed Lilliput Effect lack size data showing a return to pre-extinction sizes (e.g. Kaljo 1996; Keller and Abramovich 2009; Huang *et al.* 2010; Song *et al.* 2011; Martínez-Díaz *et al.* 2016; Belben *et al.* 2017), or the taxonomic rank is often generic or higher (e.g. Borths and Ausich 2011; Chen *et al.* 2013; Chu *et al.* 2015; Weronika *et al.* 2017), or it is applied to whole assemblages irrespective of taxonomy (Mander *et al.* 2008; Belben *et al.* 2017). Under such circumstances it may not be possible to detect if individual species crossed the extinction event, exhibit a reduced body size in the aftermath and then increased in size during the recovery, as per the Lilliput Effect. Alternatively, a surviving genus could be represented by new species with small bodies that then undergo a within-species size increase, as per the Brobdingnag Effect. These can only be tested with more studies conducted at the species level and for the entire recovery interval. One such study (Chen *et al.* 2019) testing for the Lilliput Effect in brachiopods following the end-Permian mass extinction shows that species originating in the aftermath did so with small body sizes and subsequently increased in size, thus following a Brobdingnag trend. Additionally Morten and Twitchett (2009) showed that, what is here termed the Brobdingnag Effect, occurred amongst three species following the early Toarcian mass extinction event (*Acrocoelites subtriscissus, Melegrinella substriata, Gresslya donaciformis*). With an increase in studies conducted at the

species level it may be found that the Brobdingnag Effect was more prevalent through geological time than the Lilliput Effect.

2.7 Conclusions

Three species of Limidae (*Plagiostoma giganteum, Antiquilima succincta* and *Pseudolimea* pectinoides) show increased body size during the first 2 million years of the Jurassic following the end-Triassic mass extinction. Of these *P. giganteum* is the most impressive case with a substantial increase in mean shell size (179%) from the *planorbis* to the *bucklandi* Zone. The larger specimens of *P. giganteum* from the *bucklandi* interval show an increase in the number and spacing of growth lines when compared to those from earlier times, indicating larger size was achieved by faster growth and greater longevity. We proposed that this within-species size increase in the aftermath of a mass extinction be termed the Brobdingnag Effect and argue that many so-called example of the Lilliput Effect (reduction in size of species across a mass extinction horizon) need to be re-evaluated. They may represent the origination of small, new species followed by subsequent size increase. The Brobdingnag Effect was not ubiquitous within the Early Jurassic Limidae though, because *Ctenostreon philocles* did not undergo significant size changes and *Plagiostoma punctatum* decreased in size.

The cause of the Brobdingnag Effect is unclear. There is apparently no connection with temperature fluctuations although a paucity of reliable Early Jurassic temperature records makes this factor difficult to evaluate. Oxygen-poor conditions clearly caused Limidae populations to become smaller in body size, because of increased juvenile mortality, but this is a local/regional effect and does not influence the long-term size-increase trend. It remains a remarkable finding

that some bivalves are capable of substantial changes in size that presumably involved changes in ecological style, whilst remaining a morphologically distinct species.

Acknowledgements. We thank the following people for their assistance: Tom Sunderland, Bob Corns and Tom Charman of Natural England and Hugh Luttrell of East Quantoxhead Estate for permissions to sample at Pinhay Bay, along the Blue Anchor-Lilstock Coast SSSI and along the Yorkshire Coast; Peter Hodges, Caroline Buttler and Lucy McCobb of the National Museum of Wales, Cardiff; Deborah Hutchinson at the Bristol Museum and Art Gallery; Jon Radley from Warwickshire Museum Service; Matt Williams at the Bath Royal Literary and Scientific Institute; Sarah King and Stuart Ogilvy of the Yorkshire Museums Trust, and Roger Osborne and Tim Burnhill of Whitby Museum. Additional thanks go to field assistant Karolina Zarzyczny, Mike Simms and Mick Oates for showing us field sites in Northern Ireland and Conesby Quarry respectively. JWA was funded by a NERC postgraduate studentship.

References

Aberhan, M. 1994. Early Jurassic bivalvia of northern Chile. Part 1. Subclasses Palaeotaxodonta, Pteriomorphia, and Isofilibranchia. *Beringeria*, **13**, 3–115.

Aberhan, M., Scholz, A. & Schubert, S. 2011. Das Ober-Pliensbachium (Domerium) der Herforder Liasmulde - Teil 3 - Taxonomie und paläoökologie der bivalvia aus der Amaltheenton-Formation (Unterjura) der Herforder Liasmulde. *Geologie und Paläeontologie in Westfalen*, **80**, 61–109.

Alroy, J. 1998. Cope's Rule and the dynamics of body mass evolution in North American fossil mammals. *Science*, **280**, 731–734, https://doi.org/10.1126/science.280.5364.731.

Arendt, J.D. 2011. Size-fecuncity relationships, growth trajectories, and the

Temperature-Size Rule for ectotherms. *Evolution*, **65**, 43–51, https://doi.org/10.1111/j.1558-5646.2010.01112.x.

Atkinson, D. 1994. Temperature and organism size—a biological law for ectotherms? *Advances in Ecological Research*, **25**, 1–58, https://doi.org/10.1016/S0065-2504(08)60212-3.

Atkinson, D. & Sibly, R.M. 1997. Why are organisms usually bigger in cold environments? Making sense of a life history puzzle. *Trends in Ecology & Evolution*, **12**, 235–239.

Attrill, M.J., Hartnoll, R.G., Rice, A.L. & Thurston, M.H. 1990. A depth-related distribution of the red crab, Geryon trispinosus (Herbst) [=G. tridens KrÃ‚yer]: indications of vertical migration. *Progress in Oceanography*, **24**, 197–206.

Barras, C.G. & Twitchett, R.J. 2007. Response of the marine infauna to Triassic – Jurassic environmental change: Ichnological data from southern England. *Palaeogeography, Palaeoclimatology, Palaeoecology*, **244**, 223–241, https://doi.org/10.1016/j.palaeo.2006.06.040.

Belben, R.A., Underwood, C.J., Johanson, Z. & Twitchett, R.J. 2017. Ecological impact of the end-Cretaceous extinction on lamniform sharks. *PLoS ONE*, **12**, e0178294.

Bergmann, C. 1847. Ueber die Verhältnisse der Wärmeökonomie der Thiere zu ihrer Grösse. *Grottinger studien*, **3**, 595–708.

Berke, S.K., Jablonski, D., Krug, A.Z., Roy, K. & Tomašových, A. 2013. Beyond Bergmann's Rule: size–latitude relationships in marine bivalvia world-wide. *Global Ecology and Biogeography*, **22**, 173–183, https://doi.org/10.1111/j.1466-8238.2012.00775.x.

Bloos, G. & Page, K.N. 2002. Global stratotype section and point for base of the Sinemurian Stage (Lower Jurassic). *Episodes*, **25**, 22–28.

Bonis, N.R. 2010. *Palaeoenvironmental Changes and Vegetation History during the Triassic-Jurassic Transition*. Unpublished PhD thesis, Utrecht University, Utrecht.

Bonis, N.R., Ruhl, M. & Kürschner, W.M. 2010. Climate change driven black shale deposition during the end-Triassic in the western Tethys. *Palaeogeography, Palaeoclimatology, Palaeoecology*, **290**, 151–159, https://doi.org/10.1016/j.palaeo.2009.06.016.

Boomer, I.D., Duffin, C.J. & Swift, A. 1999. Arthropods 1: Crustaceans. *In*: Swift, A. & Martill, D. M. (eds) *Fossils of the Rhaetian Penarth Group*. London, The Palaeontological Association, 129–148.

Borths, M.R. & Ausich, W.I. 2011. Ordovician – Silurian Lilliput crinoids during the end-Ordovician biotic crisis. *Swiss Journal of Palaeontology*, **130**, 7–18, https://doi.org/10.1007/s13358-010-0003-2.

Bottini, C., Jadoul, F., Rigo, M., Zaffani, M., Artoni, C. & Erba, E. 2016. Calcareous nannofossils at the Triassic/Jurassic boundary: Stratigraphic and paleoceanogrpahic characterization. *Rivista Italiana di Paleontologia E Stratigrafia*, **122**, 141–164.

Bottrell, S.H. & Raiswell, R. 1989. Primary versus diagenetic origin of Blue Lias rhythms (Dorset, UK): evidence from sulphur geochemistry. *Terra Nova*, **1**,

451–456, https://doi.org/10.1111/j.1365-3121.1989.tb00409.x.

Brom, K.R., Salamon, M.A., Ferré, B., Brachaniec, T. & Szopa, K. 2015. The Lilliput Effect in crinoids at the end of the Oceanic Anoxic Event 2: a case study from Poland. *Journal of Paleontology*, **89**, 1076–1081.

Brown, M.R., Jeffrey, S.W., Volkman, J.K. & Dunstan, G.A. 1997. Nutritional properties of microalgae for mariculture. *Aquaculture*, **151**, 315–331.

Chen, J., Song, H., He, W., Tong, J., Wang, F. & Wu, S. 2019. Size variation of brachiopods from the Late Permian through the Middle Triassic in South China: Evidence for the Lilliput Effect following the Permian-Triassic extinction. *Palaeogeography, Palaeoclimatology, Palaeoecology*, **519**, 248–257, https://doi.org/10.1016/j.palaeo.2018.07.013.

Chen, Y., Twitchett, R.J., et al. 2013. Size variation of conodonts during the Smithian–Spathian (Early Triassic) global warming event. *Geology*, **41**, 823–826, https://doi.org/10.1130/G34171.1.

Chown, S.L. & Gaston, K.J. 2010. Body size variation in insects: a macroecological perspective. *Biological Reviews*, **85**, 139–169, https://doi.org/10.1111/j.1469-185X.2009.00097.x.

Chu, D., Tong, J., Song, H., Benton, M.J., Song, H., Yu, J. & Qiu, X. 2015. Lilliput Effect in freshwater ostracods during the Permian – Triassic extinction. *Palaeogeography, Palaeoclimatology, Palaeoecology*, **435**, 38–52, https://doi.org/10.1016/j.palaeo.2015.06.003.

Clémence, M.-E., Bartolini, A., Gardin, S., Paris, G., Beaumont, V. & Page, K.N. 2010. Early Hettangian benthic–planktonic coupling at Doniford (SW England): Palaeoenvironmental implications for the aftermath of the end-Triassic crisis. *Palaeogeography, Palaeoclimatology, Palaeoecology*, **295**, 102–115, https://doi.org/10.1016/j.palaeo.2010.05.021.

Cope, E.D. 1887. *The Origin of the Fittest* . New York, D. Appleton and Co.

Cox, L.R. 1944. On Pseudolimea Arkell. *Proceedings of the Malacological Society, London*, **26**, 74–88.

Cox, L.R., Newell, N., et al. 1969. Part N bivalvia. *In*: Moore, R. C. (ed.) *Treatise on Invertebrate Paleontology*. The Geological Society of America, Inc. and The Universtiy of Kansas, N385–N393.

Craig, G.Y. & Hallam, A. 1963. Size-frequency and growth-ring analyses of Mytilus edulis and Cardium edule, and their palaeoecological significance. *Palaeontology*, **6**, 731–750.

Deconinck, J., Hesselbo, S.P., Debuisser, N. & Averbuch, O. 2003. Environmental controls on clay mineralogy of an Early Jurassic mudrock (Blue Lias Formation, southern England). *International Journal of Earth Sciience (Geol Rundsch)*, **92**, 255–266, https://doi.org/10.1007/s00531-003-0318-y.

Dommergues, J.-L., Montuire, S. & Neige, P. 2002. Size patterns through time: the case of the Early Jurassic ammonite radiation. *Paleobiology*, **28**, 423–434, https://doi.org/10.1666/0094-8373(2002)028<0423:SPTTTC>2.0.CO;2.

Epifanio, C.E. 1979. Growth in bivalve molluscs: nutritional effects of two or more species of algae in diets fed to the american oyster Crassostrea

virginica (Gmelin) and the hard clam Mercenaria mercenaria (L.). *Aquaculture*, **18**, 1–12.

Gallois, R.W. 2007. The stratigraphy of the Penarth Group (late Triassic) of the east Devon coast. *Geoscience in South-West England*, **11**, 287–297.

Gallois, R.W. 2008. The lithostratigraphy of the Shales-with-Beef Member of the Charmouth Mudstone Formation, Lower Jurassic. *Proceedings of the Ussher Society*, **12**, 32–40.

Gallois, R.W. 2009. Lithostratigraphy of the Penarth Group (Late Triassic) of the Severn Estuary area. *Geoscience in South-West England*, **12**, 71–84.

Geist, V. 1987. Bergmann's Rule is invalid. *Canadian Journal of Zoology*, **65**, 1035–1038, https://doi.org/10.1139/z87-164.

Hallam, A. 1960. A sedimentary and faunal study of the Blue Lias of Dorset and Glamorgan. *Philosophical Transactions of the Royal Society of London B: Biological Sciences*, **243**, 1–44, https://doi.org/10.1098/rstb.1960.0003.

Hallam, A. 1963. Observations on the palaeoecology and ammonite sequence of the Frodingham Ironstone (Lower Jurassic). *Palaeontology*, **6**, 554–574.

Hallam, A. 1965. Environmental causes of stunting in living and fossil marine benthonic invertebrates. *Palaeontology*, **8**, 132–155.

Hallam, A. 1975. Evolutionary size increase and longevity in Jurassic bivalves and ammonites. *Nature*, **258**, 493–496.

Hallam, A. 1978. How rare is phyletic gradualism and what is its evolutionary significance? Evidence from Jurassic bivalves. *Paleobiology*, **4**, 16–25.

Hallam, A. 1981. A revised sea-level curve for the early Jurassic. *Journal of the Geological Society*, **138**, 735–743.

Hallam, A. 1987. Radiations and extinctions in relation to environmental change in the marine Lower Jurassic of Northwest Europe. *Paleobiology*, **13**, 152–168.

Hallam, A. 1996. Recovery of the marine fauna in Europe after the end-Triassic and early Toarcian mass extinctions. *Geological Society, London, Special Publications*, **102**, 231–236, https://doi.org/10.1144/GSL.SP.1996.001.01.16.

Hallam, A. 1998. Speciation patterns and trends in the fossil record. *GEOBIOS*, **30**, 921–930.

Hallam, A. & El Shaarawy, Z. 1982. Salinity reduction of the end- Triassic sea from the Alpine region into northwestern Europe. *Lethaia*, **15**, 169–178, https://doi.org/10.1111/j.1502-3931.1982.tb01136.x.

Hammer, Ø., Harper, D.A.T. & Ryan, P.D. 2001. Past: Paleontological Statistics software package for education and data analysis.

Harries, P.J. & Knorr, P.O. 2009. What does the 'Lilliput Effect' mean? *Palaeogeography, Palaeoclimatology, Palaeoecology*, **284**, 4–10, https://doi.org/10.1016/j.palaeo.2009.08.021.

Hautmann, M. 2004. Effect of end-Triassic CO2 maximum on carbonate sedimentation and marine mass extinction. *Facies*, **50**, 257–261, https://doi.org/10.1007/s10347-004-0020-y.

He, W.-H., Twitchett, R.J., Zhang, Y., Shi, G.R., Feng, Q., Yu, J. & Wu, S. 2010. Controls on body size during the Late Permian mass extinction event. *Geobiology*, **8**, 391–402, https://doi.org/10.1111/j.1472-4669.2010.00248.x.

Hesselbo, S.P. & Jenkyns, H.C. 1995. Lower and Middle Jurassic of Dorset and Yorkshire. *In*: Taylor, P. D. (ed.) *The Field Geology of the British Jurassic*. Bath, Geological Society of London, 110–115.

Hodges, P. 1987. *Lower Lias (Lower Jurassic) Bivlavia from South Wales and Adjacent Areas*. Unpublished PhD thesis, University College of Swansea, Swansea.

Huang, B., Harper, D.A.T., Zhan, R. & Rong, J. 2010. Can the Lilliput Effect be detected in the brachiopod faunas of South China following the terminal Ordovician mass extinction? *Palaeogeography, Palaeoclimatology, Palaeoecology*, **285**, 277–286.

Jablonski, D. 1996. Body size and macroevolution. *In*: Jablonski, D., Erwin, D. H. & Lipps, J. H. (eds) *Evolutionary Paleobiology*. Chicago, University of Chicago Press.

James, A.C., Azevedo, R.B.R. & Partridge, L. 1995. Cellular basis and developmental timing in a size cline of Drosophila melanogaster. *Genetics*, **140**, 659–666.

James, F.C. 1970. Geographic size variation in birds and its relationship to climate. *Ecology*, **51**, 365–390, https://doi.org/10.2307/1935374.

Jaraula, C.M.B., Grice, K., Twitchett, R.J., Böttcher, M.E., Lemetayer, P., Dastidar, A.G. & Opazo, L.F. 2013. Elevated pCO_2 leading to Late Triassic extinction, persistent photic zone euxinia, and rising sea levels. *Geology*, **41**, 955–958, https://doi.org/10.1130/G34183.1.

Johnson, A. 1994. Evolution of European Lower Jurassic Gryphaea (Gryphaea) and contemporaneous bivalves. *Historical Biology*, **7**, 167–186.

Johnson, M.E. & McKerrow, W.S. 1995. The Sutton Stone: an Early Jurassic rocky shore deposit in South Wales. *Palaeontology*, **38**, 529–541.

Kaariainen, J.I. & Bett, B.J. 2006. Evidence for benthic body size miniaturization in the deep sea. *Journal of the Marine Biological Association of the United Kingdom*, **86**, 1339–1345, https://doi.org/10.1017/S0025315406014366.

Kaljo, D. 1996. Diachronous recovery patterns in Early Silurian corals, graptolites and acritarchs. *In*: Hart, M. B. (ed.) *Biotic Recovery from Mass Extinction Events*. Geological Society, London, Special Publications, **102**, 127–134.

Kauffman, E.G. & Erwin, D.H. 1995. Surviving mass extinctions. *Geotimes*, **14**, 14–17.

Keller, G. & Abramovich, S. 2009. Lilliput Effect in late Maastrichtian planktic foraminifera : Response to environmental stress. *Palaeogeography, Palaeoclimatology, Palaeoecology*, **284**, 47–62, https://doi.org/10.1016/j.palaeo.2009.08.029.

Kingsolver, J.G. & Huey, R.B. 2008. Size, temperature, and fitness: Three rules. *Evolutionary Ecology Research*, **10**, 251–268.

Korte, C., Hesselbo, S.P., Jenkyns, H.C., Rickaby, R.E.M. & Spotl, C. 2009.

Palaeoenvironmental significance of carbon- and oxygen-isotope stratigraphy of marine Triassic-Jurassic boundary sections in SW Britain. *Journal of the Geological Society*, **166**, 431–445, https://doi.org/10.1144/0016-76492007-177.

Kosnik, M.A., Jablonski, D., Lockwood, R. & Novack-Gottshall, P.M. 2006. Quantifying molluscan body size in evolutionary and ecological analyses: Maximizing the return on data-collection efforts. *Palaios*, **21**, 588–597.

Łaska, W., Rodríguez-tovar, F.J. & Uchman, A. 2017. Evaluating macrobenthic response to the Cretaceous-Palaeogene event: A high-resolution ichnological approach at the Agost section (SE Spain). *Cretaceous Research*, **70**, 96–110.

Linse, K., Barnes, D.K.A. & Enderlein, P. 2006. Body size and growth of benthic invertebrates along an Antarctic latitudinal gradient. *Deep Sea Research Part II: Topical Studies in Oceanography*, **53**, 921–931, https://doi.org/10.1016/j.dsr2.2006.03.006.

Lutz, R.A. 1976. Annual growth patterns in the inner shell layer of Mytilus edulis L. *Journal of the Marine Biological Association of the United Kingdom*, **56**, 723–731.

Lutz, R.A. & Rhoads, D.C. 1980. Growth patterns within the molluscan shell. *In*: Rhoads, D. C. & Lutz, R. A. (eds) *Skeletal Growth of Aquatic Organisms: Biological Records of Environmental Change*. New York and London, Plenum Press, 203–254.

Mander, L., Twitchett, R.J. & Benton, M.J. 2008. Palaeoecology of the Late Triassic extinction event in the SW UK. *Journal of the Geological Society*, **165**, 319–332, https://doi.org/10.1144/0016-76492007-029.

Mander, L., Kürschner, W.M. & McElwain, J.C. 2013. Palynostratigraphy and vegetation history of the Triassic – Jurassic transition in East Greenland. *Journal of the Geological Society, London*, **170**, 37–46, https://doi.org/10.1144/jgs2012-018.Palynostratigraphy.

Marshall, L.G. & Corruccini, R.S. 1978. Variability, evolutionary rates, and allometry in dwarfing lineages. *Paleobiology*, **4**, 101–119.

Martínez-Díaz, L., Phillips, G.E., Nyborg, T., Espinosa, B., de Araújo Tavora, V., Centeno-garcía, E. & Vega, F.J. 2016. Lilliput Effect in a retroplumid crab (Crustacea: Decapoda) across the K/Pg boundary. *Journal of South American Earth Sciences*, **69**, 11–24, https://doi.org/10.1016/j.jsames.2016.03.007.

McElwain, J.C., Beerling, D.J. & Woodward, F.I. 1999. Fossil plants and global warming at the Triassic-Jurassic boundary. *Science*, **285**, 1386–1391.

McGowan, A.J., Smith, A.B. & Taylor, P.D. 2009. Faunal diversity, heterogeneity and body size in the Early Triassic: Testing post-extinction paradigms in the Virgin Limestone of Utah, USA. *Australian Journal of Earth Sciences*, **56**, 859–872, https://doi.org/10.1080/08120090903002839.

McNab, B.K. 1971. On the ecological significance of Bergmann's Rule. *Ecology*, **52**, 845–854, https://doi.org/10.2307/1936032.

Metcalfe, B., Twitchett, R.J. & Price-Lloyd, N. 2011. Changes in size and growth rate of 'Lilliput' animals in the earliest Triassic. *Palaeogeography,*

Palaeoclimatology, Palaeoecology, **308**, 171–180, https://doi.org/10.1016/j.palaeo.2010.09.011.

Moghadam, H. V & Paul, C.R.C. 2000. Trace fossils of the Jurassic, Blue Lias, Lyme Regis, southern England. *Ichnos*, **7**, 283–306, https://doi.org/10.1080/10420940009380167.

Morten, S.D. & Twitchett, R.J. 2009. Fluctuations in the body size of marine invertebrates through the Pliensbachian-Toarcian extinction event. *Palaeogeography, Palaeoclimatology, Palaeoecology*, **284**, 29–38, https://doi.org/10.1016/j.palaeo.2009.08.023.

Morton, J.D., Whiteside, D.I., Hethke, M. & Benton, M.J. 2017. Biostratigraphy and geometric morphometrics of conchostracans (Crustacea, Branchiopoda) from the Late Triassic fissure deposits of Cromhall Quarry, UK. *Palaeontology*, **60**, 349–374, https://doi.org/10.1111/pala.12321.

Mousseau, T.A. 1997. Ectotherms follow the converse to Bergmann's Rule. *Evolution*, **51**, 630–632, https://doi.org/10.2307/2411138.

Nürnberg, S., Aberhan, M. & Krause, R.A. 2012. Evolutionary and ecological patterns in body size, shape, and ornamentation in the Jurassic bivalve Chlamys (Chlamys) textoria (Schlotheim, 1820). *Fossil Record*, **15**, 27–39, https://doi.org/10.1002/mmng.201200002.

Olabarria, C. & Thurston, M.H. 2003. Latitudinal and bathymetric trends in body size of the deep-sea gastropod Troschelia berniciensis (King). *Marine Biology*, **143**, 723–730, https://doi.org/10.1007/s00227-003-1116-6.

Page, K.N. 2002. A review of the ammonite faunas and standard zonation of the Hettangian and Lower Sinemurian succession (Lower Jurassic) of the east Devon coast (south west England). *Geoscience in South-West England*, **10**, 293–303.

Page, K.N. 2010. Stratigraphical Framework. *In*: Lord, A. R. & Davis, P. G. (eds) *Fossils from the Lower Lias of the Dorset Coast*. London, The Palaeontological Association, 33–53.

Paris, G., Beaumont, V., Bartolini, A., Clémence, M.-E., Gardin, S. & Page, K.N. 2010. Nitrogen isotope record of a perturbed paleoecosystem in the aftermath of the end-Triassic crisis, Doniford section, SW England. *Geochem. Geophys. Geosyst*, **11**, 1–15, https://doi.org/10.1029/2010GC003161.

Payne, J.L. 2005. Evolutionary dynamics of gastropod size across the end-Permian extinction and through the Triassic recovery interval. *Paleobiology*, **31**, 269–290.

Peck, L.S. & Harper, E.M. 2010. Variation in size of living articulated brachiopods with latitude and depth. *Marine Biology*, **157**, 2205–2213, https://doi.org/10.1007/s00227-010-1486-5.

Powell, J.H. 2010. Jurassic sedimentation in the Cleveland Basin : a review. *Proceedings of the Yorkshire Geological Society*, **58**, 21–72, https://doi.org/10.1144/pygs.58.1.278.

Pugh, A.C., Danise, S., Brown, J.R. & Twitchett, R.J. 2014. Benthic ecosystem dynamics following the Late Triassic mass extinction event : Palaeoecology of the Blue Lias Formation, Lyme Regis, UK. *Proceedings of the Ussher*

Society, **13**, 255–266.

Radley, J.D., Twitchett, R.J., Mander, L. & Cope, J. 2008. Disscussion on palaeoecology of the Late Triassic extinction event in the SW UK. *Journal of the Geological Society*, **165**, 988–992, https://doi.org/10.1144/0016-76492007-029.

Rensch, B. 1948. Histological changes correlated with evolutionary changes of body size. *Evolution*, **2**, 218–230.

Rex, M.A. & Etter, R.J. 1998. Bathymetric patterns of body size: implications for deep-sea biodiversity. *Deep Sea Research Part II: Topical Studies in Oceanography*, **45**, 103–127.

Rhoads, D.C. & Morse, J.W. 1971. Evolutionary and ecologic significance of oxygen-deficient marine basins. *Lethaia*, **4**, 413–428.

Richardson, L. 1911. The Rhaetic and contiguous deposits of west, mid part of east Somerset. *Proceedings of the Geologists' Association, London*, **67**, 1–74.

Richmond, C., Marcus, N.H., Sedlacek, C., Miller, G.A. & Oppert, C. 2006. Hypoxia and seasonal temperature: Short-term effects and long-term implications for Acartia tonsa dana. *Journal of Experimental Marine Biology and Ecology*, **328**, 177–196, https://doi.org/10.1016/j.jembe.2005.07.004.

Richoz, S., van de Schootbrugge, B., et al. 2012. Hydrogen sulphide poisoning of shallow seas following the end-Triassic extinction. *Nature Geoscience*, **5**, 662–667, https://doi.org/10.1038/ngeo1539.

Roy, K. & Martien, K.K. 2001. Latitudinal distribution of body size in north-eastern Pacific marine bivalves. *Journal of Biogeography*, **28**, 485–493, https://doi.org/10.1046/j.1365-2699.2001.00561.x.

Ruhl, M., Deenen, M.H.L., Abels, H.A., Bonis, N.R., Krijgsman, W. & Kürschner, W.M. 2010. Astronomical constraints on the duration of the early Jurassic Hettangian Stage and recovery rates following the end-Triassic mass extinction (St Audrie's Bay / East Quantoxhead, UK). *Earth and Planetary Science Letters*, **295**, 262–276, https://doi.org/10.1016/j.epsl.2010.04.008.

Schmidt, D.N., Thierstein, H.R. & Bollmann, J. 2004. The evolutionary history of size variation of planktic foraminiferal assemblages in the Cenozoic. *Palaeogeography, Palaeoclimatology, Palaeoecology*, **212**, 159–180, https://doi.org/10.1016/j.palaeo.2004.06.002.

Sheppard, T.H. 2006. Sequence architecture of ancient rocky shorelines and their response to sea-level change: an Early Jurassic example from South Wales, UK. *Journal of the Geological Society, London*, **163**, 595–606, https://doi.org/10.1144/0016-764920-015.

Sheppard, T.H., Houghton, R.D. & Swan, A.R.H. 2006. Bedding and pseudo-bedding in the Early Jurassic of Glamorgan: deposition and diagenesis of the Blue Lias in South Wales. *Proceedings of the Geologists' Association*, **117**, 249–264.

Shi, G.R., Zhang, Y.-C., Shen, S.-Z. & He, W.-H. 2016. Nearshore-offshore-basin species diversity and body size variation patterns in Late Permian (Changhsingian) brachiopods. *Palaeogeography, Palaeoclimatology, Palaeoecology*, **448**, 96–107, https://doi.org/10.1016/j.palaeo.2015.07.046.

Shirayama, Y. 1983. Size structure of deep-sea meio- and macrobenthos in the western Pacific. *Internationale revue der gesamten hydrobiologie und hydrographie*, **68**, 799–810.

Simms, M.J. 2003. Uniquely extensive seismite from the latest Triassic of the United Kingdom: Evidence for bolide impact? *Geology*, **31**, 557–560.

Simms, M.J. 2004. The Mendip and South Wales massifs. *In*: Simms, M. J., Chidlaw, N., Morton, N. & Page, K. N. (eds) *British Lower Jurassic Stratigraphy*. Peterborough, Geological Conservation Review Series, No. 30, Joint Nature Conservation Committee, 111–157.

Simms, M.J. & Chidlaw, N. 2004. The Severn Basin. *In*: Simms, M. J., Chidlaw, N. & Morton, N. (eds) *British Lower Jurassic Stratigraphy*. Peterborough, Geological Conservation Review Series, No. 30, Joint Nature Conservation Committee, 164–170.

Simms, M.J. & Jeram, A. 2007. Waterloo Bay, Larne, Northern Ireland: a candidate Global Stratotype Section and Point for the base of the Hettangian Stage and Jurassic System. *ISJS Newsletter*, **34**, 50–68.

Simms, M.J. & Page, K.N. 2004. The East Midlands Shelf. *In*: Simms, M. J., Chidlaw, N., Morton, N. & Page, K. N. (eds) *British Lower Jurassic Stratigraphy, Geolocial Conservation Review Series No. 30*. Peterborough, Joint Nature Conservation Committee, 215–223.

Smith, W. 1797. *An Early List of Strata by William Smith*. MSS pubulished by Douglas, J.A and Cox, L.R. (1949).

Sogot, C.E., Harper, E.M. & Taylor, P.D. 2014. The Lilliput Effect in colonial organisms: Cheilostome bryozoans at the Cretaceous-Paleogene mass extinction. *PLoS ONE*, **9**, e87048.

Song, H., Tong, J. & Chen, Z.-Q. 2011. Evolutionary dynamics of the Permian – Triassic foraminifer size: evidence for Lilliput Effect in the end-Permian mass extinction and its aftermath. *Palaeogeography, Palaeoclimatology, Palaeoecology*, **308**, 98–110, https://doi.org/10.1016/j.palaeo.2010.10.036.

Swift, A. 1999a. Conodonts. *In*: Swift, A. & Martill, D. M. (eds) *Fossils of the Rhaetian Penarth Group*. London, The Palaeontological Association, 183–190.

Swift, A. 1999b. Stratigraphy (including biostratigraphy). *In*: Swift, A. & Martill, D. M. (eds) *Fossils of the Rhaetian Penarth Group*. London, The Palaeontological Association, 15–30.

Timofeev, S.F. 2001. Bergmann's principle and deep-water gigantism in marine crustaceans. *Biology Bulletin of the Russian Academy of Sciences*, **28**, 646–650, https://doi.org/10.1023/A:1012336823275.

Twitchett, R.J. 2006. The palaeoclimatology , palaeoecology and palaeoenvironmental analysis of mass extinction events. *Palaeogeography, Palaeoclimatology, Palaeoecology*, **232**, 190–213, https://doi.org/10.1016/j.palaeo.2005.05.019.

Twitchett, R.J. 2007. The Lilliput Effect in the aftermath of the end-Permian extinction event. *Palaeogeography, Palaeoclimatology, Palaeoecology*, **252**, 132–144, https://doi.org/10.1016/j.palaeo.2006.11.038.

Twitchett, R.J. & Barras, C.G. 2004. Trace fossils in the aftermath of mass

extinction events. *Geological Society, London, Special Publications*, **228**, 397–418, https://doi.org/10.1144/gsl.sp.2004.228.01.18.

Urbanek, A. 1993. Biotic crises in the history of Upper Silurian graptoloids: A Palaeobiological model. *Historical Biology*, **7**, 29–50, https://doi.org/10.1080/10292389309380442.

van de Schootbrugge, B. & Gollner, S. 2013. Altered primary productivity during mass-extinction events. *The Paleontological Society Papers*, **19**, 87–114.

van de Schootbrugge, B., Tremolada, F., et al. 2007. End-Triassic calcification crisis and blooms of organic-walled 'disaster species'. *Palaeogeography, Palaeoclimatology, Palaeoecology*, **244**, 126–141, https://doi.org/10.1016/j.palaeo.2006.06.026.

van Der Have, T.M. & De Jong, G. 1996. Adult size in ectotherms: Temperature effects in growth and differentiation. *Journal of Theoretical Biology*, **183**, 3329–3340.

van Voorhies, W.A. 1996. Bergmann size clines: A simple explanation for their occurrence in ectotherms. *Evolution*, **50**, 1259–1264, https://doi.org/10.2307/2410666.

von Elert, E., Martin-creuzburg, D. & Le Coz, J.R. 2003. Absence of sterols constrains carbon transfer between cyanobacteria and a freshwater herbivore (Daphnia galeata). *Proceedings of the Royal Society of London B*, **270**, 1209–1214, https://doi.org/10.1098/rspb.2003.2357.

Wacker, A. & von Elert, E. 2008. Body size and food thresholds for zero growth in Dressena polymorpha: a mechanism underlying intraspecific competition. *Freshwater Biology*, **53**, 2356–2363.

Ward, P.D., Garrison, G.H., Haggart, J.W., Kring, D.A. & Beattie, M.J. 2004. Isotopic evidence bearing on Late Triassic extinction events , Queen Charlotte Islands, British Columbia , and implications for the duration and cause of the Triassic / Jurassic mass extinction. *Earth and Planetary Science Letters*, **224**, 589–600, https://doi.org/10.1016/j.epsl.2004.04.034.

Waters, R.A. & Lawrence, D.J.D. 1987. *Geology of the South Wales Coalfield, Part III, the Country around Cardiff*. London, Memoirs of the Geological Survey, England and Wales. HMSO.

Weedon, G.P. 1986. Hemipelagic shelf sedimentation and climatic cycles: The basal Jurassic (Blue Lias) of S. Britain. *Earth and Planetary Science Letters*, **76**, 321–335, https://doi.org/10.1016/0012-821X(86)90083-X.

Weiss, M.B., Curran, P.B., Peterson, B.J. & Gobler, C.J. 2007. The influence of plankton composition and water quality on hard clam (Mercenaria mercenaria) populations across Long Island's south shore lagoon estuaries (New York, USA). *Journal of Experimental Marine Biology and Ecology*, **345**, 12–25.

Wignall, P.B. 1990. Benthic palaeocology of the Late Jurassic Kimmeridge Clay of England. *Special papers in palaeontology*, **43**.

Wignall, P.B. 2001. Sedimentology of the Triassic-Jurassic boundary beds in Pinhay Bay (Devon, SW England). *Proceedings of the Geologists' Association*, **112**, 349–360, https://doi.org/10.1016/S0016-7878(01)80014-6.

Wignall, P.B. & Bond, D.P.G. 2008. The end-Triassic and Early Jurassic mass extinction records in the British Isles. *Proceedings of the Geologists' Association*, **119**, 73–84, https://doi.org/10.1016/S0016-7878(08)80259-3.

Wignall, P.B. & Hallam, A. 1991. Biofacies, stratigraphic distribution and depositional models of British onshore Jurassic black shales. *Geoogical Society Special Publications*, **58**, 291–309.

Wobber, F.J. 1965. Sedimentology of the Lias (Lower Jurassic) of South Wales. *Journal of sedimentary petrology*, **35**, 683–703, https://doi.org/10.1306/74D71325-2B21-11D7-8648000102C1865D.

Chapter 3: How quick was marine recovery after the end-Triassic mass extinction and what role did anoxia play?

Published in Palaeogeography, Palaeoclimatology, Palaeoecology

Atkinson, J.W. & Wignall, P.B. 2019. How quick was marine recovery after the end-Triassic mass extinction and what role did anoxia play? *Palaeogeography, Palaeoclimatology, Palaeoecology*, **528**, 99–119, https://doi.org/10.1016/j.palaeo.2019.05.011.

How quick was marine recovery after the end-Triassic mass extinction and what role did anoxia play?

J.W Atkinson* and P. B. Wignall

School of Earth and Environment, University of Leeds, Leeds, LS2 9JT

*gy12jwa@leeds.ac.uk

3.1 Abstract

Oxygen restricted conditions were widespread in European shelf seas after the end-Triassic mass extinction event and they are reported to have hindered the recovery of marine benthos. Here we reconstruct the redox history of the Early Jurassic Blue Lias Formation of southwest Britain using pyrite framboid size analysis and compare this with the recovery of bivalves based on field and museum collections. Results suggest widespread dysoxia punctuated by periods of anoxia in the region, with the latter developing frequently in deeper water settings. Despite these harsh conditions, initial benthic recovery occurred rapidly in the British Jurassic, especially in shallowest settings, and shows no relationship with the intensity of dysoxia. A stable diversity was reached by the first recognised ammonite zone after the end-Triassic mass extinction. This contrasts with the deeper-water, more oxygen-poor sections where the diversity increase was still continuing in the earliest Sinemurian Stage, considerably longer than previously reported. Similar recovery rates are seen amongst other groups (brachiopods and ammonites). Oxygen-poor conditions have been suggested to delay recovery after the Permo-Triassic mass extinction, but this is not the case after the end-Triassic crisis. We suggest that this was because the European

dysoxia was only a regional phenomenon and there were plenty of well-ventilated regions available to allow an untrammelled bounce back.

Keywords: Pyrite framboids, Early Jurassic, Blue Lias Formation, benthic recovery, diversification

3.2 Introduction

Marine anoxia has been implicated as a cause of delayed biotic recovery from the end-Triassic mass extinction event, especially in Western Europe (Hallam 1996; Mander *et al.* 2008; Clémence *et al.* 2010; Richoz *et al.* 2012; Jost *et al.* 2017; Luo *et al.* 2018). The evidence for oxygen-restriction includes widespread black shale deposition in the epicontinental seaway of Europe during the earliest Hettangian and again during the Sinemurian (Wignall & Hallam 1991; Richoz *et al.* 2012; van de Schootbrugge *et al.* 2013). The intensity of oxygen deficiency has been assessed using a range of proxies: redox sensitive trace metals such as Th/U (Hallam 1995; Wignall 2001) and molybdenum (Breward *et al.* 2015), pyrite sulphur isotopes (Jaraula *et al.* 2013; Luo *et al.* 2018), uranium isotopes (Jost *et al.* 2017) and the presence of isorenieratene (Richoz *et al.* 2012; Jaraula *et al.* 2013; Naeher & Grice 2015; Blumenberg *et al.* 2016).

Many studies have only focussed on short stratigraphic intervals in the earliest Hettangian sedimentary record in Western Europe, because this is the immediate post-mass extinction interval. These show that dysoxic conditions, punctuated by episodic anoxia and photic zone euxinia (PZE), were widespread at this time (e.g. Hallam 1995, 1997; Wignall 2001; Paris *et al.* 2010; Richoz *et al.* 2012; Jaraula *et al.* 2013; Naeher & Grice 2015). Studies in Germany, Luxemburg and

Switzerland demonstrate that these conditions persisted from the middle Hettangian to the lowermost Sinemurian (Schwab & Spangenberg 2007; Richoz *et al.* 2012; Luo *et al.* 2018). Away from the European epicontinental sea there is some suggestion of PZE from north-eastern Panthalassa (Kasprak *et al.* 2015) but oxic deposition is suggested in other regions of this ocean recorded in accreted terranes of Japan (Wignall *et al.* 2010; Fujisaki *et al.* 2016). In no region is it clear how long the marine recovery took and how it relates to the redox record.

This study aims to reconstruct redox conditions of southwestern Britain from the beginning of recovery following the end-Triassic mass extinction through to the Sinemurian Stage, using pyrite framboid size analysis. This will then be compared with the bivalve recovery, based on field and museum collections, to evaluate the notion that anoxia delayed recovery at this time. The size distribution of pyrite framboids is a powerful tool used to assess redox conditions (e.g. Wignall & Newton 1998; Huang *et al.* 2017). Framboids are spheres of aggregated pyrite microcrysts that form at the boundary between oxic and sulphidic waters (Wilkin *et al.* 1996). Under euxinic conditions the redox boundary occurs in the water column where framboids grow, but they do not achieve diameters much beyond 5 μm before sinking to the seabed (Wilkin *et al.* 1996). In contrast, in dysoxic settings the redox boundary is within the uppermost sediments and framboids grow to a wide range of sizes with a larger mean diameter (Wilkin *et al.* 1996). This size distribution has been shown for the modern (Wilkin *et al.* 1996) and also in ancient sediments where framboid analyses have been corroborated by independent palaeontological and geochemical redox indicators (Wignall & Newton 1998; Huang *et al.* 2017).

Variable degrees of oxygen restriction are thought to be represented by differing size classes of framboid populations (Table 1 in Bond & Wignall 2010).

Defining a biotic recovery can be problematic, and several different alternatives have been used. The onset of recovery is often defined as the point when origination rates exceed extinction rates and recovery is assumed complete once pre-extinction diversity is attained (Kauffman & Erwin 1995). Such a simple measure is not suitable for the British record of the recovery from the end-Triassic mass extinction, because diversity in the pre-extinction interval was low due to unusual salinities that were quite different to the fully marine settings that develop in the aftermath (Hallam & El Shaarawy 1982). A period of rising diversity followed by stabilisation may provide a better assessment of the recovery interval (Damborenea *et al.* 2017). An alternative four-phase model for recovery, incorporating ecological parameters, was created based on observations of the recovery following the end-Permian mass extinction (Twitchett 2006, referred to here as the Twitchett recovery model). Phase one consists of high abundance, low diversity faunas (low evenness) with small body sizes and minimal ecological tiering. The following stages of recovery see an expansion of benthic tiering levels, an increase in evenness, species richness, body size and appearance of key ichnotaxa.

3.3 Geological setting

The Cotham Member of the Lilstock Formation features rippled fine sandstones, deep fissures and severe soft sediment deformation (Simms 2003). It is within this member that the end-Triassic extinction is located (Wignall & Bond 2008), and is succeeded by the Langport Member of the same formation. Micritic

carbonates dominate the Langport Member and were deposited within a shallow epicontinental sea of uncertain salinity (Hallam & El Shaarawy 1982). An erosion surface and intraformational conglomerate caps the Member in Devon (Wignall 2001), although in other areas the contact is more gradational and apparently conformable.

The Hettangian to lowermost Sinemurian (Early Jurassic) Blue Lias Formation of southwestern Britain was deposited in an epicontinental sea that covered much of north-western Europe during the Lower Jurassic (Hallam 1960). The Formation consists of rhythms of limestone, marl and shale (Hallam 1960; Paul *et al.* 2008), which are thought to record climate-driven cycles in seafloor oxygenation and sedimentation due to Milankovitch periodicities (Weedon 1986; Bottrell & Raiswell 1989; Moghadam & Paul 2000; Wignall 2001; Clémence *et al.* 2010; Ruhl *et al.* 2010). Weedon (1986) defined the five lithotypes of the Blue Lias used here:

Bioturbated limestones may occur as semi-continuous beds, or nodular horizons within pale marls. These often bear irregular and uneven bed contacts though they can also be planar. Beds are homogenous and bioturbated with up to seven ichnotaxa recorded and are considered to have formed under a fully aerated water column (Weedon 1986; Moghadam & Paul 2000). Bivalves, including *Plagiostoma, Gryphaea* and *Pinna*, are typically common. Total organic carbon (TOC) is variable, with values ranging from 0.14-1.64 wt% (Weedon *et al.* 2018a). These beds become increasingly dominant in shallower water sections (Hallam 1964).

Pale marls are light blue-grey, homogenous beds bearing a diverse trace fossil assemblage, suggesting good seafloor oxygenation. TOC is typically higher

than in the limestones at 0.38-4.41 wt% (Weedon *et al.* 2018a), and silt-grade quartz grains are more common (Hallam 1960).

Dark marls are similar to pale marls, however they have a weak fissility, especially when weathered. These marls show planar contacts with the pale marls and have an increased TOC range of 0.51-6.51 wt% (Weedon *et al.* 2018a). Dark marls also have less diverse trace fossil assemblages dominated by *Chondrites* and only one or two additional ichnospecies, suggesting weaker oxygenation than seen in the pale marls (Moghadam & Paul 2000).

Shales appear as dark brown or black beds, these weather to become very fissile, occasionally showing millimetre-scale laminae. Fossils are usually confined to nektic organisms and small bivalves (Hallam 1960). Of the five lithologies of the Blue Lias, the shale beds have the highest TOC values, typically between 1.53 -12.8 wt%, and record intervals of anoxia (Ebukanson & Kinghorn 1990; Wignall & Hallam 1991; Weedon *et al.* 2018a).

Laminated limestones exhibit planar bedding surfaces and are laminated. TOC values can be twice as great as seen in bioturbated limestones with values of 0.9-3 wt% and they have a fetid odour when freshly broken (Weedon 1986; Weedon *et al.* 2018a). The laminated limestones are considered to have originally been black shales that have been diagenetically-overprinted by carbonate (Arzani 2004).

The relative contribution of each lithology varies between location and stratigraphic interval allowing regional members of the Blue Lias Formation to be defined and correlated using ammonite biozonation schemes (Fig. 3.1).

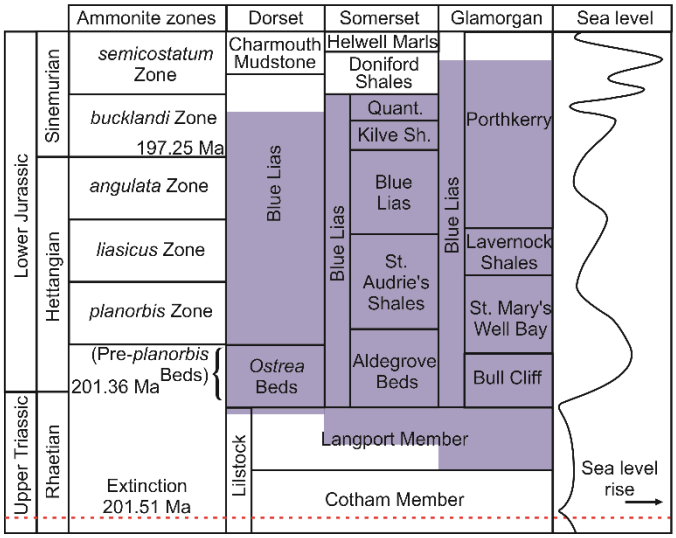

Figure 3.1 Lithological correlation of members of the Blue Lias Formation, after Hodges (2000). Quant. – Quantock Beds, Kilve Sh. – Kilve Shales. Shaded regions depict sampled interval, dashed line position of extinction horizon. Relative sea level curve from Hesselbo and Jenkyns (1998); Hesselbo et al. (2004) and Wignall and Bond (2008), extinction and boundary ages from Wotzlaw *et al*. (2014) and Weedon *et al*. (2018b).

Limestone beds are most prevalent in the Pre-*planorbis* Beds and *planorbis* and *angulata* zones, whereas the *liasicus* Zone has lower proportions of limestones and is thought to be due to deepening caused by accelerated sea level rise at this time (Hesselbo and Jenkyns 1998; Sheppard 2006; Weedon *et al.* 2018a). The higher proportions of limestones in the succeeding *angulata* Zone is attributed to a lowering of relative sea level prior to another deepening episode during the *bucklandi* Zone (Sheppard 2006). Limestone-rich sections on the Glamorgan coastline were deposited closer to a palaeo-shoreline than the mud-dominated Somerset sections (Wobber 1965; Johnson & McKerrow 1995).

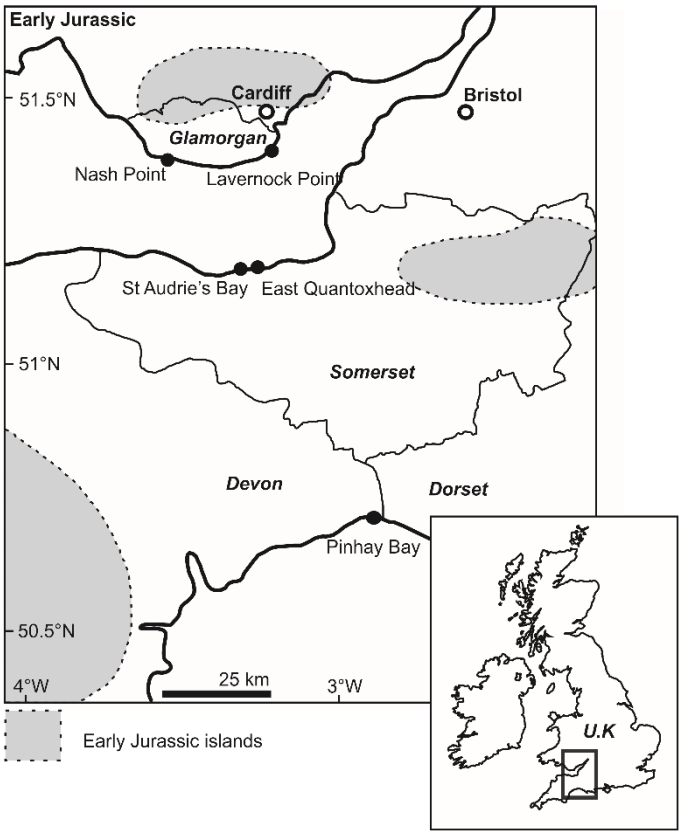

Fig. 3.2 Location map and palaeogeography of southwestern Britain, Early Jurassic islands indicated by shaded regions, modified from Martill *et al.* (2016).

3.4 Materials and methods

Sampling was undertaken in three regions (Fig. 3.2): Glamorgan (South Wales), Somerset and Devon (southwest England). Stratigraphic height of sampling was determined using published sedimentary logs where available (Hesselbo & Jenkyns 1995; Bloos & Page 2002; Simms 2004) or logged by the authors during sampling and dated by use of ammonites. For Glamorgan two localities were sampled: Lavernock Point (ST 188 682 – ST 183 679) spanning the Langport Member to *liasicus* Zone and Nash Point (SS 911 692 – SS 921 679) covering the *angulata* to *bucklandi* zones. For Somerset, again two localities

were sampled: St Audrie's Bay (ST 103 434 – ST 099 433) and East Quantoxhead (ST 134 442 – ST 142 444), spanning the upper Langport Member to *liasicus* Zone and *angulata* to *bucklandi* zones respectively. For Devon only Pinhay Bay (SY 317 907 – SY 333 914) was sampled, this spanning topmost Langport Member to *bucklandi* Zone. The five lithologies of the Blue Lias: bioturbated limestone, pale marl, dark marl, shale and laminated limestone (described above) were recorded and sampled.

At each sample horizon bivalve diversity was assessed by species counts and life modes assigned from published sources (Supplementary appendix B). First occurrence of crinoids was also noted. In mudstones, marls and shales bivalves were identified from freshly split surfaces of approximately equal volume of rock (~0.5 x 0.5 x 0.3 m). For limestone beds fossils were identified *in situ* on weathered bedding surfaces, owing to this different sampling method abundance data are presented separately. In addition, bivalve diversity was also assessed by combining field observations with occurrences based on museum specimens. This was undertaken only for Glamorgan due to the extensive collection of stratigraphically-tied specimens housed within the National Museum of Wales (NMW) and conducted at the resolution of ammonite zone. For the lower interval of the Blue Lias Formation lacking ammonites the Pre-*planorbis* Beds are used here as a time bin as is the Langport Member.

For each section a subset of sampled horizons was used to test for changes in oxygenation regime using pyrite framboids. The method was adapted from that of Wignall and Newton (1998). Pyrite framboid diameters were measured from polished stone chips approximately 2 x 1 cm in size set into resin blocks. These were carbon coated and viewed using a Tescan VEGA3 XM scanning electron microscope (SEM) with a backscatter electron detector. By

adjusting the brightness and contrast this allows pyrite to stand out from the matrix. Framboids were then located by scanning across the sample surface and diameters measured using inbuilt measurement applications of the SEM. Each sample was analysed for up to one hour or until 100 framboids had been measured. Mean framboid diameter and standard deviation were then calculated per sample and plotted on what are referred to herein as a Wilkin diagram (Wilkin *et al.* 1996). Results of framboid analysis of bed H1 from Pinhay Bay presented in Wignall (2001) are incorporated into this study. It is important to note that each 1 cm-thick sample area can record up to several thousands of years of deposition (Weedon *et al.* 2018b). Thus, each sample potentially records a range of oxygenation regimes developed during such intervals and accounts for the fact that euxinic populations can sometimes occur in samples with benthic fossils that record seafloor oxygenation (Bond & Wignall 2010).

Mean framboid diameters and standard deviations are correlated with raw species richness per sample horizon using Spearman's rank correlation, conducted in PAST statistical software (Hammer *et al.* 2001).

3.5 Results

3.5.1 Pyrite framboids

3.5.1.1 Lithological variability

Pyrite framboids were found in all samples from both the Langport Member and the Blue Lias Formation irrespective of lithology. Photographic representations of pyrite framboids formed under anoxic and dysoxic regimes are shown in Fig. 3.3.

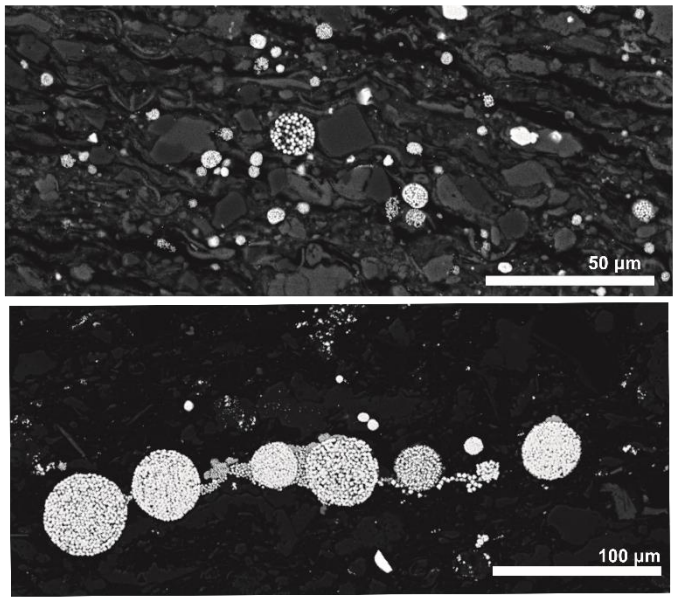

Fig. 3.3 Example populations of pyrite framboids from an anoxic mudstone (Q39, top) and a dysoxic marl (NP15, bottom).

In the Langport Member, only two samples are examined for framboids, these were collected from Lavernock Point (LP9 and LP21). Framboids are not abundant but both samples still yield at least 100, although euhedral crystals of pyrite are more common. These samples have an average framboid diameter of 10.7 µm, but show wildly different standard deviations placing LP21 in the mid-dysoxic region of a framboid mean-standard deviation plot (Wilkin diagram), whilst LP9 plots as being uppermost dysoxic (Fig. 3.4).

Fifty-one samples of bioturbated limestone are analysed and, of the five Blue Lias lithotypes, they are found to have the least pyrite, with euhedral crystals, and pyrite-replaced bioclasts being more common than framboids. Despite this observation, only four samples failed to yield 100 framboids within the allotted one-hour analysis time. Framboids are typically concentrated into discrete clusters or loose patches. Average diameter of framboids is 8.7 µm, with

the largest being 70.0 µm. The populations typically plot in the mid to upper dysoxic region of the Wilkin diagram (Fig. 3.4).

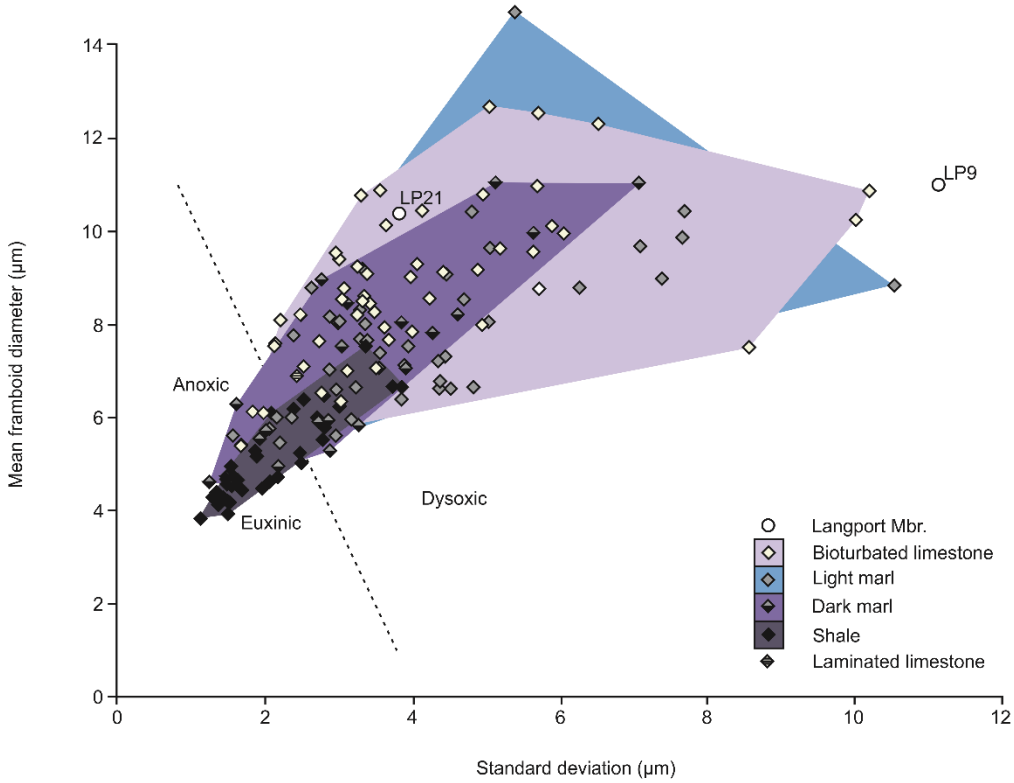

Fig. 3.4 Mean framboid diameter (µm) against standard deviation of framboid diameters (Wilkin diagram), samples plotted according to lithology. Dashed line dictated anoxic-dysoxic threshold. Shaded regions illustrate spread of results.

Three samples plot in the anoxic field, these are two from St. Audrie's Bay (SAB52, SAB53) and one from East Quantoxhead (Q76) – these are not laminated limestones although they do exhibit planar contacts in the field (Figs. 3.5 & 3.6).

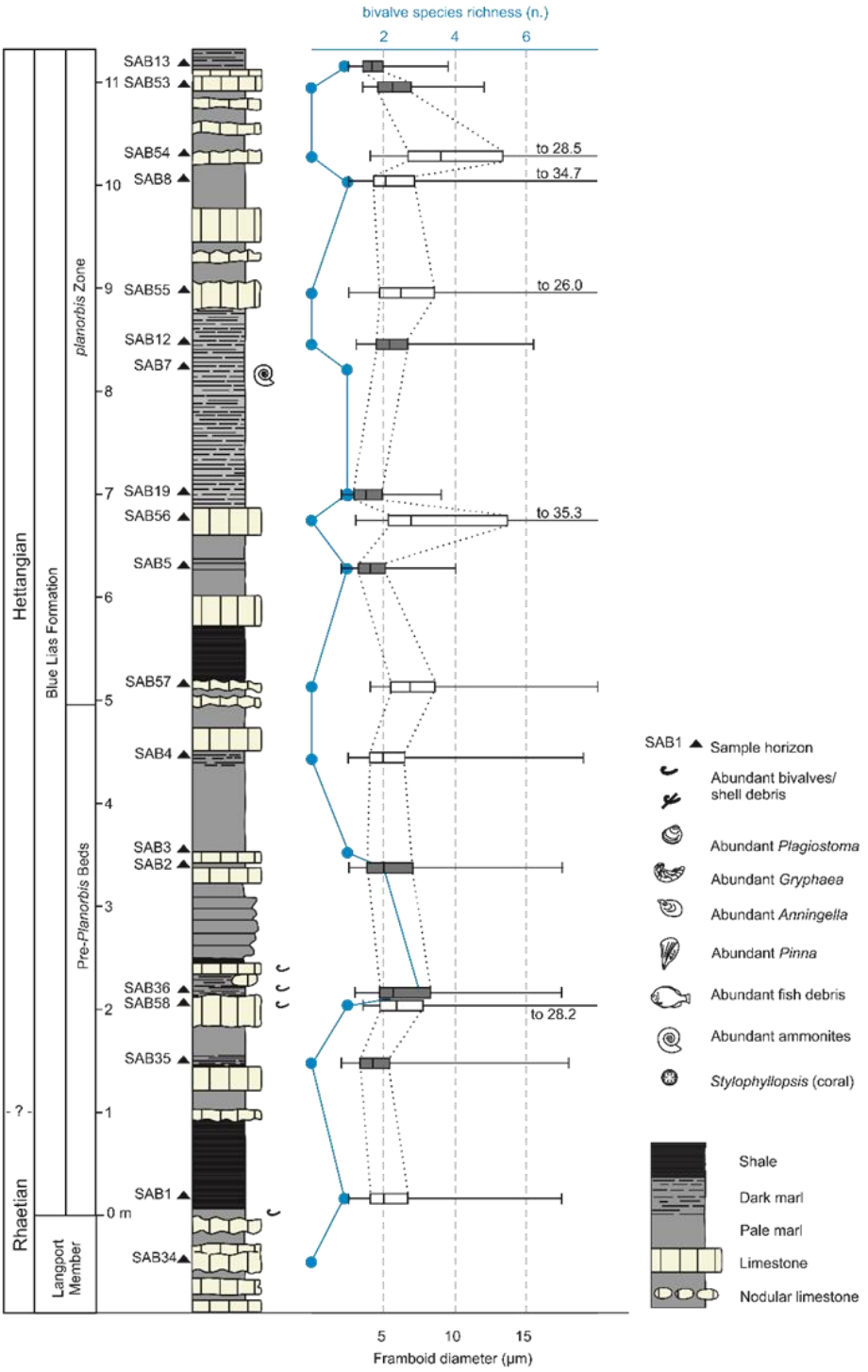

Fig. 3.5 St. Audrie's Bay, Somerset. Box and whisker plots, box depicts 25th and 75th percentiles, central line is median, whiskers illustrating minimum and maximum framboid diameters. Shaded boxes indicate samples that plot below the oxic-anoxic line on a Wilkin diagram. Solid circles record raw species richness per sampled horizon. Approximate position of Triassic-Jurassic boundary from Weedon *et al.* (2018b).

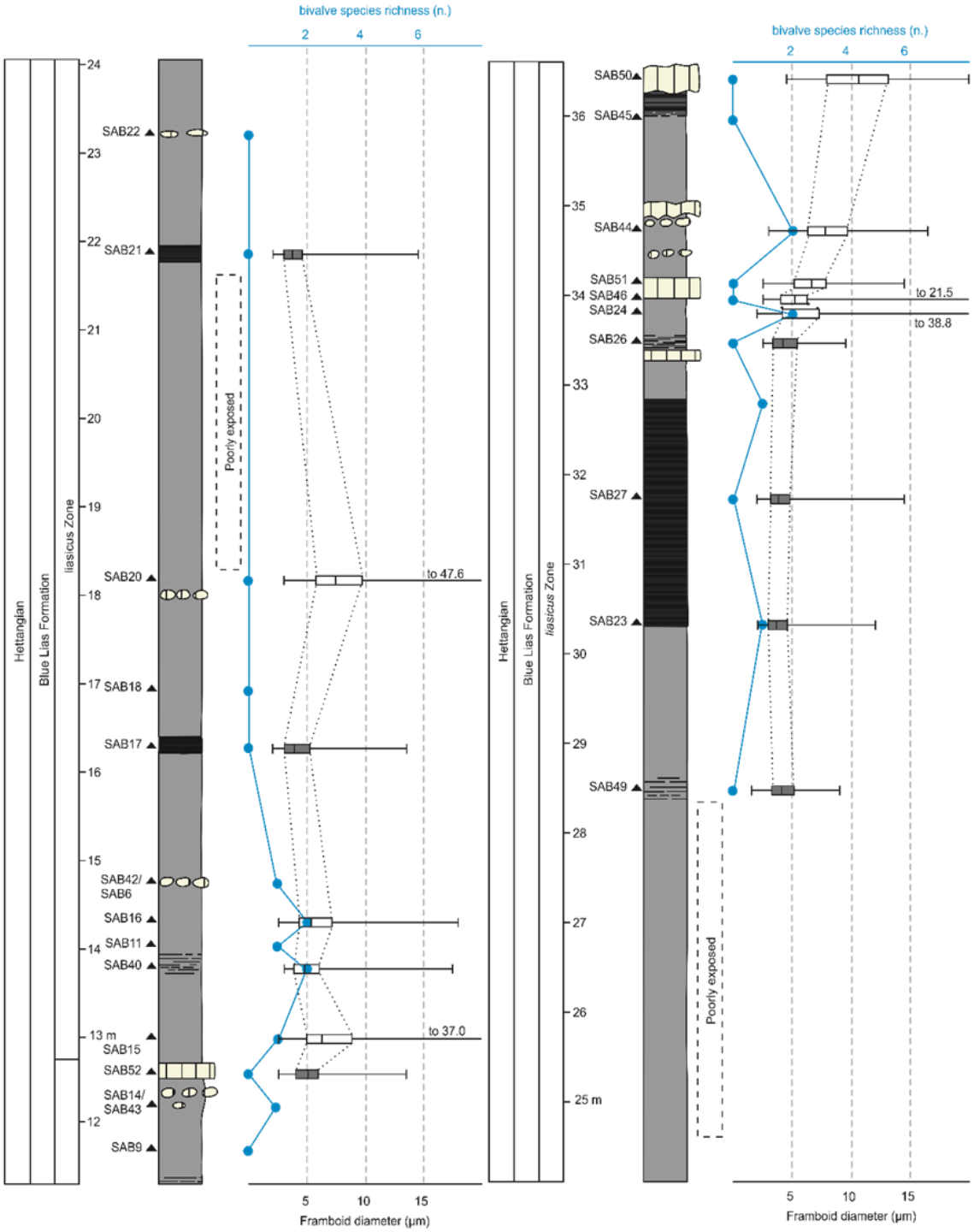

(Fig. 3.5 continued)

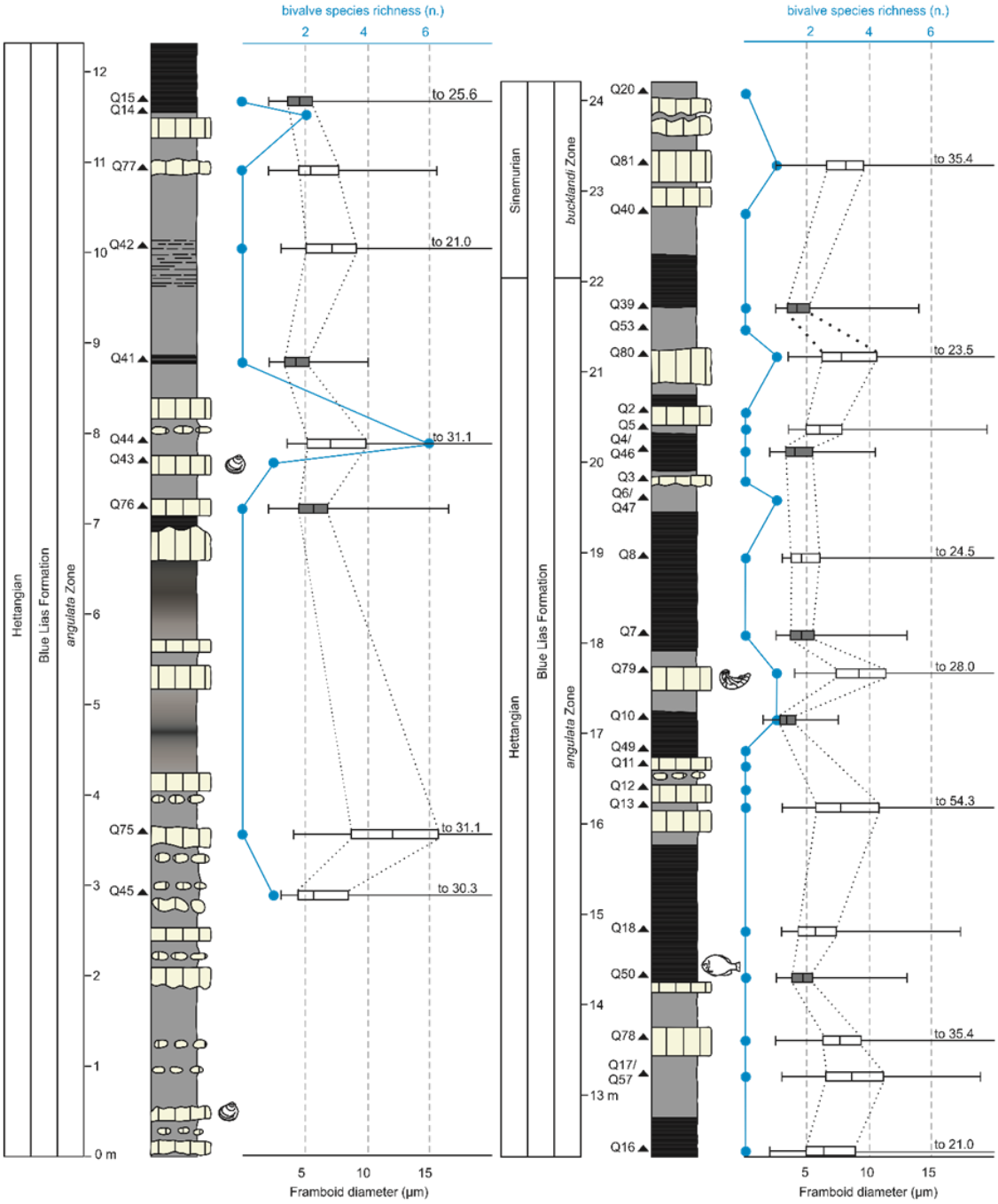

Fig. 3.6 East Quantoxhead Somerset, sedimentary log modified from Bloos and Page (2002) see Fig. 3.5 for details.

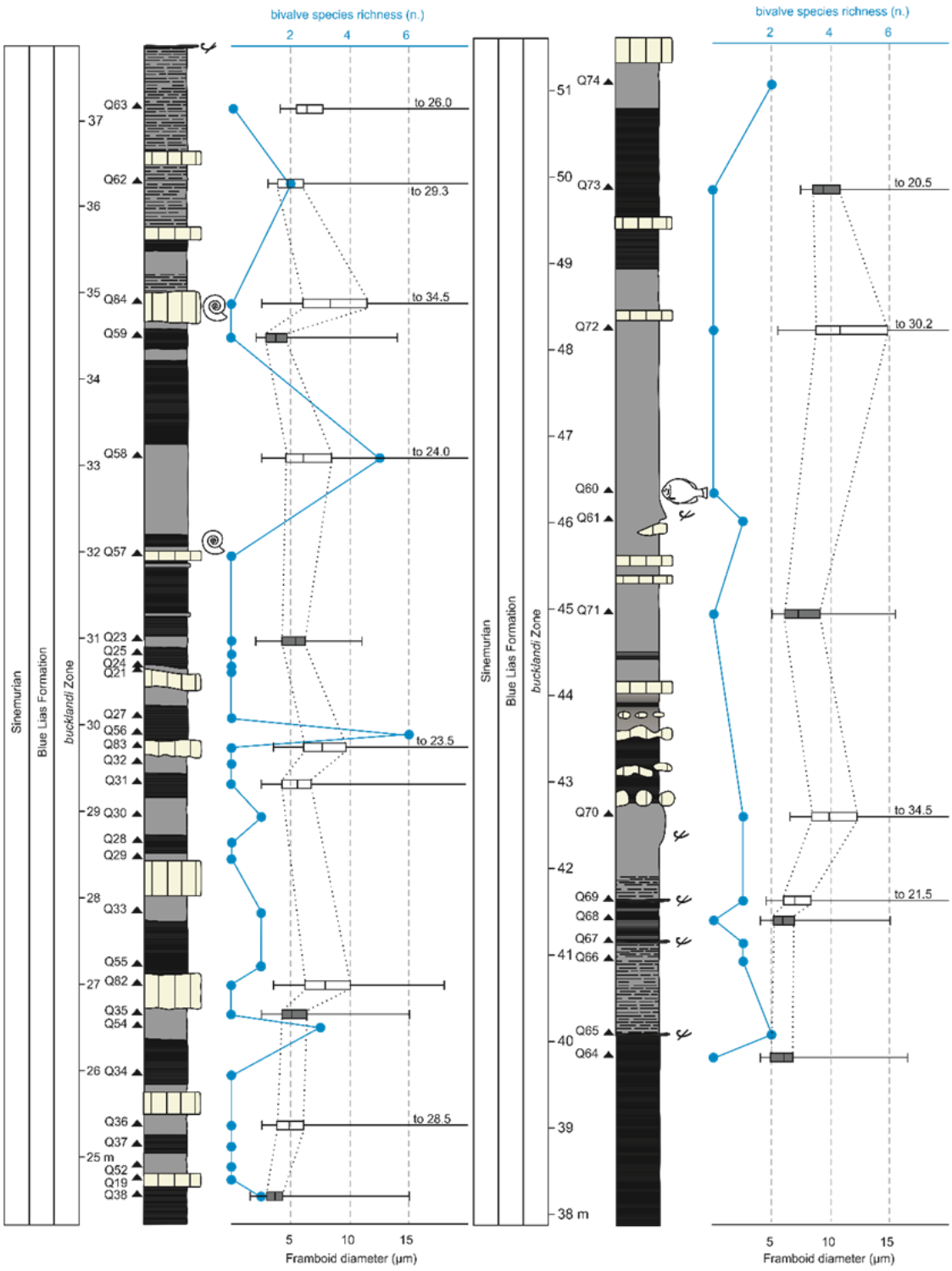

(Fig. 3.6 continued)

Forty-seven samples of bioturbated, pale marls are analysed, these typically contain a low to moderate abundance of pyrite with a mixture of framboidal and euhedral forms and void-filling internal spaces of bioclasts. Pyrite framboids are restricted to specific horizons or clusters often bound by a dense carbonate cement. Average framboid diameter is 7.9 μm with largest being 75.3 μm (Fig. 3.4). The framboids exhibit the largest variability of all Blue Lias lithotypes on the Wilkin diagram, with four samples plotting as anoxic (Fig. 3.4).

Twenty-three samples of dark marl are analysed which reveal a mixture of euhedral and, more commonly, framboidal forms of pyrite. In contrast to the framboids found in pale marls, they occur evenly distributed throughout the samples. Average framboid diameter is 6.9 μm, the largest being 43.2 μm. Most dark marl samples plot within the anoxic—mid dysoxic field (Fig. 3.4).

Thirty-one samples of shale are studied. These contain very high concentrations of pyrite, with the majority being small framboids. Average diameter is 5.2 μm although rare, large framboids attain a maximum of 33.9 μm (Fig .3.4). Most plot within the euxinic/anoxic field.

Only one sample of laminated limestone is analysed, collected from between two shale beds at Lavernock Point (Fig. 3.7). Pyrite is common with small framboids scattered evenly throughout. Average diameter is 6.9 μm placing it in the lower dysoxic field (Fig. 3.4).

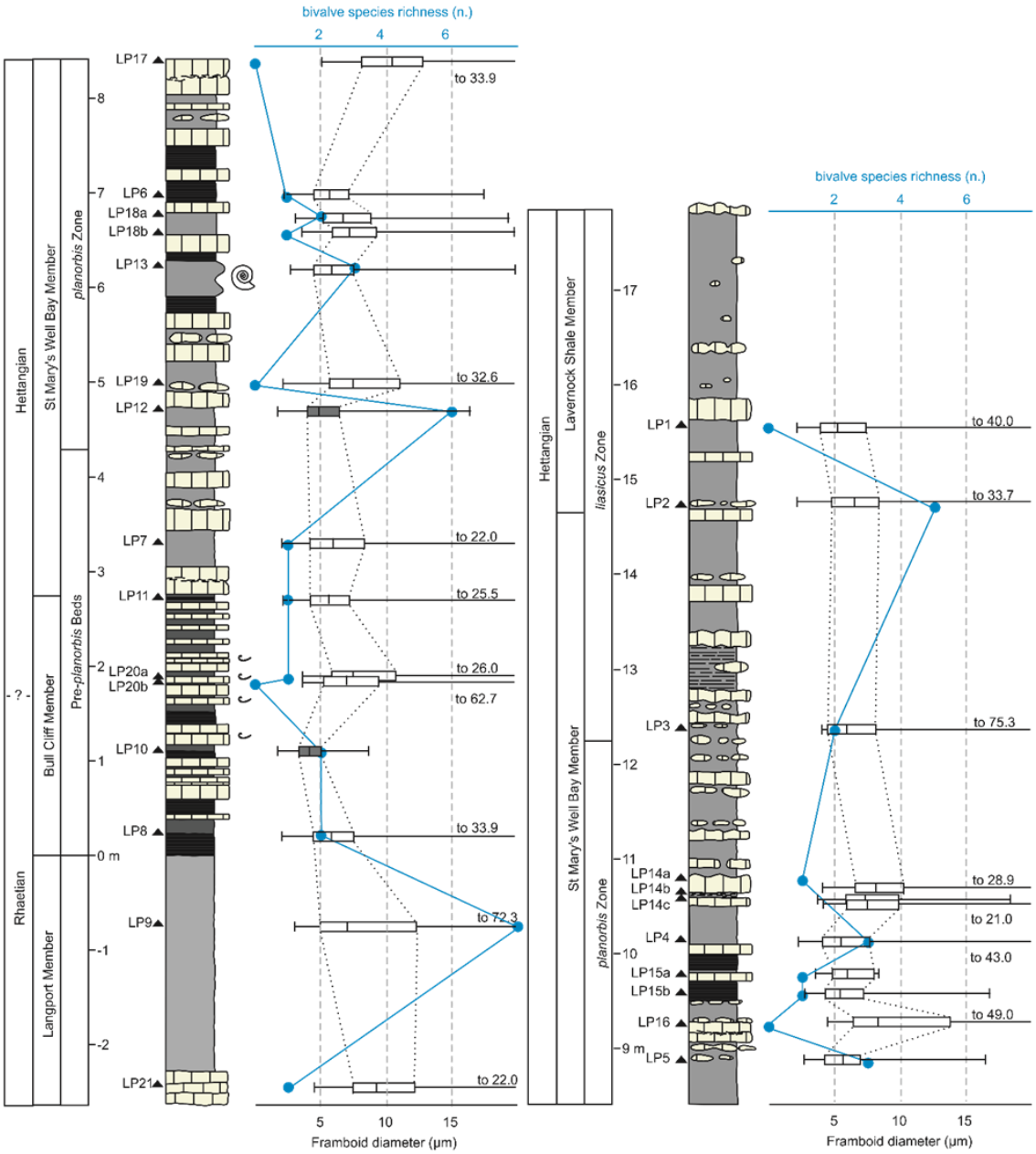

Fig. 3.7 Lavernock Point, Glamorgan. Sedimentary log modified from Simms (2004). See Fig. 3.5 for details

3.5.1.2 Regional variability

As framboids were only analysed in the Langport Member of Glamorgan regional variability is only assessed for Blue Lias Formation samples. Glamorgan sections were deposited close to a palaeo-shoreline and are the most proximal

ones examined in this study (Wobber 1965; Johnson & McKerrow 1995). Overall, the framboids from this region have the largest average diameter (8.13 μm), and the greatest variability with an average standard deviation of 4.23 μm indicating the highest oxygenation levels. At Lavernock Point two of the beds plot in the anoxic field (LP10 and LP12; Fig. 3.7). The former (LP10) being from the Bull Cliff Member, which is distinct from other levels of the Blue Lias Formation in showing planar beds with a high abundance of fossil oysters. That aside, the remaining four samples from the Bull Cliff Member plot as mid-upper dysoxic populations. Despite shales and laminated limestones featuring in the *planorbis* Zone of Lavernock Point these beds do not plot as anoxic. The greater part of the Lavernock section plots as variably dysoxic. Very little of the Lavernock Shale Member was sampled as these are poorly exposed in the foreshore, however the succeeding Porthkerry Member is well exposed at Nash Point. This section shows a marked upward increase in both the abundance and thickness of limestone beds and lacks shales (Fig. 3.8).

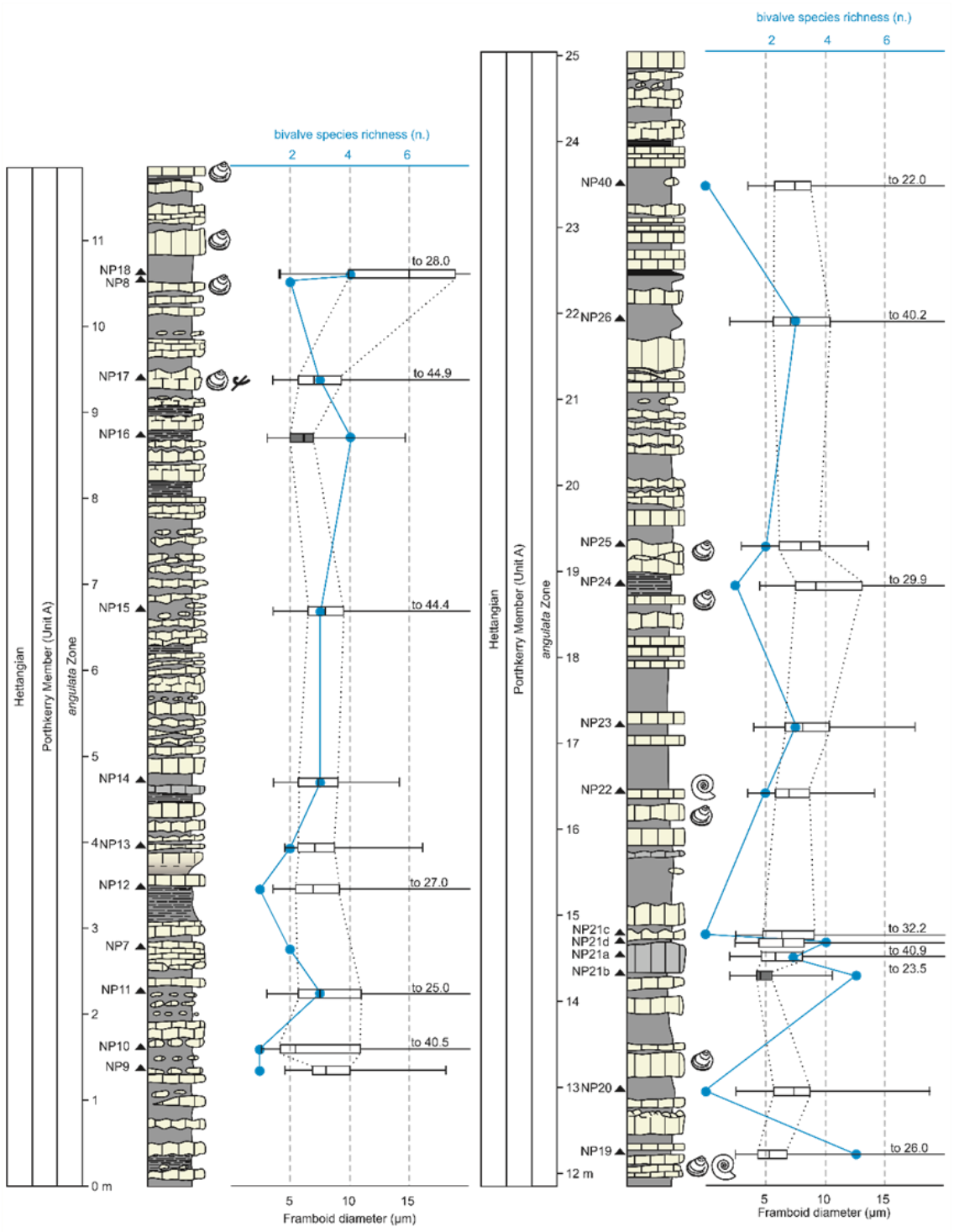

Fig. 3.8 Nash Point, Glamorgan, see Fig. 3.5 for details.

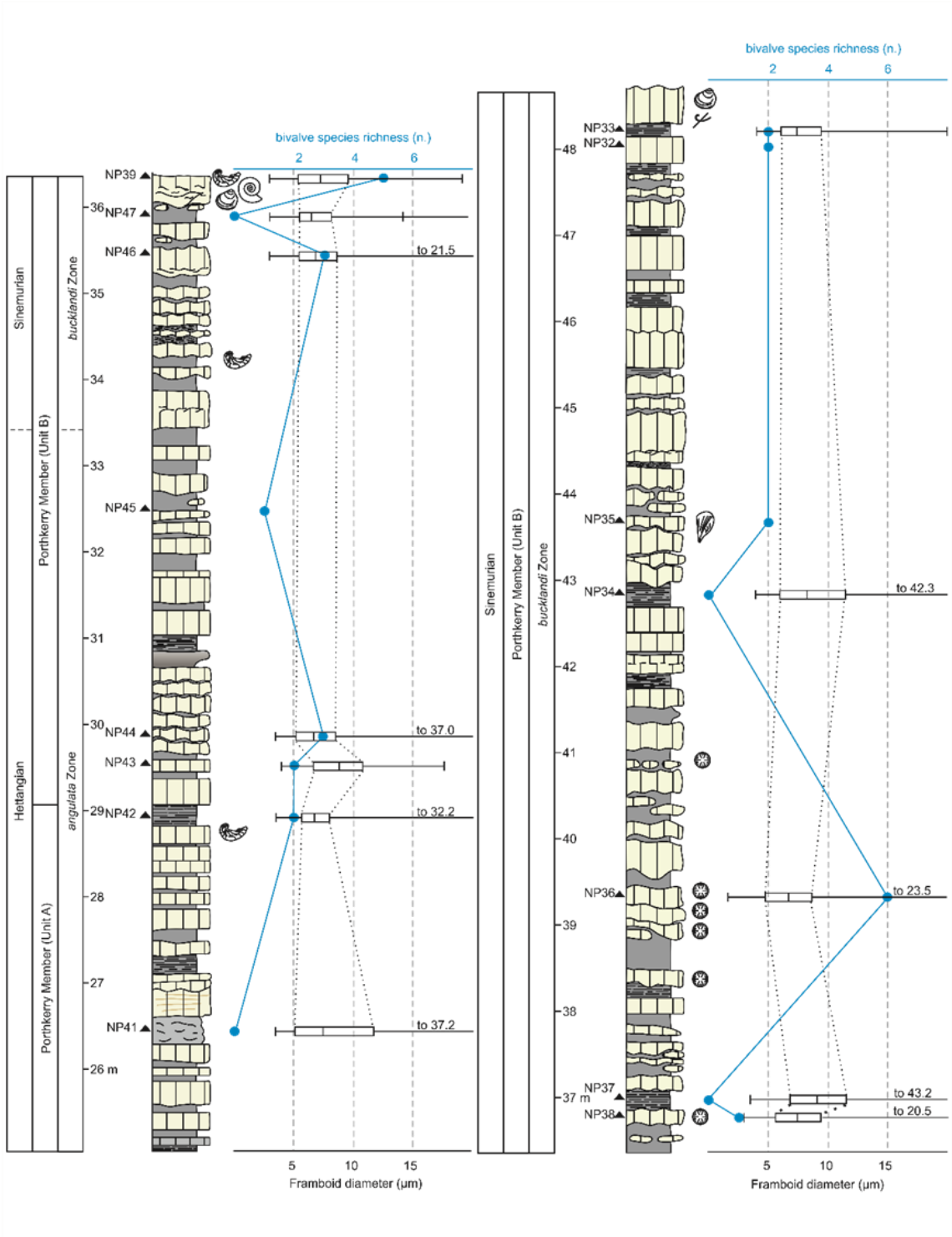

(Fig. 3.8 continued)

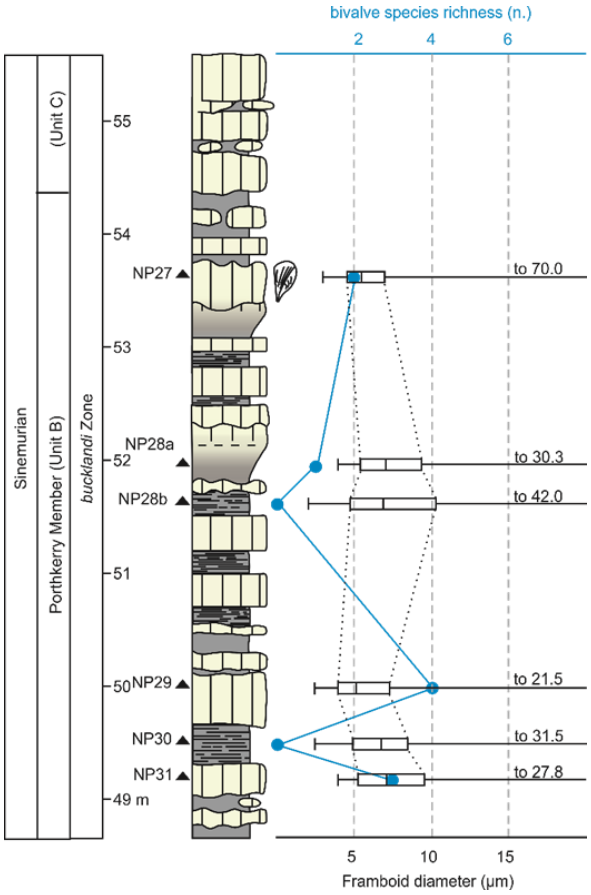

(Fig. 3.8 continued)

A total of 38 of the 40 samples from this section plot as mid-upper dysoxic, with pale marls and limestones potting within the same region and dark marls nestled within (Fig. 3.9).

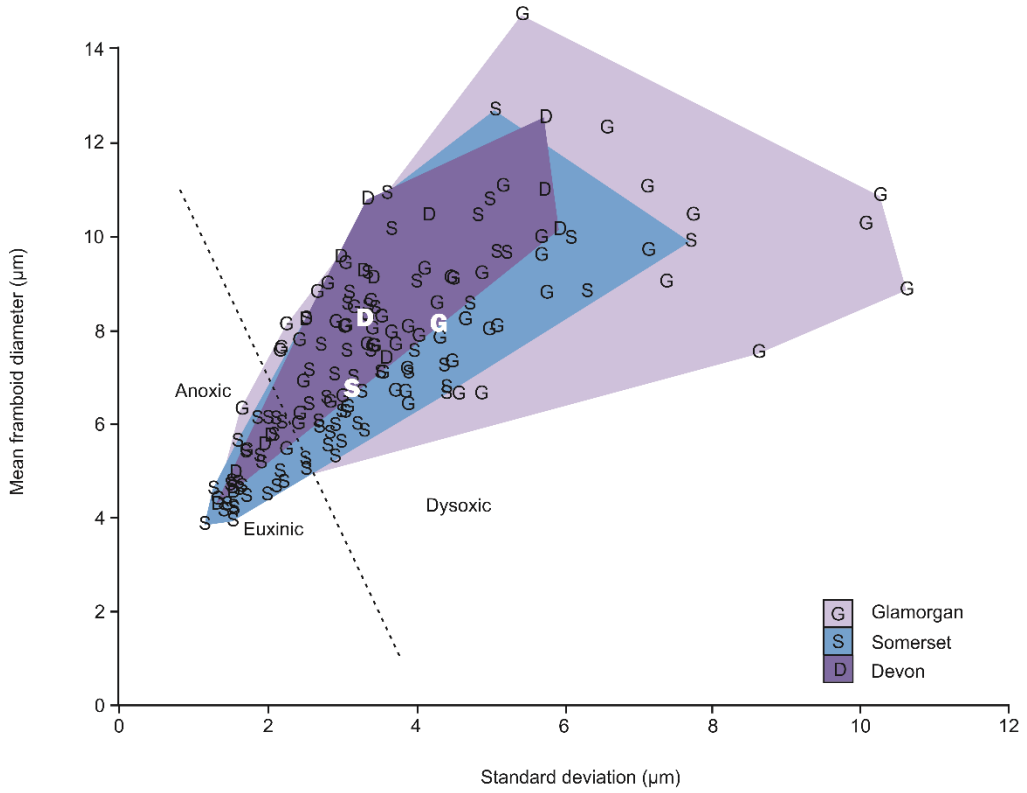

Fig. 3.9 Wilkin diagram, samples plotted according to geographic region. D – Devon, S – Somerset, G – Glamorgan. Means of each location indicated as a bold white letter.

two anoxic beds are recorded, the lower of these occurs within a dark, weakly laminated marl in the lower portion of the section where limestones are thin and nodular. The second occurs directly below a distinct thick, grey limestone. The limestone itself (NP21a) plots within the dysoxic field and makes a good marker bed, being one of the few limestones not of yellow-beige colour.

The Somerset sections record the deepest-water settings studied (Fig. 3.2). SEM analysis shows the sediments contain less silt-grade quartz than seen in Glamorgan and are more coccolith- and clay-rich. Across the span of the study interval the classic lithological rhythms of the Blue Lias are well developed. Somerset, overall has the smallest average framboid diameters of the three

regions studied (6.72 μm and standard deviation of 3.07 μm). The framboid size distributions with the shales and most of the dark marls plot within the euxinic-anoxic region whilst pale marls and limestones generally plot in the mid-upper dysoxic field (Figs. 3.5 & 3.6). Across Somerset an approximately 2 m-thick, blue-grey weathering shale occurs, that contains large numbers of the ammonite *Psiloceras*, the bivalve *Anningella* and fish debris. The framboids from this level plot in the anoxic field (Fig. 3.5). Unlike the Nash Point section, East Quantoxhead (which is of equivalent age) features many euxinic, paper shales, that are often thickly developed (Figs. 3.6 & 3.8).

Pinhay Bay is a limestone-dominated section that is by far the most condensed of all the sections in the three regions studied. All limestones beds contain framboids that plot within the dysoxic field (Figs. 3.9 & 3.10). Of the few marls and shales sampled the greater majority plot as anoxic, suggesting the anoxic-dysoxic rhythms seen in Somerset are also present in Devon (Fig. 3.10). Devon has an overall mean framboid diameter of 8.22 μm (standard deviation of 3.24 μm), this being comparable to the Glamorgan average, albeit with a smaller standard deviation. Both Devon and Glamorgan represent deposition in shallower, better oxygenated waters than those of Somerset and the average framboid diameters reflect this, being smaller in the deeper water.

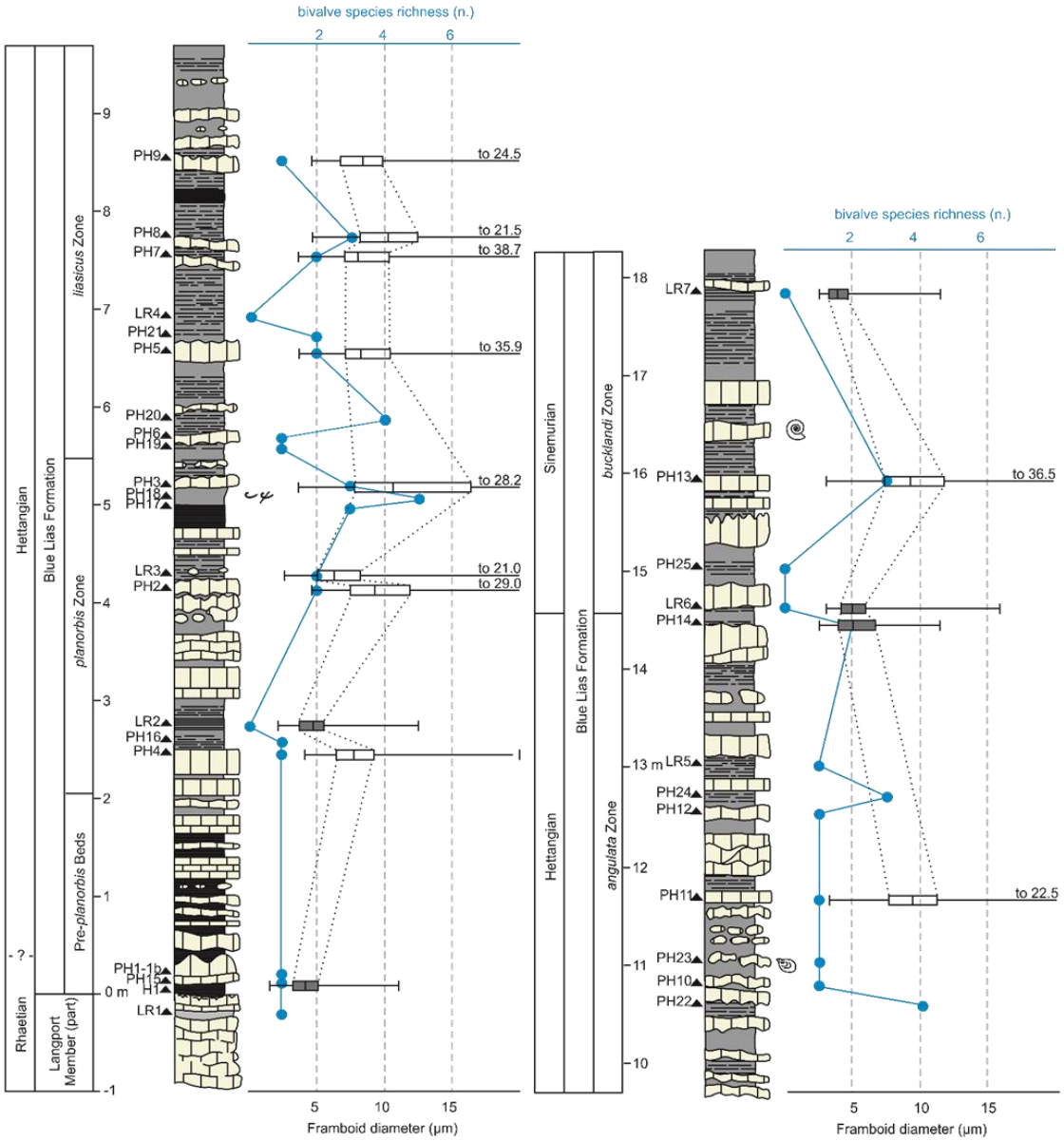

Fig. 3.10 Pinhay Bay, Devon. Sedimentary log modified from Hesselbo and Jenkyns (1995). See Fig. 3.5 for details.

3.5.1.3 Temporal variability

Dividing the 155 samples from all localities into ammonite zone time bins (including the Pre-*planorbis* Beds and the Langport Member) allows for long-term temporal trends to be tested. All zones plot as mostly dysoxic with occasional forays into anoxic or euxinic conditions (Fig. 3.11).

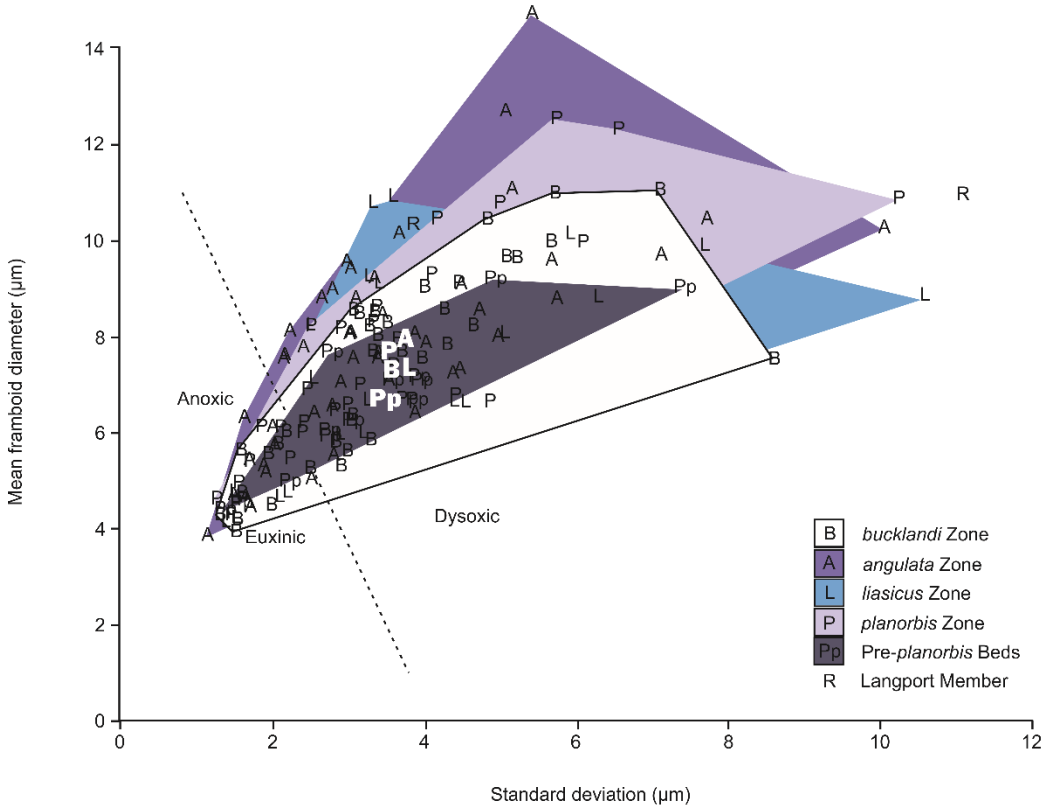

Fig. 3.11 Wilkin diagram, samples plotted according to ammonite zone/time bin. R – Langport, Pp – Pre-*planorbis* Beds, P – *planorbis* Zone, L – *liasicus* Zone, A – *angulata* Zone, B – *bucklandi* Zone. Average for each zone indicated as a bold white symbol, no average is given for the Langport (R) owing to the large disparity in standard deviations of the two samples.

The average of mean framboid diameters and standard deviations varies little between each zone (Fig. 3.11), with no two subsequent zones showing a significant difference (t-test, $p(a) > 0.05$). There is a distinct lack of directional trend through time, with the only significant size increase in framboid diameters found when populations of the Pre-*planorbis* Beds and *angulata* Zone are compared (t-test, $p(a) = 0.05$), however these zones are indistinct from all other zones. The same result is found when ammonite zones are compared for individual areas.

3.5.2 Faunas

3.5.2.1 Field collections

Bed-by-bed raw species counts are shown in Figs. 3.5-8 and 3.10 alongside pyrite framboid size distributions whilst range charts for the bivalves are shown in Figs. 3.12-14 (for raw sampling data see supplementary appendix C).

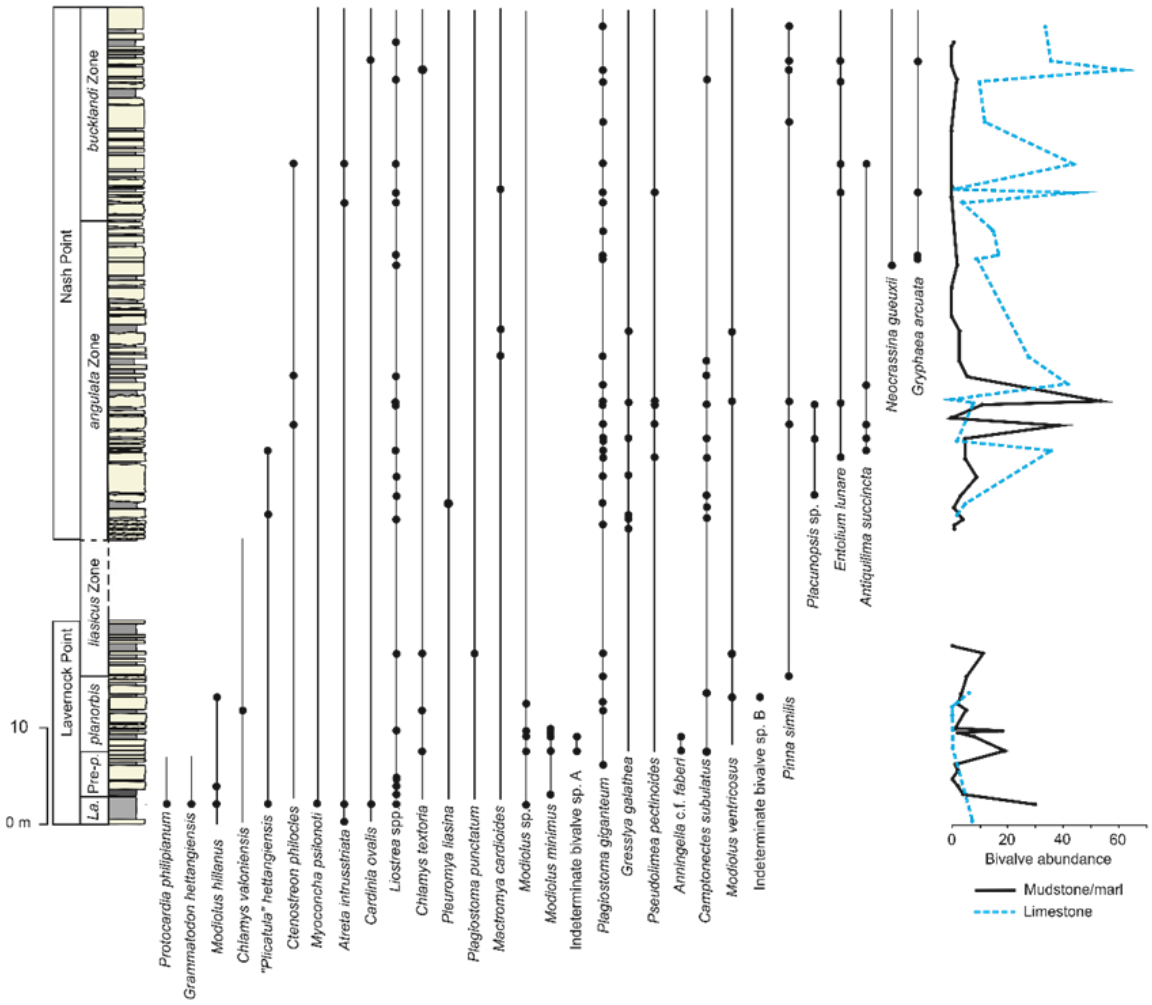

Fig. 3.12 Species range chart and bivalve abundances for Glamorgan (Lavernock Point and Nash Point). For range chart dark circles show horizons species were encountered during field collections. Connecting line indicates range of species, extensions to ranges based on personal observations, museum collections of NMW, Bath Royal Literary and Scientific Institute, Bristol City Museum and Art Gallery, and published literature (Ivimey-Cook *et al.* 1999; Hodges 2000, 2018; Palmer 2010). For abundance plot solid line depicts bivalve abundances from mudstones and marls, dashed line from limestones.

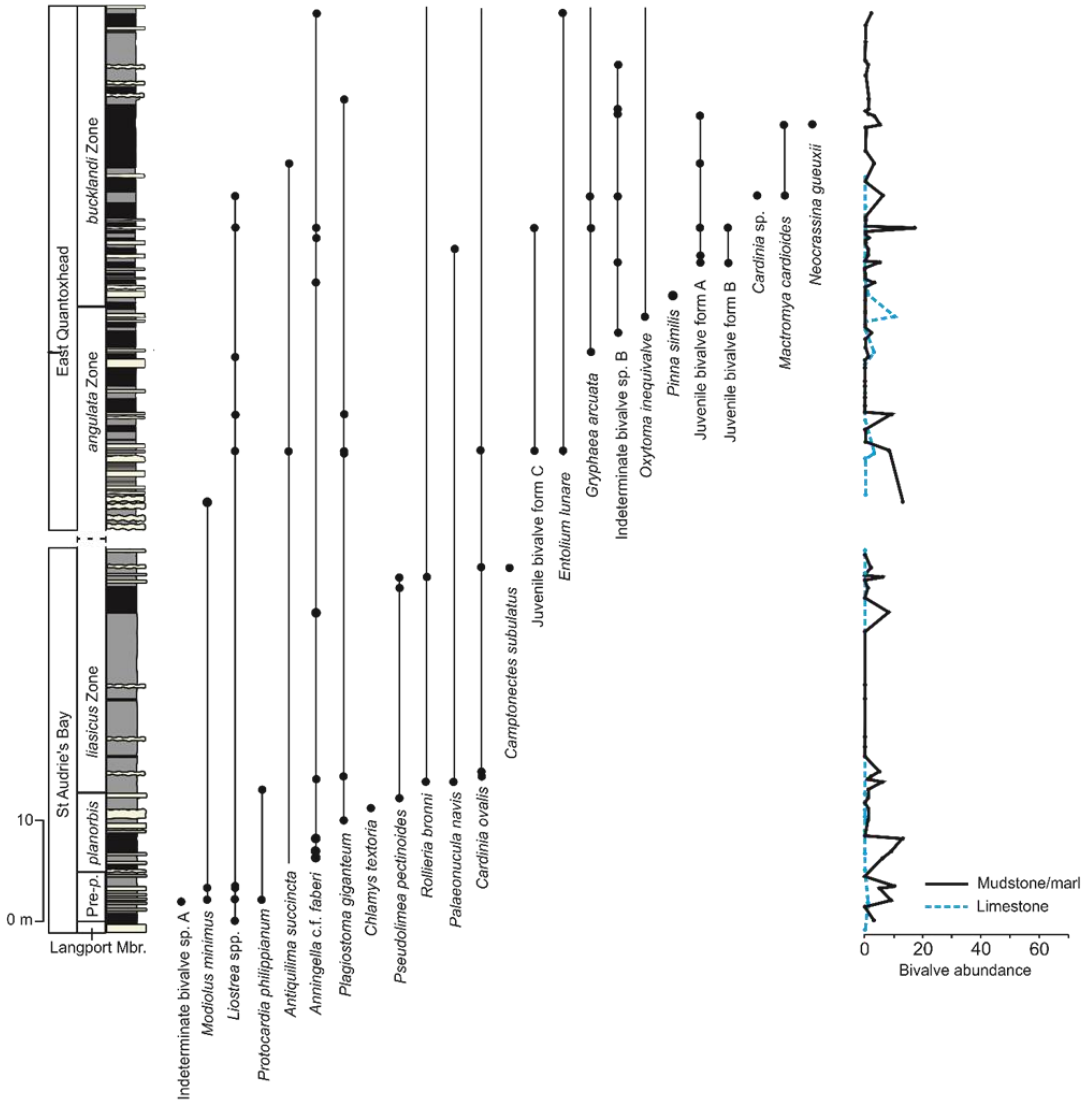

Fig. 3.13 Species range chart for Somerset (St Audrie's Bay and East Quantoxhead). See Fig. 3.12 for details.

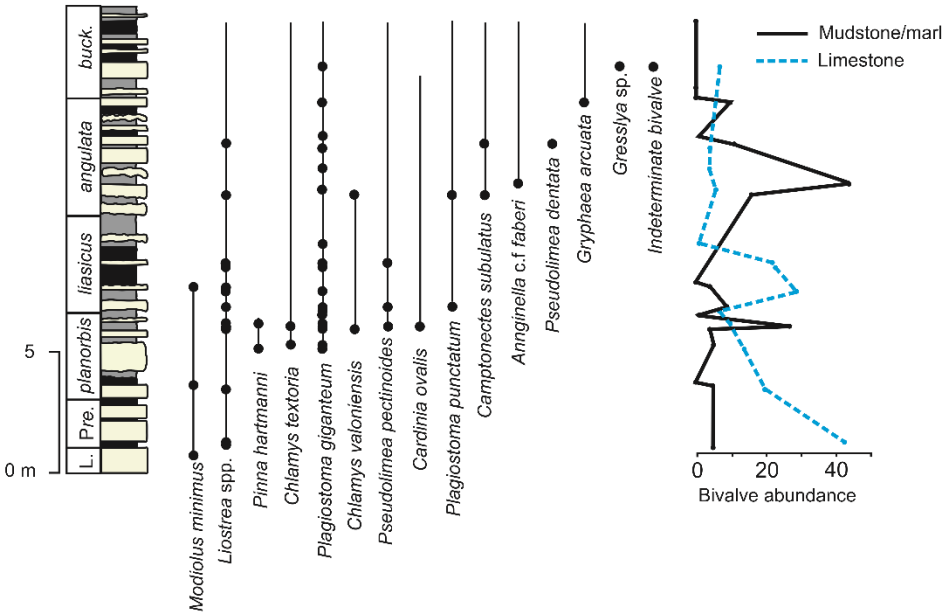

Fig. 3.14 Species range chart for Devon (Pinhay Bay). See Fig. 3.12 for details.

These show that bivalve diversity does not correlate with mean framboid diameters or standard deviation (r = +0.18, *p*(a) = 0.02, n = 155 and r = +0.22, *p*(a) = 0.01, n = 155 respectively). Although a higher diversity occurs in beds that show a larger mean framboid diameter, the converse is not always true. Similarly beds with an anoxic signal have been found to contain bivalves. LP12 is a pale marl from the base of the *planorbis* Zone of Lavernock Point and, despite its anoxic framboid population, it also contains a relatively diverse fauna including *Modiolus* and *Chlamys.* Another bivalve associated with framboid populations suggestive of anoxia is *Anningella* (SAB19 and SAB23; Fig. 3.5), but they are occasionally found attached to fossil drift wood suggesting a pseudoplanktonic lifestyle unhindered by seafloor conditions. In contrast, the anoxic beds from Devon are associated with low diversity bivalve assemblages (0-1 typically) with diversity showing a weak positive correlation to framboid diameters and standard deviations (r = +0.81, *p*(a) = 0.0003, n = 15 and r = +0.81, *p*(a) = 0.0003, n = 15

respectively). Generally, Glamorgan hosts the greatest bivalve diversity per zone (Fig. 3.15) and includes deep infaunal bivalve species (*Pleuromya liasina*, and *Gresslya galathea*; Fig. 3.12). The Nash Point section features several beds that contain the solitary coral *Stylophyllopsis* and large, disarticulated and occasionally stacked *Plagiostoma* shells that are heavily encrusted on all surfaces by *Liostrea*, *Atreta* and corals. Two of the coral beds at Nash Point (NP36, NP38), have framboid mean diameters that are indistinct from the rest of the limestone and marl beds (Fig. 3.8). Overall there is a temporal trend of increasing species richness per zone (Fig. 3.15). For Glamorgan and Devon the main rise occurs between the Pre-*planorbis* Beds and *planorbis* Zone. With bivalve species richness per zone remaining between seven and nine for Devon. The greatest species richness is achieved in the *angulata* Zone of Glamorgan, before falling slightly in the *bucklandi* Zone (Fig. 3.15). For Somerset species richness rises at a lessening rate throughout the Hettangian and into the Sinemurian and fossils are rare throughout (Fig. 3.5 & 3.6).

At the bed level the Langport Member of Glamorgan can host four times the diversity of species than the Pre-*planorbis* Beds, however in regards to ecological tiering this is only greater by one – featuring shallow infaunal species. Benthic tiering is reduced to epifauna with subordinate semi-infaunal components in the Pre-*planorbis* Beds, for Somerset the middle Pre-*planorbis* Beds also feature rare shallow infaunal bivalves (*Protocardia philippianum*). This latter tiering level is not seen in Devon until the upper *planorbis* Zone. Deep infaunal life modes are not encountered in Somerset, however they are recorded in the *angulata* and *bucklandi* zones of Glamorgan and Devon respectively. An increase in epifaunal tiering levels is noted by the presence of ossicles of the crinoid

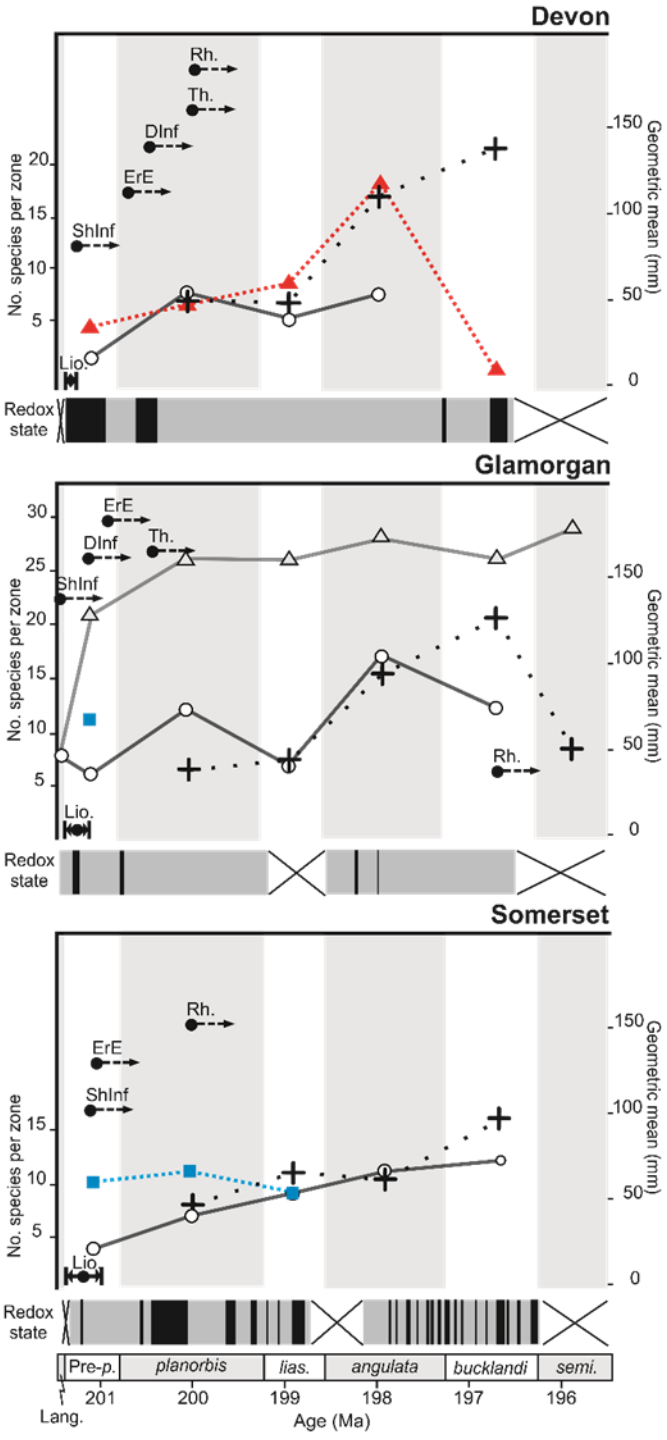
Devon
Rh.
Th.
DInf
ErE
ShInf
Lio.
No. species per zone
Geometric mean (mm)
Redox state
Glamorgan
ErE
DInf
Th.
ShInf
Rh.
Lio.
Somerset
Pre-p.
planorbis
lias.
angulata
bucklandi
semi.
Lang.
Age (Ma)

Fig. 3.15 Compiled recovery metrics and oxygenation states for each of the three studied regions. Hollow circles show number of species encountered per zone, from this study. Hollow triangles show number of species per zone from combined field and museum collections of Glamorgan. Squares show species richness per zone and from range charts published in Mander *et al.* (2008) and solid triangle the same from Pugh *et al.* (2014). Crosses depict average geometric mean shell size of *Plagiostoma giganteum* per location per zone from Atkinson *et al*. (2019). Filled circles and arrows show first recorded position of key recovery features of stages from Twitchett recovery model, codes as follows: Lio. – *Liostrea* shell beds (stage 1), ShInf – shallow infauna (stage 2), Rh. – *Rhizocorallium* burrows (stage 3), Th. – *Thalassinoides* burrows, ErE – erect epifauna (crinoids, stage 3), DInf – Deep infauna. Medium grey bars indicate periods with dysoxic framboid size distributions, black bars anoxic distributions, regions crossed out lack data. Time scaled to Weedon *et al*. (2018b).

Isocrinus psilonoti, these first appear in the Pre-*planorbis* Beds of Lavernock Point and the *planorbis* Zone of St Audrie's Bay and Pinhay Bay.

3.5.2.2 Museum collections

Bivalve diversity by zone for Glamorgan is assessed by incorporating bivalve specimens housed in the NMW alongside field observations. For the Langport Member incorporation of these specimens does not enhance diversity from that encountered in the field (eight species). Between the Langport Member and the Pre-*planorbis* Beds diversity increases greatly with 21 species present this rising to a stable diversity of around 26 species in the *planorbis* Zone and persisting into younger levels (Fig. 3.15). Deep infaunal suspension feeding bivalves are also recognised far sooner than seen during the field study, occurring in the Pre-*planorbis* Beds, and further members of this guild appear in the *planorbis* Zone (supplementary appendix D). Species richness rises to 29 in the *semicostatum* Zone, however this is represented by a silicified fauna that has been shown to be more diverse than un-silicified time-equivalent sections (Wright *et al.* 2003).

3.6 Discussion

3.6.1 Recovery

Most studies of recovery from the end-Triassic mass extinction in Britain have concentrated on the initial aftermath (*planorbis* to the early part of the *liasicus* zones) (Mander *et al.* 2008; Clémence *et al.* 2010). Here we extend the time interval of our analysis to the *bucklandi* Zone, of the Sinemurian Stage.

The majority of the beds from Pinhay Bay (Devon) suggest an environment with moderate oxygen restriction, with occasional intervals of anoxia. In spite of this, biotic recovery occurs rapidly, with a sharp increase in species richness by the *planorbis* Zone and ecological tiering being also well developed by this time.

Our field observations show low diversity with assemblages dominated by *Liostrea* in the lower Pre-*planorbis* Beds. This is consistent with the findings of Pugh *et al*. (2014), and conforms to phase one of the Twitchett recovery model. The definition of recovery phase two is the expansion of infaunal tiering levels. This was reported by Pugh *et al.* (2014) from the upper Pre-*planorbis* Beds using the trace fossil data of Barras and Twitchett (2007) and Twitchett and Barras (2004). However, the range charts of Pugh *et al.* (2014) show the infaunal tier was occupied before this time by *Pteromya tatei* in the lower Pre-*planorbis* Beds (Bed H2). This is earlier than our own field observations which show the appearance of *Cardinia ovalis* in the *planorbis* Zone being the first infaunal species.

Defined as an expansion in the epifaunal tiering levels, phase three occurs in the *planorbis* Zone in both our data and that of Pugh *et al*. (2014). The *planorbis* Zone also contains the key ichnotaxa for phase three with *Rhizocorallium* and *Thalassinoides* that are, at this interval, small in size (Twitchett & Barras 2004).

Defining the final stage of recovery is less clear-cut. Pugh *et al*. (2014) use the presence of deep infaunal bivalves in the *angulata* Zone, however their range charts show that this ecology was already present in the *planorbis* Zone (cf. Paul *et al.* 2008). Our data shows species richness had broadly stabilised by the *planorbis* Zone, considerably earlier than reported previously (Pugh *et al.* 2014). However, a trend of shell-size increase is seen after this time which persisted until the late *angulata* Zone (Atkinson *et al.* 2019).

In Somerset, this deep-water region records a greater number of episodes of anoxia than the shallower regions in Glamorgan. A background of dysoxic condition was punctuated by anoxic intervals, a situation that persists from the Pre-*planorbis* Beds and into the *bucklandi* Zone. Biotic recovery is still seen, even in these adverse conditions, albeit represented by a gradual rise in species richness, several of the key features of Twitchett's recovery model occur by the *planorbis* Zone.

As with Devon the lower beds of the Pre-*planorbis* interval are dominated by oysters and is again consistent with phase one of recovery. The appearance of infaunal tiering occurs in the upper Pre-*planorbis* Beds according to the range charts of Mander *et al*. (2008) who reported the shallow infaunal bivalve *Rollieria* at this level and is broadly consistent with our data which shows shallow infaunal tiers occupied from the mid Pre-*planorbis* interval. There is a discordance with the trace fossils, Barras and Twitchett (2007) do not report any trace fossils from the Pre-*planorbis* Beds of St Audrie's Bay.

Phase three (epifaunal tiering development) was not reported by Mander *et al*. (2008) from Somerset. However, this is contradicted by our finding of *Isocrinus psilonoti* in the mid-*planorbis* Zone at St Audrie's Bay and in upper Pre-*planorbis* Beds at Lilstock. Ichnotaxa are slower to recover, although rare *Rhizocorallium* occur in the *planorbis* Zone, and becomes more frequent from the *angulata* Zone (Barras & Twitchett 2007). Our results show that diversity continues to rise steadily in the earliest Jurassic of Somerset up to the *bucklandi* Zone but at no point is benthos abundant, and deep infaunal bivalves do not appear. Thus, recovery phase four is much later in the offshore Somerset sections than in the nearer, shallower sections of Devon.

Glamorgan represents the most near-shore region in this study, and also shows fewer anoxic intervals than the more distal Somerset sections. All the same, no sample lacked pyrite framboids, suggesting that oxygen restriction, to some degree, was still present even in these shallower waters up to the Sinemurian. Nonetheless, biotic recovery occurred promptly as seen in both field and museum collections which show an early rise in species richness into the *planorbis* Zone.

The Langport Member is discordant with the expectations of the Twitchett recovery model for an initial post extinction because several ecological tiers are occupied and no single species dominates the assemblage. At the bed level the Langport Member can attain a greater diversity than the succeeding Pre-*planorbis* Beds however when considered as a time bin, with the inclusion of NMW specimens this interval is comparably depleted in bivalve diversity, with a great increase occurring with the transition to Blue Lias facies (Fig. 3.15). This may be driven by a rapid sea level rise and development of fully marine conditions

The lower Pre-*planorbis* Beds, with their high numbers of *Liostrea* and *Modiolus minimus,* are far more characteristic of phase one than the earlier Langport Member. Two shallow infaunal species are present in the Langport Member but our field collecting did not find further infaunal bivalves until the lower *angulata* Zone, where deep infauna also appeared (*Gresslya*, *Pleuromya* and *Pholadomya*). However, Mander *et al*. (2008) recorded shallow infaunal deposit feeding bivalves in the upper Pre-*planorbis* Beds and specimens housed in the NMW include *Pteromya*, *Protocardia*, *Pleuromya*, *Rollieria*, *Mactromya* and *Cardina* all in the Pre-*planorbis* Beds. Thus, this tiering level was not lost with the changing facies. The expansion of epifaunal tiering (recovery phase three) is seen in upper Pre-*planorbis* Beds with the presence of *Isocrinus psilonoti*.

However, as with Somerset, key ichnotaxa of these phases are lacking, with *Thalassinoides* occurring later in the lower *planorbis* Zone and rare *Rhizocorallium* later still in the *bucklandi* Zone (Wobber 1968). The ordered succession of recovery phases does not match the record seen in Glamorgan.

Based on field collecting alone, diversity rose rapidly into the *planorbis* Zone and was highest in the *angulata* Zone – a time when all the tiering levels were filled. The largest limid bivalves and *Thalassinoides* burrows were recorded from the *bucklandi* Zone (Hallam 1960; Wilson *et al.* 1990; Atkinson *et al.* 2019). However, using the data from museum collections shows that diversity and tiering had stabilised far earlier (in the *planorbis* Zone). Diversity from combined field and NMW collections was also far higher than direct field observations alone this likely relates to the ability of museum collections to capture rare faunal elements based on many years of collecting effort and samples from temporary exposures.

In both Devon and Glamorgan recovery occurs quickly and was complete by the *planorbis* Zone, as monitored by stable, high diversity and restoration of tiering levels (Figs. 3.12, 3.14 & 3.15). Diversity is slower to increase in the offshore/deeper water Somerset sections. Based on body and burrow sizes the recovery is more gradual and slower taking up to the *angulata* and *bucklandi* zones. The recovery patterns do not fit Twitchett's recovery model with its progressive development of tiers and diversity in the shelly fauna occurring out of synch with trace fossil records. The model only accords with the recovery pattern seen at Pinhay Bay, there trace fossils recover hand-in-hand with the shelly fauna. The timing of the appearance of key ichnotaxa and shelly fauna tiering and diversity is ill fitted in Somerset and Glamorgan. For example, there is a near absence of trace fossils in Somerset until the *angulata* Zone (Barras &

Twitchett 2007), despite the recovery of the bivalves. Recovery should be deemed complete once a stable diversity is attained, however we acknowledge the necessity for ecological factors to be also considered and retain the ideas of Twitchett (1999) that benthic tiering is an important indicator of recovery also. Body size and presence of particular trace fossils are perhaps controlled by other factors (substrate, sea level and so on) and do not appear relatable across different regions or recovery intervals.

Looking further afield recovery also appears to have been rapidly completed within the Hettangian. High diversity shell beds with low dominance and highly specialised forms are reported from early Hettangian of Tibet (Hautmann *et al.* 2008). In the Neuquén Basin, Argentina, recovery appears slower than Tibet, because there is an interval barren of bivalves roughly equivalent to the *planorbis* Zone, followed by rising diversity and increased occupation of tiering until the *canadensis* Zone equivalent to the upper *angulata* Zone (Damborenea *et al.* 2017).

Ammonites also recovered very quickly, with a rapid diversification in the immediate aftermath of the end-Triassic mass extinction with peak originations occurring in the *planorbis* Zone (Guex *et al.* 2012). This diversification was also accompanied by an increase in size disparity over the first four standard ammonite zones of the Jurassic, with some of the largest forms of the Lower Jurassic occurring in the *bucklandi* Zone (Dommergues *et al.* 2002). Recovery amongst the brachiopods occurs on broadly the same time span as seen amongst bivalves (Tomašových & Siblík 2007). In the Northern Calcareous Alps of Germany and Austria, brachiopod recovery occurs in the *calliphyllum* and *megastoma* zones (equivalent to *planorbis* to lower *angulata* zones of the UK, cf. Page 2003).

3.6.2 Duration of recovery

A recent reappraisal of the cyclostratigraphy of the Blue Lias has suggested that the Hettangian stage was longer than previously thought, being perhaps >4.1 Myr (Weedon *et al.* 2018b) compared to earlier estimates of 1.7- 2 million years (Schaltegger *et al.* 2008; Ruhl *et al.* 2010, 2016; Guex *et al.* 2012; Hüsing *et al.* 2014). This has clear implications for the timing of the recovery. Evidence for a short Hettangian comes from U-Pb dating of poorly biostratigraphically constrained ash beds in northern Peru (Schaltegger *et al.* 2008; Schoene *et al.* 2010; Wotzlaw *et al.* 2014) and cyclostratigraphic study of the St Audrie's Bay and East Quantoxhead sections (Ruhl *et al.* 2010, 2016; Hüsing *et al.* 2014), but Weedon et al.'s (2018b) work improves on these earlier cyclostratigraphies by including the *tilmanni* Zone (encompassing part of the Pre-*planorbis* Beds), and also constructing chronologies from several Blue Lias sites. This has allowed for the detection of hiatuses and missing sedimentary cycles, and so generated a longer composite chronology for the Hettangian (Weedon *et al.* 2018a, b). Based on this new >4.1 Myr duration for the Hettangian and accounting for the 0.15 Myr between the End-Triassic extinction and the Triassic-Jurassic boundary (Wotzlaw *et al.* 2014) the pace of recovery can be assessed.

Despite Somerset recording a greater level of oxygen restriction, the duration of early recovery phases between all three regions are broadly similar. The biotic recovery from the end-Triassic mass extinction event appears to have begun extremely rapidly; it was substantially complete within <0.7 Myr in both Somerset and Glamorgan (excluding trace fossils). Devon lagged behind

and took > 2 Myr to reach a similar stage. Following the initial rapid recovery later, incremental diversity increases were ongoing for > 4 Myr. Although we favour the most recent Hettangian time scale, as some controversy remains we also present an alternative duration of recovery using the time scales of Ruhl *et al*. (2016), under this chronology recovery was exceedingly rapid, significant expansion of tiering was restored within 0.22 Myr for Somerset and Glamorgan and with stable diversity and fully restored tiers in both Devon and Glamorgan within 0.53 Myr, and equally the incremental diversity increases seen in Somerset were ongoing for >2.14 Myr.

3.6.3 Role of anoxia in recovery

There is no suggestion of the involvement of anoxia in the end-Triassic extinction event itself in the region (Wignall & Bond 2008), but oxygen restriction clearly occurred during the earliest Jurassic and this has been suggested to have impeded the recovery (e.g. Hallam 1996; Mander *et al.* 2008; Clémence *et al.* 2010; Luo *et al.* 2018). Our redox study fails to shows this link. Anoxic and dysoxic conditions were regularly developed during the Hettangian and lower Sinemurian in Somerset and Devon, whilst less intense dysoxia persisted in the nearer shore/shallower Glamorgan sections with fewer anoxic intervals recorded. Much the same redox history has been demonstrated for other regions of the European Shelf Sea (Schwab & Spangenberg 2007; Quan *et al.* 2008; Richoz *et al.* 2012). Despite the oxygen restriction, rapid recovery in the basal Jurassic occurred unhindered (Fig. 3.15). Nonetheless, some influence of dysoxia can be seen because the greatest diversity increase occurred in nearshore sections whilst the continued deposition of anoxic, black shales in

Somerset into the *bucklandi* Zone lowered the diversity and abundances at least at the bed level and prolonged the local recovery.

The rapid initial recovery of the Early Jurassic is in marked contrast to the muted recovery seen during the Early Triassic when anoxia has also been proposed to have hindered recovery (e.g. Hallam 1991; Dai *et al.* 2018). However, the environmental extent of anoxia in the earlier interval was much greater, with anoxia frequently extending into shallow, inner shelf settings (Wignall & Twitchett 1996; Wignall *et al.* 2016). During the Early Jurassic it is possible that species from the shallower, dysoxic setting of South Wales replenished deeper water populations following periods of anoxia in the Early Jurassic, thereby allowing punctuated recovery even in the deeper waters. It is important to remember that this is a regional story for two basins, each responding in subtly different ways. Although episodic anoxia continued into the Sinemurian, uranium isotope ratios suggest that, on a global scale, a major expansion of sea-floor anoxia lasted for only around 45 kyr after the extinction, before improving gradually in the next 200 kyr (Jost *et al.* 2017). However, Jost *et al*.'s (2017) work used the astrochronological timescale of Ruhl *et al.* (2010). The more recent timescale of Weedon *et al*. (2018b) doubles the duration of the widespread anoxia episode. The oxygen-poor environmental conditions in NW Europe were unusually harsh compared to elsewhere in the Early Jurassic, ensuring that there were sufficient locations beyond this region where benthic diversity was able to diversify unimpeded.

3.7 Conclusions

The Hettangian and lowermost Sinemurian shelf seas of Britain show pyrite framboid size distributions that suggest conditions were commonly dysoxic especially in more distal, offshore settings. Despite this observation, the poor aeration did not hinder biotic recovery from the end-Triassic mass extinction event as recorded by the dominant bivalve fauna. Even in deeper water where a greater severity of oxygen restriction was recorded a rapid initial recovery can be detected. It may be that diversification took place in the best oxygenated shallowest-water settings and helped stock the benthos in offshore, dysoxic settings during transient times of improved oxygenation. This is supported by the evidence form the nearshore sections of Glamorgan where recovery was potentially faster (achieved within 0.7 Myr). Other facets of the recovery, seen in benthic tiering levels, both epifaunal and infaunal, improved rapidly and synchronously: there is little support for models that view recovery to occur in a set of distinct stages or phases.

Acknowledgements: We thank the following people for their assistance: Tom Sunderland and Bob Corns of Natural England and Hugh Luttrell of East Quantoxhead Estate for permissions to sample at Pinhay Bay and along the Blue Anchor-Lilstock Coast SSSI; Peter Hodges, Caroline Buttler and Lucy McCobb of the National Museum of Wales, Cardiff. Additional thanks go to field assistants Jacob Morton and Karolina Zarzyczny, SEM assistance from Duncan Hedges and to two anonymous reviewers and Thomas Algeo for constructive reviews.

Funding: This work was supported by a NERC studentship at the University of Leeds.

References

Arzani, N. 2004. Diagenetic evolution of mudstones: black shales to laminated limestones, an example from the Lower Jurassic of SW Britain. *Journal of Sciences, Islamic Republic of Iran*, **15**, 257–267.

Atkinson, J.W., Wignall, P.B., Morton, J.D. & Aze, T. 2019. Body size changes in bivalves of the family Limidae in the aftermath of the end-Triassic mass extinction: the Brobdingnag Effect. *Palaeontology*, https://doi.org/10.1111/pala.12415.

Barras, C.G. & Twitchett, R.J. 2007. Response of the marine infauna to Triassic – Jurassic environmental change: Ichnological data from southern England. *Palaeogeography, Palaeoclimatology, Palaeoecology*, **244**, 223–241, https://doi.org/10.1016/j.palaeo.2006.06.040.

Bloos, G. & Page, K.N. 2002. Global stratotype section and point for base of the Sinemurian Stage (Lower Jurassic). *Episodes*, **25**, 22–28.

Blumenberg, M., Heunisch, C., Lückge, A., Scheeder, G. & Wiese, F. 2016. Photic zone euxinia in the central Rhaetian Sea prior the Triassic-Jurassic boundary. *Palaeogeography, Palaeoclimatology, Palaeoecology*, **461**, 55–64, https://doi.org/10.1016/j.palaeo.2016.08.007.

Bond, D.P.G. & Wignall, P.B. 2010. Pyrite framboid study of marine Permian – Triassic boundary sections: A complex anoxic event and its relationship to contemporaneous mass extinction. *GSA Bulletin*, **122**, 1265–1279, https://doi.org/10.1130/B30042.1.

Bottrell, S.H. & Raiswell, R. 1989. Primary versus diagenetic origin of Blue Lias rhythms (Dorset, UK): evidence from sulphur geochemistry. *Terra Nova*, **1**, 451–456, https://doi.org/10.1111/j.1365-3121.1989.tb00409.x.

Breward, N., Kemp, S.J., Ambrose, K., Powell, J.H., Morigi, A. & Wagner, D. 2015. Anomalous enrichment of molybdenum and associated metals in Lower Jurassic (Lias Group) black shales of central England, as revealed by systematic geochemical surveys. *Proceedings of the Geologists' Association*, **126**, 346–366, https://doi.org/10.1016/j.pgeola.2015.03.007.

Clémence, M.-E., Bartolini, A., Gardin, S., Paris, G., Beaumont, V. & Page, K.N. 2010. Early Hettangian benthic–planktonic coupling at Doniford (SW England): Palaeoenvironmental implications for the aftermath of the end-Triassic crisis. *Palaeogeography, Palaeoclimatology, Palaeoecology*, **295**, 102–115, https://doi.org/10.1016/j.palaeo.2010.05.021.

Dai, X., Song, H., et al. 2018. Rapid biotic rebound during the late Griesbachian indicates heterogeneous recovery patterns after the Permian-Triassic mass extinction. *Geological Society of America Bulletin*, **130**, 2015–2030, https://doi.org/https://doi.org/10.1130/30/B31969.1.

Damborenea, S.E., Echevarría, J. & Ros-Franch, S. 2017. Biotic recovery after the end-Triassic extinction event: Evidence from marine bivalves of the Neuquén Basin, Argentina. *Palaeogeography, Palaeoclimatology, Palaeoecology*, **487**, 93–104, https://doi.org/10.1016/j.palaeo.2017.08.025.

Dommergues, J.-L., Montuire, S. & Neige, P. 2002. Size patterns through time:

the case of the Early Jurassic ammonite radiation. *Paleobiology*, **28**, 423–434, https://doi.org/10.1666/0094-8373(2002)028<0423:SPTTTC>2.0.CO;2.

Ebukanson, E.J. & Kinghorn, R.R.F. 1990. Jurassic mudrock formations of southern England: lithology, sedimentation rates and organic carbon content. *Journal of Petroleum Geology*, **13**, 221–228, https://doi.org/10.1111/j.1747-5457.1990.tb00841.x.

Fujisaki, W., Sawaki, Y., Yamamoto, S., Sato, T., Nishizawa, M., Windley, B.F. & Maruyama, S. 2016. Tracking the redox history and nitrogen cycle in the pelagic Panthalassic deep ocean in the Middle Triassic to Early Jurassic: Insights from redox-sensitive elements and nitrogen isotopes. *Palaeogeography, Palaeoclimatology, Palaeoecology*, **449**, 397–420, https://doi.org/10.1016/j.palaeo.2016.01.039.

Guex, J., Schoene, B., et al. 2012. Geochronological constraints on post-extinction recovery of the ammonoids and carbon cycle perturbations during the Early Jurassic. *Palaeogeography, Palaeoclimatology, Palaeoecology*, **346**–**347**, 1–11, https://doi.org/10.1016/j.palaeo.2012.04.030.

Hallam, A. 1960. A sedimentary and faunal study of the Blue Lias of Dorset and Glamorgan. *Philosophical Transactions of the Royal Society of London B: Biological Sciences*, **243**, 1–44, https://doi.org/10.1098/rstb.1960.0003.

Hallam, A. 1964. Origin of the limestone-shale rhythm in the Blue Lias of England: a composite theory. *The Journal of Geology*, **72**, 157–169, https://doi.org/10.1086/626974.

Hallam, A. 1991. Why was there a delayed radiation after the end-Palaeozoic extinction? *Historical Biology*, **5**, 257–262, https://doi.org/10.1080/10292389109380405.

Hallam, A. 1995. Oxygen-restricted facies of the basal Jurassic of North West Europe. *Historical Biology*, **10**, 247–257, https://doi.org/10.1080/10292389509380523.

Hallam, A. 1996. Recovery of the marine fauna in Europe after the end-Triassic and early Toarcian mass extinctions. *Geological Society, London, Special Publications*, **102**, 231–236, https://doi.org/10.1144/GSL.SP.1996.001.01.16.

Hallam, A. 1997. Estimates of the amount and rate of sea-level change across the Rhaetian – Hettangian and Pliensbachian – Toarcian boundaries (latest Triassic to early Jurassic). *Journal of the Geological Society*, **154**, 773–779, https://doi.org/10.1144/gsjgs.154.5.0773.

Hallam, A. & El Shaarawy, Z. 1982. Salinity reduction of the end- Triassic sea from the Alpine region into northwestern Europe. *Lethaia*, **15**, 169–178, https://doi.org/10.1111/j.1502-3931.1982.tb01136.x.

Hammer, Ø., Harper, D.A.T. & Ryan, P.D. 2001. Past: Paleontological Statistics software package for education and data analysis.

Hautmann, M., Stiller, F., Cai, H.W. & Sha, J.-G. 2008. Extinction-recovery pattern of level-bottom faunas across the Triassic-Jurassic boundary in Tibet: implications for potential killing mechanisms. *Palaios*, **23**, 711–718, https://doi.org/10.2110/palo.2008.p08-005r.

Hesselbo, S.P. & Jenkyns, H.C. 1995. Lower and Middle Jurassic of Dorset and Yorkshire. *In*: Taylor, P. D. (ed.) *The Field Geology of the British Jurassic*. Bath, Geological Society of London, 110–115.

Hesselbo, S.P. & Jenkyns, H.C. 1998. British Lower Jurassic sequence stratigraphy. *In*: *Mesozoic and Cenozoic Sequence Stratigraphy of European Basins*. SEPM Special Publications No. 60.

Hesselbo, S.P., Robinson, S.A. & Surlyk, F. 2004. Sea-level change and facies development across potential Triassic – Jurassic boundary horizons, SW Britain. *Journal of the Geological Society*, **161**, 365–379.

Hodges, P. 2000. *The Early Jurassic Bivalvia from the Hettangian and Lower Sinemurian of South-West Britain Part 1*. London, Monograph of the Palaeontographical Society.

Hodges, P. 2018. *The Early Jurassic Bivalvia from the Hettangian and Lower Sinemurian of South-West Britain Part 2*. London, Monograph of the Palaeontographical Society, https://doi.org/10.1080/02693445.2017.11963960.

Huang, Y., Chen, Z., Wignall, P.B. & Zhao, L. 2017. Latest Permian to Middle Triassic redox condition variations in ramp settings, South China: Pyrite framboid evidence. *Geological Society of America Bulletin*, **129**, 229–243, https://doi.org/10.1130/B31458.1.

Hüsing, S.K., Beniest, A., van der Boon, A., Abels, H.A., Deenen, M.H.L., Ruhl, M. & Krijgsman, W. 2014. Astronomically-calibrated magnetostratigraphy of the Lower Jurassic marine successions at St. Audrie's Bay and East Quantoxhead (Hettangian-Sinemurian; Somerset, UK). *Palaeogeography, Palaeoclimatology, Palaeoecology*, **403**, 43–56, https://doi.org/10.1016/j.palaeo.2014.03.022.

Ivimey-Cook, H.C., Hodges, P., Swift, A. & Radley, J.D. 1999. Bivalves. *In*: Swift, A. & Martill, D. M. (eds) *Fossils of the Rhaetian Penarth Group*. London, The Palaeontological Association, 83–127.

Jaraula, C.M.B., Grice, K., Twitchett, R.J., Böttcher, M.E., Lemetayer, P., Dastidar, A.G. & Opazo, L.F. 2013. Elevated pCO2 leading to Late Triassic extinction, persistent photic zone euxinia, and rising sea levels. *Geology*, **41**, 955–958, https://doi.org/10.1130/G34183.1.

Johnson, M.E. & McKerrow, W.S. 1995. The Sutton Stone: an Early Jurassic rocky shore deposit in South Wales. *Palaeontology*, **38**, 529–541.

Jost, A.B., Bachan, A., van de Schootbrugge, B., Lau, K. V, Weaver, K.L., Maher, K. & Payne, J.L. 2017. Uranium isotope evidence for an expansion of marine anoxia during the end-Triassic extinction. *Geochem. Geophys. Geosyst*, **18**, 3093–3108, https://doi.org/10.1002/2017GC006941.

Kasprak, A.H., Sepúlveda, J., et al. 2015. Episodic photic zone euxinia in the northeastern Panthalassic Ocean during the end-Triassic extinction. *Geology*, **43**, 307–310, https://doi.org/10.1130/G36371.1.

Kauffman, E.G. & Erwin, D.H. 1995. Surviving mass extinctions. *Geotimes*, **14**, 14–17.

Luo, G., Richoz, S., van de Schootbrugge, B., Algeo, T.J., Xie, S., Ono, S. & Summons, R.E. 2018. Multiple sulfur-isotopic evidence for a shallowly

stratified ocean following the Triassic-Jurassic boundary mass extinction. *Geochimica et Cosmochimica Acta*, **231**, 73–87, https://doi.org/10.1016/j.gca.2018.04.015.

Mander, L., Twitchett, R.J. & Benton, M.J. 2008. Palaeoecology of the Late Triassic extinction event in the SW UK. *Journal of the Geological Society*, **165**, 319–332, https://doi.org/10.1144/0016-76492007-029.

Martill, D.M., Vidovic, S.U., Howells, C. & Nudds, J.R. 2016. The oldest Jurassic dinosaur: a basal neotheropod from the Hettangian of Great Britain. *PLoS ONE*, **11**, e0145713, https://doi.org/10.1371/journal.pone.0145713.

Moghadam, H. V & Paul, C.R.C. 2000. Trace fossils of the Jurassic, Blue Lias, Lyme Regis, southern England. *Ichnos*, **7**, 283–306, https://doi.org/10.1080/10420940009380167.

Naeher, S. & Grice, K. 2015. Novel 1H-Pyrrole-2,5-dione (maleimide) proxies for the assessment of photic zone euxinia. *Chemical Geology*, **404**, 100–109, https://doi.org/10.1016/j.chemgeo.2015.03.020.

Page, K.N. 2003. The Lower Jurassic of Europe: its subdivision and correlation. *Geological Survey of Denmark and Greenland Bulletin*, **1**, 23–59.

Palmer, C.P. 2010. Mollusca - Bivalves. *In*: Lord, A. R. & Davis, P. G. (eds) *Fossils from the Lower Lias of the Dorset Coast*. London, The Palaeontological Association, 124–146.

Paris, G., Beaumont, V., Bartolini, A., Clémence, M.-E., Gardin, S. & Page, K.N. 2010. Nitrogen isotope record of a perturbed paleoecosystem in the aftermath of the end-Triassic crisis, Doniford section, SW England. *Geochem. Geophys. Geosyst*, **11**, 1–15, https://doi.org/10.1029/2010GC003161.

Paul, C.R.C., Allison, P.A. & Brett, C.E. 2008. The occurrence and preservation of ammonites in the Blue Lias Formation (lower Jurassic) of Devon and Dorset, England and their palaeoecological, sedimentological and diagenetic significance. *Palaeogeography, Palaeoclimatology, Palaeoecology*, **270**, 258–272, https://doi.org/10.1016/j.palaeo.2008.07.013.

Pugh, A.C., Danise, S., Brown, J.R. & Twitchett, R.J. 2014. Benthic ecosystem dynamics following the Late Triassic mass extinction event : Palaeoecology of the Blue Lias Formation, Lyme Regis, UK. *Proceedings of the Ussher Society*, **13**, 255–266.

Quan, T.M., van de Schootbrugge, B., Field, P.M., Rosenthal, Y. & Falkowski, P.G. 2008. Nitrogen isotope and trace metal analyses from the Mingolsheim core (Germany): Evidence for redox variations across the Triassic-Jurassic boundary. *Global Biogeochemical Cycles*, **22**, 1–14, https://doi.org/10.1029/2007GB002981.

Richoz, S., van de Schootbrugge, B., et al. 2012. Hydrogen sulphide poisoning of shallow seas following the end-Triassic extinction. *Nature Geoscience*, **5**, 662–667, https://doi.org/10.1038/ngeo1539.

Ruhl, M., Deenen, M.H.L., Abels, H.A., Bonis, N.R., Krijgsman, W. & Kürschner, W.M. 2010. Astronomical constraints on the duration of the early Jurassic Hettangian stage and recovery rates following the end-Triassic mass extinction (St Audrie's Bay / East Quantoxhead, UK). *Earth and Planetary*

Science Letters, **295**, 262–276, https://doi.org/10.1016/j.epsl.2010.04.008.

Ruhl, M., Hesselbo, S.P., et al. 2016. Astronomical constraints on the duration of the Early Jurassic Pliensbachian Stage and global climatic fluctuations. *Earth and Planetary Science Letters*, **455**, 149–165, https://doi.org/10.1016/j.epsl.2016.08.038.

Schaltegger, U., Guex, J., Bartolini, A., Schoene, B. & Ovtcharova, M. 2008. Precise U–Pb age constraints for end-Triassic mass extinction, its correlation to volcanism and Hettangian post-extinction recovery. *Earth and Planetary Science Letters*, **267**, 266–275, https://doi.org/10.1016/j.epsl.2007.11.031.

Schoene, B., Guex, J., Bartolini, A., Schaltegger, U. & Blackburn, T.J. 2010. Correlating the end-Triassic mass extinction and flood basalt volcanism at the 100 ka level. *Geology*, **38**, 387–390, https://doi.org/10.1130/G30683.1.

Schwab, V.F. & Spangenberg, J.E. 2007. Molecular and isotopic characterization of biomarkers in the Frick Swiss Jura sediments: A palaeoenvironmental reconstruction on the northern Tethys margin. *Organic Geochemistry*, **38**, 419–439, https://doi.org/10.1016/j.orggeochem.2006.06.013.

Sheppard, T.H. 2006. Sequence architecture of ancient rocky shorelines and their response to sea-level change: an Early Jurassic example from South Wales, UK. *Journal of the Geological Society, London*, **163**, 595–606, https://doi.org/10.1144/0016-764920-015.

Simms, M.J. 2003. Uniquely extensive seismite from the latest Triassic of the United Kingdom : Evidence for bolide impact ? *Geology*, **31**, 557–560.

Simms, M.J. 2004. The Mendips and South Wales Massif. *In*: Simms, M. J., Chidlaw, N., Morton, N. & Page, K. N. (eds) *British Lower Jurassic Stratigraphy, Geolocial Conservation Review Series No. 30*. Peterborough, Joint Nature Conservation Committee, 112–156.

Tomašových, A. & Siblík, M. 2007. Evaluating compositional turnover of brachiopod communities during the end-Triassic mass extinction (Northern Calcareous Alps): Removal of dominant groups, recovery and community reassembly. *Palaeogeography, Palaeoclimatology, Palaeoecology*, **244**, 170–200, https://doi.org/10.1016/j.palaeo.2006.06.028.

Twitchett, R.J. 1999. Palaeoenvironments and faunal recovery after the end-Permian mass extinction. *Palaeogeography, Palaeoclimatology, Palaeoecology*, **154**, 27–37.

Twitchett, R.J. 2006. The palaeoclimatology, palaeoecology and palaeoenvironmental analysis of mass extinction events. *Palaeogeography, Palaeoclimatology, Palaeoecology*, **232**, 190–213, https://doi.org/10.1016/j.palaeo.2005.05.019.

Twitchett, R.J. & Barras, C.G. 2004. Trace fossils in the aftermath of mass extinction events. *Geological Society, London, Special Publications*, **228**, 397–418, https://doi.org/10.1144/gsl.sp.2004.228.01.18.

van de Schootbrugge, B., Bachan, A., Suan, G., Richoz, S. & Payne, J.L. 2013. Microbes, mud and methane: cause and consquence of recurrent Early Jurassic anoxia following the end-Triassic mass extinction. *Palaeontology*, **56**, 685–709, https://doi.org/10.1111/pala.12034.

Weedon, G.P. 1986. Hemipelagic shelf sedimentation and climatic cycles: The basal Jurassic (Blue Lias) of S. Britain. *Earth and Planetary Science Letters*, **76**, 321–335, https://doi.org/10.1016/0012-821X(86)90083-X.

Weedon, G.P., Jenkyns, H.C. & Page, K.N. 2018a. Combined sea-level and climate controls on limestone formation, hiatuses and ammonite preservation in the Blue Lias Formation, South Britain (uppermost Triassic–Lower Jurassic). *Geological Magazine*, **155**, 1117–1149, https://doi.org/10.1017/S001675681600128X.

Weedon, G.P., Page, K.N. & Jenkyns, H.C. 2018b. Cyclostratigraphy, stratigraphic gaps and the duration of the Hettangian Stage (Jurassic): insights from the Blue Lias Formation of southern Britain. *Geological Magazine*, 1–41, https://doi.org/10.1017/S0016756818000808.

Wignall, P.B. 2001. Sedimentology of the Triassic-Jurassic boundary beds in Pinhay Bay (Devon, SW England). *Proceedings of the Geologists' Association*, **112**, 349–360, https://doi.org/10.1016/S0016-7878(01)80014-6.

Wignall, P.B. & Bond, D.P.G. 2008. The end-Triassic and Early Jurassic mass extinction records in the British Isles. *Proceedings of the Geologists' Association*, **119**, 73–84, https://doi.org/10.1016/S0016-7878(08)80259-3.

Wignall, P.B. & Hallam, A. 1991. Biofacies, stratigraphic distribution and depositional models of British onshore Jurassic black shales. *Geoogical Society Special Publications*, **58**, 291–309.

Wignall, P.B. & Newton, R.J. 1998. Pyrite framboid diameter as a measure of oxygen deficiency in ancient mudrocks. *American Journal of Science*, **298**, 537–552, https://doi.org/10.2475/ajs.298.7.537.

Wignall, P.B. & Twitchett, R.J. 1996. Oceanic anoxia and the end Permian mass extinction. *Science*, **272**, 1155–1158, https://doi.org/10.1126/science.272.5265.1155.

Wignall, P.B., Bond, D.P.G., Kuwahara, K., Kakuwa, Y., Newton, R.J. & Poulton, S.W. 2010. An 80 million year oceanic redox history from Permian to Jurassic pelagic sediments of the Mino-Tamba terrane , SW Japan , and the origin of four mass extinctions. *Global and Planetary Change*, **71**, 109–123, https://doi.org/10.1016/j.gloplacha.2010.01.022.

Wignall, P.B., Bond, D.P.G., Sun, Y., Grasby, S.E., Beauchamp, B., Joachimski, M.M. & Blomeier, Dierk, P.G. 2016. Ultra-shallow-marine anoxia in an Early Triassic shallow-marine clastic ramp (Spitsbergen) and the suppression of benthic radiation. *Geol. Mag.*, **153**, 316–331, https://doi.org/10.1017/S0016756815000588.

Wilkin, R.T., Barnes, H.L. & Brantley, S.L. 1996. The size distribution of framboidal pyrite in modern sediments: An indicator of redox conditions. *Geochimica et Cosmochimica Acta*, **60**, 3897–3912, https://doi.org/10.1016/0016-7037(96)00209-8.

Wilson, D., Davies, J.R., Fletcher, C.J.N. & Smith, M. 1990. Geology of the South Wales coalfield, part VI, the country around Bridgend. *Memoir of the 1:50 000 geological sheets 261 and 262 (England and Wales). London: HMSO.*

Wobber, F.J. 1965. Sedimentology of the Lias (Lower Jurassic) of South Wales.

Journal of sedimentary petrology, **35**, 683–703, https://doi.org/10.1306/74D71325-2B21-11D7-8648000102C1865D.

Wobber, F.J. 1968. A faunal analysis of the Lias (Lower Jurassic) of South Wales (Great Britain). *Palaeogeography, Palaeoclimatology, Palaeoecology*, **5**, 269–308, https://doi.org/10.1016/0031-0182(68)90072-2.

Wotzlaw, J., Guex, J., et al. 2014. Towards accurate numerical calibration of the Late Triassic: High-precision U-Pb geochronology constraints on the duration of the Rhaetian. *Geology*, **42**, 571-574,https://doi.org/10.1130/G35612.1.

Wright, P., Cherns, L. & Hodges, P. 2003. Missing molluscs: Field testing taphonomic loss in the Mesozoic through early large-scale aragonite dissolution. *Geology*, **31**, 211–214, https://doi.org/10.1130/0091-7613(2003)031<0211:MMFTTL>2.0.CO;2.

Chapter 4: The Hettangian-Sinemurian (Lower Jurassic) strata of Redcar, Cleveland Basin, NE England: facies and palaeoecology

Submitted for publication in Proceedings of the Yorkshire Geological Society

The Hettangian-Sinemurian (Lower Jurassic) strata of Redcar, Cleveland Basin, NE England: facies and palaeoecology

J.W. Atkinson[1]*, P.B. Wignall[1] & K.N. Page[2]

[1]School of Earth and Environment, University of Leeds, Leeds. LS2 9JT, UK

*gy12jwa@leeds.ac.uk

[2]Camborne School of Mines, University of Exeter, Penryn Campus, Penryn, Cornwall TR10 9FE, UK

4.1 Abstract

Redcar hosts the earliest Jurassic succession exposed on the Yorkshire Coast but has received little attention since the late 19th century owing to beach sand cover. Temporary removal of these sands by winter storms in early 2018 allowed for a sedimentological and palaeontological study to be undertaken of a nearly 60 m-thick foreshore section. The rocks date to the latest Hettangian and early Sinemurian stages (Early Jurassic) and consist of five coarsening-upward cycles (parasequences) that grade from mudstones through siltstones into *Gryphaea*-rich shell beds. Ammonites are reasonably common along with a diverse benthos that, in addition to *Gryphaea arcuata* Lamarck, includes abundant bivalves (e.g. *Cardinia, Luciniola, Plagiostoma* and *Oxytoma*) and rarer serpulids, gastropods, foraminifers and solitary corals. In the upper part of the section, the thicker-shelled taxa are commonly bored, most frequently by cirripedes. Despite the diversity of the benthos and intense bioturbation, pyrite framboids are common with size distributions, suggesting deposition occurred under an oxic-dysoxic water column. Deposition at Redcar occurred 4 million

years after the end-Triassic mass extinction (during the latest Hettangian to Sinemurian Stage) and the diverse marine assemblages indicate recovery was substantially complete by this time.

Keywords: End-Triassic mass extinction, pyrite framboid, marine recovery

4.2 Introduction

The Cleveland Basin (Yorkshire) contains one of the classic Early Jurassic (Liassic) records that has provided important evidence on numerous aspects of the Early Jurassic world, such as the Toarcian Oceanic Anoxic Event (e.g. Little & Benton 1995; Wignall *et al.* 2005; Danise *et al.* 2013) and it also hosts the Global Boundary Stratotype Section and Point (GSSP) for the Sinemurian-Pliensbachian stage boundary (Meister *et al.* 2004). Older stratigraphic intervals have however been largely neglected because of poor coastal exposures and limited inland sites (mostly exposed in the 19th century) or borehole studies (Tate & Blake 1876; Ivimey-Cook & Powell 1991; Powell *et al.* 1992). Redcar Rocks is the only coastal locality available in the Cleveland Basin where rocks of the Hettangian and lowermost Sinemurian are exposed. The intertidal platforms were meticulously sampled by Tate and Blake and published in 1876. Their bed descriptions are somewhat difficult to interpret but they provided a useful sketch map of the foreshore depicting the location of key ammonite finds (expanded in Page 2004a). The succession was subsequently reported in Gad's (1966) unpublished Ph.D thesis and van Buchem and McCave (1989) although neither provided a detailed section or any palaeontological study. The problem with the Redcar sequence is its frequent cover beneath beach sand, as Tate and Blake (1876, p. 56) noted:- "the occasions, however, when so large an expanse of rock

is in view, as we have shown on the plan, are few". Fortunately, the storms in February-March 2018 removed great quantities of the sand cover exposing a section almost as good as seen by Tate and Blake over 140 years before. Our study provides a detailed sedimentary succession and record of fossil occurrences. We assess the palaeoenvironments through fossil occurrences, sedimentary facies and reconstruction of palaeoredox conditions using framboidal pyrite size distributions (cf. Atkinson & Wignall 2019). Redcar Rocks provide a new perspective on the Hettangian and Sinemurian interval that allows comparison with the well-documented Blue Lias Formation of southwest Britain and contributes new data on the changing environmental conditions and biotic recovery following the end-Triassic mass extinction event.

4.3 Geological setting

The Cleveland Basin formed as part of a series of small extensional basins within a shallow epicontinental seaway (Powell 2010). During the Lower Lias the basin was bordered by the Pennine High landmass to the west and the Market Weighton High to the south. The oldest Jurassic-aged rocks within the Cleveland Basin are assigned to the Redcar Mudstone Formation, a mud and silt rich succession that is divided into the following members: a lowermost Calcareous Shale Member defined by the presence of carbonate nodules, the Siliceous Shale Member (bearing sandy horizons), the Pyritous Shale Member (a dark shale, rich in pyrite) and the Ironstone Shale Member (characterized by beds of siderite nodules). Combined, the Redcar Mudstone Formation is *c*. 283 m thick near Redcar thinning southward (Powell 1984). The Redcar Rocks outcrop exposes much of the Redcar Mudstone, whilst the nearby Coatham Rocks feature the

overlying lower Pliensbachian-aged Staithes Sandstone Formation, albeit exposed only at very low tide (Fig. 4.1). Only intermittent exposure of this sequence is available however, even when much of the beach sand has been removed. A companion section is well exposed in the cliffs and reefs of Robin Hood's Bay some 40 km to the southeast, but only the upper 20 m or so of the Calcareous Shale is exposed there, meaning that these lower beds can only be studied at Redcar.

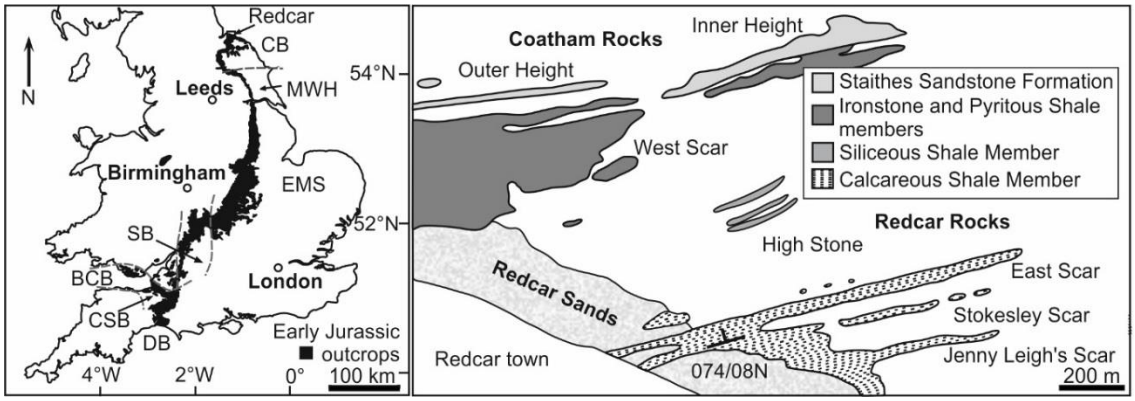

Fig. 4.1 UK location map showing Lower Jurassic outcrop and key sedimentary basins modified from Gründel *et al.* (2011) Basin codes as follows: BCB – Bristol Channel Basin; DB – Dorset Basin; CSB – Central Somerset Basin; EMS – East Midlands Shelf; SB – Severn Basin; MWH – Market Weighton High; CB – Cleveland Basin. Foreshore map of Redcar and Coatham rocks with geological units and scar names (Page 2004a).

4.4 Materials and methods

Logging of the Calcareous Shale Member was undertaken along the foreshore at Redcar Rocks using a high-precision Jacob's staff with laser sight (Patacci 2016), and sampled beds were allocated numbers (Red 1 – 31). At these semi-regular intervals benthic diversity was assessed by species counts. In mudstone bivalves were identified from freshly split surfaces of approximately equal volume of rock (~0.5 x 0.5 x 0.3 m). For shell beds fossils were identified *in situ* from bedding surfaces. Species range extensions are inferred from occurrences higher in the section at Robin Hood's Bay, Staithes and Hawsker Bottoms using occurrence data presented in Atkinson and Wignall (*under review;* Appendix E). Sediments were also studied in thin sections which allowed occurrences of microfossils (especially foraminifera) and shell fragments to be noted.

A subset of sampled horizons were used to test for changes in oxygenation regime using pyrite framboids. Employing the method from Wignall and Newton (1998), pyrite framboid diameters were measured on carbon-coated polished stone chips approximately 2 x 1 cm in size set into resin blocks and viewed using a Tescan VEGA3 XM scanning electron microscope (SEM) with a backscatter electron detector. Diameters were measured using inbuilt measurement applications of the SEM. Ideally 100 framboids were measured from each sample, if this could be achieved within a designated one-hour analysis time. Mean framboid diameter and standard deviation were calculated for each sample and plotted on what are referred to herein as a Wilkin diagram (cf. Wilkin *et al.* 1996).

4.5 Results

4.5.1 Sedimentology

The measured section spans some 50 metres predominantly of mudstone and silty-mudstone, with thin calcareous shell-rich beds (Fig. 4.2). Spacing of shell beds occurs with some degree of cyclicity. Between 16-22 m (beds 66-98 of Tate and Blake) there are 16 closely stacked shell beds, these form a projection out to sea known as Jenny Leigh's Scar (Fig. 4.1). The alternate regions dominated by softer mudstones produces a series of embayments between harder weathering reefs or "scars". Shell beds between 36-38 m form Stokesley Scar (beds 35-53 of Tate and Blake). Towards the top of the measured section these cycles become closer in their spacing, with sandy beds measured at 42 m and above, forming East Scar (beds 32-11 of Tate and Blake). The mudstones are medium to light grey in colour with little of the primary fabric retained owing to pervasive bioturbation, resulting in silt-grade quartz and detrital carbonate grains being scattered throughout, and shell fragments often rotated to high angles (Fig. 4.3A). Occasional horizons of carbonate concretions occur within the mudstone intervals usually in close association with shell beds. Between around 24-32 m (beds 55-64 of Tate and Blake) siderite nodules are found either scattered or forming distinct horizons. This part of the succession bears the lowest concentration of shell beds (Fig. 4.2).

The shell beds are up to 0.3 m thick and are formed of abundant thin shelled debris, including recognisable bivalve and echinoderm fragments and also large numbers of disarticulated *Gryphaea* and *Cardinia* shells (Figs. 4.3B & 4.4). The bases of the shell beds are seen as a mudstone with a high proportion

of thin shell fragments, grading up into siltier and sandier strata with larger and more numerous bioclasts (mostly *Gryphaea*) and culminating in shelly limestones cemented by sparite (i.e. biosparite, Fig. 4.3C). Small patches of mudstone can persist between shells. Shell beds sampled at horizons Red 8, 9, 15 and 17 all contain glauconite-replaced echinoderm fragments.

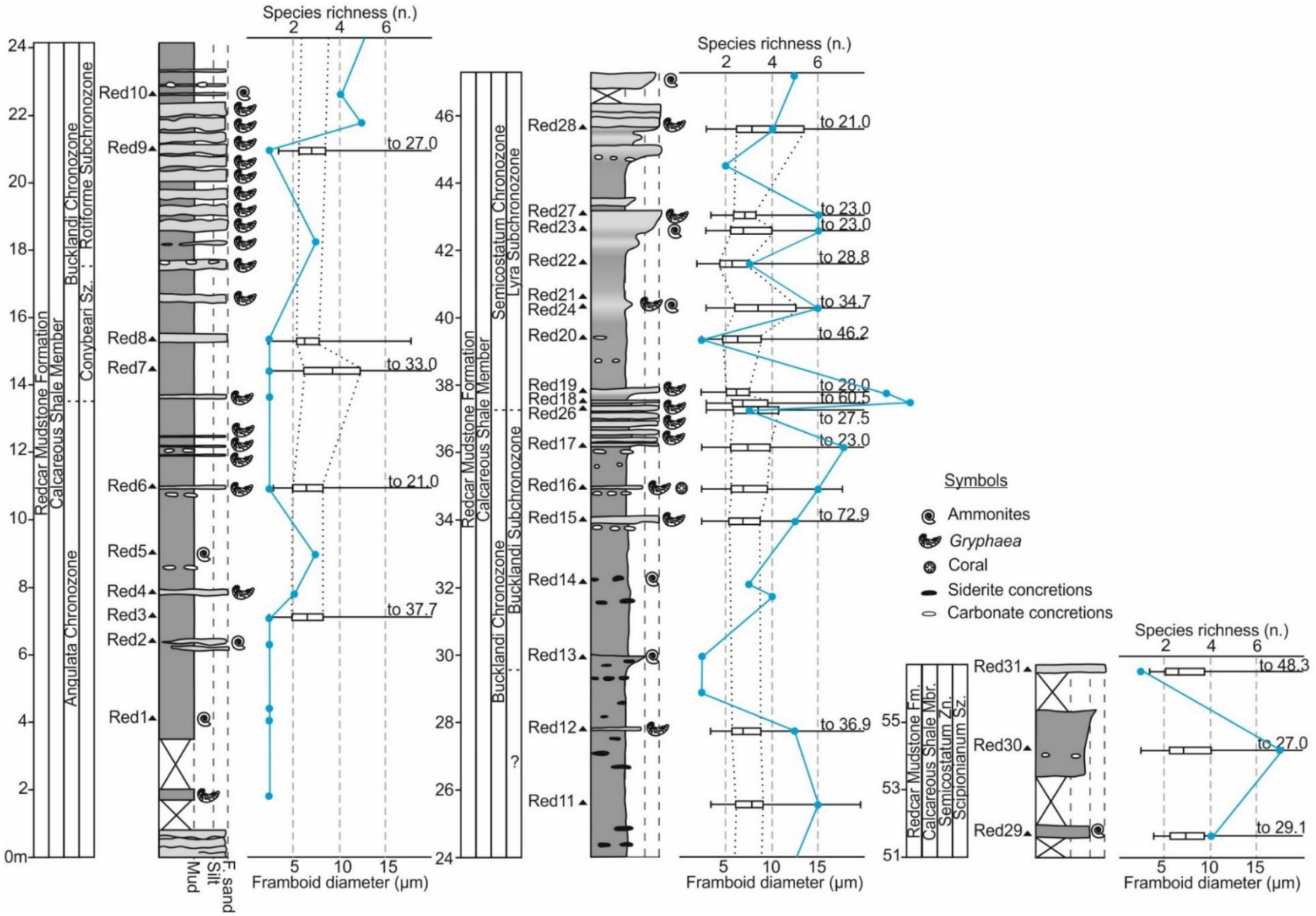
Species richness (n.)
Framboid diameter (µm)
Redcar Mudstone Formation
Calcareous Shale Member
Angulata Chronozone
Bucklandi Chronozone
Semicostatum Chronozone
Lyra Subchronozone
Bucklandi Subchronozone
Scipionianum Sz.
Rotiforme Subchronozone
Convybeari Sz.
Red1
Red2
Red3
Red4
Red5
Red6
Red7
Red8
Red9
Red10
Red11
Red12
Red13
Red14
Red15
Red16
Red17
Red18
Red19
Red20
Red21
Red22
Red23
Red24
Red26
Red27
Red28
Red29
Red30
Red31
to 27.0
to 33.0
to 21.0
to 37.7
to 21.0
to 23.0
to 23.0
to 28.8
to 34.7
to 46.2
to 28.0
to 60.5
to 27.5
to 23.0
to 72.9
to 36.9
to 48.3
to 27.0
to 29.1
Symbols
Ammonites
Gryphaea
Coral
Siderite concretions
Carbonate concretions
Mud
Silt
F sand

Fig. 4.2 Graphic log of Redcar Rocks including box and whisker plots of pyrite framboid results. Box and whisker plots, box depicts 25th and 75th percentiles, central line is median, whiskers illustrating minimum and maximum framboid diameters. Solid circles show record raw species richness per sampled horizon.

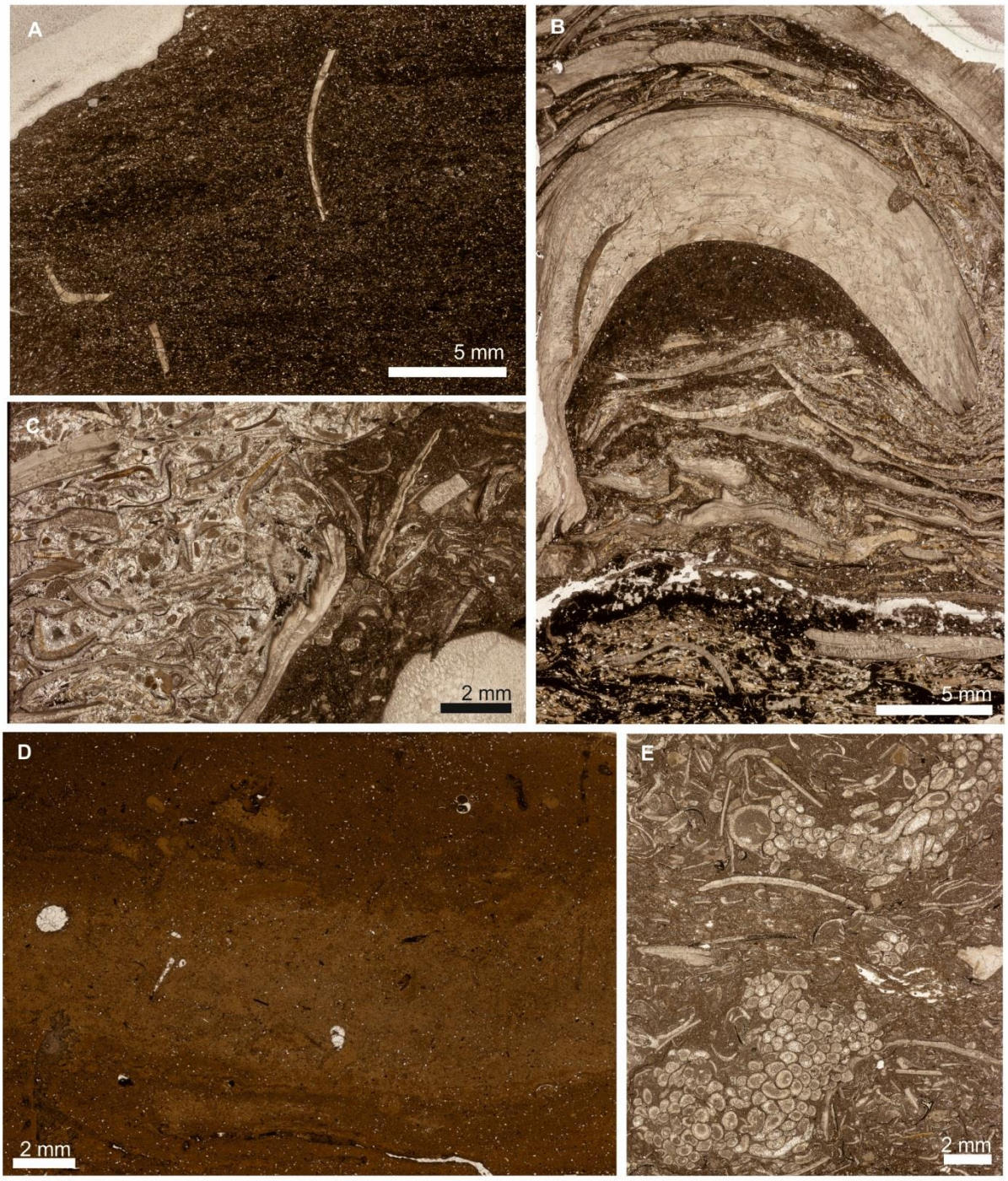

Fig. 4.3 Photomicrographs of thin sections. A, Red 23, shell fragment rotated by burrowing. B, Red 28, example shell bed including *Gryphaea* shell with simple boring on the right. C, Red 6, example of biosparite D, Red 24, phosphatic nodule featuring burrow mottling. E, Red 8, two nests of serpulid tubes.

Above 40 m the succession increases in grain size becoming increasingly silty, until at 42-47 m height fine sandstone beds form East Scar (Fig. 4.2). Initially these are composed of homogeneous siltstone of quartz and detrital carbonate grains that then grade up into carbonate-cemented fine sandstones rich in shell debris and *Gryphaea*. This part of the succession also features elongate, cigar-shaped phosphatic nodules, approximately 5 cm long, which preserve burrow mottling (Fig. 4.3D).

Viewed under a SEM many of the Redcar beds feature rice-shaped ankerite grains, typically <10 µm in length, often at high abundances within some samples (Fig. 4.5A). Red 27 and 29 also feature numerous iron oxide grains and infilling chambers of foraminifera seen in thin section, which may originally have been siderite or pyrite grains and pyrite infills respectively, prior to oxidation.

Fig. 4.4 *Gryphaea*-rich shell bed at outcrop. Hammer 30 cm long.

4.5.2 Fauna

Ammonite faunas of the lower 9 m of the section are dominated by *Schlotheimia* of the *angulata* Zone, of latest Hettangian age (Fig. 4.6A). These are replaced by Arietitidae in the basal Sinemurian, *conybeari* Subzone

(*bucklandi* Zone), including *Metophioceras* spp.. No ammonites were found from Jenny Leigh's Scar during this survey, although previously reported finds include *Coroniceras* ex grp *rotiforme* (J. de C. Sowerby) and ?*Arietites* sp. indicating the *rotiforme* and *bucklandi* subzones respectively (Page 2004a).

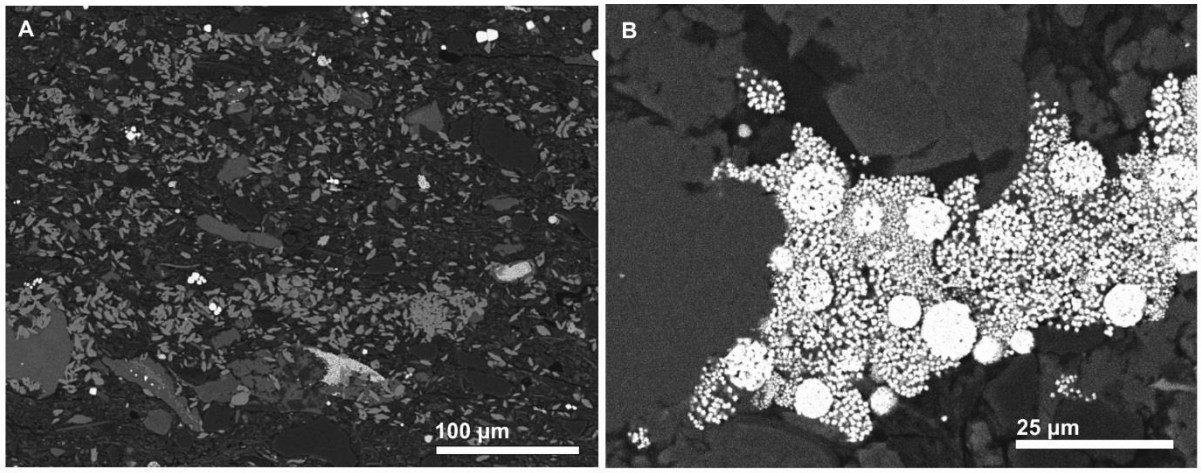

Fig. 4.5 SEM images. A, Red 11, abundant rice-shaped ankerite grains (pale grey). B, Red 15, pyrite framboids surrounded by a cloud of dissociated pyrite microcrysts,

Placement of the *rotiforme-bucklandi* Subzone boundary is unclear although *Coroniceras* ex grp *multicostatum* (J. Sowerby) suggests late *bucklandi* Subzone by horizon Red 14. The lowest part of the succeeding *semicostatum* Zone is recognisable from the upper beds of Stokesley Scar on the basis of *Paracoroniceras* sp. with well preserved and encrusted examples of *Arnioceras* also collected from the mudstones above (Fig. 4.6B). The *scipionanum* Subzone is recognised by *Agassiceras* with *Arnioceras acuticarinatum* (Simpson).

Using range-through species richness benthic diversity was modest during the *angulata* Zone, with fewer than 10 species present, but then rises markedly to 15 species in the first shell bed of Jenny Leigh's Scar. Above this level diversity

increases further to a stable diversity of around 22 for the remainder of the succession (Fig. 4.7). The assemblages are dominated by bivalves with a full range of ecologies present. Of the suspension feeding guilds of bivalve there is one epifaunal reclining species, two cementing, one epifaunal facultative motile, nine epibyssate and three endobyssate, three shallow infaunal, and two deep infaunal (Table 4.1). There are also six species of deposit-feeding, shallow infaunal bivalves and one abundant species that likely hosted sulphur-oxidising chemosymbiotic bacteria. After bivalves, gastropods form the next significant component with large forms present (up to 66 mm height, and width) such as *Pleurotomaria cognata* Chapuis & Dewalque (Fig. 4.6C), however the majority of gastropods are small (~1-2 mm) high spired forms identified only in thin section (Fig. 4.6D). Echinoderms are a common component with shell beds especially echinoid spines and ophiuroid plates. Red 12 also contained articulated specimens of *Isocrinus psilonoti* (Quenstedt) including cirri (Fig. 4.6E). Serpulids are locally common, with several species present, with dense, intergrown nests of small diameter specimens found in Red 8 (Fig. 4.3E).

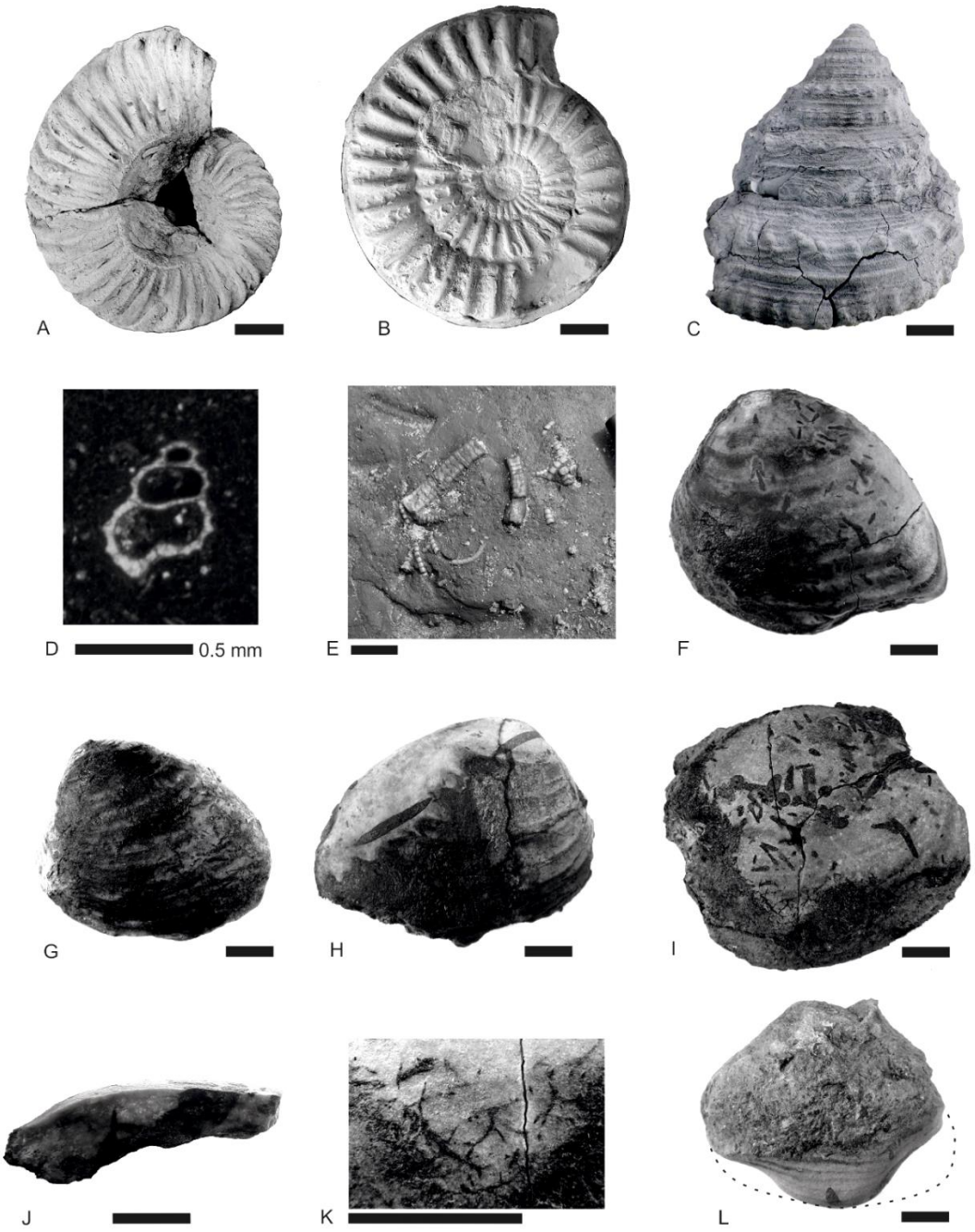
A
B
C
D
0.5 mm
E
F
G
H
I
J
K
L

Fig. 4.6 Examples of fossils collected from Redcar. A, Red 1, *Schlothemia* sp.; B, Red 21, *Arnioceras* sp. encrusted by *Liostrea irregularis* (Munster); C, Red 17, *Pleurotomaria cognata* Chapuis & Dewalque; D, Red 2 photomicrograph of microgastropod in thin section; E, Red 12 *Isocrinus psilonoti* (Quenstedt), partially articulated specimen with cirri, photographed *in situ;* F-I, Red 15, *Cardinia listeri* (J. Sowerby) featuring a range of cirripede borings. J, cross-section through part of *C. listeri* shell (I) showing potential *Simonizapfes*; K, detail of *C. listeri* shell (I) with possible bryozoan borings; L, *C. listeri* with growth defect, dashed line projects normal shell outline. A-C, whitened using ammonium chloride, scales bars 1 cm unless otherwise stated.

Gryphaea arcuata occurs throughout the entire succession and is the most notable fossil especially in the shell beds where their thick shells dominate (Fig. 4.4). In the upper shell beds of Jenny Leigh's Scar *Cardinia listeri* (J. Sowerby) is also found in high numbers alongside *G. arcuata*, again a thick shelled species. Shell beds also contain subordinate faunas including *Luciniola limbata* (Terquem & Piette) and the solitary coral *Trocharea guettardi* (Blaniville) (c. 35 m, bed 55 of Tate and Blake). *Cardinia* and *Gryphaea* specimens in the shell beds of Stokesley and East Scar frequently display a range of borings, which are infilled by matrix testifying they are of Jurassic origin (Fig. 4.6F-L). The majority of the bore marks are slit-like in form and pinched at one end, typical of barnacle borings (Häntzschel 1975) such as *Zapfella, Rogerella* and *Simonizapfes;* the last has a distinctive sock-shaped cross section, seen a in broken *Cardinia* from Red 15 (Fig. 4.6J). A fine network-like boring was seen on *Cardinia* shells. These do not penetrate the shell to any significant depth however, and may have been formed by boring bryozoans (Fig. 4.6K). Other borings include simple rounded holes and elongate gashes (Fig. 4.6H). Evidence for constrained growth in a specimen of *Cardinia* was also found, this specimen shows normal growth was impeded partway during the individual's life resulting in irregular growth lines and a miss-shaped outline (Fig. 4.6L). In the shell beds of Jenny Leigh's Scar almost no boring was seen and shells are generally in a better state of preservation with more articulated *Cardinia* fossils.

SPECIES	***ECOLOGY***
Gryphaea arcuata Lamarck	surficial, non-motile, reclining suspension feeder
Atreta intusstriata (Emmrich)	surficial, cemented, suspension feeder
Terquemia difformis (Schlotheim)	surficial, cemented, suspension feeder
Liostrea irregularis (Munster)	surficial, cemented, suspension feeder
Plagiostoma giganteum J. Sowerby	surficial, byssate, suspension feeder
Plagiostoma punctatum J. Sowerby	surficial, byssate, suspension feeder
Pseudolimea pectinoides (J. Sowerby)	surficial, byssate, suspension feeder
Antiquilima succincta (Schlotheim)	epibyssate, suspension feeder
Grammatodon (Cosmetodon) sp.	epibyssate, suspension feeder
Oxytoma inequivalvis (J. Sowerby)	epibyssate, suspension feeder
Camptonectes cf. auritus (Schlotheim)	epibyssate, suspension feeder
Chlamys textoria (Schlotheim)	epibyssate, suspension feeder
Entolium lunare (Roemer)	surficial, facultative motile, suspension feeder
Modiolus sp.	endobyssate, suspension feeder
Pinna sp.	endobyssate, suspension feeder
Gervillia hagenowi (Dunker)	endobyssate, suspension feeder
Neocrassina sp.	shallow infaunal, suspension feeder
Cardinia listeri (J. Sowerby)	shallow infaunal, suspension feeder
Protocardia philippianum (Dunker)	shallow infaunal, suspension feeder
Luciniola limbata (Terquem & Piette)	shallow infaunal suspension feeder with chemosymbionts
Dacryomya heberti (Martin)	shallow infaunal, deposit feeder
Palaeonucula navis (Piette)	shallow infaunal, deposit feeder
Ryderia doris (d'Orbigny)	shallow infaunal, deposit feeder
Rollieria bronni (Andler)	shallow infaunal, deposit feeder
Palaeoneilo elliptica (Goldfuss)	shallow infaunal, deposit feeder
indeterminate protobranch	shallow infaunal, deposit feeder
Gresslya sp.	deep infaunal, suspension feeder
Pleuromya liasina (Zieten)	deep infaunal, suspension feeder

Table 4.1 Bivalve ecologies encountered within the Redcar sequence, assigned from published literature (Johnson 1984; Hodges 1991, 2018; Wignall 1990; Damborenea & Manceñido 2005; Ros-Franch *et al.* 2014).

Fossils are most conspicuous in the shell beds, but many species occur within the mudstones. These often include thin-shelled protobranch species as well as *Luciniola limbata, Oxytoma inequivalvis* (J. Sowerby) and *Pseudolimea pectinoides* (J. Sowerby) (Fig. 4.7). Large logs of fossilised wood were also noted.

Several foraminifera were identified from thin sections these are predominately elongate, uniserial forms (*Pseudonodosaria*, *Paralingula*, *Dentalina*), these are shallow infaunal forms (Rita *et al.* 2016). Discoidal coiled forms (*Glomospirella*) was found in Red 2 this being an epifaunal morphology (Rita *et al.* 2016). Red 27 hosted the greatest abundance of foraminifera with numerous examples of *Lenticulia,* an opportunistic form. Ostracods were also encountered in several beds (Red 2, 3, 15, 20, 24).

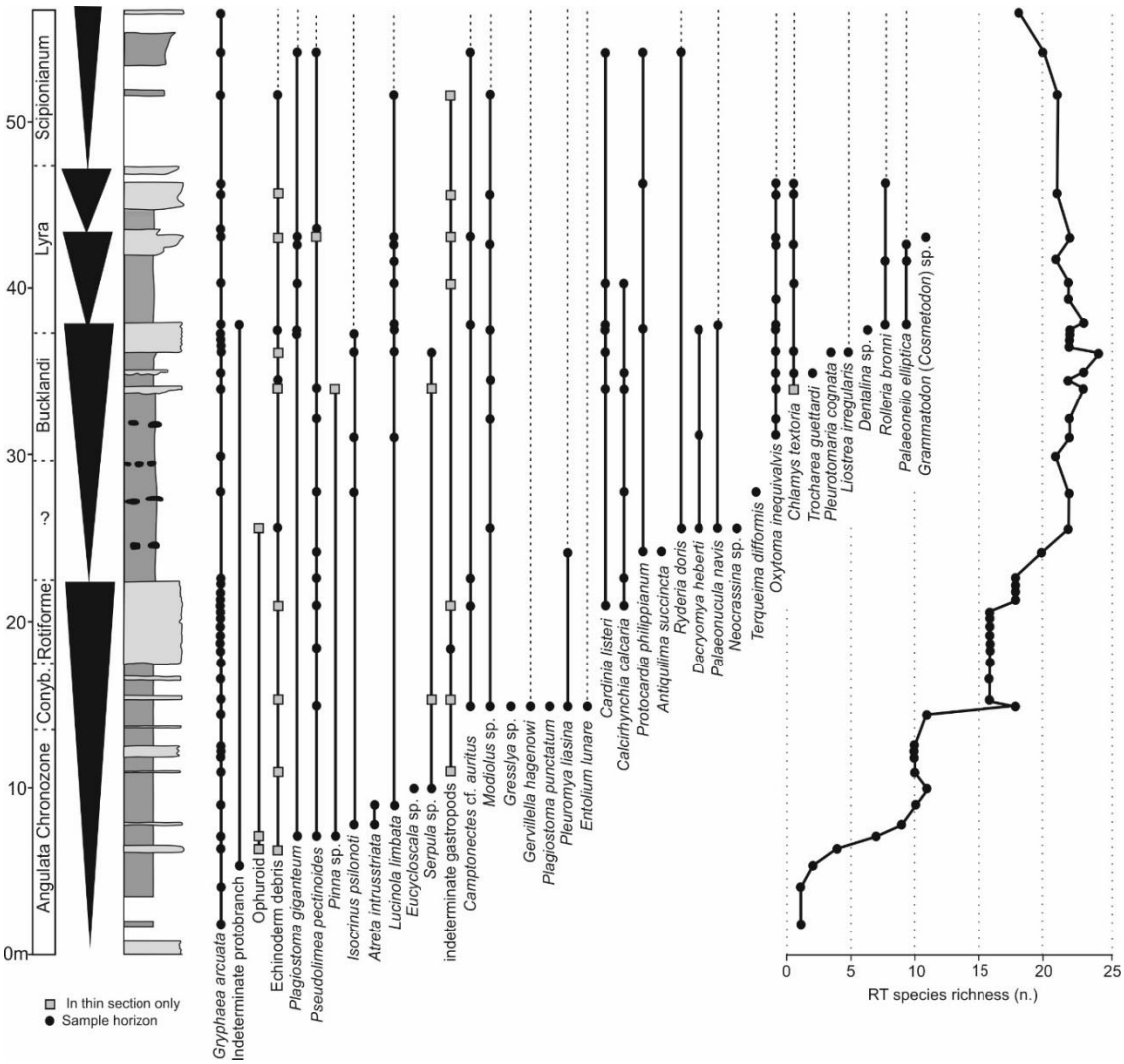

Fig. 4.7 Species range chart and range through (RT) species richness for Redcar Rocks. For range chart dark circles show horizons species were encountered during field collections, shaded squares for species only encountered in thin sections. Connecting line indicates range of species, extensions to ranges based on personal observations and species occurrence data presented in Atkinson and Wignall (*under review,* Appendix E). Inverted black triangles on the left depict the five parasequences.

4.5.3 Framboid analysis

Pyrite was found in all samples, both as euhedral crystals and framboidal pyrite and locally replaces the matrix (Red 28). Framboids often occur in clusters or streamers surrounded by clouds of dissociated pyrite microcrysts (Fig. 4.5B). In all bar two samples over 100 framboids were counted within the one-hour analysis time (however the two samples still contained >70 framboids each). All samples show framboid populations that plot in the oxic-dysoxic field of the Wilkin diagram (Fig. 4.2 & 4.8). There is no distinction between framboid populations measured from shell beds and mudstones and, equally, no systematic change in framboid diameters or standard deviation up-section. Overall the Redcar Rocks have an average framboid diameter of 8.35 microns and standard deviation of 4.31 microns.

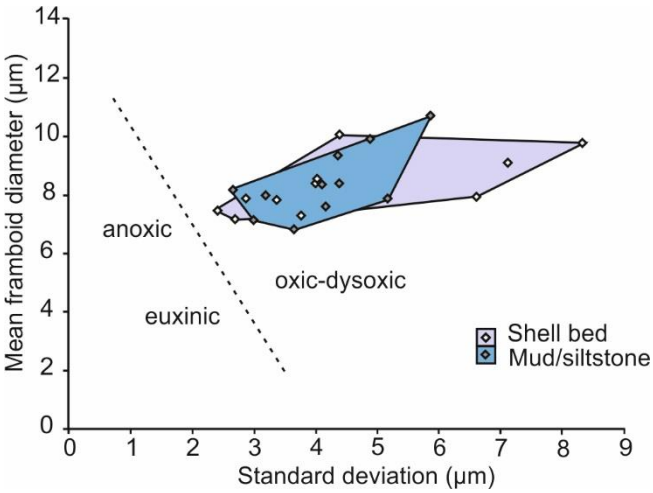

Fig. 4.8 Mean framboid diameter (µm) against standard deviation of framboid diameters (Wilkin diagram) for Redcar. Dashed line dictated anoxic/euxinic-oxic/dysoxic threshold (Wilkin *et al.* 1996). Samples plotted as either being from shell beds or the intervening mudstones and siltstones with shaded regions illustrating the spread of results.

4.6 Discussion

Redcar presents a mudstone dominated succession encompassing the Hettangian-Sinemurian boundary (*angulata-bucklandi* zonal boundary) with a reasonably diverse benthic fauna. Quiet water mudstone deposition was interspersed by periods of prolonged winnowing generating shell beds dominated by the thick-shelled *Cardinia* and especially *Gryphaea*. The associated grain size increase suggests the shelly horizons represent shallower/more proximal environments.

There are five distinct parasequences (shallowing-up cycles) each passing from mudstone-dominated to shell bed-dominated facies. The first parasequence forms the base of the section to the top of Jenny Leigh's Scar, the second culminates in the top of Stokesley Scar, the third and fourth occur in East Scar and the base of the fifth is at the top of the section (Fig. 4.7). Superimposed on this succession there is a long-term, weakly expressed, upwards coarsening that coincides with a reduction in parasequence thickness, suggesting that accommodation space was declining. The long-term increase in boring intensity, culminating in the shells found in Stokesley and East Scar, indicates more prolonged exposure on the sea floor compared with shells from the stratigraphically older, and more expanded, Jenny Leigh's Scar shell beds. The mud/siltstone-shell bed cycles continue into higher levels of the *semicostatum* Zone with similar beds reported from the younger succession at Robin Hood's Bay 40 km to the south east (Page 2004b).

An Early Jurassic eustatic sea level curve has been developed, based primarily on data from UK sections (Hesselbo & Jenkyns 1998; Hesselbo 2008). Relative water depths seen in the Redcar succession are only partially in accord

with this curve. Thus, a relative sea level fall during the *rotiforme* Subzone is coincident with the formation of the Jenny Leigh's Scar shell bed but, deepening then purportedly occurs through the *bucklandi* Subzone to peak in a *lyra* Subzone highstand (Hesselbo 2008). At Redcar this initial deepening is coincident with the deposition of mudstones (24-32 m, beds 55-64 of Tate and Blake), but intervals of shallowing saw the formation of the Stokesley Scar shell beds in the *bucklandi* Subzone. The *lyra* Subzone at Redcar records relatively shallow deposition in parasequences of relatively limited thickness compared with the underlying examples. This could record a transition from early, aggradation-dominated parasequences to late, progradation-dominated, highstand deposition expressed in a relatively nearshore setting.

The faunal assemblage recorded from Redcar is diverse and features a wide range of ecological groups also seen elsewhere in contemporary British Liasic successions (Atkinson & Wignall 2019). It differs slightly from these other records in the paucity of large *Plagiostoma giganteum* J. Sowerby and *Pinna similis* Chapuis & Dewalque which abound, most notably in the limestone dominated successions of Glamorgan (Hallam 1960; Atkinson & Wignall 2019; Atkinson *et al.* 2019). The most distinctive faunal component of the Redcar rocks is *Gryphaea arcuata* which inspired Tate and Blake (1876) to propose the term "Gryphites" for the shell-rich strata. The uppermost *angulata* to *semicostatum* zones of the British Lias is characterised by high numbers of *Gryphaea*, that are often prolifically abundant, possibly owing to the preservability of their robust shells (Pugh *et al.* 2014), espciealy so in condenesd and winowed settings. Similar Gryphites to those seen at Redcar are reported from near Scunthorpe, on the East Midland Shelf, and Hock Cliff in the Severn Basin (Simms 2004; Radley 2008). In both instances these are *bucklandi* Zone in age, and are developed as

comparably thin beds within mudstone-dominated sections (Simms 2004; Radley 2008).

Although Tate and Blake reported four coral-hosting beds at Redcar only their second uppermost coral bed (bed 55 of Tate and Blake), was seen during this study, which hosts solitary coral *Trocharea guettardi* (Blainville) and scallop *Chlamys textoria* (Schlotheim). Solitary corals like *Trocharea* are widespread in the British Isles of the *angulata* and *bucklandi* zones, being recorded from Lincolnshire, Larne in Northern Island and Glamorgan (Trueman 1930; Negus 1983).

Basin	***angulata***	***bucklandi***
Cleveland	7	25
Dorset	8	Nd.
Central Somerset	11	12
Bristol Channel	17	13
Severn	Nd.	13

Table 4.2 Bivalve species richness per zone for four basins of the classic Blue Lias Formation compared to the Cleveland Basin. Bivalve species richness data from Atkinson and Wignall (2019) and Atkinson and Wignall (*under review,* Appendix E).

The Redcar succession records an interval of marine recovery > 4 Myr after the end-Triassic mass extinction, based on the most recent age model of Weedon *et al.* (2019). Sections elsewhere in the UK show that this recovery was rapid, with bivalve diversity essentially stabilised by the mid-Hettangian (Atkinson & Wignall 2019). Bivalve diversity per ammonite zone in the Calcareous Shale Member at Redcar can be compared with the recovery trend in the contemporary Blue Lias Formation of the southern UK (Table 4.2). For the *angulata* Zone the Redcar section has an equivalent bivalve species richness to that of the Blue Lias in southwest Britain, but this then increases greatly in the *bucklandi* Zone, far exceeding the numbers from field collections of the Blue Lias (Atkinson & Wignall 2019). This may reflect the more habitable conditions of the shallower water Cleveland Basin site, although the prevalence of framboidal pyrite and common occurrences of *Luciniola* suggest the presence of H_2S within the sediment, no horizons contained a framboid size distribution suggestive of an anoxic water column. With this respect the Cleveland Basin was similar to the Bristol Channel Basin of South Wales (Fig. 4.9).

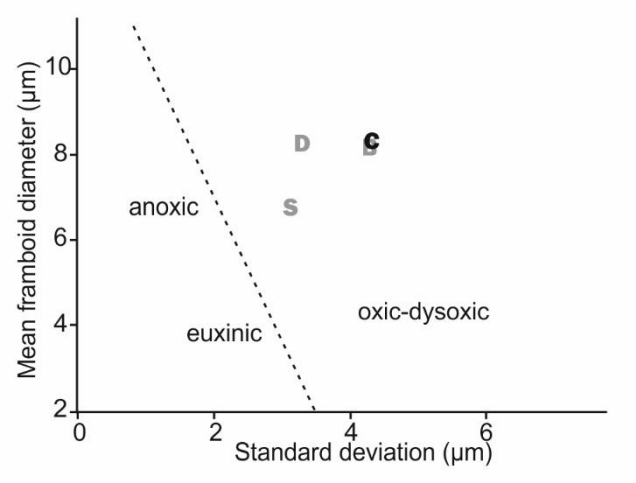

Fig 4.9 Average framboid diameter and standard deviation for three Blue Lias hosting basins in southwest Britain. D – Dorset Basin; B – Bristol Channel Basin; S – Central Somerset Basin (from Atkinson and Wignall 2019); C – Cleveland Basin (this study).

4.7 Conclusions

Redcar Rocks provide an alternative section to the classical Blue Lias sequences of southwest Britain and adds new insights to possible sea level changes around the Hettangian/Sinemurian boundary. The Calcareous Shale Member lacks the cyclical development of limestone-marl-shale as seen in the Blue Lias Formation of equivalent age, but, instead, features coarsening-up cycles that range from mudstones to mass accumulations of *Gryphaea arcutata* and *Cardinia listeri* in sandy shell beds or limestones. Benthic diversity is comparably high through much of the section with a wide range of ecologies represented suggesting advanced levels of recovery from the end-Triassic mass extinction event some 4 Myr earlier. Reconstructing marine oxygenation from pyrite framboid populations, suggests oxic-upper dysoxia conditions in the

Cleveland Basin and compliments the recent findings of Atkinson and Wignall (2019).

Acknowledgements

We wish to thank the YGS for providing funding for this project via the Yorkshire Geological Society Research Fund in its inaugural year. Tom Charman of Natural England for permissions to sample the Redcar Rocks. Harri Wyn Williams for his excellent thin-section making and Dave Bond for the use of his slide scanner.

References

Atkinson, J.W. & Wignall, P.B. 2019. How quick was marine recovery after the end-Triassic mass extinction and what role did anoxia play? *Palaeogeography, Palaeoclimatology, Palaeoecology*, **528**, 99–119, https://doi.org/10.1016/j.palaeo.2019.05.011.

Atkinson, J.W., Wignall, P.B., Morton, J.D. & Aze, T. 2019. Body size changes in bivalves of the family Limidae in the aftermath of the end-Triassic mass extinction: the Brobdingnag Effect. *Palaeontology*, https://doi.org/10.1111/pala.12415.

Damborenea, S. & Manceñido, M.O. 2005. Biofacies analysis of Hettangian-Sinemurian bivalve/brachiopod associations from the Neuquén Basin (Argentina). *Geologica Acta*, **3**, 163–178, https://doi.org/10.1344/105.000001405.

Danise, S., Twitchett, R.J., Little, C.T.S. & Clémence, M.-E. 2013. The impact of global warming and anoxia on marine benthic community dynamics : an example from the Toarcian (Early Jurassic). *PLoS ONE*, **8**, e56255, https://doi.org/10.1371/journal.pone.0056255.

Gad, M.A.M.A. 1966. *A Geochemical Study of the Liassic Rocks of the Yorkshire Coast*. University of London.

Gründel, J., Kaim, A., Nützel, A. & Little, C.T.S. 2011. Early Jurassic gastropods from England. *Palaeontology*, **54**, 481–510, https://doi.org/10.1111/j.1475-4983.2011.01043.x.

Hallam, A. 1960. A sedimentary and faunal study of the Blue Lias of Dorset and Glamorgan. *Philosophical Transactions of the Royal Society of London B: Biological Sciences*, **243**, 1–44, https://doi.org/10.1098/rstb.1960.0003.

Häntzschel, W. 1975. *Treatise on Invertebrate Paleontology Part W Miscellanea Supliment 1. Trace Fossils and Problematica*, 2nd ed. Teichert, C. (ed.). Boulder, The Geological Society of America, Inc. and The Universtiy of

Kansas.

Hesselbo, S.P. 2008. Sequence stratigraphy and inferred relative sea-level change from the onshore British Jurassic. *Proceedings of the Geologists' Association*, **119**, 19–34, https://doi.org/10.1016/S0016-7878(59)80069-9.

Hesselbo, S.P. & Jenkyns, H.C. 1998. British Lower Jurassic sequence stratigraphy. *In*: *Mesozoic and Cenozoic Sequence Stratigraphy of European Basins*. SEPM Special Publications No. 60.

Hodges, P. 1991. The relationship of the Mesozoic bivalve Atreta to the Dimyidae. *Palaeontology*, **34**, 963–970.

Hodges, P. 2018. *The Early Jurassic Bivalvia from the Hettangian and Lower Sinemurian of South-West Britain Part 2*. London, Monograph of the Palaeontographical Society, https://doi.org/10.1080/02693445.2017.11963960.

Ivimey-Cook, H.C. & Powell, J.H. 1991. Late Triassic and early Jurassic biostratigraphy of the Felixkirk Borehole, North Yorkshire. *Proceedings of the Yorkshire Geological Society*, **48**, 367–374.

Johnson, A. 1984. *The Palaeobiology of the Bivalve Families Pectinidae and Propeamussiidae in the Jurassic of Europe*. München, Zitteliana.

Little, C.T.S. & Benton, M.J. 1995. Early Jurassic mass extinction : A global long-term event. *Geology*, **23**, 495–498, https://doi.org/10.1130/0091-7613(1995)023<0495.

Meister, C., Aberhan, M., et al. 2004. The Global Boundary Stratotype Section and Point (GSSP) for the base of the Pliensbachian Stage (Lower Jurassic), Wine Haven, Yorkshire, UK. *Episodes*, **29**, 93–106.

Negus, P.E. 1983. Distribution of the British Jurassic corals. *Proceedings of the Geologists' Association*, **94**, 251–257, https://doi.org/10.1016/S0016-7878(83)80043-1.

Page, K.N. 2004a. Redcar Rocks. *In*: Simms, M. J., Chidlaw, N., Morton, N. & Page, K. N. (eds) *British Lower Jurassic Stratigraphy*. Peterborough, Geological Conservation Review Series, No. 30, Joint Nature Conservation Committee, 245–250.

Page, K.N. 2004b. Normanby Stye Batts-Miller's Nab (Robin Hood's Bay). *In*: Simms, M. J., Chidlaw, N., Morton, N. & Page, K. N. (eds) *British Lower Jurassic Stratigraphy*. Peterborough, Geological Conservation Review Series, No. 30, Joint Nature Conservation Committee, 250–262.

Patacci, M. 2016. A high-precision Jacob's staff with improved spatial accuracy and laser sighting capability. *Sedimentary Geology*, **335**, 66–69, https://doi.org/ 10.1016/j.sedgeo.2016.02.001.

Powell, J.H. 1984. Lithostratigraphical nomenclature of the Lias Group in the Yorkshire Basin. *Proceedings of the Yorkshire Geological Society*, **45**, 51–57.

Powell, J.H. 2010. Jurassic sedimentation in the Cleveland Basin : a review. *Proceedings of the Yorkshire Geological Society*, **58**, 21–72, https://doi.org/10.1144/pygs.58.1.278.

Powell, J.H., Cooper, A.C. & Benfield, A.C. 1992. *Geology of the County around*

Thirsk. British Geological Survey Memoir, England and Wales, Sheet 52.

Pugh, A.C., Danise, S., Brown, J.R. & Twitchett, R.J. 2014. Benthic ecosystem dynamics following the Late Triassic mass extinction event : Palaeoecology of the Blue Lias Formation, Lyme Regis, UK. *Proceedings of the Ussher Society*, **13**, 255–266.

Radley, J.D. 2008. Gryphaea beds (upper Scunthorpe Mudstone Formation; Lower Jurassic) at Scunthorpe, North Lincolnshire, north-east England. *Proceedings of the Yorkshire Geological Society*, **57**, 107–111.

Rita, P., Reolid, M. & Duarte, L. V. 2016. Benthic foraminiferal assemblages record major environmental perturbations during the Late Pliensbachian – Early Toarcian interval in the Peniche GSSP, Portugal. *Palaeogeography, Palaeoclimatology, Palaeoecology*, **454**, 267–281, https://doi.org/10.1016/j.palaeo.2016.04.039.

Ros-Franch, S., Márquez-aliaga, A. & Damborenea, S.E. 2014. Comprehensive database on Induan (Lower Triassic) to Sinemurian (Lower Jurassic) marine bivalve genera and their paleobiogeographic record. *Paleontological Contributions*, **8**, 1–219, https://doi.org/10.17161/PC.1808.13433.

Simms, M.J. 2004. Hock Cliff. *In*: Simms, M. J., Chidlaw, N., Morton, N. & Page, K. N. (eds) *British Lower Jurassic Stratigraphy*. Peterborough, Geological Conservation Review Series, No. 30, Joint Nature Conservation Committee, 164–170.

Tate, R. & Blake, J.F. 1876. *The Yorkshire Lias*. London.

Trueman, A.E. 1930. The lower Lias (bucklandi Zone) of Nash Point, Glamorgan. *Proceedings of the Geologists' Association*, **41**, 148–159.

van Buchem, F.S.P. & McCave, I.N. 1989. Cyclic sedimentation patterns in Lower Lias mudstones of Yorkshire (GB). *Terra Nova*, **1**, 461–467.

Weedon, G.P., Page, K.N. & Jenkyns, H.C. 2019. Cyclostratigraphy, stratigraphic gaps and the duration of the Hettangian Stage (Jurassic): insights from the Blue Lias Formation of southern Britain. *Geological Magazine,* **156**, 1469–1509, https://doi.org/10.1017/S0016756818000808.

Wignall, P.B. 1990. Benthic palaeocology of the Late Jurassic Kimmeridge Clay of England. *Special papers in palaeontology*, **43**.

Wignall, P.B. & Newton, R.J. 1998. Pyrite framboid diameter as a measure of oxygen deficiency in ancient mudrocks. *Amer*, **298**, 537–552, https://doi.org/10.2475/ajs.298.7.537.

Wignall, P.B., Newton, R.J. & Little, C.T.S. 2005. The timing of paleoenvironmental change ans cause-and-effect relationships during the Early Jurassic mass extinction in Europe. *American Midland Naturalist*, **305**, 1014–1032.

Wilkin, R.T., Barnes, H.L. & Brantley, S.L. 1996. The size distribution of framboidal pyrite in modern sediments: An indicator of redox conditions. *Geochimica et Cosmochimica Acta*, **60**, 3897–3912, https://doi.org/10.1016/0016-7037(96)00209-8.

Chapter 5: Body size trends and recovery amongst bivalves following the end-Triassic mass extinction

Submitted for publication in Palaeogeography, Palaeoclimatology, Palaeoecology

Body size trends and recovery amongst bivalves following the end-Triassic mass extinction

Jed W. Atkinson* and Paul B. Wignall

School of Earth and Environment, University of Leeds, Leeds, UK, LS2 9JT.

*gy12jwa@leeds.ac.uk

5.1 Abstract

Fossils in the immediate aftermath of mass extinctions are often of small size, a phenomenon attributed to the Lilliput Effect (temporary, size reduction of surviving species). There has been little attempt to study size trends during subsequent recovery intervals nor has the relationship between size, diversity and environmental controls been evaluated. Here we examine the recovery following the end-Triassic mass extinction amongst bivalves of the British Lias. Three distinct phases of size change are seen that are independent of other recovery metrics: initially bivalves are small but the Lilliput Effect is a minor factor, the majority of small taxa belong to new species that undergo an intraspecific size increase (the Brobdingnag Effect) throughout the subsequent Hettangian Stage. New species that appeared during the Hettangian were also progressively larger and Cope's Rule (size increase between successive species) is reported – notably amongst ammonites. The size increase was reversed during the Sinemurian Stage, when bivalves once again exhibited small body sizes. During the Pliensbachian Stage another phase of size increase occurred with further evidence of the Brobdingnag Effect. These three phases of size change are seen across all suspension feeding ecological guilds of bivalve but are not expressed

among deposit feeding life modes. Local environmental conditions explain some aspects of size patterns, but factors such as temperature, marine oxygenation and sea level, do not correlate with the long-term size trends. The Brobdingnag Effect may record increased availability/quality of food during the recovery interval: a factor that controlled bivalve size but not evolution.

Keywords: Brobdingnag Effect; Lilliput Effect; Cope's Rule; Lower Jurassic palaeoenvironments

5.2 Introduction

The causes and nature of size changes during mass extinction events have been much debated (Twitchett 2007; Harries & Knorr 2009; Brayard *et al.* 2010; Metcalfe *et al.* 2011; Song *et al.* 2011; Sogot *et al.* 2014; Brom *et al.* 2015; Wiest *et al.* 2018; Atkinson *et al.* 2019; Chen *et al.* 2019). Species that survive mass extinctions are often unusually small and are termed "Lilliput taxa" (Urbanek 1993), although the more general term "Lilliput Effect" is used to describe the prevalence of smaller species at this time. The cause of the size reduction is often unclear and there are several possible mechanisms including preferential extinction of large taxa, dwarfing of species that cross the extinction boundary and proliferation of small, fecund species (opportunists) in the high stress conditions of the extinction interval (Batten & Stokes 1986; Payne 2005; Twitchett 2007; Harries & Knorr 2009). Implicit in the Lilliput concept is that species return to larger sizes in the subsequent post-extinction interval as the stressful conditions ameliorate. However, a recent study of sizes changes in limid bivalves in the aftermath of the end-Triassic mass extinction revealed a prolonged size

increase of species that first appeared after the extinction but with no precursory size reduction (Atkinson *et al.* 2019). This has been termed the Brobdingnag Effect, after the race of giants in *Gulliver's Travels*, and its importance during post-extinction recovery remains unexplored. The Brobdingnag Effect is an intraspecific size increase and is thus distinct from Cope's Rule which is an increase in size between successive species in a lineage (Cope 1887; Rensch 1948; Jablonski 1997; Alroy 1998).

Here we examine the size-recovery relationships of the entire bivalve fauna from the British Lower Jurassic record to determine the extent of the Brobdingnag Effect and its possible causes following the end-Triassic mass extinction event. Body size of marine invertebrates is influenced by factors like water temperature, dissolved oxygen content, salinity and nutrient availability (e.g. Rhoads & Morse 1971; His *et al.* 1989; Atkinson 1994; Wacker & von Elert 2008). It is likely that each species responds to environmental changes in their own unique manner with each species having a different optimal body size for a certain environment (Hallam 1965; Carey & Sigwart 2014).

Oxygen restriction has been demonstrated as a cause of reduced body sizes (Rhoads & Morse 1971; Richmond *et al.* 2006) due to reduced metabolic and growth rates (Richmond *et al.* 2006), although some low-oxygen tolerant species can increase in size as oxygen levels decline (Wignall 1990). Temperature exerts a control on the concentration of dissolved gasses within the waters, but it can also affect body size directly. Perhaps the most renowned temperature-size trend is Bergmann's Rule, although this is strictly a positive correlation with body size and latitude – taken as an approximation of temperature (Bergmann 1847; James 1970; Blackburn *et al.* 1999). As the current study has little in the way of a latitudinal gradient it is perhaps better, in order to

avoid confusion, to refer to the rather unambiguously named Temperature-Size Rule (Atkinson 1994; Atkinson & Sibly 1997). This rule explains how growth rates and development rates are affected unequally by temperature with the latter being more sensitive. For example, under low temperatures both growth and development rates are slowed, the latter more so thereby delaying sexual maturity allowing an increased duration of growth which can result in larger animals.

Food availability and quality are known controls on body size (von Elert *et al.* 2003; Wacker & von Elert 2003). Amongst bivalves, red algae (dinoflagellates) are preferable for good growth over green algae (prasinophytes and acritarchs) because the latter are smaller which reduces the capture rate by the gills of bivalves, and also green algae lack key long-chained polyunsaturated fatty acids essential for growth (Brown *et al.* 1997; von Elert *et al.* 2003; Weiss *et al.* 2007). Turbidity of the water has also been suggested as a factor affecting body size because it lowers filtration rate in the bivalves, and causes them to spend more time with valves closed (Loosanoff & Tommers 1948).

Single species distributed over a broad range of water depths are often (although not exclusively) smaller at greater bathymetries (Attrill *et al.* 1990; Olabarria & Thurston 2003; Kaariainen & Bett 2006). This is likely a manifestation of numerous depth-linked factors such as food and dissolved oxygen concentrations (Shirayama 1983; Peck & Harper 2010; Shi *et al.* 2016).

Most of the size-control factors that are outlined above can be evaluated in the geological record and are considered here in order to distinguish environmental controls from temporal trends in bivalve body size in the Lower Jurassic following the end-Triassic mass extinction.

5.3 Geological setting

During the Rhaetian and Lower Jurassic the British Isles formed part of an epicontinental sea that extended across much of northwest Europe (Hallam 1960). This Rhaetic sea was likely of variable salinity, as it lacked stenohaline taxa (Hallam & El Shaarawy 1982; Swift 1999). Fully marine conditions developed around the Triassic-Jurassic boundary and persisted into the Early Jurassic. Many islands dotted this Jurassic sea, and consequently a range of depositional environments are recorded across different basins in relation to proximity to these landmasses (Fig. 5.1). For example the Bristol Channel Basin passes onto the Welsh Massif, where Carboniferous limestones are onlapped by marginal facies (Sheppard 2006). Likewise, there are similar facies around the Shepton Mallet area of Somerset (Simms 2004).

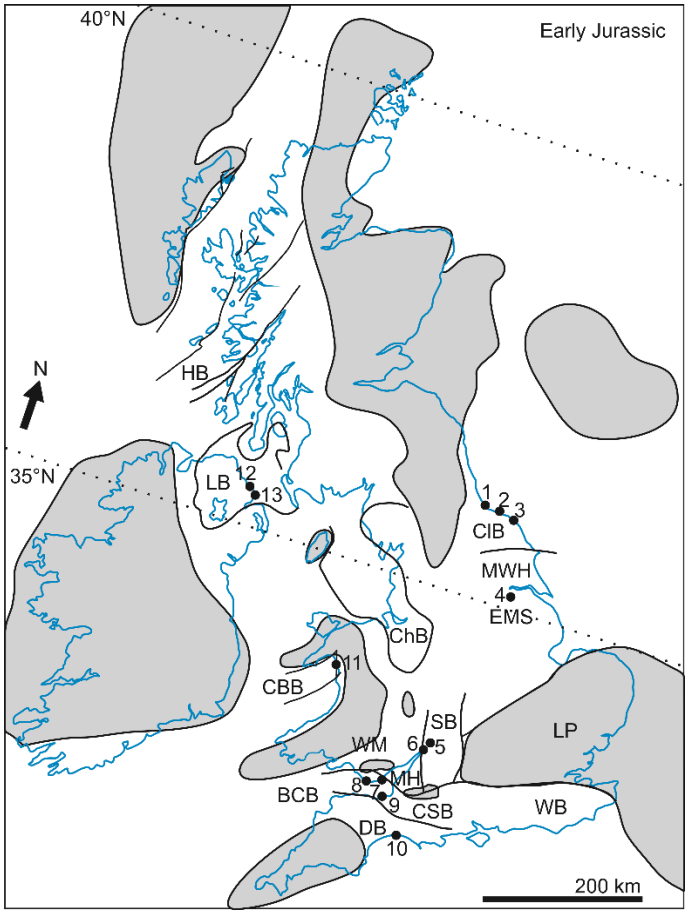
Early Jurassic
40°N
35°N
N
HB
LB
12
13
1
2
3
CIB
MWH
4
EMS
ChB
11
CBB
SB
WM
6
5
LP
MH
8
BCB
9
CSB
WB
DB
10
200 km

Fig. 5.1 Palaeogeography of the British Isles with Hettangian landmasses (indicated by shaded regions) and sedimentary basins. Based on Deconinck *et al.* (2003)*;* Simms *et al.* (2004)*;* Copestake & Johnson (2014); Martill *et al.* (2016)*;* Lindström *et al.* (2017). Codes as follows: HB – Hebrides Basin; LB – Larne Basin; ClB – Cleveland Basin; MWH – Market Weighton High; EMS – East Midlands Shelf; ChB – Cheshire Basin; CBB – Cardigan Bay Basin; BCB – Bristol Channel Basin; CSB – Central Somerset Basin; SB – Severn Basin; WM – Welsh Massif; WB – Wessex Basin; MH – Mendips High; DB – Dorset Basin; LP – London Platform. Location numbers: 1 – Redcar, North Yorkshire (NZ 613 253); 2 – Staithes, North Yorkshire (NZ 781 190); 3 – Hawsker Bottoms (NZ 952 076) and Robin Hood's Bay, North Yorkshire (NZ 971 028); 4 – Conesby Quarry, Scunthorpe (SE 889 145); 5 – Robin's Wood Hill Quarry, Gloucestershire (SO 835 148); 6 – Hock Cliff, Gloucestershire (SO 725 093); 7 – Lavernock Point, Glamorgan (ST 188 682 – ST183.679); 8 – Nash Point, Glamorgan (SS 911 692 – SS 921 679); 9 – Doniford (ST 083 431), St Audire's Bay (ST 103 434 – ST 099 433), East Quantoxhead to Kilve (ST 134 442 – 142 444), and Lilstock (ST 178 453), Somerset; 10 – Pinhay Bay to Charmouth (SY 317 907 – SY 970 929), Devon/Dorset; 11 – Llanbedr (Mochras Farm) borehole, North Wales (SH 553 259); 12 – Larne (NW 558 582) and Portmuck Harbour (NW 558 582) County Antrim; 13 – Cloghfin Port (NW 624 490) and Cloghfin Point (NW 608 454), County Antrim.

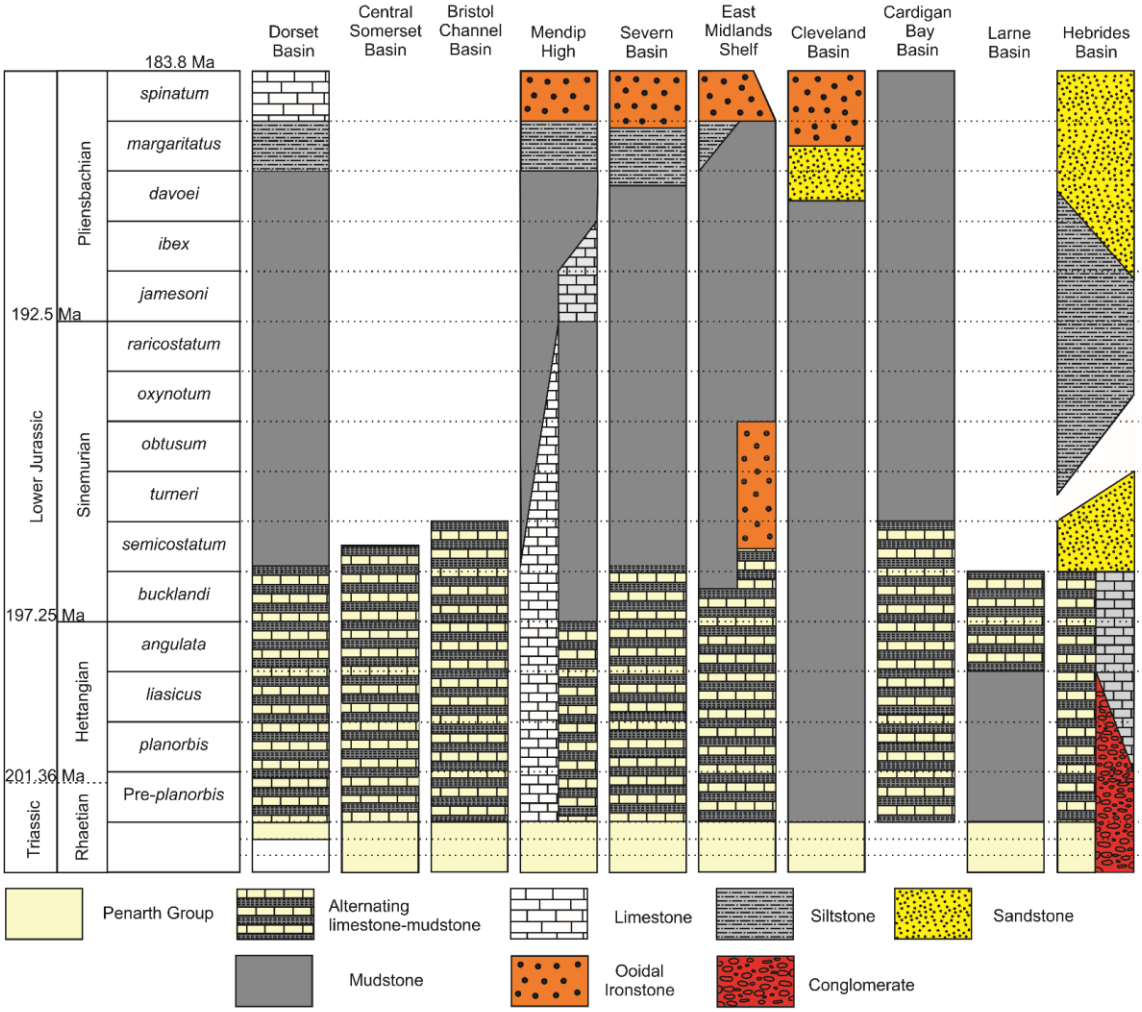

Fig. 5.2 Schematic lithostratigraphy of studied sedimentary basins. Modified from Ivimey-Cook (1971); Simms *et al.* (2004); Simms & Jeram (2007). Stage boundary ages from Wotzlaw *et al*. (2014); Ruhl *et al.* (2016), Weedon *et al*. (2019).

There were, broadly speaking, four phases of sedimentation in the British Lias (outlined below). Between the basins and shelves these intervals are correlated using a well-defined ammonite biostratigraphy (Fig. 5.2).

Rhaetic sedimentation in the British Isles is recorded in the Penarth Group, consisting of the shallow-water, quasimarine Westbury and Lilstock formations. The end-Triassic mass extinction occurs within the Cotham Member of the Lilstock Formation during a regressive interval (Wignall & Bond 2008).

Subsequent deposition saw progressive deepening, although a minor sea level fall occurred at the top of the Group (Wignall 2001).

Pre-*planorbis* to *bucklandi* zones sees the onset of the Blue Lias Formation, a cyclic limestone-marl-shale unit that represents offshore deposition (Hallam 1960; Weedon 1986; Moghadam & Paul 2000). In the *liasicus* Zone limestone beds are rarer – likely due to deepening (Ivimey-Cook 1975; Weedon *et al.* 2018). The Blue Lias Formation is found chiefly in southern regions of Britain, and passes northwards into mudstone-dominated successions (Fig. 5.2; Simms and Page 2004). However, the Blue Lias is also developed in the Hebrides Basin of north-west Scotland and passes laterally into the shallower-water bioclastic limestones of the Breakish or Broadford Formation (Oates 1978).

Mudstone dominates sedimentation from the *semicostatum* to *davoei* zones (e.g. the Charmouth Mudstone, Redcar Mudstone and Pabay Shale formations, Fig. 5.2). Within the *semicostatum* to *obtusum* interval deposition within the Dorset Basin is characterised by sediments of high organic carbon content and evidence for sea-floor anoxia, these being the Shales-with-Beef and Black Ven Marls of the Charmouth Mudstone Formation (Wignall & Hallam 1991; Gallois 2008). Similarly the *obtusum* Zone of the Mendips is represented by dark laminated limestones (Simms 2004). To the north of this region lithologies are more variable. The northern part of the East Midlands Shelf (EMS) is especially distinct during the *semicostatum* to *obtusum* zones with the deposition of the Frodingham Ironstone Member of the Scunthorpe Mudstone Formation (Hallam 1963). Deposition in the Hebrides Basin during this interval was dominated by siltstones of the misleadingly named Pabay Shale Formation (Oates 1978; Morton 1989). Deposition here occurred under shallower water depths than seen

in several basins at this time and was above the storm wave-base (Morton & Oates 2004).

Siltstone deposition dominated the *davoei* to *margaritatus* interval across much of the British Isles (Fig. 5.2). Once again conditions were shallower than elsewhere in the Hebrides Basin where the Scalpay Sandstone Formation formed (Hesselbo *et al.* 1998; Radley 2003; Donovan *et al.* 2005). Within the Cleveland Basin the later part of this interval saw the Staithes Sandstone Formation replaced by the Cleveland Ironstone Formation, that shows coarsening-up cycles capped by oolitic ironstone beds (Howarth 1955; Howard 1985). Indeed many basins show an overall coarsening upwards during this interval that culminates in the *spinatum* Zone (Fig. 5.2). This is not expressed in the Cardigan Bay Basin where siltstone dominates the thick succession from the *jamesoni* Zone upwards (Ivimey-Cook 1971).

5.4 Materials and methods

Bivalve size data were collected from the Westbury Formation to the topmost *spinatum* Zone, encompassing the Rhaetian, Hettangian, Sinemurian and Pliensbachian stages. The bivalves *Plagiostoma giganteum* J. Sowerby and all species of *Gryphaea* were excluded from our analysis because their size trends are already well documented (Hallam 1978; Johnson 1994; Atkinson *et al.* 2019). Latest Rhaetian and Liassic bivalve data were collected via two methods: direct field observations and museum collections. Field collections were made from coastal locations in Devon, Dorset, Somerset, Glamorgan, North Yorkshire, and County Antrim, a river cliff section and quarry in Gloucestershire, a quarry in North Lincolnshire and material retrieved from the Llanbedr (Mochras Farm)

borehole, Wales housed in the British Geological Survey, Keyworth, Nottingham (Fig. 5.1). These sections represent the full spectrum of sedimentary basins and depositional settings of the epicontinental sea that covered much of the British Isles in the Early Jurassic. For softer lithologies (mudstones, siltstones, shales and marls), fossils were measured and collected from freshly split surfaces from approximately equal volumes of rock (50 cm^2 width and 20-30 cm depth). For the harder limestone and ironstone beds, which could not easily be split, fossils were measured *in situ* from upper bedding surfaces or from scree if zonal affinity could be confirmed.

Museum collections include specimens with sufficient biostratigraphic context from the following institutes: National Museum of Wales, Cardiff (NMW); Warwickshire Museum, Warwick (WARMS); Bristol City Museum and Art Gallery, Bristol (BRSMG); Yorkshire Museum, York (YORYM); Whitby Museum, Whitby (WHITM); Bath Royal Literary and Scientific Institute, Bath (BRLSI). In addition, personal collections made by Michael Oates and JWA from the Hebrides Basin, material from Blockley Station Quarry, Long Itchington Quarry and Somerset collected previously by PBW housed in the School of Earth and Environment, University of Leeds and specimens from Northern Ireland donated by Michael Simms, are included. These are amalgamated under ‘museum collections’ as no conscious effort to avoid size biased sampling could be guaranteed.

For each specimen a series of measurements were recorded (Fig. 5.3) using a pair of digital callipers with a measurement error of +/-0.02 mm. For inequivalved species the larger, left valves were measured. Growth line spacing was measured from high resolution photographs in order to assess changes in growth rates. Height and length measurements were used to calculate geometric mean body size (GMBS). This being the square root of the product of height and

length. For incomplete specimens the missing values are calculated based on height to length ratios of coeval, complete specimens.

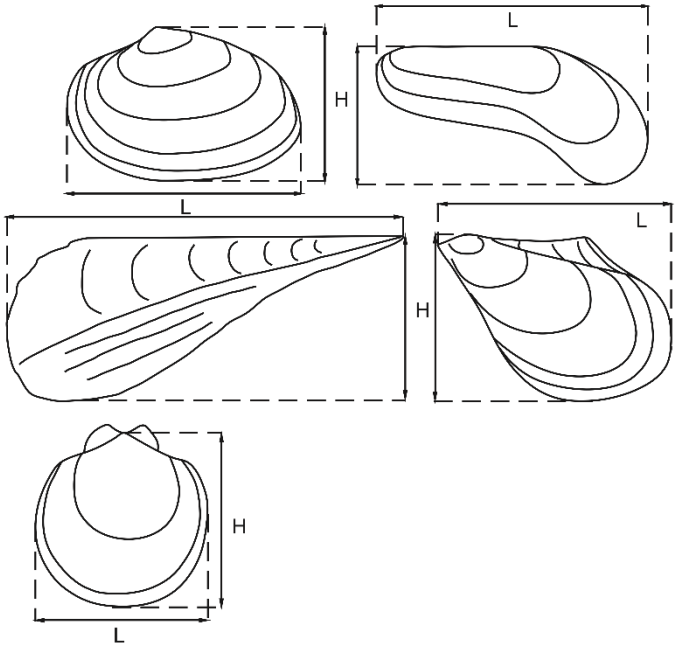

Fig. 5.3 Measurement schematic for a variety of bivalve morphologies.

GMBS is used for size analysis as it provides a better representation of a specimen's overall size than a single linear measurement, and correlates well with other, more complex, body size measurements, whilst being easy to obtain (cf. Kosnik *et al.* 2006).

Ammonite zones are selected for time bins providing a high-resolution age model suitable for both museum specimens (with sufficient context), and field observations. In some instances, data from the *semicostatum* and *turneri* zones were pooled, owing to low sample sizes. Durations of ammonite zones (including Pre-*planorbis* Beds) are primarily from astrochronological timescales of Weedon *et al.* (2019) and Ruhl *et al*. (2016) with exception to the interval spanning the *semicostatum* to *oxynotum* zones, duration for these zones are based on the assumption of equal duration of subzones. For the Rhaetian, which lacks

ammonites, the Westbury Formation and the constituent members of the Lilstock Formation are used as time bins, although these are of uncertain durations. The resultant floating chronology is tied using the U-Pb radiometric dates for the end-Triassic mass extinction and Triassic-Jurassic boundary of Wotzlaw *et al*. (2014).

Size plots feature mean GMBS and maximum GMBS per time bin. Error bars on mean body size depict 95% confidence intervals, representing the range of population body sizes. Maximum body size is herein referring to mean of the largest 10% of the population, rather than the single largest specimen and is only calculated when n ≥ 10. This approach was used in order to reduce the effects of abnormally large outliers (Johnson 1994). Percentage size changes are quoted relative to the size in the previous time bin, unless otherwise stated. The autecology of each species is assigned using a modified version of the scheme presented in Ros-Franch *et al*. (2014) (See supplementary appendix B).

Where sufficient sample sizes are available from an ammonite zone, size differences between locations (and thereby environment) are considered. For species present within the Blue Lias Formation there is a further test as a single ammonite zone at a single location may encompass a variety of lithologies (Atkinson & Wignall 2019). In order to test for the effects of lithology related variation on body size, specimens were divided into samples from limestones, pale marls, dark marls and shales: - the succession of lithologies seen in the Blue Lias Formation.

Additionally, body size of specimens housed in museum collections are compared to field observations in order to test for size bias and assess the usability of the wealth of material housed in museums for these such studies. To test for the statistical significance of size changes between time bins a

Kolmogorov-Smirnov test (K-S test) was performed and for correlation a Spearman's rank test, *p*-values are quoted with a 95% significance threshold ($p(a) < 0.05$). These analyses were carried out using PAST 3.12 statistical software (Hammer *et al.* 2001). All other analyses were carried out using Microsoft Office Excel 2013.

5.5 Results

5.5.1 All bivalves

A total of 6509 bivalve specimens, belonging to 145 species, were measured (Supplementary Appendix E). When the entire dataset is plotted three distinct phases of size change can be seen: the Westbury Formation to the *angulata* Zone; *bucklandi* Zone to *oxynotum* Zone and *raricostatum* Zone to *spinatum* Zone. The first phase is one of increasing body size (Fig. 5.4A). Over this interval maximum size increases by 195%. Mean size increases also, this reaches a plateau of 23-25 mm from the *liasicus* to *bucklandi* Zone. Between the Westbury Formation and the *liasicus* Zone mean body size increases by 182%. During this phase newly appearing taxa are typically larger within successive time bins (Fig. 5.4B).

The second phase spans much of the Sinemurian Stage. This period saw a decline in maximum body size that began in the *bucklandi* Zone and continued into the *semicostatum* Zone (Fig. 5.4A). From the body size peak in the *angulata* Zone to the *semicostatum* Zone the maximum size of bivalves fell by 47% resulting in a return to body sizes seen in the Pre-*planorbis* Beds. Mean body size only decreases after the *bucklandi* Zone but still shows a Sinemurian trough. The few newly originating species in this interval are typically smaller than those

that originated during the Hettangian (Fig. 5.4B). The prolonged period of low body sizes is punctuated by a positive spike in both maximum and mean size centred on the *obtusum* Zone (Fig. 5.4A). This produces a mean body size 32% larger than the *liasicus* Zone and returns maximum body size to a par with those seen during the *angulata* Zone.

The third phase corresponds broadly to the Pliensbachian Stage (but also includes the last ammonite zone of the Sinemurian) and saw body size increase again (Fig. 5.4A). Mean body size rises progressively from the *oxynotum* Zone to the *ibex* Zone, increasing by 234%. Maximum size also shows this increase into the *ibex* Zone increasing by 155%, however this is less gradual with a near doubling of size occurring between the *oxynotum* and *raricostatum* zones. There then follows a shallow depression of both mean and maximum size (however these remain higher than much of the Hettangian and Sinemurian) until the culmination of the Pliensbachian Stage size increase in the *spinatum* Zone, when maximum size attained 115.2 mm.

During the entire study interval (Westbury Formation to *spinatum* Zone) maximum size of bivalves increases by 347% and mean size by 328%, with an overall average bivalve body size of 19.1 mm. The typical maximum size of the same interval is 57.6 mm. The *angulata*, *obtusum* and *raricostatum-spinatum* zones have a maximum size that is larger than the average for the Lias.

Body size and bivalve diversity exhibit no significant correlation (mean size and diversity r = +0.23, *p*(a) = 0.35; maximum size and diversity r = +0.29, *p*(a) =

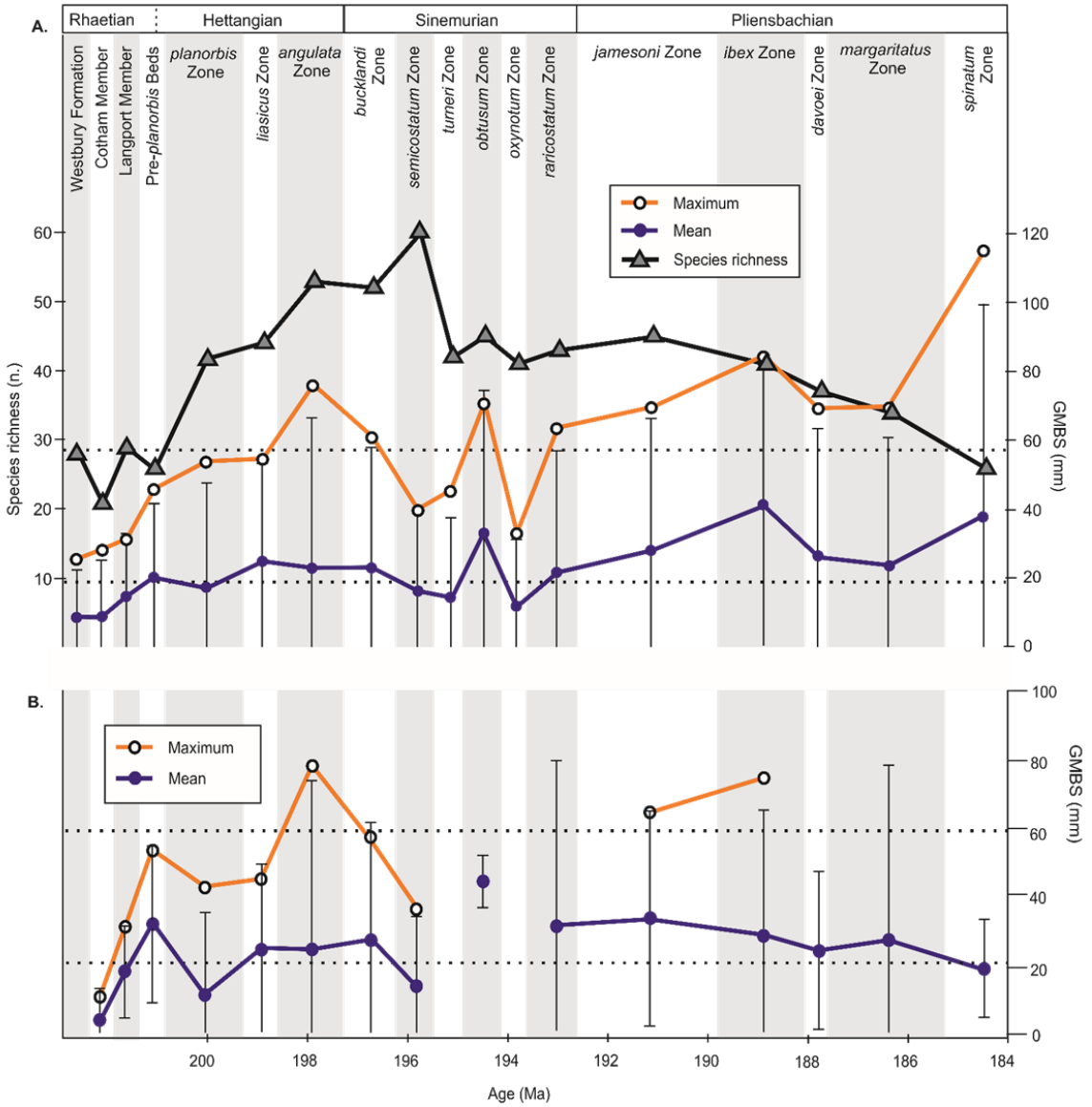

Fig. 5.4 Time-binned geometric mean size plots for all Rhaetian and Lower Jurassic bivalves, hollow circles depict maximum size (see methods), filled circles show mean bivalve size, error bars show 95% confidence interval representing range of sizes within a time bin. Dashed horizontal lines show Lias average for maximum and mean size. A, All bivalves measured per time bin, additionally bivalve species richness per time bin (grey triangles). B, size of newly arriving bivalve species per zone.

0.25; Fig. 5.4A). Diversity drops in the Cotham Member due to the end-Triassic mass extinction event and is followed by a diversity increase (albeit with a slight decline in the Pre-*planorbis* Beds), that continues to the *semicostatum* Zone, after which it declines to between 40-45 species. This stability continues to the *davoei* Zone and then begins to decline.

5.5.2 Basin trends

A Rhaetian to latest Hettangian size increase is seen within most of the basins studied, although the magnitude of the increase and precise timing of the peak varies slightly (Fig. 5.5A-D). The Dorset Basin and Mendip High (and surrounding areas) exhibit a peak size in the *liasicus* Zone, indeed bivalves from this latter region are the largest of the entire study. For the Bristol Channel Basin – Welsh Massif and Larne Basin the largest bivalves were encountered in the *angulata* Zone, whilst in the Hebrides Basin and EMS these occur in the *bucklandi* Zone. Large bivalves were not encountered in every basin, bivalves are consistently small in the Central Somerset and Cardigan Bay basins and do not show the Hettangian phase of size increase (Fig. 5.5D).

Size troughs are seen in many of the basins following the Hettangian (or earliest Sinemurian) size maxima (Fig. 5.5A-D). There is a well-developed depression in the mean body size of bivalves from the Cleveland Basin from the *semicostatum* Zone to the *raricostatum* Zone although, in most basins, this decrease is poorly constrained because the sample size diminishes after the *semicostatum* Zone. Nonetheless the decline is seen in the Mendips, Bristol Channel Basin-Welsh Massif and the Dorset Basin when bivalve sizes returns to values similar to those of the Penarth Group. The size decrease is even noted on

the EMS, following a high in the *bucklandi* Zone (when bivalves are the largest of any of the British basins). It should also be noted that even with a size reduction the bivalves of the EMS from the *semicostatum* and *obtusum* zones remain the largest of any of the basins and were collected from the Frodingham Ironstone Member of the Scunthorpe Mudstone Formation.

A phase of size increase during the Pliensbachian is clearly seen in the Cleveland Basin, starting from the *jamesoni* Zone and culminating with bivalves over 100 mm from the *spinatum* Zone (similar *spinatum* Zones sizes are recorded from the Hebrides Basin). Although sampling is sporadic during the Pliensbachian from many of the basins, when sampled, there is a fairly consistent occurrence of large bivalves from the *ibex* Zone (Dorset, Severn, and Cardigan Bay basins).

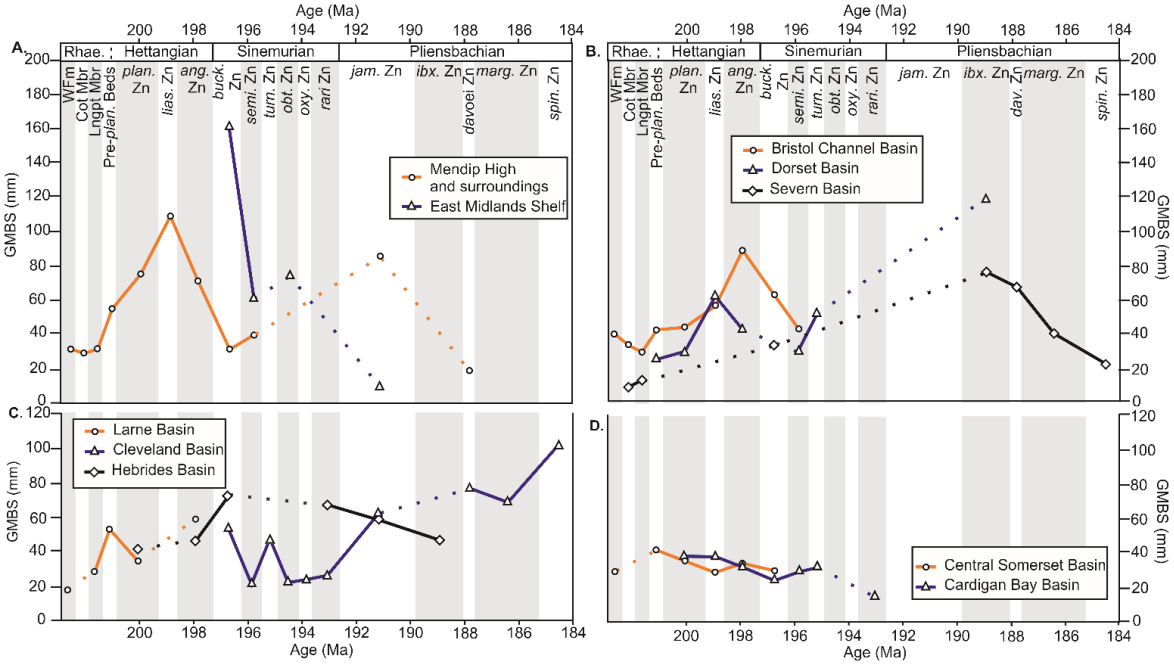

Fig. 5.5A-D Maximum GMBS of bivalves per time bin per basin/shelf. Time bin abbreviations: WFm – Westbury Formation; Cot Mbr – Cotham Member; Lngpt Mbr – Langport Member; Pre-*plan.* Beds – Pre-*planorbis* Beds; *plan.* Zn – *planorbis* Zone; *lias.* Zn – *liasicus* Zone; *ang.* Zn – *angulata* Zone; *buck.* Zn – *bucklandi* Zone; *semi.* Zn – *semicostatum* Zone; *turn*. Zn – *turneri* Zone; *obt*. Zn – *obtusum* Zone; *oxy*. Zn – *oxynotum* Zone; *rari.* Zn – *raricostatum* Zone; *jam*. Zn – *jamesoni* Zone; *ibx*. Zn – *ibex* Zone; *dav*. Zn – *davoei* Zone; *marg*. Zn – *margaritatus* Zone; *spin*. Zn – *spinatum* Zone. See individual legends for basin information.

5.5.3 Trends within ecological groups

Within the majority of the ecological guilds employed by bivalves, the three main size phases can be readily noted. All recorded suspension feeding guilds, irrespective of attachment style or burrow depth show a size increase in both mean and maximum body size from the Rhaetian and across the Hettangian (Fig. 5.6A). A suppressed body size during the Sinemurian is best expressed in endo- and epibyssate suspension feeding bivalves (Fig. 5.6A). This trend is weaker in shallow infaunal suspension feeders and cementing bivalves, and is however first expressed earlier during the *angulata* Zone. The brief *obtusum* Zone reversal of the size decline is exhibited only in shallow infaunal and epibyssate suspension feeders. The third phase, a Pliensbachian size increase is again seen in all suspension feeding guilds of bivalve (except cementing bivalves), however epibyssate bivalves show a maximum and mean peak size centred on the *ibex* Zone, with later Pliensbachian members of this ecology being progressively smaller.

Shallow infaunal, deposit feeding bivalves show fundamentally different size trends to the suspension feeders (Fig. 5.6B). Thus, there does not appear to be a Hettangian size increase, instead mean size is similar between the *planorbis* and *angulata* zones (~10 mm) whilst maximum size decreases slightly (18%). Mean body size decreases from the *angulata* to the *bucklandi* Zone, while the maximum size remains the same. During the o*btusum* Zone mean and maximum sizes are comparable to the *planorbis* Zone and for the Pliensbachian mean body size remains around 10 mm and maximum, as seen within the *planorbis* and *obtusum* zones, remains around 20 mm, only seeming large due to a decline in both mean and maximum size in the *jamesoni* Zone.

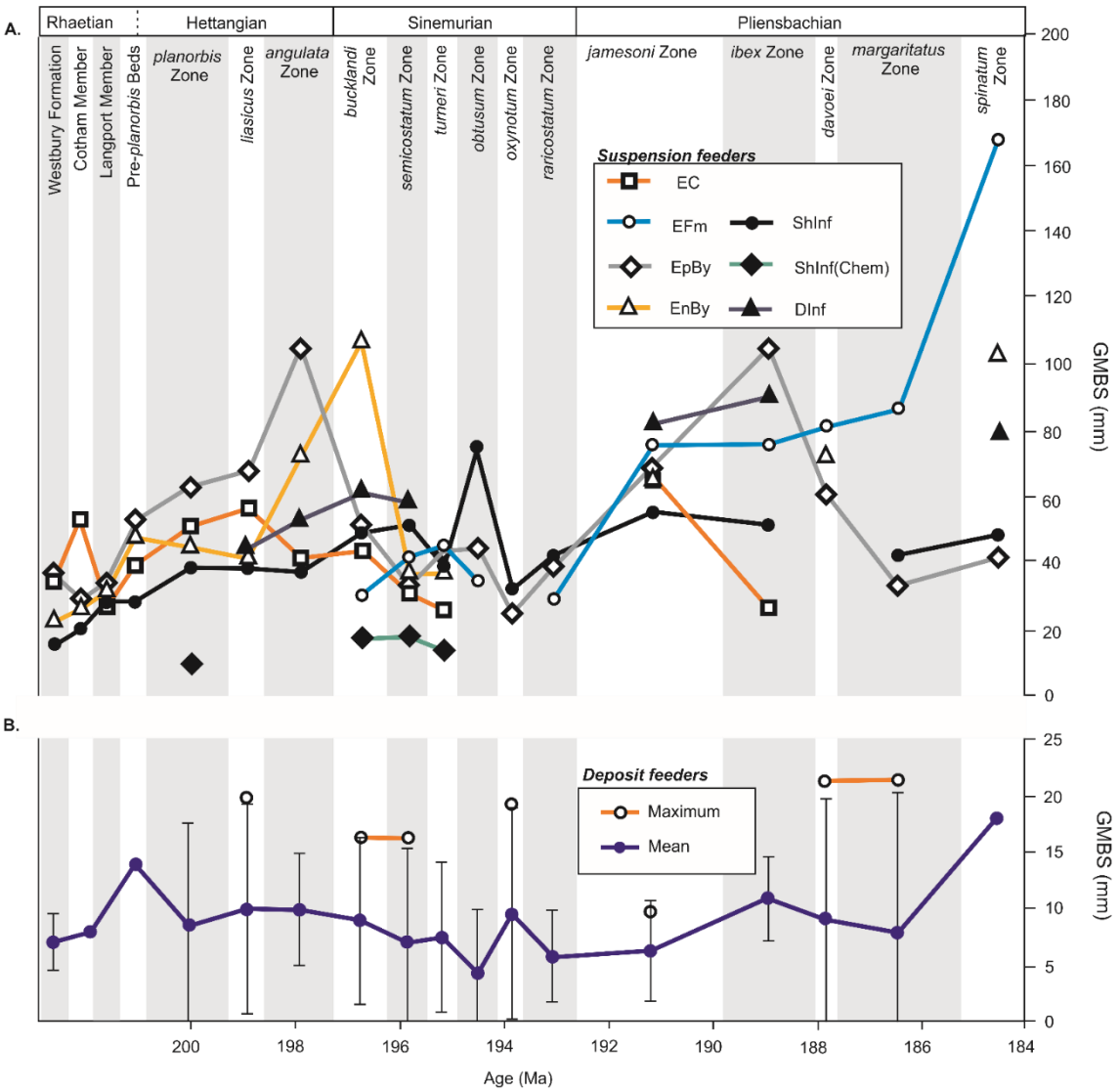

Fig. 5.6 Maximum GMBS for bivalves per ecological guild. A, Suspension feeding bivalves. Ecological abbreviations as follows: EC – epifaunal cemented; EFm – epifaunal facultative motile; EpBy – epibyssate; EnBy – endobyssate; ShInf – shallow infaunal; ShInf(Chem) – shallow infaunal with chemosymbionts (primarily represented by *Luciniola limbata* Terquem & Piette); DInf – deep infaunal. B, Deposit feeding bivalves; see Fig. 5.4 caption for details.

5.5.4 Within lineage trends

A subset of the 145 bivalve species studied herein have sufficient occurrence data to examine both intraspecific and lineage size trends. For a full species-by-species account see supplementary appendix E.

Pseudopecten equivalvis J. Sowerby remains small in both mean and maximum size throughout the Hettangian and Sinemurian, only to increase dramatically in size during the Pliensbachian (Fig. 5.7A). There are three pulses of drastic size increase: the first is between the *raricostatum* and *jamesoni* zones when there is a doubling in mean and 133% increase in maximum. The next is only reflected in the mean with a 90% increase from the *jamesoni* to *ibex* zones. And, lastly a 68% increase in mean size from the *margaritatus* to the *spinatum* Zone and 94% increase in the maximum. Overall from the *semicostatum* to *spinatum* zones there is an increase of 254% in mean and 476% increase in maximum. There are however also phases of size reduction, between the *semicostatum* and the *raricostatum* there is a decrease in mean by 37% although maximum stays around the same (2% decrease).

The size trend in *P. equivalvis* predominantly reflects changes within the Cleveland Basin, although there is a similar but more subdued size change in the Hebrides Basin around the Sinemurian and Pliensbachian and in both basins the giants were found in the *spinatum* Zone. The size increase is independent of lithology: initially small individuals are from the *semicostatum* Zone oolitic ironstone facies – the Frodingham Ironstone Member – whilst the *raricostatum* and *jamesoni* size increase in the Cleveland Basin occurs within mudstones and the *margaritatus* to *spinatum* increase is within ironstones again. Museum and

field collections show the same trend for this species, although for the *oxynotum* and *raricostatum* zones the largest specimens are found in museum collections.

Entolium lunare (Roemer) increases between the *bucklandi* and *semicostatum-turneri* zones by 46% in mean size, 51% in maximum (p(a) <0.001, Fig. 5.7B). This is however only temporary with mean size decreasing in the subsequent zone by 29%, thereby returning the mean size to approximately 19 mm. The maximum size reflects the trends in the mean. Specimens are scarce thereafter until the *jamesoni* Zone, when the largest mean and maximum sizes were attained. The next time bin with >10 specimens is the *margaritatus* Zone. At this interval the maximum size is 50% larger than that during the early Sinemurian. Museum and field collections seldom have large numbers of *E. lunare* from the same time, but nonetheless the *angulata* and *obtusum* zone trends in each collection are the same. The *semicostatum-turneri* zone is the only zone that has a large sample size in both collections, the museum specimens are however 43% larger than the field collections.

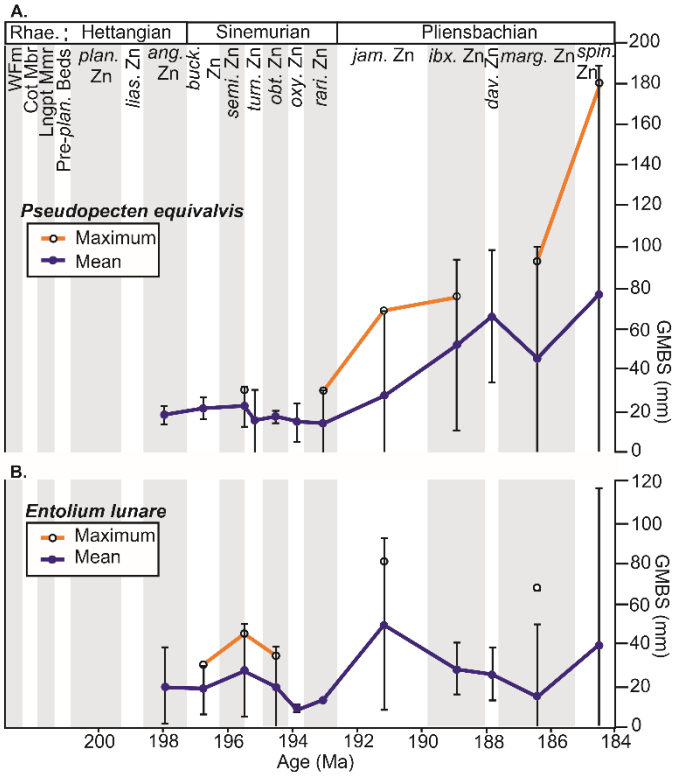

Fig. 5.7 Time-binned GMBS plot for A, *Pseudopecten equivalvis* and B, *Entolium lunare.* See Fig. 5.4 caption for details and Fig. 5.5 for time bin abbreviations.

Chlamys valoniensis (Defrance) is one of the few common species to survive the end-Triassic mass extinction in the study region. Initially very common in the Westbury Formation, and a basal shell bed of the Cotham Member, it is then absent from the remaining Cotham, before reoccurring in the Langport Member and is abundant again in the *planorbis* Zone. Specimens are plentiful from the Sutton Stone, a marginal/coastal facies. From the Westbury to Cotham mean body size declines by 10%. The communities of the *planorbis* Zone are 16% smaller than the Westbury and 7% smaller than the Cotham (Fig. 5.8), but only the former is a significant change (p(a) < 0.05). The *liasicus* Zone

populations from marginal facies are significantly larger than those from the offshore Blue Lias *planorbis* Zone (75%, *p*(a) < 0.001).

Due to the bountiful supply of specimens from the Westbury Formation variation between locations and collection styles can be tested for. The sizes are broadly consistent between locations, albeit with a slight northwards size increase: Somerset 26.1 mm, Glamorgan 27.2 mm, Aust 30.5 mm and Larne 34.0 mm. Both field and museum collections show comparable sizes.

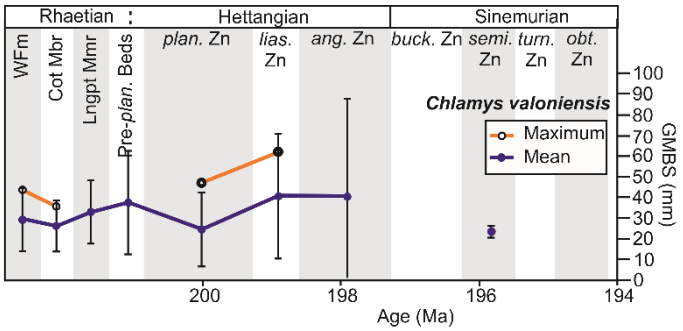

Fig. 5.8 Time-binned GMBS plot for *Chlamys valoniensis.* See Fig. 5.4 caption for details and Fig. 5.5 for time bin abbreviations.

Camptonectes body size trends are here reported at the generic level as many specimens were not preserved with shell material, which contains the diagnostic ornament for species determination. This genus occurs commonly throughout the Lower Jurassic and its size trends are somewhat out of kilter with the overall Hettangian/earliest Sinemurian size patterns: maximum size progressively declining from the *planorbis* to *angulata* Zone by 19% before increasing into the *semicostatum-turneri* zone by 37% (Fig. 5.9A). Mean body size is broadly similar showing a dip in the *angulata* Zone. Use of K-S tests defines three intervals of significant size changes, the 20% (*p*(a) = 0.002) decrease between the *semicostatum-turneri* and *obtusum* zones. This initiates a

period of reduced body size within *Camptonectes* which is ended by a 38% (*p*(a) = 0.002) increase between the *raricostatum* and *jamesoni* zones. During the Pliensbachian there is again a period of reduced body size there being a 28% decline between the *jamesoni* and *davoei* zones.

Two main species of *Oxytoma* occur: *O. fallax* (Pflücker) and *O. inequivalvis* (J. Sowerby). The former is present in Rhaetic-aged strata and measurements are based entirely on museum collections, in most instances these were shell covered slabs. There is an increase of 49% in the maximum size between the Cotham and the Langport members though only a slight but significant change in the mean (increase by 10%, *p*(a) <0.001). *O. inequivalvis* is typically larger than its predecessor, *O. fallax*, and is well-represented from the *angulata* Zone to *semicostatum-turneri* Zone. This species shows an increase in both the mean and maximum size, expressed best in the maximum size however (Fig. 5.9B). From the *angulata* Zone to the *jamesoni* Zone maximum size increases by 107%, slightly declining by 9% during the *davoei* Zone.

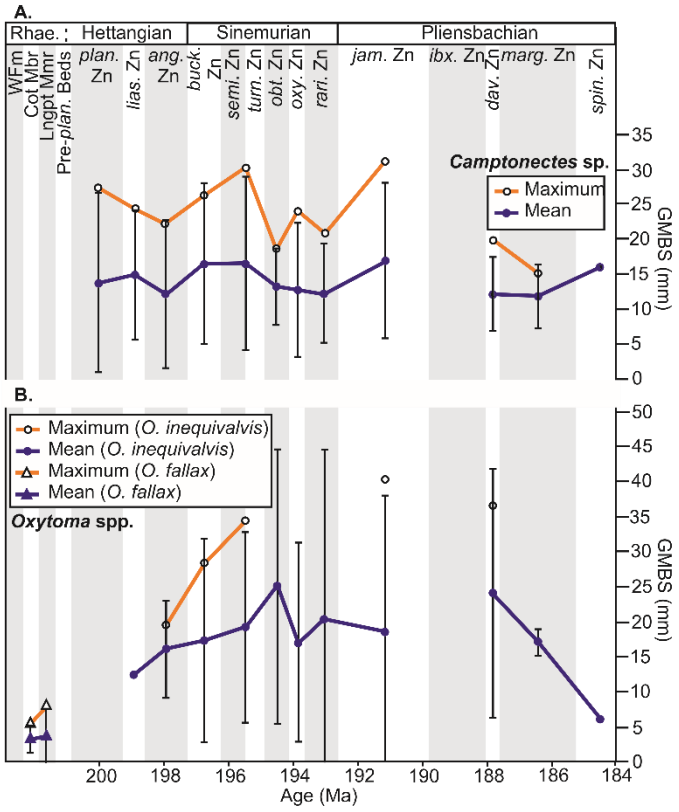

Fig. 5.9 Time-binned GMBS plot for A, species of *Camptonectes* and B, species of *Oxytoma,* see in-figure legend for induvial species present. See Fig. 5.4 caption for details and Fig. 5.5 for time bin abbreviations.

Anningella cf. *faberi* (Oppel) first occurs within a 2 m thick blue-grey shale bed, associated with abundant *Psiloceras* ammonites, where specimens are common (n. 56) with the largest individual attaining a GMBS of 34.0 mm from this bed. During the *liasicus* Zone, specimens were found pyritised in a black shale associated with drift wood from St Audrie's Bay. Both mean and maximum body size is reduced at this point by 36% and 27% respectively (p(a) < 0.05). The *angulata* Zone specimens were collected from a single shale bed in Pinhay Bay. Maximum size decreased while mean size increased slightly by 13%. Thereafter the species is too scarce to comment on body size changes.

Parainoceramus ventricosus (J. de C. Sowerby) is recorded from *jamesoni* to *margaritatus* zones with a single earlier occurrence in the *semicostatum* Zone. Greatest sizes occur in the *ibex* Zone when maximum size attains 109.0 mm. There does not appear be any directional trends within this species, merely appearing in the British Lias as an already large species.

Analysis for *Liostrea* was conducted at the generic level because the two species (*Liostrea hisingeri* (Nilsson) and *L. irregularis* (Münster)) have considerable morphological overlap. *L. hisingeri* is the primary faunal component of the Ostrea Beds of the Pre-*planorbis* interval. The latter species is usually attached to other shelly faunas and has a variable outline. The genus is well represented having 379 specimens from the Westbury Formation to the *jamesoni* Zone. They first appear in any significant numbers in the Langport Member, becoming very abundant in the lower to middle Pre-*planorbis* Beds. Mean body size remains fairly constant for the Hettangian between 18.8- 20 mm (Fig. 5.10A). Maximum size increases almost smoothly from the Langport to the *bucklandi* Zone, with a total increase of 49% before dropping away in the *semicostatum* Zone.

For the *liasicus*, *angulata* and *bucklandi* zones there is a good relationship between host lithology in the Blue Lias Formation and body size: the darker the lithology the smaller the bivalve. In the Pre-*planorbis* Beds specimens come from laminated limestones and share similar body sizes to those from shales. Museum and field collections show a good correspondence until the *angulata* and *bucklandi* zones when field collections show a declining mean size.

Atreta intusstriata (Emmrich) is common in the Langport Member (n. 57), and in the *angulata* Zone (n. 23). Between these two time bins there is a 26% decline in mean body size, mirrored by a 25% decline in the maximum (p(a) < 0.001, Fig. 5.10B). Body size increases thereafter into the *bucklandi* Zone (mean by 21%, this time not a significant change p(a) = 0.38) and does not regain the shell sizes of the Langport community being still 10% smaller. The reduction in body size between the Rhaetian and Hettangian is accompanied by a change in attachment style. The Langport communities were by-and-large found as independent entities, cementing, presumably to a firm substrate, whereas specimens from the Blue Lias Formation were attached to larger shells, typically *Plagiostoma giganteum* or *Gryphaea arcuate* Lamarck.

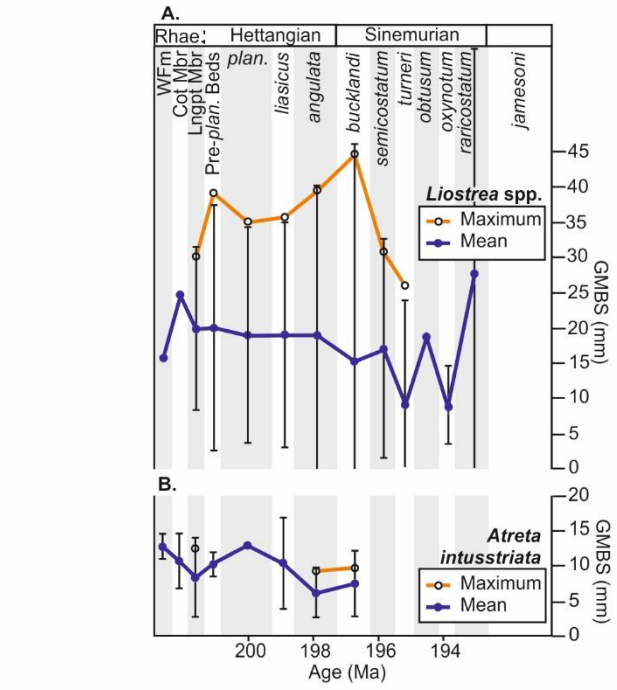

Fig. 5.10 Time-binned GMBS plot for A, undifferentiated of species of *Liostrea* and B, *Atreta intusstriata.* See Fig.5.4 caption for details and Fig. 5.5 for time bin abbreviations.

Two species of *Modiolus* have sufficient sample sizes to report within-species changes: - *M. hillanus* (J. Sowerby) and *M. minimus* (J. Sowerby). The former has a fairly constant maximum size, being around 30 mm in all time bins (Fig. 5.11A). The exception to this being for the Cotham Member, where both mean and maximum size decrease (59% and 67% respectively, p(a) <0.001). The Langport Member specimens increase in size, to an average size 33% larger than the Westbury Formation. Mean body size is reduced in the *planorbis* Zone, down by 22% from the Langport Member.

M. minimus increases in abundance from the Langport Member to the *planorbis* Zone and decreases in size over this same interval (mean size by 54% and maximum by 56%, Fig. 5.11B), and remain small until the *angulata* Zone when their mean size increases insignificantly (11%, p(a) = 0.2). There is no relationship between the size of a specimen and its host lithology. Museum and field collections show the same temporal trend in body size.

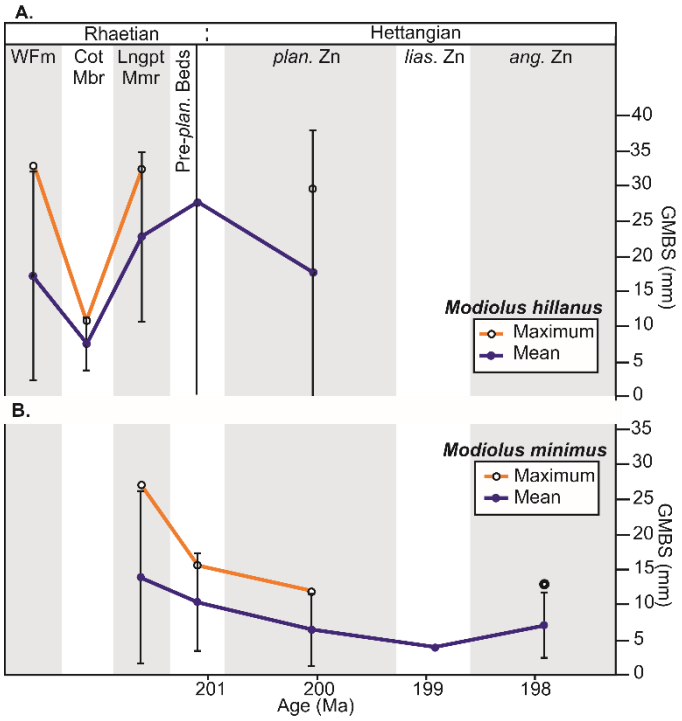

Fig. 5.11 Time-binned GMBS plot for species of *Modiolus*. A, *M. hillanus* and B, *M. minimus*. See Fig. 5.4 caption for details and Fig. 5.5 for time bin abbreviations.

Pteromya crowcombeia Moore is one of the few species to remain reasonably common across the end-Triassic crisis, it ranges from the Penarth Group and the *planorbis* Zone. Mean body size decreases in the Cotham Member by 28% accompanied by a 24% decline in maximum size (p(a) = 0.02*;* Fig. 5.12A). This is a brief decrease in size with an immediate, large increase of 53% in mean and 111% in maximum size during the Langport Member. The trend continues in the Pre-*planorbis* interval, with mean body size rising by a further 43%.

Isocyprina ewaldi (Bornemann) is abundant in the Westbury Formation, forming shell pavements. From sections in Northern Ireland, bed-by-bed sampling shows this species increases in size through the Westbury Formation.

This trend is sustained into the Cotham Member, when using the time-binned approach, with mean size increasing by 24% (Fig. 5.12B). There is however a marked reduction in sample size at this time because it was a victim of the end-Triassic mass extinction.

Neocrassina gueuxii (d'Orbigny) undergoes an extraordinary increase in body size between the *planorbis* and *liasicus* zones of 215% (Fig. 5.12C). This is followed by a slight decline into the *angulata* Zone, but maximum size continues to increase resulting in an overall 283% increase in maximum size from the *planorbis* to the *angulata* Zone. The mean and maximum size then decrease in the *semicostatum-turneri* Zone by 24% and 12% ($p(a) < 0.05$) respectively.

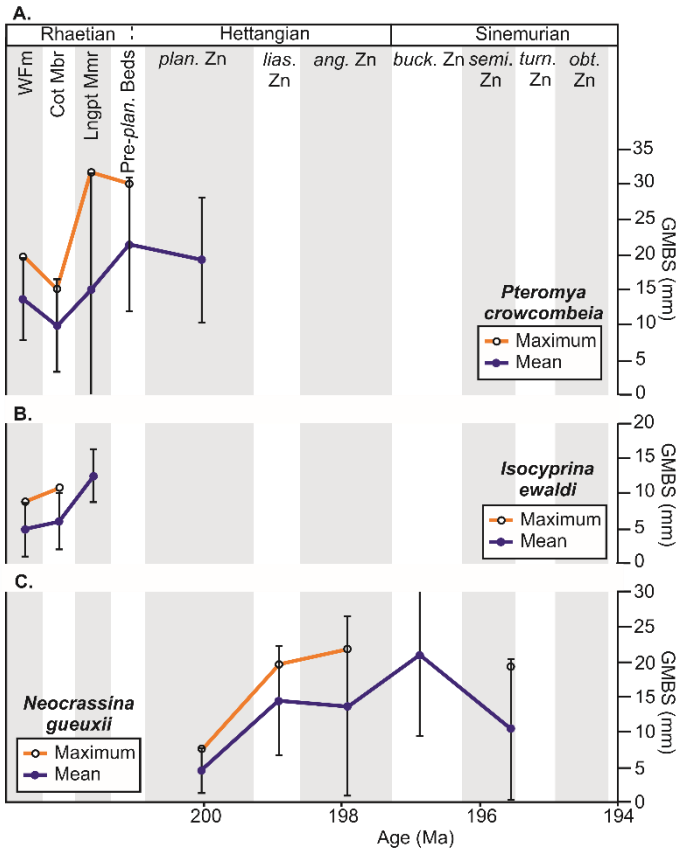

Fig. 5.12 Time-binned GMBS plot for A, *Pteromya crowcombeia,* B, *Isocyprina ewaldi,* C, *Neocrassina gueuxii.* See Fig. 5.4 caption for details and Fig. 5.5 for time bin abbreviations.

Cardinia ovalis (Stutchbury) survived the end-Triassic mass extinction event. Size plot shows two distinct size classes, smaller individuals from the Penarth Group and consistently larger ones from the Hettangian (Fig. 5.13A). Each population shows little in the way of size variation but a single stepped increase in size between the two with mean and maximum increasing by 75% and 67% respectively, between the Cotham Member and *planorbis* Zone. Growth line analyses show the Cotham specimens have fewer and more closely spaced primary growth lines than those of the Blue Lias and Waterloo Mudstone formations (Fig. 5.13B).

C. ovalis is common in the *planorbis* Zone of Northern Ireland, and the *liasicus* Zone elsewhere in Britain. In the latter zone, samples from Glamorgan have the largest average, followed by those from Mochras and smallest being of the Somerset coast indicating a likely offshore decreasing size trend. In all the time bins with sufficient material, museum and field collections have a comparable mean size.

Cardinia ovalis is replaced by *Cardinia listeri* (J. Sowerby) in the Sinemurian, with a *bucklandi* Zone maximum size 47% larger than its predecessor.

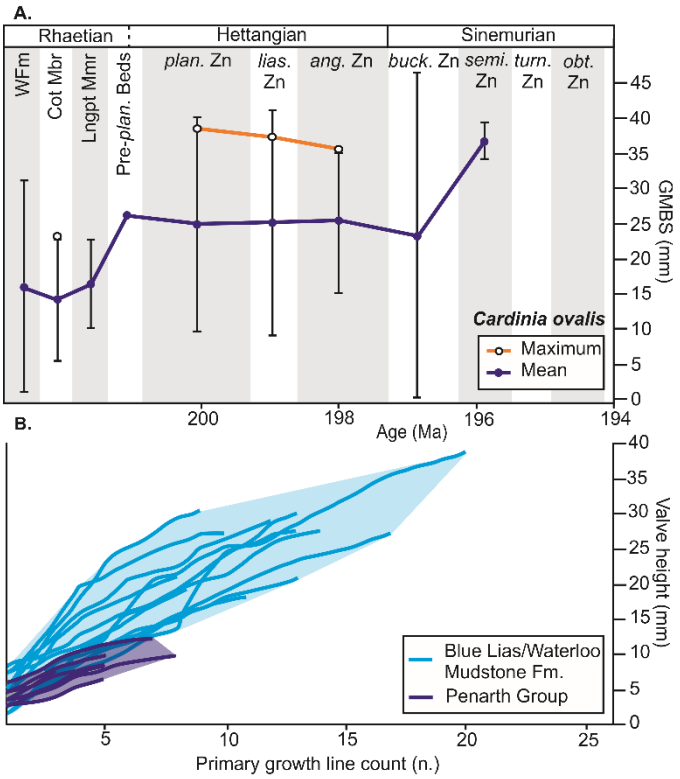

Fig. 5.13 A, Time-binned GMBS plot for *Cardinia ovalis,* see Fig. 5.4 caption for details and Fig. 5.5 for time bin abbreviations. B, Primary growth line plot for *C. ovalis* specimens from the Penarth Group and Blue Lias/Waterloo Mudstone formations.

Mactromya cardioideum (Phillips) shows mean and maximum body size fluctuations in the Hettangian and early Sinemurian but without any long term trends over that time. Subsequently, there is a 54% (p(a) <0.001) increase in mean size from the *semicostatum* Zone to the *ibex* Zone (Fig. 5.14A). The larger specimens, from the Blockley Quarry site in the Severn Basin, have more growth lines than their Blue Lias predecessor (Fig. 5.14B) indicating they achieved their greater size due to increased longevity.

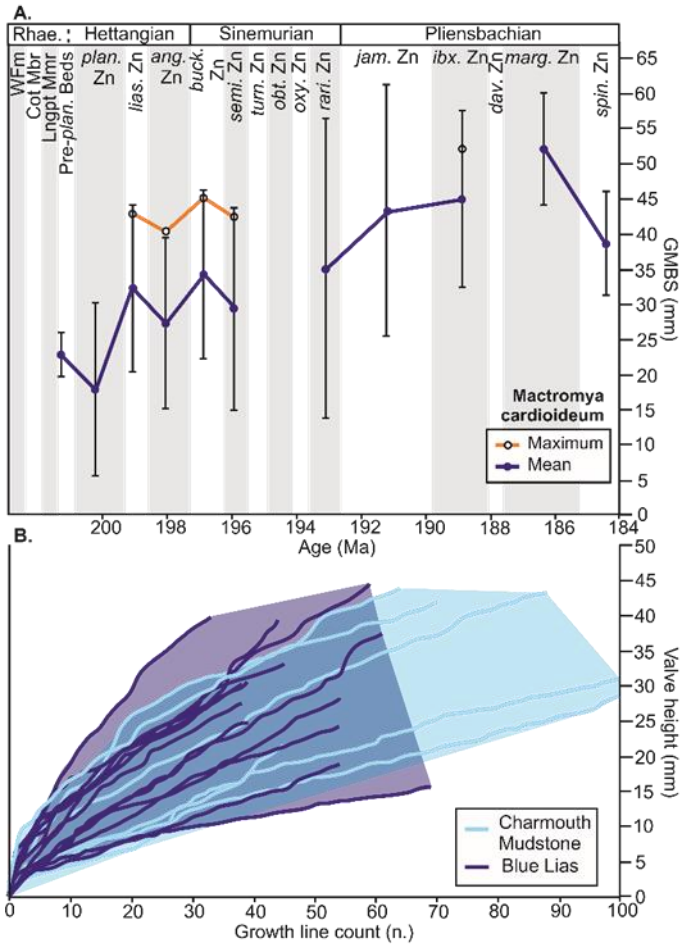

Fig. 5.14 A, Time-binned GMBS plot for *Mactromya cardioideum,* see Fig. 5.4 caption for details and Fig. 5.5 for time bin abbreviations. B, Growth line plot also for *M. cardioideum* specimens from the Blue Lias Formation and from Blockley Quarry, Severn Basin (Charmouth Mudstone Formation).

Four species of *Protocardia* are recognised within the study interval, distinguished by strength of carina, position and number of radial ribs (see Appendix F) and show minimal range overlap (Fig. 5.15). *P. rhaetica* (Merian) is abundantly recorded in the Westbury Formation before going extinct in the lower Cotham Member. There is no change in the mean nor the range of sizes. *P. philippianum* (Dunker) appears in the aftermath of the end-Triassic mass extinction and is plentiful in the Langport Member and Pre-*planorbis* Beds but dwindles in abundance rapidly thereafter, finally disappearing in the *angulata* Zone. Between the Langport Member and Pre-*planorbis* Beds there is no significant size change (p(a) > 0.05) but the rarely occurring, geologically youngest individuals are far smaller, being around one third the size of those from the Pre-*planorbis* Beds. The next *Protocardia species* – *P. oxynoti* (Quenstedt) is also the smallest species, and ranges from the *bucklandi* to *raricostatum* zones. It is common in the Mochras core from the *semicostatum* to *turneri* zones and at Robin Hood's Bay for the *turneri* to *raricostatum* Zone but there is little change in size except in the *oxynotum* Zone where specimens are slightly smaller. *P. truncata* (J. de C. Sowerby) is the youngest stratigraphically and largest species encountered in this study, and is common only in the *margaritatus* and *spinatum* zones, especially in the Staithes Sandstone and the Marlstone Rock formations. These were measured from museum collections with few from direct field observations. Between the *margaritatus* Zone and the *spinatum* Zone there is a 20% (p(a) <0.001) decrease in the mean whilst maximum is broadly similar.

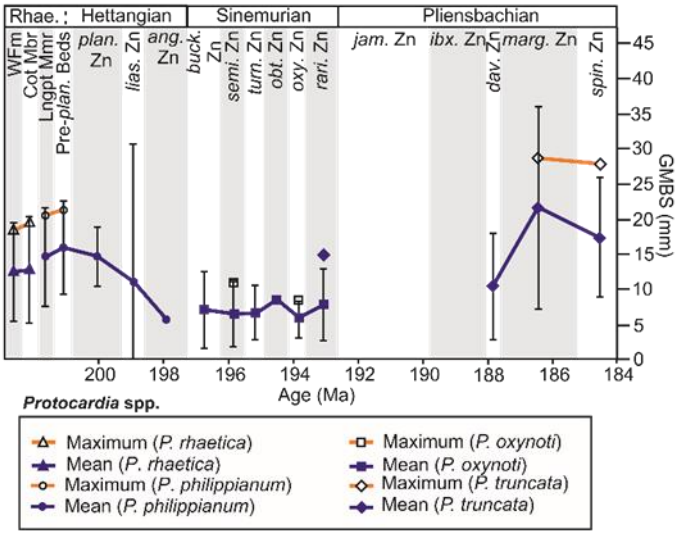

Fig. 5.15 Time-binned GMBS plot for species of *Protocardia,* see figure legend for species details, and also see figure captions for Figs. 5.4 and 5.5 for details of error bars and abbreviations.

Gresslya galathea (Agassiz) occurs during the Hettangian and early Sinemurian but samples are almost entirely restricted to Glamorgan. This species shows a single stepped increase in size between the *liasicus* and *angulata* zones (30% mean, 58% max, Fig. 5.16A). Thereafter, mean body size is fairly consistent. *G. galathea* is followed by the far larger *G. intermedius* (Simpson), which has an average size of 40 mm compared to 20 mm of its predecessor, this species is primarily seen in the *margaritatus* and *spinatum* zones.

Pleuromya liasina Agassiz first occurs (rarely) in the Pre-*planorbis* Bed and becomes more abundant in the *angulata* and *bucklandi* zones, with an insignificant (p(a) > 0.05) increase in mean and maximum size of around 10%. *P. liasina* is succeeded by *P. costata* (Young & Bird), which is recognised by its stronger concentric ornament and more truncated anterior (Appendix F). This

species has a first questionable appearance in the *semicostatum* Zone (n. 3). There are however only two times when the species is sufficiently abundant to make comment on any size trends: *ibex* and *spinatum* zones when mean sizes are 32.5 mm and 33.6 mm respectively. There is however quite a marked increase (43%) in the maximum size 38.3 mm to 54.6 mm (Fig. 5.16B).

Two main species of *Pholadomya* were recorded in this study, *P. glabra* Agassiz and *P. ambigua* J. Sowerby (a single specimen of *P. "ovalis"* was also measured from the *ibex* Zone). *P. glabra* is chiefly recorded from Glamorgan and has a mean body size around 30 mm which increases from the *liasicus* Zone to the *bucklandi* Zone by 62%, accompanied by a 41% increase in the maximum size (Fig. 5.16C). Between the *angulata* and *bucklandi* zones there is a 36% increase in size which may be attributable to an increase in growth rate and longevity. This is suggested by several of the *bucklandi* specimens which attain a larger size for the same number of growth lines, and continue to grow thereafter, thereby also show a greater number of growth lines (Fig. 5.16D). *P. glabra* is replaced by *P. ambigua* during the late Sinemurian, with the geologically younger species featuring stronger and fewer radial ribs and more inflated valves (see Appendix F). This later species shows little in the way of a within-species size change with an 8% increase in the mean and a 15% in the maximum size between the *ibex* and *spinatum* zones ($p(a) > 0.05$). *P. ambigua* does however form part of a long-term generic body size increase. Between the mean size of *P. glabra* in the *liasicus* Zone and the mean size of *P. ambigua* during the *spinatum* Zone there is a doubling of size.

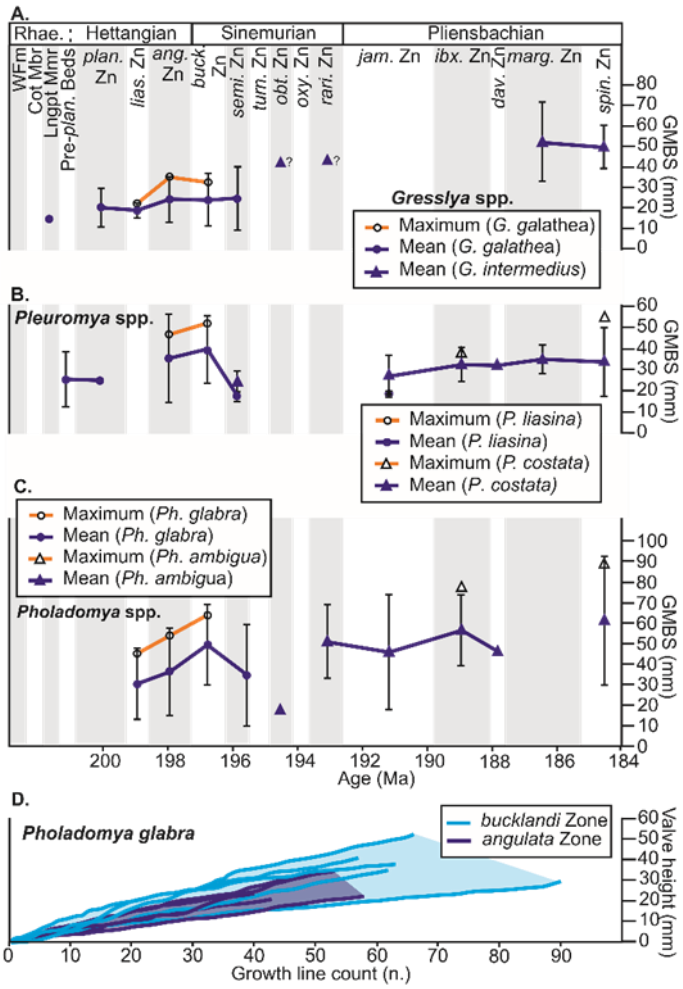

Fig. 5.16 Time-binned GMBS plot for A, species of *Gresslya,* B, species of *Pleuromya,* and C, species of *Pholadomya,* see subfigure legends for individual species featured. See Fig. 5.4 caption for details and Fig. 5.5 for time bin abbreviations. D, Growth line plot for *Pholadomya glabra* from the Blue Lias Formation comparing specimens of the *angulata* and *bucklandi* zones.

5.6 Discussion

5.6.1 Body size trends

5.6.1.1 Lilliputians

Of the 25 species discussed in detail there are only six species that survived the mass extinction and have sufficient data to assess size trends. Of these, two species could be considered as exhibiting the Lilliput Effect: *Modiolus hillanus* and *Pteromya crowcombeia,* and possibly two others: *Chlamys valoniensis* and *Cardinia ovalis*. In *M. hillanus* and *P. crowcombeia* pre-extinction body sizes were restored by the Langport Member, less than 0.15 Myr following the event. It is questionable if *C. valoniensis* is an example of the Lilliput Effect because it is very rare post extinction, making it difficult to judge its size. It was not common again until 2.3 Myr after the extinction, in the *liasicus* Zone, when it had re-attained its pre-extinction size. *Cardinia ovalis* also cannot unequivocally be shown to have a Lilliput trend, because the species is poorly known/very rare prior to the extinction interval. During the Cotham Member (the extinction interval) *C. ovalis* is small with specimens having few, closely spaced growth lines when compared to the Hettangian when this species is bigger and has more growth lines that are typically spaced at wider intervals. In summary, despite claims that the Lilliput Effect was common during the end-Triassic mass extinction (Barras & Twitchett 2007; Mander *et al.* 2008; Clémence & Hart 2013), it can only be clearly demonstrated to have occurred for two species.

5.6.1.2 Brobdingnagians

Alongside *Plagiostoma giganteum*, Atkinson *et al*. (2019) reported the Brobdingnag Effect in two other species of limid bivalves, here a further five species of bivalve exhibit a clear Brobdingnag trend in the aftermath of the mass extinction: *Luciniola limbata, Neocrassina gueuxii, Oxytoma inequivalvis, Gresslya galathea* and *Pholadomya glabra.* These all exhibit a size increase over a similar interval of time to that of *P. giganteum*. From growth lines analysis of *P. giganteum* it was found that the size increase reflected increased growth rates and, to some extent, a greater longevity (Atkinson *et al.* 2019). A similar case in point is seen with *Ph. glabra* although there is a greater overlap in growth rates between specimens measured from the *angulata* and *bucklandi* zones. The *bucklandi* Zone specimens often have a greater number of growth lines, here likely indicating an increased life span. Species of *Liostrea* may also show a Brobdingnag trend as the genus exhibits increasing maximum size following the mass extinction.

A further three species show a size increase over the span of the study interval, *Entolium lunare, Pseudopecten equivalvis* and *Mactromya cardioideum.* These three differ in having a delayed size increase that does not begin until the Sinemurian or Pliensbachian, some 9 Myr after the end-Triassic mass extinction. The size increase of *M. cardioideum* was driven solely by greater longevity as the larger Pliensbachian specimens have similar growth line spacing but more growth lines than those in the Hettangian/earliest Sinemurian.

The Brobdingnag Effect was a significant feature of the aftermath of the end-Triassic mass extinction and was still important 17 Myr later, at the end of the Pliensbachian Stage. The generally large size of bivalves in the *spinatum* Zone was caused by the culmination of long-term size increase trends amongst

species that appeared earlier. The average size of newly arriving bivalves, does not feature a size increase for this time (Fig. 5.4B).

5.6.1.3 Cope's Rule

It is hard to assess the role of Cope's Rule during the Hettangian and Pliensbachian phases of size increase as the ancestry of the new species is not always clear. If assumptions are made that a geologically younger species is the descendant of a geologically older species of the same genus (in cases where there are multiple potential ancestors the most morphologically similar is chosen) then size changes between these can be assessed. As demonstrated above, the Hettangian size increase is facilitated by both the appearance of increasingly large new taxa and also larger new species of pre-existing genera. However, when broken down further there are as many instances of new species of a lineage being smaller than their potential ancestor as there are those that display a Cope's Rule pattern. The succession of species within the genera~~:~~ *Gresslya*, *Pholadomya, Oxytoma* and also *Cardinia* show perhaps the best candidates for Cope's Rule. Although insufficient material was measured during this study, Hodges (2000) also found an increase in size between *Dacryomya heberti* (Martin) and *D. gaveyi* Cox between the Sinemurian and Pliensbachian, a size trajectory that appears to have been sustained in to the Toarcian with *D. ovum* (J. de C. Sowerby) (Caswell & Dawn 2019).

This therefore suggests that Cope's Rule did play a role in the size increase in the Lower Jurassic, but the Brobdingnag Effect is more crucial to explain the large bivalves found during the *spinatum* Zone.

5.6.1.4 No trends

Not all bivalves show a size trend in the Lower Jurassic. Some simply do not alter their size (either significantly or with any distinct direction) across the duration of the study. Examples of this include most species of protobranchs and *Parainoceramus ventricosus*. *Camptonectes* size fluctuates during the Lower Jurassic, but only shows a distinct pattern during the Sinemurian, when they show a size reduction.

5.6.1.5 Those that get smaller

Alongside the previously reported *Plagiostoma punctatum* J. Sowerby (Atkinson *et al.* 2019), there are three cases of bivalves reducing in size over the same interval that others show a Brobdingnag trend. These are *Anningella* cf. *faberi*, *Atreta intusstriata* and *Modiolus minimus*. These inverse-Brobdingnags are not Lilliputians because they exhibit a progressive reduction in body size during the recovery.

The Sinemurian is marked by a general suppression of body size in the bivalves (excluding the *obtusum* Zone; Fig. 5.4A); a phase herein referred to as the Sinemurian Small Episode (SSE). The lowest point of the SSE is in the *oxynotum* Zone when the data are all from the Cleveland Basin. Although this particular basin hosts bivalves that are usually smaller than most other basins until the Pliensbachian, the SSE is not merely an artefact of the relative contribution of material measured from each basin because the SSE in the Cleveland Basin is bracketed by comparably larger bivalves in the *bucklandi* and *jamesoni* zones. The Mendips, East Midlands Shelf, Dorset and Bristol Channel Basin all show the SSE where it is primarily expressed as an initial size reduction

following the *angulata* Zone size peak. *Plagiostoma giganteum* also shows a decrease in body size at this time (Atkinson *et al.* 2019).

Other taxa that show concurrent size reductions are: *Cardinia listeri*, *Neocrassina gueuxii*, *Camptonectes* and *Liostrea.* The SSE is expressed not only as intraspecific size reduction but also, those species that originate during this interval, are smaller compared to the *angulata* Zone. Thus, *Entolium lunare* and *Pseudopecten equivalvis* both originate at small body sizes during this interval and increase in size during the Pliensbachian. Additionally, new species of *Protocardia* and *Modiolus* are smaller than their Hettangian predecessors.

5.6.1.6 *Gryphaea*

The evolutionary lineage of the oyster *Gryphaea* (*Gryphaea arcuata* - *G. mccullochi* J. de C. Sowerby – *G. gigantea* J. de C. Sowerby) has been widely reported (Hallam 1968, 1975; Johnson 1994; Jones & Gould 1999; Nori & Lathuiliére 2003). *Gryphaea arcuata* first appeared in the *angulata* Zone and increases in size into the *bucklandi* Zone before decreasing in the *semicostatum* Zone (Johnson 1994). It is then replaced by the *G. mccullochi* which is larger than the youngest *G. arcuata* specimens but does not exceed the sizes of *Gryphaea* in the *bucklandi* Zone. Ironically, *G. gigantea* first appears at a smaller size than its predecessor *G. mccullochi* before increasing in size from the upper *jamesoni* Zone onwards (Johnson 1994). The *angulata* – *bucklandi* Zone size increase and subsequent reduction during the *semicostatum* Zone seen within *G. arcuata* matches that seen in other bivalve species featured in this study. There is a paucity of measured *Gryphaea* samples from the interval of the SSE with the only sample in the *obtusum* Zone.

5.6.1.7 Bivalve-size changes across Europe and beyond

No other studies have systematically documented body size changes during the Lower Jurassic, but the available information suggest that the trends seen in British bivalves are repeated elsewhere. Johnson (1984) reported size changes within the Pectinidae and Propeamussidae and showed a size increase in *Entolium lunare* and *Psuedopecten equivalvis* in Germany, also *Camptonectes* and *Chlamys textoria* (Schlotheim) show a size increase from the Sinemurian to upper Pliensbachian of Germany. Data for the Hettangian are very limited, only Hallam (1975) covers this interval albeit in scant detail: only the initial and final maximum size of a species is documented. Hallam measured bivalves from the collections of the British Museum (Natural History) that includes collections from Germany and France, and found a Hettangian to Pliensbachian size increase indicating the trends occurred across the European shelf sea. Unfortunately there are no other size data available from other regions such as the Tethyan realm, although it is potentially noteworthy that sizes of Pliensbachian bivalves from Serbia are comparable to those reported here (Radulović 2013).

Panthalassic records of bivalves from the South America have received considerable attention (e.g. Damborenea 1987a, b; Aberhan 1994; Damborenea *et al.* 2017), although temporal size data is mostly absent. Nonetheless, Damborenea's monographs (Damborenea 1987a, b, 2002) present some 240 measured specimens from Argentina at stage resolution but with a dearth of Hettangian specimens. These indicate there is a size increase between the Sinemurian and the Pliensbachian at the community level.

5.6.1.8 Size trends in other groups

Body size trend studies of other marine invertebrates are restricted to the well-known Liassic ammonites. Dommergues *et al*. (2002) provide a compendium of ammonite shell volumes per zone that can be compared to our bivalve maximum body sizes (Fig. 5.17). For the Hettangian and Sinemurian, the two datasets are remarkably consistent, both bivalves and ammonites show increasing maximum sizes through the Hettangian. Peak ammonite size is attained in the *bucklandi* Zone, slightly later than the bivalves (although if *Plagiostoma giganteum* data of Atkinson *et al*. (2019) are included with our data herein the two maxima coincide). Ammonites also show a size trough (the SSE) for much of the Sinemurian and both feature a brief renewal of size increase in the *obtusum* Zone, just as bivalves do. The SSE is ended in both datasets by an increase in size from the *oxynotum* to the *raricostatum* Zone. The remarkable congruence of bivalve and ammonite data disappears in the Pliensbachian when ammonite shell volume decreased whilst the bivalves showed two further increases in size during the *ibex* and *spinatum* zones.

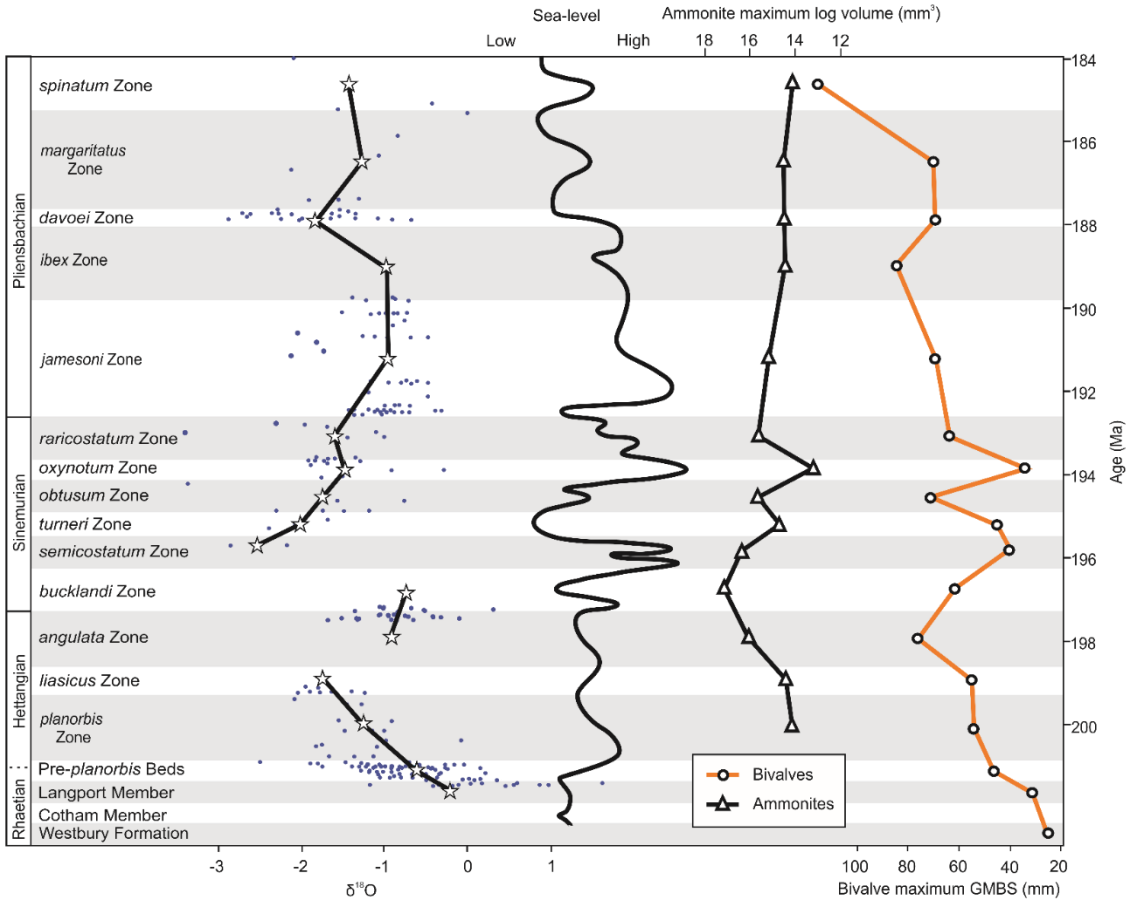

Fig. 5.17 Temperature and sea level changes in relation to maximum GMBS of all bivalves and maximum log volume of ammonites. $\delta^{18}O$ isotope curve compiled from Korte *et al*. (2009); van de Schootbrugge *et al.* (2007); Weedon (1987); Korte and Hesselbo (2011); hollow stars depict time bin average $\delta^{18}O$ values. Sea level curve derived from Hesselbo (2008); Hesselbo and Jenkyns (1998) and Wignall and Bond (2008). Maximum GMBS of bivalves from this study and maximum log volume of ammonites per ammonite zone from Dommergues *et al.* (2002).

5.6.2 Possible causes of size change

5.6.2.1 Sea level, sediments and size

Three phases of size change occur amongst Rhaetian and Lower Jurassic bivalves whereas there are four distinct phases of sedimentation in the British Isles. The faunas of the Penarth Group (Westbury and Lilstock formations) lack any large bivalves, never exceeding 60 mm. This has been attributed to abnormal salinities (Hallam & El Shaarawy 1982; Márquez-aliaga *et al.* 2010), and large bivalves are found elsewhere in normal marine settings at this time (Hallam 2002). The reduced body size seen in three species during the extinction interval recorded in the Cotham Member could be linked to a salinity control because this unit likely accumulated in hypersaline, brackish or even freshwater conditions (Wignall & Bond 2008), but other causes are considered below.

Maximum size increases markedly from the Penarth Group to the Blue Lias Formation and coincides with the development of normal marine conditions (Hallam & El Shaarawy 1982; Hesselbo *et al.* 2004). This change may have played a role in bivalve size increase as demonstrated by *Cardinia ovalis*, which exhibited stunting of growth and size during deposition of the Penarth Group but both improved during the onset of fully marine conditions with no subsequent size change thereafter. The change from the Lilstock to the Blue Lias Formation is also a change in substrate consistency and this may explain the size reduction seen in *Atreta intusstriata* because, during periods of firm substrate, this species is found attached to the seabed, something unachievable on soupy substrates when *A. intusstriata* could attach only to other shells. This change is accompanied by a size reduction, perhaps owing to limitations of space thus imposed.

For the remainder of the Hettangian, size increase occurs within the same formation (the Blue Lias) whilst sea levels were fluctuating (Fig. 5.17). In itself these sea level changes seem unlikely to have been responsible for the increased size although bivalves generally decrease in size in deeper waters as shown by the smaller average size of bivalves in deeper water setting of the Central Somerset Basin. Oxygen deficiency was more prevalent in deeper waters, which may account for the undersized nature of the bivalves there (Atkinson & Wignall 2019). The temporal size increase of bivalves in the Hettangian is superimposed on this proximal-distal size trend and is not related to relative water depth changes.

The initiation of the SSE is largely coincident with deepening (Hesselbo 2008), and so could represent a depth control on size. This is supported during the *turneri* Zone when a brief shallowing is coincident with a temporary size increase seen in both the Dorset and Cleveland basins. The total bivalve database (Fig. 5.17) shows this size increase continues into the *obtusum* Zone but this is only seen on the EMS and is likely an effect of the Frodingham Ironstone, discussed below. The end of the SSE coincides with a lowering of sea levels. But this tenuous link to sea level falls apart in the *jamesoni* Zone when there is a significant deepening and no consequent size reduction.

It seems apt to here summarize the relationship between large body sizes and ironstones. For the *obtusum* Zone the largest bivalves occur in the Frodingham Ironstone Member and likewise the largest bivalves from the *spinatum* Zone are mostly from ironstone facies. Such sediments are thought to have accumulated slowly on seafloor highs or shoals (Hallam & Bradshaw 1979). The well-aerated, clear waters together with increased nutrient supply likely favoured bivalve growth in such settings (Nicol 1967; Johnson 1984). However,

there remains a question over the size increase seen in *Pseudopecten equivalvis* and *Entolium lunare* between the *obtusum* and *spinatum* zones, which occurred within similar ironstone facies, suggesting some other influence at play.

5.6.2.2 Redox

The degree of oxygenation within the Hettangian and earliest Sinemurian of the British Isles has been assessed using pyrite framboid populations (Atkinson & Wignall 2019). This study recorded high abundances of framboidal pyrite throughout the study interval. The size distribution of the framboids suggest oxic/dysoxic bottom waters with no significant changes in framboid size distributions between the *planorbis* and *bucklandi* zones. Bivalve sizes increased at this time (Fig. 5.18), indicating there was little or no overall long-term redox control. The deeper waters of the Central Somerset Basin do however show more intervals of intense water column anoxia than seen in the shallower Glamorgan sections, which may account for the smaller size of bivalves measured in the former location.

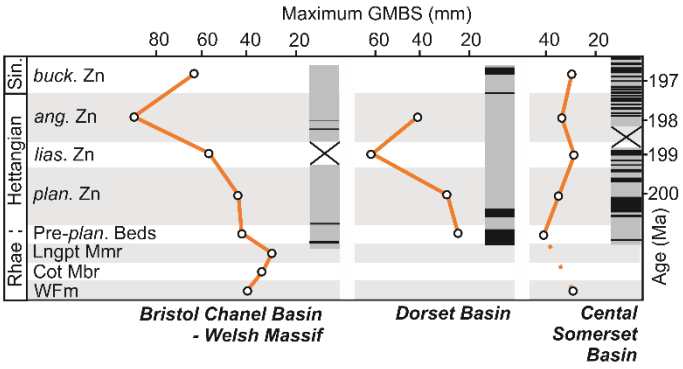

Fig. 5.18 Maximum GMBS trends for the Bristol Channel Basin-Welsh Massif, Dorset and Central Somerset basins and oxygenation states for each of the three basins from Atkinson & Wignall (2019). Hollow circles show maximum GMBS, from this study. Redox states are depicted as alternating grey and black bars, the former indicate periods with oxic/dysoxic framboid size distributions, black bars anoxic distributions, regions crossed out lack data. Time bin abbreviations same as Fig. 5.5. Time scaled to Weedon *et al.* (2019).

5.6.2.3 Temperature

The relationship between temperature and size is difficult to evaluate because of a paucity of Lower Jurassic proxy data. The release of large volumes of greenhouse gases during emplacement of the Central Atlantic Magmatic Province is suggested to have caused intense global warming during the end-Triassic mass extinction (Beerling & Berner 2002). Evidence from decreasing leaf stomatal density at the time suggests 3-4°C of atmospheric temperature increase across the extinction interval (McElwain *et al.* 1999). Subsequent temperature fluctuations in the Lower Jurassic are ill constrained, but the available data indicate no major changes (Fig. 5.17). Korte *et al.* (2009) suggest sea-floor temperatures of between 7 and 14°C for the upper Langport Member (and

ostensibly a dramatic cooling from the preceding hot conditions of the extinction event during Cotham deposition, presuming salinity has not affected these results), rising to 12-22°C for the *planorbis* and lowermost *liasicus* zones based on oxygen isotope ratios from oyster calcite. Oxygen isotope data from the *angulata* and *bucklandi* zones indicate temperatures still within this range (Weedon 1987; Weedon *et al.* 2018), suggesting temperatures did not drive the contemporaneous size increases.

The later Sinemurian to Pliensbachian has a more continuous oxygen isotope record that indicates potentially warmer conditions (Korte & Hesselbo 2011). Temperature estimates for the *semicostatum* and *turner* zones are 19-25°C, however these progressively cool to values again similar to the Hettangian (13-21°C, Korte & Hesselbo, 2011), again suggesting that temperature was not the cause of the SSE.

The patterns of size changes seen in the Pliensbachian are also unlikely to be related to temperatures as no covariation is seen. Sizes increase in both mean and maximum towards the *ibex* Zone, but temperature is poorly constrained at this time (Fig. 5.17). The succeeding *davoei* Zone is considered a period of brief warming (Dera *et al.* 2009; Gómez *et al.* 2016), prior to cooling in the latest Pliensbachian (Bailey *et al.* 2003; Rosales *et al.* 2004; Suan *et al.* 2010; Korte & Hesselbo 2011) but bivalves show no significant body size change over this interval.

5.6.2.4 Food availability

Food supply is a major factor affecting body size in modern marine molluscs (Olabarria & Thurston 2003; Linse *et al.* 2006; Smith *et al.* 2008; Berke

et al. 2013; Munroe *et al.* 2013) and some authors use the size of bivalves as a proxy for primary productivity (e.g. Vermeij 2011). To simply use a "size = productivity" approach in this study would clearly be a case of circular reasoning. However, there are other patterns that suggest improved food supply may have been a factor for the size increase amongst Lower Jurassic bivalves. It is noteworthy that the deposit feeding bivalve species, whose nutrition comes from within-sediment organic detritus, do not show the increasing sizes seen amongst suspension feeding bivalves. A Brobdingnag trend was also seen within *Luciniola limbata*, which is considered to have hosted sulphur-oxidising bacteria within the gills, thereby supplying the mollusc with an alternative energy source independent of water column productivity (Distel & Felbeck 1987). For modern lucinid bivalves a large proportion of their energy demands are supplied by their symbionts, although, these bivalves are still capable of suspension feeding and so may have been susceptible to the same productivity controls as regular suspension feeding bivalves discussed herein (Distel & Felbeck 1987; Cary *et al*. 1989). A Brobdingnag trend amongst suspension feeding molluscs could reflect an increased total abundance of suspended organic matter at the seafloor or a change in the quality of the organic matter to larger planktonic forms such as dinoflagellates. The works of van de Schootbrugge and colleagues (van de Schootbrugge *et al.* 2007; van de Schootbrugge & Gollner 2013) suggest major changes amongst algal communities during the early Hettangian when green algae dominated. The latter provide poor-quality food for bivalves because of their small size and lack of essential nutrients and can result in poor growth of bivalves (Brown *et al.* 1997; von Elert *et al.* 2003; Weiss *et al.* 2007). The intervals of green algal dominance also coincided with periods of more frequent black shale deposition (van de Schootbrugge *et al.* 2007, 2013; Xu *et al.* 2017). As many of

the black shales in the Blue Lias were shown to have a framboid population suggesting deposition under euxinic (or euxinic punctuated by dysoxic) bottom waters implying also a possible influence of redox conditions (Atkinson & Wignall 2019). Although for the pre-*planorbis* Beds and *planorbis* Zone algal communities were depleted in dinoflagellates apparently independent of redox (van de Schootbrugge *et al.* 2007; Atkinson & Wignall 2019), during this time bivalves remained small suggesting that improved food supply/quality may be a key control on size. This hypothesis requires testing with further studies of algal composition in the Lower Jurassic from understudied, younger intervals.

5.6.3 Body size and biotic recovery

The importance of the Lilliput Effect in producing small bodied assemblages in the aftermath of a mass extinction was recently questioned (Atkinson *et al.* 2019), owing to its requirement for a species to survive the extinction to be considered a true Lilliput (Urbanek 1993). Instead the Brobdingnag Effect was proposed, whereby new species originate during recovery at small size and subsequently increase in size, thereby producing not only the small faunas in the immediate aftermath but also the increasing size suggested as a feature of biotic recovery (Atkinson *et al.* 2019). Following the end-Triassic mass extinction the Brobdingnag Effect has been shown for 11 (possibly 12) bivalve species whilst the Lilliput Effect only occurred in two (possibly three). The Brobdingnag Effect therefore dominated in the aftermath of the end-Triassic mass extinction and, in conjunction with Cope's Rule, produced bivalve communities of increasingly large sizes.

Size increase provides an indicator of marine recovery that is unconnected from other factors that have been used to monitor post-extinction progress. Thus, ecological tiering recovers rapidly, in the early Hettangian, whilst bivalve diversity increase continued into the Pliensbachian (Hallam 1996; Atkinson & Wignall 2019). Body size increase follows neither of these trends and is clearly monitoring a different and under-explored aspect of environmental recovery or change. As discussed above, temperature may exert some control on body size although food supply is potentially more important. The role of such factors and their significance during the recovery from other extinction crises remains to be explored.

5.7 Conclusions

The recovery of bivalve communities following the end-Triassic mass extinction saw substantial, intraspecific size increase amongst many bivalves that persisted for 17 million years and saw some bivalves increase their size by up to 476%. Such trends have been traditionally attributed to the Lilliput Effect: – the stunting of species in the harsh environmental conditions of the extinction interval and their subsequent size increase during recovery. However, this effect was minor, only 2-3 Lilliput species are found, instead the size trend is caused by the Brobdingnag Effect: – a within-species size increase of newly originated taxa. The Brobdingnag Effect has been demonstrated for 11 filter-feeding species displaying diverse lifestyles but is not manifest amongst the deposit-feeding bivalves. In conjunction with this, newly appearing species are also progressively larger, with some aspect of this relating to Cope's Rule evolution (seen also in ammonite lineages). The mollusc populations of the Hettangian show an increase in average and maximum body size that was followed by a phase of reduced

body size, here referred to as the Sinemurian Small Episode, before renewed size increase during the Pliensbachian. The geographic distribution of theses size trends remains uncertain although the evidence available suggests that it occurred across much of the European shelf seas and possibly in the Tethys and Panthalassa oceans.

Local environmental factors can be attributed to size changes (small bivalves in the deeper, less well-ventilated waters, large bivalves in the ironstones) but they cannot explain secular trends in body size of both benthos and nekton. The size trends appear unrelated to temperature and redox trends but may link to improvements in food supply (both abundance and quality) available to filter-feeding bivalves. Body size trends in the aftermath of the end-Triassic mass extinction occurred over longer time scales compared to other recovery metrics such as diversity and ecological complexity which indicate recovery was achieved in less than a million years (Atkinson & Wignall 2019). Future investigations of long-term body size trends following other crises may reveal the legacy of such crises is considerably longer than appreciated.

Acknowledgements: We wish to extend our gratitude to Tom Sunderland, Bob Corns and Tom Charman of Natural England and Hugh Luttrell of East Quantoxhead Estate for permissions to sample at Pinhay Bay, along the Blue Anchor-Lilstock Coast SSSI and along the Yorkshire Coast; Peter Hodges, Caroline Buttler and Lucy McCobb of the National Museum of Wales, Cardiff; Deborah Hutchinson at the Bristol Museum and Art Gallery; Jon Radley from Warwickshire Museum Service; Matt Williams at the Bath Royal Literary and Scientific Institute; Sarah King and Stuart Ogilvy of the Yorkshire Museums Trust, and Roger Osborne and Tim Burnhill of Whitby Museum. Additional thanks go to field assistants Jacob Morton, Karolina Zarzyczny and Ovye Yohanna; to Mike Simms for showing us field sites in Northern Ireland and to Mick Oates for

supplying a wealth of specimens from the Hebrides Basin and showing us the Conesby Quarry site. JWA was funded by a NERC DTP postgraduate studentship at the University of Leeds.

References

Aberhan, M. 1994. Early Jurassic bivalvia of northern Chile. Part 1. Subclasses Palaeotaxodonta, Pteriomorphia, and Isofilibranchia. *Beringeria*, **13**, 3–115.

Alroy, J. 1998. Cope's Rule and the dynamics of body mass evolution in North American fossil mammals. *Science*, **280**, 731–734, https://doi.org/10.1126/science.280.5364.731.

Atkinson, D. 1994. Temperature and organism size—a biological law for ectotherms? *Advances in Ecological Research*, **25**, 1–58, https://doi.org/10.1016/S0065-2504(08)60212-3.

Atkinson, D. & Sibly, R.M. 1997. Why are organisms usually bigger in cold environments? Making sense of a life history puzzle. *Trends in Ecology & Evolution*, **12**, 235–239.

Atkinson, J.W. & Wignall, P.B. 2019. How quick was marine recovery after the end-Triassic mass extinction and what role did anoxia play? *Palaeogeography, Palaeoclimatology, Palaeoecology*, **528**, 99–119, https://doi.org/10.1016/j.palaeo.2019.05.011.

Atkinson, J.W., Wignall, P.B., Morton, J.D. & Aze, T. 2019. Body size changes in bivalves of the family Limidae in the aftermath of the end-Triassic mass extinction: the Brobdingnag Effect. *Palaeontology*, **62**, 561-582 https://doi.org/10.1111/pala.12415.

Attrill, M.J., Hartnoll, R.G., Rice, A.L. & Thurston, M.H. 1990. A depth-related distribution of the red crab, Geryon trispinosus (Herbst) [=G. tridens KrÃ‚yer]: indications of vertical migration. *Progress in Oceanography*, **24**, 197–206.

Bailey, T.R., Rosenthal, Y., McArthur, J.M. & van de Schootbrugge, B. 2003. Paleoceanographic changes of the Late Pliensbachian-Early Toarcian interval : a possible link to the genesis of an Oceanic Anoxic Event. *Earth and Planetary Science Letters*, **212**, 307–320, https://doi.org/10.1016/S0012-821X(03)00278-4.

Barras, C.G. & Twitchett, R.J. 2007. Response of the marine infauna to Triassic – Jurassic environmental change: Ichnological data from southern England. *Palaeogeography, Palaeoclimatology, Palaeoecology*, **244**, 223–241, https://doi.org/10.1016/j.palaeo.2006.06.040.

Batten, R.L. & Stokes, W.M.L. 1986. Early Triassic gastropods from the Sinbad Member of the Moenkopi Formation, San Rafael Swell, Utah. *American Musuem Novitates*, 1–33.

Beerling, D.J. & Berner, R.A. 2002. Biogeochemical constraints on the Triassic-Jurassic boundary carbon cycle event. *Global Biogeochemical Cycles*, **16**, 1–13.

Bergmann, C. 1847. Ueber die Verhältnisse der Wärmeökonomie der Thiere zu ihrer Grösse. *Grottinger studien*, **3**, 595–708.

Berke, S.K., Jablonski, D., Krug, A.Z., Roy, K. & Tomašových, A. 2013. Beyond Bergmann's Rule: size–latitude relationships in marine bivalvia world-wide. *Global Ecology and Biogeography*, **22**, 173–183, https://doi.org/10.1111/j.1466-8238.2012.00775.x.

Blackburn, T.M., Gaston, K.J. & Loder, N. 1999. Geographic gradients in body size: a clarification of Bergmann's Rule. *Diversity and Distributions*, **5**, 165–174, https://doi.org/10.1046/j.1472-4642.1999.00046.x.

Brayard, A., Nützel, A., Stephen, D.A., Bylund, K.G., Jenks, J. & Bucher, H. 2010. Gastropod evidence against the Early Triassic Lilliput Effect. *Geology*, **38**, 147–150, https://doi.org/10.1130/g30553.1.

Brom, K.R., Salamon, M.A., Ferré, B., Brachaniec, T. & Szopa, K. 2015. The Lilliput Effect in crinoids at the end of the Oceanic Anoxic Event 2: a case study from Poland. *Journal of Paleontology*, **89**, 1076–1081.

Brown, M.R., Jeffrey, S.W., Volkman, J.K. & Dunstan, G.A. 1997. Nutritional properties of microalgae for mariculture. *Aquaculture*, **151**, 315–331.

Carey, N. & Sigwart, J.D. 2014. Size matters: plasticity in metabolic scaling shows body-size may modulate responses to climate change. *Biology letters*, **10**, https://doi.org/DOI: 10.1098/rsbl.2014.0408.

Cary, S.C., Vetter, R.D., & Felbeck, H. 1989. Habitat characterization and nutritional strategies of the endosymbiont-bearing bivalve *Lucinoma aequizonata. Marine Ecology Progress Series,* **55**, 31-45, https://doi.org/10.3354/meps055031.

Caswell, B.A. & Dawn, S.J. 2019. Recovery of benthic communities following the Toarcian Oceanic Anoxic Event in the Cleveland Basin , UK. *Palaeogeography, Palaeoclimatology, Palaeoecology*, **521**, 114–126, https://doi.org/10.1016/j.palaeo.2019.02.014.

Chen, J., Song, H., He, W., Tong, J., Wang, F. & Wu, S. 2019. Size variation of brachiopods from the Late Permian through the Middle Triassic in South China: Evidence for the Lilliput Effect following the Permian-Triassic extinction. *Palaeogeography, Palaeoclimatology, Palaeoecology*, **519**, 248–257, https://doi.org/10.1016/j.palaeo.2018.07.013.

Clémence, M.-E. & Hart, M.B. 2013. Proliferation of Oberhauserellidae during the recovery following the Late Triassic extinction: paleoecological implications. *Journal of Paleontology*, **87**, 1004–1015, https://doi.org/10.1666/13-021.

Cope, E.D. 1887. *The Origin of the Fittest* . New York, D. Appleton and Co.

Copestake, P. & Johnson, B. 2014. *Lower Jurassic Foraminifera from the Llanbedr (Mochras Farm) Borehole, North Wales, UK*. London, Monograph of the Palaeontographical Society.

Damborenea, S.E. 1987a. Early Jurassic bivalvia of Argentina. Part 1: stratigraphical introduction and superfamilies Nuculanacea, Arcacea, Mytilacea and Pinnacea. *Palaeontographica Abteilung A*, **199**, 23–111.

Damborenea, S.E. 1987b. Early Jurassic bivalvia of Argentina. Part 2: superfamilies Pteriacaea, Buchiacea and part of Pectinacea.

Palaeontographica Abteilung A, **199**, 113–216.

Damborenea, S.E. 2002. Early Jurassic bivalvia of Argentina. Part 3: superfamilies Monotoidea, Pectinoidea, Plicatuloidea and Dimyoidea. *Palaeontographica Abteilung A*, **265**, 1–119.

Damborenea, S.E., Echevarría, J. & Ros-Franch, S. 2017. Biotic recovery after the end-Triassic extinction event: Evidence from marine bivalves of the Neuquén Basin, Argentina. *Palaeogeography, Palaeoclimatology, Palaeoecology*, **487**, 93–104, https://doi.org/10.1016/j.palaeo.2017.08.025.

Deconinck, J., Hesselbo, S.P., Debuisser, N. & Averbuch, O. 2003. Environmental controls on clay mineralogy of an Early Jurassic mudrock (Blue Lias Formation, southern England). *International Journal of Earth Sciience (Geol Rundsch)*, **92**, 255–266, https://doi.org/10.1007/s00531-003-0318-y.

Dera, G., Pellenard, P., Neige, P., Deconinck, J., Pucéat, E. & Dommergues, J. 2009. Distribution of clay minerals in Early Jurassic Peritethyan seas: palaeoclimatic significance inferred from multiproxy comparisons. *Palaeogeography, Palaeoclimatology, Palaeoecology*, **271**, 39–51, https://doi.org/10.1016/j.palaeo.2008.09.010.

Distel, D.L. & Felbeck, H. 1987. Endosymbiosis in the lucinid clams *Lucinoma aequizonata, Lucinoma annulata* and *Lucina floridana:* a reexamination of the functional morphology of the gills as bacteria-bearing organs. *Marine Biology*, **96**, 79-86, https://doi.org/10.1007/BF00394840.

Dommergues, J.-L., Montuire, S. & Neige, P. 2002. Size patterns through time: the case of the Early Jurassic ammonite radiation. *Paleobiology*, **28**, 423–434, https://doi.org/10.1666/0094-8373(2002)028<0423:SPTTTC>2.0.CO;2.

Donovan, D.T., Curtis, M.L.K. & Fry, T.R. 2005. The lower part of the Lias Group in south Gloucestershire: zonal stratigraphy and structure. *Proceedings of the Geologists' Association*, **116**, 45–59, https://doi.org/10.1016/S0016-7878(05)80016-1.

Gallois, R.W. 2008. The lithostratigraphy of the Shales-with-Beef Member of the Charmouth Mudstone Formation, Lower Jurassic. *Proceedings of the Ussher Society*, **12**, 32–40.

Gómez, J.J., Comas-rengifo, M.J. & Goy, A. 2016. Palaeoclimatic oscillations in the Pliensbachian (Early Jurassic) of the Asturian Basin (Northern Spain). *Climate of the Past*, **12**, 1199–1214, https://doi.org/10.5194/cp-12-1199-2016.

Hallam, A. 1960. A sedimentary and faunal study of the Blue Lias of Dorset and Glamorgan. *Philosophical Transactions of the Royal Society of London B: Biological Sciences*, **243**, 1–44, https://doi.org/10.1098/rstb.1960.0003.

Hallam, A. 1963. Observations on the palaeoecology and ammonite sequence of the Frodingham Ironstone (Lower Jurassic). *Palaeontology*, **6**, 554–574.

Hallam, A. 1965. Environmental causes of stunting in living and fossil marine benthonic invertebrates. *Palaeontology*, **8**, 132–155.

Hallam, A. 1968. Morphology, palaeoecology and evolution of the genus Gryphaea in the British Lias. *Philosophical Transactions of the Royal*

Society of London B: Biological Sciences, **254**, 91–128, https://doi.org/10.1098/rstb.1968.0014.

Hallam, A. 1975. Evolutionary size increase and longevity in Jurassic bivalves and ammonites. *Nature*, **258**, 493–496.

Hallam, A. 1978. How rare is phyletic gradualism and what is its evolutionary significance? Evidence from Jurassic bivalves. *Paleobiology*, **4**, 16–25.

Hallam, A. 1996. Recovery of the marine fauna in Europe after the end-Triassic and early Toarcian mass extinctions. *Geological Society, London, Special Publications*, **102**, 231–236, https://doi.org/10.1144/GSL.SP.1996.001.01.16.

Hallam, A. 2002. How catastrophic was the end-Triassic mass extinction ? *Lethaia*, **35**, 147–157.

Hallam, A. & Bradshaw, M.J. 1979. Bituminous shales and oolitc ironstones as indicators of transgressions and regressions. *Journal of the Geological Society, London*, **136**, 157–164, https://doi.org/10.1144/gsjgs.136.2.0157.

Hallam, A. & El Shaarawy, Z. 1982. Salinity reduction of the end- Triassic sea from the Alpine region into northwestern Europe. *Lethaia*, **15**, 169–178, https://doi.org/10.1111/j.1502-3931.1982.tb01136.x.

Hammer, Ø., Harper, D.A.T. & Ryan, P.D. 2001. Past: Paleontological statistics software package for education and data analysis.

Harries, P.J. & Knorr, P.O. 2009. What does the 'Lilliput Effect' mean? *Palaeogeography, Palaeoclimatology, Palaeoecology*, **284**, 4–10, https://doi.org/10.1016/j.palaeo.2009.08.021.

Hesselbo, S.P. 2008. Sequence stratigraphy and inferred relative sea-level change from the onshore British Jurassic. *Proceedings of the Geologists' Association*, **119**, 19–34, https://doi.org/10.1016/S0016-7878(59)80069-9.

Hesselbo, S.P. & Jenkyns, H.C. 1998. British Lower Jurassic sequence stratigraphy. *In*: *Mesozoic and Cenozoic Sequence Stratigraphy of European Basins*. SEPM Special Publications No. 60.

Hesselbo, S.P., Oates, M.J. & Jenkyns, H.C. 1998. The Lower Lias Group of the Hebrides Basin. *Scottish Journal of Geology*, **34**, 23–60.

Hesselbo, S.P., Robinson, S.A. & Surlyk, F. 2004. Sea-level change and facies development across potential Triassic – Jurassic boundary horizons , SW Britain. *Journal of the Geological Society*, **161**, 365–379.

His, E., Robert, R. & Dinet, A. 1989. Combined effects of temperature and salinity on fed and starved larvae of the Mediterranean mussel Mytilus galloprovincialis and the Japanese oyster Crassostrea gigas. *Marine Biology*, **100**, 455–463.

Hodges, P. 2000. *The Early Jurassic Bivalvia from the Hettangian and Lower Sinemurian of South-West Britain Part 1*. London, Monograph of the Palaeontographical Society.

Howard, A.S. 1985. Lithostratigraphy of the Staithes Sandstone and Cleveland Ironstone formations (Lower Jurassic) of north-east Yorkshire. *Proceedings of the Yorkshire Geological Society*, **45**, 261–275, https://doi.org/10.1144/pygs.45.4.261.

Howarth, M.K. 1955. Domerian of the Yorkshire coast. *Proceedings of the Yorkshire Geological Society*, **30**, 147–175.

Ivimey-Cook, H.C. 1971. Stratigraphical palaeontology of the Lower Jurassic of the Llanbedr (Mochras Farm) Borehole. *In*: Woodland, A. W. (ed.) *The Llanbedr (Mochras Farm) Borehole*. Institute of Geological Sciences Report No.71/18, 87–92.

Ivimey-Cook, H.C. 1975. The stratigraphy of the Rhaetic and Lower Jurassic in eastern Antrim. *Bulletin of the Geological Survey of Great Britain*, **50**, 51–69.

Jablonski, D. 1997. Body-size evolution in Cretaceous molluscs and the status of Cope's Rule. *Nature*, **385**, 250–252.

James, F.C. 1970. Geographic size variation in birds and its relationship to climate. *Ecology*, **51**, 365–390, https://doi.org/10.2307/1935374.

Johnson, A. 1984. *The Palaeobiology of the Bivalve Families Pectinidae and Propeamussiidae in the Jurassic of Europe*. München, Zitteliana.

Johnson, A. 1994. Evolution of European Lower Jurassic Gryphaea (Gryphaea) and contemporaneous bivalves. *Historical Biology*, **7**, 167–186.

Jones, D.S. & Gould, S.J. 1999. Direct measurements of age in fossil Gryphaea: the solution to a classic problem in heterochrony. *Paleobiology*, **25**, 158–187.

Kaariainen, J.I. & Bett, B.J. 2006. Evidence for benthic body size miniaturization in the deep sea. *Journal of the Marine Biological Association of the United Kingdom*, **86**, 1339–1345, https://doi.org/10.1017/S0025315406014366.

Korte, C. & Hesselbo, S.P. 2011. Shallow marine carbon and oxygen isotope and elemental records indicate icehouse-greenhouse cycles during the Early Jurassic. *paleoceanography*, **26**, 1–18, https://doi.org/10.1029/2011PA002160.

Korte, C., Hesselbo, S.P., Jenkyns, H.C., Rickaby, R.E.M. & Spotl, C. 2009. Palaeoenvironmental significance of carbon- and oxygen-isotope stratigraphy of marine Triassic-Jurassic boundary sections in SW Britain. *Journal of the Geological Society*, **166**, 431–445, https://doi.org/10.1144/0016-76492007-177.

Kosnik, M.A., Jablonski, D., Lockwood, R. & Novack-Gottshall, P.M. 2006. Quantifying molluscan body size in evolutionary and ecological analyses: Maximizing the return on data-collection efforts. *Palaios*, **21**, 588–597.

Lindström, S., van de Schootbrugge, B., et al. 2017. A new correlation of Triassic–Jurassic boundary successions in NW Europe, Nevada and Peru, and the Central Atlantic Magmatic Province: A time-line for the end-Triassic mass extinction. *Palaeogeography, Palaeoclimatology, Palaeoecology*, **478**, 80–102, https://doi.org/10.1016/j.palaeo.2016.12.025.

Linse, K., Barnes, D.K.A. & Enderlein, P. 2006. Body size and growth of benthic invertebrates along an Antarctic latitudinal gradient. *Deep Sea Research Part II: Topical Studies in Oceanography*, **53**, 921–931, https://doi.org/10.1016/j.dsr2.2006.03.006.

Loosanoff, V.L. & Tommers, F.D. 1948. Effect of suspended silt and other substances on rate of feeding of oysters. *Science*, **107**, 69–70,

https://doi.org/10.1126/science.107.2768.69.

Mander, L., Twitchett, R.J. & Benton, M.J. 2008. Palaeoecology of the Late Triassic extinction event in the SW UK. *Journal of the Geological Society*, **165**, 319–332, https://doi.org/10.1144/0016-76492007-029.

Márquez-aliaga, A., Damborenea, S., Gómez, J.J. & Goy, A. 2010. Bivalves from the Triassic-Jurassic transition in Northern Spain (Asturias and Western Basque-Cantabrian Basin). *Ameghiniana*, **47**, 185–205, https://doi.org/10.5710/AMGH.v47i2.3.

Martill, D.M., Vidovic, S.U., Howells, C. & Nudds, J.R. 2016. The oldest Jurassic dinosaur: a basal neotheropod from the Hettangian of Great Britain. *PLoS ONE*, **11**, e0145713, https://doi.org/10.1371/journal.pone.0145713.

McElwain, J.C., Beerling, D.J. & Woodward, F.I. 1999. Fossil plants and global warming at the Triassic-Jurassic boundary. *Science*, **285**, 1386–1391.

Metcalfe, B., Twitchett, R.J. & Price-Lloyd, N. 2011. Changes in size and growth rate of 'Lilliput' animals in the earliest Triassic. *Palaeogeography, Palaeoclimatology, Palaeoecology*, **308**, 171–180, https://doi.org/10.1016/j.palaeo.2010.09.011.

Moghadam, H. V & Paul, C.R.C. 2000. Trace fossils of the Jurassic, Blue Lias, Lyme Regis, southern England. *Ichnos*, **7**, 283–306, https://doi.org/10.1080/10420940009380167.

Morton, N. 1989. Jurassic sequence stratigraphy in the Hebrides Basin, NW Scotland. *Marine and Petroleum Geology*, **6**, 243–260.

Morton, N. & Oates, M.J. 2004. The Hebrides Basin. *In*: Simms, M. J., Chidlaw, N., Morton, N. & Page, K. N. (eds) *British Lower Jurassic Stratigraphy, Geolocial Conservation Review Series No. 30*. Peterborough, Joint Nature Conservation Committee, 313–374.

Munroe, D.M., Powell, E.N., Mann, R., Klinck, J.M. & Hofmann, E.E. 2013. Underestimation of primary productivity on continental shelves: evidence from maximum size of extant surfclam (Spisula solidissima) populations. *Fisheries Oceanography*, **22**, 220–233, https://doi.org/10.1111/fog.12016.

Nicol, D. 1967. Some characteristics of cold-water marine pelecypods. *Journal of Paleontology*, **41**, 1330–1340.

Nori, L. & Lathuiliére, B. 2003. Form and environment of Gryphaea arcuata. *Lethaia*, **36**, 83–96, https://doi.org/10.1080/00241160310003081.

Oates, M.J. 1978. A revised stratigraphy for the western Scottish Lower Lias. *Proceedings of the Yorkshire Geological Society*, **42**, 143–156.

Olabarria, C. & Thurston, M.H. 2003. Latitudinal and bathymetric trends in body size of the deep-sea gastropod Troschelia berniciensis (King). *Marine Biology*, **143**, 723–730, https://doi.org/10.1007/s00227-003-1116-6.

Payne, J.L. 2005. Evolutionary dynamics of gastropod size across the end-Permian extinction and through the Triassic recovery interval. *Paleobiology*, **31**, 269–290.

Peck, L.S. & Harper, E.M. 2010. Variation in size of living articulated brachiopods with latitude and depth. *Marine Biology*, **157**, 2205–2213, https://doi.org/10.1007/s00227-010-1486-5.

Radley, J.D. 2003. Warwickshire's Jurassic geology: past, present and future. *Mercian Geologist*, **15**, 209–218.

Radulović, B. 2013. Lower Jurassic bivalves of eastern Serbia. *Beringeria*, **43**, 3–61.

Rensch, B. 1948. Histological changes correlated with evolutionary changes of body size. *Evolution*, **2**, 218–230.

Rhoads, D.C. & Morse, J.W. 1971. Evolutionary and ecologic significance of oxygen-deficient marine basins. *Lethaia*, **4**, 413–428.

Richmond, C., Marcus, N.H., Sedlacek, C., Miller, G.A. & Oppert, C. 2006. Hypoxia and seasonal temperature: Short-term effects and long-term implications for Acartia tonsa dana. *Journal of Experimental Marine Biology and Ecology*, **328**, 177–196, https://doi.org/10.1016/j.jembe.2005.07.004.

Ros-Franch, S., Márquez-aliaga, A. & Damborenea, S.E. 2014. Comprehensive database on Induan (Lower Triassic) to Sinemurian (Lower Jurassic) marine bivalve genera and their paleobiogeographic record. *Paleontological Contributions*, **8**, 1–219, https://doi.org/10.17161/PC.1808.13433.

Rosales, I., Quesada, S. & Robles, S. 2004. Paleotemperature variations of Early Jurassic seawater recorded in geochemical trends of belemnites from the Basque-Cantabrian basin, northern Spain. *Palaeogeography, Palaeoclimatology, Palaeoecology*, **203**, 253–275, https://doi.org/10.1016/S0031-0182(03)00686-2.

Ruhl, M., Hesselbo, S.P., et al. 2016. Astronomical constraints on the duration of the Early Jurassic Pliensbachian Stage and global climatic fluctuations. *Earth and Planetary Science Letters*, **455**, 149–165, https://doi.org/10.1016/j.epsl.2016.08.038.

Sheppard, T.H. 2006. Sequence architecture of ancient rocky shorelines and their response to sea-level change: an Early Jurassic example from South Wales, UK. *Journal of the Geological Society, London*, **163**, 595–606, https://doi.org/10.1144/0016-764920-015.

Shi, G.R., Zhang, Y.-C., Shen, S.-Z. & He, W.-H. 2016. Nearshore-offshore-basin species diversity and body size variation patterns in Late Permian (Changhsingian) brachiopods. *Palaeogeography, Palaeoclimatology, Palaeoecology*, **448**, 96–107, https://doi.org/10.1016/j.palaeo.2015.07.046.

Shirayama, Y. 1983. Size structure of deep-sea meio- and macrobenthos in the western Pacific. *Internationale revue der gesamten hydrobiologie und hydrographie*, **68**, 799–810.

Simms, M.J. 2004. The Mendips and South Wales Massif. *In*: Simms, M. J., Chidlaw, N., Morton, N. & Page, K. N. (eds) *British Lower Jurassic Stratigraphy, Geolocial Conservation Review Series No. 30*. Peterborough, Joint Nature Conservation Committee, 112–156.

Simms, M.J. & Jeram, A. 2007. Waterloo Bay, Larne, Northern Ireland: a candidate Global Stratotype Section and Point for the base of the Hettangian Stage and Jurassic System. *ISJS Newsletter*, **34**, 50–68.

Simms, M.J. & Page, K.N. 2004. The East Midlands Shelf. *In*: Simms, M. J., Chidlaw, N., Morton, N. & Page, K. N. (eds) *British Lower Jurassic*

Stratigraphy, Geolocial Conservation Review Series No. 30. Peterborough, Joint Nature Conservation Committee, 215–223.

Simms, M.J., Chidlaw, N., Morton, N. & Page, K.N. 2004. *British Lower Jurassic Stratigraphy*. Peterborough, Geological Conservation Review Series, No. 30, Joint Nature Conservation Committee.

Smith, C.R., Leo, F.C. De, Bernardino, A.F., Sweetman, A.K. & Arbizu, P.M. 2008. Abyssal food limitation, ecosystem structure and climate change. *Trends in Ecology & Evolution*, **23**, 518–528, https://doi.org/10.1016/j.tree.2008.05.002.

Sogot, C.E., Harper, E.M. & Taylor, P.D. 2014. The Lilliput Effect in colonial organisms: Cheilostome bryozoans at the Cretaceous-Paleogene mass extinction. *PLoS ONE*, **9**, e87048.

Song, H., Tong, J. & Chen, Z.-Q. 2011. Evolutionary dynamics of the Permian – Triassic foraminifer size : evidence for Lilliput Effect in the end-Permian mass extinction and its aftermath. *Palaeogeography, Palaeoclimatology, Palaeoecology*, **308**, 98–110, https://doi.org/10.1016/j.palaeo.2010.10.036.

Suan, G., Mattioli, E., et al. 2010. Secular environmental precursors to Early Toarcian (Jurassic) extreme climate changes. *Earth and Planetary Science Letters*, **290**, 448–458, https://doi.org/10.1016/j.epsl.2009.12.047.

Swift, A. 1999. Stratigraphy (including biostratigraphy). *In*: Swift, A. & Martill, D. M. (eds) *Fossils of the Rhaetian Penarth Group*. London, The Palaeontological Association, 15–30.

Twitchett, R.J. 2007. The Lilliput Effect in the aftermath of the end-Permian extinction event. *Palaeogeography, Palaeoclimatology, Palaeoecology*, **252**, 132–144, https://doi.org/10.1016/j.palaeo.2006.11.038.

Urbanek, A. 1993. Biotic crises in the history of Upper Silurian graptoloids: A Palaeobiological model. *Historical Biology*, **7**, 29–50, https://doi.org/10.1080/10292389309380442.

van de Schootbrugge, B. & Gollner, S. 2013. Altered primary productivity during mass-extinction events. *The Paleontological Society Papers*, **19**, 87–114.

van de Schootbrugge, B., Tremolada, F., et al. 2007. End-Triassic calcification crisis and blooms of organic-walled 'disaster species'. *Palaeogeography, Palaeoclimatology, Palaeoecology*, **244**, 126–141, https://doi.org/10.1016/j.palaeo.2006.06.026.

van de Schootbrugge, B., Bachan, A., Suan, G., Richoz, S. & Payne, J.L. 2013. Microbes, mud and methane: cause and consquence of recurrent Early Jurassic anoxia following the end-Triassic mass extinction. *Palaeontology*, **56**, 685–709, https://doi.org/10.1111/pala.12034.

Vermeij, G.J. 2011. Shifting sources of productivity in the coastal marine tropics during the Cenozoic era. *Proceedings of the Royal Society of London B*, **278**, 2362–2368, https://doi.org/10.1098/rspb.2010.2362.

von Elert, E., Martin-creuzburg, D. & Le Coz, J.R. 2003. Absence of sterols constrains carbon transfer between cyanobacteria and a freshwater herbivore (Daphnia galeata). *Proceedings of the Royal Society of London B*, **270**, 1209–1214, https://doi.org/10.1098/rspb.2003.2357.

Wacker, A. & von Elert, E. 2003. Food quality controls reproduction of the zebra

mussel (Dreissena polymorpha). *Ecophysiology*, **135**, 332–338, https://doi.org/10.1007/s00442-003-1208-5.

Wacker, A. & von Elert, E. 2008. Body size and food thresholds for zero growth in Dressena polymorpha: a mechanism underlying intraspecific competition. *Freshwater Biology*, **53**, 2356–2363.

Weedon, G.P. 1986. Hemipelagic shelf sedimentation and climatic cycles: The basal Jurassic (Blue Lias) of S. Britain. *Earth and Planetary Science Letters*, **76**, 321–335, https://doi.org/10.1016/0012-821X(86)90083-X.

Weedon, G.P. 1987. *Palaeoclimatic Significance of Open-Marine Cyclic Sequences*. Linacre College.

Weedon, G.P., Jenkyns, H.C. & Page, K.N. 2018. Combined sea-level and climate controls on limestone formation, hiatuses and ammonite preservation in the Blue Lias Formation, South Britain (uppermost Triassic–Lower Jurassic). *Geological Magazine*, **155**, 1117–1149, https://doi.org/10.1017/S001675681600128X.

Weedon, G.P., Page, K.N. & Jenkyns, H.C. 2019. Cyclostratigraphy, stratigraphic gaps and the duration of the Hettangian Stage (Jurassic): insights from the Blue Lias Formation of southern Britain. *Geological Magazine*, **156**, 1469–1509, https://doi.org/10.1017/S0016756818000808.

Weiss, M.B., Curran, P.B., Peterson, B.J. & Gobler, C.J. 2007. The influence of plankton composition and water quality on hard clam (Mercenaria mercenaria) populations across Long Island's south shore lagoon estuaries (New York, USA). *Journal of Experimental Marine Biology and Ecology*, **345**, 12–25.

Wiest, L.A., Lukens, W.E., Peppe, D.J., Driese, S.G. & Tubbs, J. 2018. Terrestrial evidence for the Lilliput Effect across the Cretaceous-Paleogene (K-Pg) boundary. *Palaeogeography, Palaeoclimatology, Palaeoecology*, **491**, 161–169, https://doi.org/10.1016/j.palaeo.2017.12.005.

Wignall, P.B. 1990. Benthic palaeocology of the Late Jurassic Kimmeridge Clay of England. *Special papers in palaeontology*, **43**.

Wignall, P.B. 2001. Sedimentology of the Triassic-Jurassic boundary beds in Pinhay Bay (Devon, SW England). *Proceedings of the Geologists' Association*, **112**, 349–360, https://doi.org/10.1016/S0016-7878(01)80014-6.

Wignall, P.B. & Bond, D.P.G. 2008. The end-Triassic and Early Jurassic mass extinction records in the British Isles. *Proceedings of the Geologists' Association*, **119**, 73–84, https://doi.org/10.1016/S0016-7878(08)80259-3.

Wignall, P.B. & Hallam, A. 1991. Biofacies, stratigraphic distribution and depositional models of British onshore Jurassic black shales. *Geoogical Society Special Publications*, **58**, 291–309.

Wotzlaw, J., Guex, J., et al. 2014. Towards accurate numerical calibration of the Late Triassic: High-precision U-Pb geochronology constraints on the duration of the Rhaetian. *Geology*, **42**, 571-574,https://doi.org/10.1130/G35612.1.

Xu, W., Ruhl, M., Hesselbo, S.P., Riding, J.B. & Jenkyns, H.C. 2017. Orbital pacing of the Early Jurassic carbon cycle, black-shale formation and

seabed methane seepage. *Sedimentology*, **64**, 127–149, https://doi.org/10.1111/sed.12329.

Chapter 6: Discussion

6.1 Recovery from the end-Triassic extinction: bivalve diversity

A primary aim of this work was to document the tempo and style of recovery amongst marine communities following the end-Triassic mass extinction within the British shelf seas. This has been monitored primarily through studying bivalve assemblages. Bivalve stratigraphic ranges shows that pre-extinction diversity is rapidly re-attained by the Langport Member, only 0.15 Myr later (Fig. 5.4A.), although diversity declined in the subsequent Pre-*planorbis* Beds after a minor extinction coincident with the base of the Blue Lias Formation. Bivalve diversity rose in a series of sharp steps thereafter. The sharpest rise in diversity occurs between the Pre-*planorbis* Beds and the *planorbis* Zone, and diversity peaks during the *semicostatum* Zone. This latter zone contains a silicified fossil assemblage that may have inflated diversity owing to its exquisite preservation (Chapter 3; Wright *et al.* 2003). Exclusion of these silicified specimens did not, however, remove the trend suggesting that preservation is not responsible. A sharp diversity loss occurs between the *semicostatum* and *turneri* zones after which a broadly stable diversity is attained 6 Myr after the extinction**,** although this gradually declines from the *jamesoni* Zone onwards. These values of diversity are similar to those recorded from the *planorbis* and *liasicus* zones.

The pattern of bivalve diversity recorded here (Fig. 5.4A), departs from that presented by Hallam (1987, 1996), who showed that bivalve diversity rose through the Hettangian to reach a stable value in the Sinemurian, and then rose once more in the Pliensbachian, again to a stable level. Here it is shown that Pliensbachian diversity was lower than in the late Hettangian-early Sinemurian.

6.2 Lilliput versus Brobdingnag effects

The widely cited Lilliput Effect has often been misapplied to taxa in the aftermath of the ETE. A frequent issue is the vague and variable use of the term. The Lilliput Effect *sensu* Urbanek (1993) is the temporary reduction in size of species that survive an extinction crisis and their subsequent size increase in the recovery interval (Fig. 6.1A). Of the 28 bivalve species present in the Westbury Formation (pre-extinction), only 15 pass into the basal Cotham Member and a further four disappear above a basal shell bed in South Glamorgan. This leaves 11 species eligible to exhibit a Lilliput trend but, of these, only six species are common enough for size trends to be assessed. Of these, only two (possibly a third) exhibit the Lilliput Effect despite claims that it is frequently seen after the ETE (Barras & Twitchett 2007; Mander *et al.* 2008; Clémence & Hart 2013).

The Lilliput Effect is also uncommon after other crises. Song *et al.* (2007; 2011) reported the sizes of foraminifera across the Permo-Triassic mass extinction at Meishan, South China and found of the 36 latest Permian species, 14 survived into the Triassic, and of these only four were shown to have a reduced body size after the extinction but these are exceptionally rare making meaningful size analysis impossible. Subsequently, an early Triassic extinction pulse wipes all of these species out, and so they do not record the subsequent size increase. These “survivors” can be regarded as holdover taxa and demonstrate the issue in identifying true Lilliputians. Nonetheless, the Lilliput Effect is considered to be significant although many authors choose a *sensu lato* version of the effect by applying it at a supra-species levels (e.g. Borths & Ausich 2011; Chen *et al.* 2013; Chu *et al.* 2015; Łaska *et al.* 2017).

At the species level this study of post-extinction body size trends suggests that the Brobdingnag Effect is more likely to be encountered (defined in Chapter 2). This is defined as an intraspecific size increase in newly originating species following a mass extinction (Fig, 6.1B). This has been demonstrated for 11 or possibly 12, species of Early Jurassic bivalve and is also seen within three species of *Gryphaea* (Johnson 1994). The degree of size increase is variable. Thus, *Pholadomya glabra* increases by 62% over 2 Myr (*liasicus* to *bucklandi*); *Plagiostoma giganteum* increases by 142% in 3.6 Myr (*planorbis* to *bucklandi*); *Neocrassina gueuxii* undergoes a 283% size increase over 2.3 Myr (*planorbis* to *angulata*); and the most dramatic being an increase of 476% in *Pseudopecten equivalvis* over a much longer 11 Myr (*semicostatum* to *spinatum*).

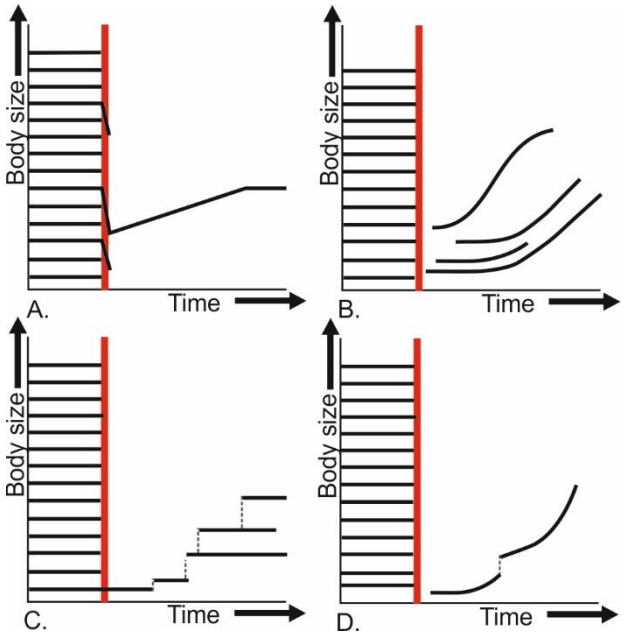

Fig. 6.1 Schematic diagrams of body size changes across extinction events (red line). Horizontal lines represent theoretical species ranges. A. The Lilliput Effect, *sensu* Urbanek; B. The Brobdingnag Effect. C. Cope's Rule, dotted vertical lines depict speciation events; D. Brobdingnag Effect in concert with Cope's Rule, as with C dotted line represents speciation.

The Brobdingnag Effect is, therefore, a more significant contributor than the Lilliput Effect to the trend of size increase during recovery from mass extinction. The size increase was shown to be a consequence of improved growth, seen as a greater spacing between growth lines, and increased longevity seen in instances where larger individuals had more growth lines. This makes the assumption that each growth increment within a single species denotes the same interval of time. In studies where fossil material preserves original shell calcite such assumptions can be tested, using oxygen isotope ratios to detect seasonal temperature oscillations allowing lifespan and growth rates to be accurately gauged and so too can growth rates (cf. Jones & Quitmyer 1996). This style of analysis was not possible with most of the species used herein as shells were usually recrystallized.

Seven *Liostrea* from the Pre-*planorbis* Beds and one from the Langport Member of Lavernock Point were used to assess growth rates through oxygen isotope compositions (Korte *et al*. 2009). Their results seem to suggest that these oysters were recording half to one annual cycle suggesting these were short lived individuals. Regrettably however, Korte *et al.* (2009) did not sample from higher in the section from some of the larger individuals to test for changes in longevity or growth rate which may have confirmed suspicions that a greater lifespan assisted in producing a Brobdingnag trend.

The extinct Cenozoic scallop *Carolinapecten eboreus* (Conrad) appears to have grown to great sizes (up to 165 mm) in less than two years (Johnson *et al.* 2019). Growth rates estimated to be as great as 145.7 mm per year, achieved through increased number of small growth increments opposed to secretion of more material per growth interval (Johnson *et al*. 2019). In Chapter 2 it was suggested that *Plagiostoma giganteum* achieved a greater size through a

combination of increased growth rates and greater longevity, however as some specimens have in excess of 1000 growth increments but few repeated cycles of high and low density growth lines, which may be interpreted as annual cycles, *Plagiostoma giganteum* may have had a similar growth strategy to *C. eboreus.*

The size increase in *Plagiostoma giganteum* might have been further facilitated by retention of the juvenile growth rates, these bivalves exhibit isometric growth, with few showing the expected condensation of growth lines towards the shell margin with increasing age (i.e. decreasing growth rate with increasing body size of the individual). Perhaps this allowed for continued growth and attainment of greater sizes in *P. giganteum,* whereas other species such as *Mactromya cardioideum* and *Cardinia ovalis* show a progressively declining growth rate with age, and so do not attain a vast relative size increase. This is especially so in *M. cardioideum* which appears to increase in size by increased longevity and so only shows a comparably small size increase through time (54%).

The Brobdingnag Effect can be seen as distinct from Cope's Rule, with stratigraphically younger individuals discernible from those of older intervals only by their larger size, being in all other respects identical. Cope's Rule is a size increase of successive species seen in phylogenetic lineages (Fig. 6.1C).

The Brobdingnag Effect and Cope's Rule were not mutually exclusive amongst Early Jurassic bivalves and several examples occur where those showing intraspecific size increase are succeeded by new species that are also successively larger. If it is assumed that a stratigraphically younger species of a particular genus is the descendant of an older species then examples of the Brobdingnag leading to Cope's Rule include species in the genera *Gresslya* and *Pholadomya*, and potentially *Oxytoma* and *Protocardia*. In each of these cases

the individual species increased in body size whilst maintaining the same morphology (as per Brobdingnag Effect), this then follows a change in morphology so as to produce a larger, new species (as per Cope's Rule; Fig. 6.1D). Such trends are seen in the succession of Early Jurassic *Gryphaea* species (Hallam 1978; Johnson 1994).

6.3 Sinemurian Small Episode

The Sinemurian sees a reversal of increasing size. Maximum body size decreases after the *angulata* Zone and (with the exception of a spike during the *obtusum* Zone, discussed below) remains low until an increase in the *raricostatum* Zone (Fig. 5.4A). This trend is herein referred to as the Sinemurian Small Episode (SSE). The cause of the SSE is perhaps manifold. During the *bucklandi* and *semicostatum* zones newly-appearing species are progressively smaller. In addition, several taxa that have an average size above the Lias mean (19.1 mm) die out in this interval. Ghost taxa are not likely to have been a major contributor. Although the *turneri* to *oxynotum* zones are characterised by the highest percentage of ghost ranges (55-70%) those species that are ghosting through are mostly below the Lias average mean size with only four larger taxa (mean size >19.1 mm) ranging through.

The *obtusum* Zone size spike is caused by *Cardinia concinna.* This bivalve is extremely common in the Frodingham Ironstone Member where it attains large size. There are 50 specimens from this time bin (which is 43% of the sample) the removal of this species from the *obutsum* Zone severely dampens the large sizes during that interval and highlights the SSE with greater clarity.

The Lilliput Effect may have played only a minor role in the ETE, but is it represented during the SSE? Regrettably this is not, at the current time, demonstrable for the usual reason that the true Lilliput effect is hard to find, the species that show a size reduction leading into the SSE die out during it and those species that appear afterwards show a size increase as per the Brobdingnag Effect. During the SSE there is a marked decline in bivalve species richness between the *semicostatum* and *turneri* zones. The Sinemurian is also associated with a transient loss in functional richness in the Boreal Oceans (Dunhill *et al*. 2018). These two factors combined with the reduction in body size, reported here, suggest this time may represent a local/regional biotic crisis hitherto unreported.

6.4 Size and recovery

Body size as an indicator of recovery has been tested here in conjunction with other recovery metrices. It was found that body size trends are independent of tiering re-occupancy and diversity. Increasingly complex tiering levels, with both deep infauna and erect epifauna, have been proposed as a measure of full recovery (Twitchett 2006). Such benthic structuring was attained very quickly after the ETE as seen in (almost) all studied sections by the *planorbis* Zone, whilst size increase is a much longer term change. This parameter was still increasing some 17 Myr after the extinction, producing an overall increase of 374% across the study interval.

Body size recovers over a much longer timescale than other metrices, and had yet to reach some form of an equilibrium among bivalves before many of them disappeared during the early Toarcian mass extinction event (Morten & Twitchett 2009). This is similar to changes seen in the ecological structure of

marine communities following the PTME (Song *et al.* 2018). This became uncoupled from taxonomic richness taking some 50 Myr for a Late Permian structure to be regained although not before it was disrupted by subsequent events. Recovery from mass extinction monitored by distinct ecological metrics thus operates over a broad range of scales.

The causes behind the observed size changes in bivalves were discussed at length in chapters 2 & 5 and despite detailed reconstruction of marine oxygenation (Chapter 3), no clear relationship is seen. Other workers, attempting to find a cause for an overarching size change in communities, have also not succeeded (e.g. Twitchett 2007; Martínez-Díaz *et al.* 2016). Any conclusion would require the explanation of why both Brobdingnag and inverse-Brobdingnag trends co-occur sometimes even within the same family.

6.5 Early Jurassic oxygenation

Results presented herein show that pyrite framboids occur in plentiful supply at locations in southwestern England, south Wales and North Yorkshire. The size distribution of framboids was considered by lithology, location and time bin revealing each basin to have its own redox history. In Chapter 3 it was proposed that the recovery from the ETE occurred against a background of dysoxia. This was proposed based on the assumption that under a fully oxygenated water column framboids would not grow within the sediment but a degree of oxygen restriction was required in order to preserve sufficient organic material for burial required for the for generation of H_2S (via sulphate reduction) necessary for pyrite formation (Raiswell & Bernrer 1985). Wilkin *et al*. (1996) suggested that it was not possible to distinguish framboids that formed under a

dysoxic water column from those that formed under a fully oxygenated water column, and reflected this by labelling the right hand side of their diagrams “oxic-dysoxic”. Replacement of Wilkin *et al.*’s “oxic-dysoxic” field with solely “dysoxic” was adopted by many following Wignall & Newton (1998) because framboid populations measured from oxygen restricted biofacies 4-5 (upper dysoxic; cf. Wignall & Hallam 1991) plot on or above dividing line on the Wilkin Diagram. These upper dysoxic samples occupy the same region as Wilkin’s oxic samples and has been implied that Wilkin *et al*’s oxic settings were not fully aerated, and it is often assumed that under a fully oxygenated water column no framboids will grow in the sediment (Bond 2004; Bond & Wignall 2010). Regardless of how well-aerated the water column is within the sediment at some depth there will be a redox boundary, at which, provided the elemental components are present, framboids will grow (Raiswell & Berner 1985; Tyson & Pearson 1991).

As question remains as to whether framboid size distributions can distinguish between those that grew within the sediment but under a dysoxic water column from those that grew under an oxygenated water column it is perhaps better for the time being to say that recovery occurred against a background of oxic-dysoxic conditions, in keeping with Wilkin *et al.* (1996).

Regardless of how one interprets the mere presence of framboids the Blue Lias has cycles of black shale deposition, many of which show a framboid population suggestive of water column euxinia and the greater majority of these beds lack benthos entirely. The only bivalve that was found in profusion was *Anningella* which, from association with fossil wood and ammonites, likely had a pseudoplanktonic existence. Black shales occur widely in the Pre-*planorbis* Beds and it is possible that oxygen restriction stalled the recovery at this time, indicated by the loss of bivalve diversity between the Langport (oxic-upper dysoxic) and the

Pre-*planorbis* Beds (anoxic-euxinic to low-mid dysoxic/oxic). Such a delay would however have been short (<0.5 Myr) because the upper beds of this interval feature signs of advancing recovery. In younger ammonite zones black shale deposition recurs, but tends not to be present across all basins at the same time, and recovery appears unaffected at the resolution of ammonite zone. For example, around the Hettangian-Sinemurian boundary Somerset experienced euxinic conditions and no benthos was found, whereas nearby Glamorgan exhibited framboid populations suggestive of oxic-dyoxic conditions and had plentiful benthos. Once conditions had improved in Somerset, these organisms were able to migrate from the shallower Glamorgan sections where diversity was high and stable from the upper Pre-*planorbis* Beds onwards.

6.6 Comparisons with other recovery intervals

The idea that the shallower, better-oxygenated Glamorgan region might provide a root stock of benthic animals to resupply deeper-water settings can be likened to the 'Habitable Zone' or Refuge Zone, proposed by Beatty *et al*. (2008) and Song *et al*. (2014) respectively, for the Early Triassic recovery. This describes inner shelf settings, with abnormally diverse fossil assemblages, that were deep enough to provide respite from the extreme heat of the Early Triassic whilst being shallow enough to avoid oxygen depletion. High temperature may also have been a factor in the ETE, with temperatures having risen by 2.5 - 5 °C (McElwain *et al.* 1999; Steinthorsdottir *et al.* 2011). The pace of cooling in the Early Jurassic is a little unclear, with oxygen isotopes suggesting that there was significant cooling in the Langport Member and the Pre-*planorbis* Beds but this was followed by a gradual warming (Korte *et al.* 2009). However, stomatal indices suggest a gradual

return to pre-extinction Rhaetian atmospheric CO_2 concentrations during the Hettangian, which implies cooling (Steinthorsdottir *et al.* 2011).

For the PTME benthic foraminifera provide good subjects for testing changing body size, and have been especially well-studied from the Permo-Triassic record of South China. Size increase during the recovery appears to have been driven largely by loss of small opportunist and disaster forms which dominated in the earliest Triassic (Payne *et al.* 2011; Song *et al.* 2011, 2016; Rego *et al.* 2012). Average body size of communities was therefore related to measures for evenness with both attaining stable, pre-extinction stable values during the middle Anisian, some 7 Myr after the extinction event. However, there are at least eight examples of a Brobdingnag trend over this interval (Payne *et al.* 2011).

Body size data for bivalves is poorly documented for the recovery from the PTME, although it is well established that they are small and thin shelled in the earliest Triassic, perhaps in response to low oxygen availability (Hautmann & Nützel 2005; Gao *et al.* 2009; Posenato 2009). *Claraia* and *Unionites* are amongst the most common earliest Triassic taxa and show an increasing size trend (Metcalfe 2011) which may reflect the Brobdingnag Effect, but only generic-level data is available.

Brachiopod body sizes have received detailed attention but, although intraspecific body size decrease was detected prior to the PTME these species ultimately died out at the extinction or shortly after (He *et al.* 2007, 2010; Chen *et al.* 2019). Therefore finding true Lilliputians is not feasible. Brachiopods do, however, show clearer evidence of the Brobdingnag Effect in the Early Triassic (Chen *et al.* 2019). Recovery begun around 1 Myr after the PTME and continued for ~10 Myr (Foster & Sebe 2017; Wang *et al.* 2017). The size increase recorded

in brachiopods is similar to that seen for bivalves in the Hettangian, because newly appearing taxa are progressively larger; a likely manifestation of Cope's Rule. Lingulid brachiopods within the Early Triassic are small (5-8 mm) and increase to 18-28 mm in the Late Triassic (Zonneveld *et al.* 2007). The older, smaller species have closer growth-line spacing than the younger species (Metcalfe *et al.* 2011), a trend that recalls *Plagiostoma giganteum* in the Early Jurassic.

The KPg event saw a reduction in size among many of the surviving marine invertebrates, which has often been referred to as the Lilliput Effect (Keller & Abramovich 2009; Martínez-Díaz *et al.* 2016; Patacci 2016; Łaska *et al.* 2017; Wiest *et al.* 2018). However, the manner by which these size reductions occurred and any subsequent size increase has not received much attention with few species-level studies. A study of veneroid bivalve body size during the KPg and Paleogene provides a rare example (Lockwood 2005). This revealed that diversity recovered in the early Eocene (around 10 Myr after the extinction), whilst average body size remained suppressed until the late Eocene, after which they show a slight increase at the Eocene-Oligocene boundary – but Maastrichtian sizes were not reattained (Lockwood 2005). As with the recovery from the ETE, body size appears to have been affected over much longer time scales than diversity suggesting the potential role of the Brobdingnag Effect amongst veneroids.

Comparison of recovery from the ETE and Permo-Triassic mass extinction suggest that the Lilliput Effect is a minor contributor to the small size of fossil assemblages following mass extinction. Instead the preferential origination of small species is more important. These may be of new or pre-existing genera

and, during recovery, many exhibit a Brobdingnag trend. Cope's Rule was likely a significant contributor also, although phylogenetic relationships are seldom well enough resolved. In both cases community level body size restoration was protracted (millions of years) and highly variable between groups**.**

References

Barras, C.G. & Twitchett, R.J. 2007. Response of the marine infauna to Triassic – Jurassic environmental change: Ichnological data from southern England. *Palaeogeography, Palaeoclimatology, Palaeoecology*, **244**, 223–241, https://doi.org/10.1016/j.palaeo.2006.06.040.

Beatty, T.W., Zonneveld, J.-P. & Henderson, C.M. 2008. Anomalously diverse Early Triassic ichnofossil assemblages in northwest Pangea: A case for a shallow-marine habitable zone. *Geology*, **36**, 771–774, https://doi.org/10.1130/G24952A.1.

Bond, D.P.G. 2004. *Oceanographic changes during the Frasnian-Framennian mass extinction.* unpublished Ph.D thesis, University of Leeds, Leeds.

Bond, D.P.G. & Wignall, P.B. 2010. Pyrite framboid study of marine Permian – Triassic boundary sections: A complex anoxic event and its relationship to contemporaneous mass extinction. *GSA Bulletin*, **122**, 1265–1279, https://doi.org/10.1130/B30042.1.

Borths, M.R. & Ausich, W.I. 2011. Ordovician – Silurian Lilliput crinoids during the end-Ordovician biotic crisis. *Swiss Journal of Palaeontology*, **130**, 7–18, https://doi.org/10.1007/s13358-010-0003-2.

Chen, J., Song, H., He, W., Tong, J., Wang, F. & Wu, S. 2019. Size variation of brachiopods from the Late Permian through the Middle Triassic in South China: Evidence for the Lilliput Effect following the Permian-Triassic extinction. *Palaeogeography, Palaeoclimatology, Palaeoecology*, **519**, 248–257, https://doi.org/10.1016/j.palaeo.2018.07.013.

Chen, Y., Twitchett, R.J., et al. 2013. Size variation of conodonts during the Smithian–Spathian (Early Triassic) global warming event. *Geology*, **41**, 823–826, https://doi.org/10.1130/G34171.1.

Chu, D., Tong, J., Song, H., Benton, M.J., Song, H., Yu, J. & Qiu, X. 2015. Lilliput Effect in freshwater ostracods during the Permian – Triassic extinction. *Palaeogeography, Palaeoclimatology, Palaeoecology*, **435**, 38–52, https://doi.org/10.1016/j.palaeo.2015.06.003.

Clémence, M.-E. & Hart, M.B. 2013. Proliferation of Oberhauserellidae during the recovery following the Late Triassic extinction: paleoecological implications. *Journal of Paleontology*, **87**, 1004–1015, https://doi.org/10.1666/13-021.

Dunhill, A.M., Foster, W.J., Sciberras, J & Twitchett, R.J. 2018. Impact of the Late Triassic mass extinction on functional diversity and composition of

marine ecoystems. *Palaeontology.* **61**, 133-148, https://doi.org/10.111/pala.12332.

Foster, W.J. & Sebe, K. 2017. Recovery and diversification of marine communities following the late Permian mass extinction event in the western Palaeotethys. *Global and Planetary Change*, **155**, 165–177, https://doi.org/10.1016/j.gloplacha.2017.07.009.

Gao, Y., Shi, G.R. & Peng, Y. 2009. A new bivalve fauna from the Permian – Triassic boundary section of southwestern China. *Alcheringa*, **33**, 33–47, https://doi.org/10.1080/03115510802618227.

Hallam, A. 1978. How rare is phyletic gradualism and what is its evolutionary significance? Evidence from Jurassic bivalves. *Paleobiology*, **4**, 16–25.

Hallam, A. 1987. Radiations and extinctions in relation to environmental change in the marine Lower Jurassic of Northwest Europe. *Paleobiology*, **13**, 152–168.

Hallam, A. 1996. Recovery of the marine fauna in Europe after the end-Triassic and early Toarcian mass extinctions. *Geological Society, London, Special Publications*, **102**, 231–236, https://doi.org/10.1144/GSL.SP.1996.001.01.16.

Hautmann, M. & Nützel, A. 2005. First record of a heterodont bivalve (mollusca) from the Early Triassic: palaeontological significance and implications for the 'Lazarus problem'. *Palaeontology*, **48**, 1131–1138.

He, W.-H., Shi, G.R., et al. 2007. Brachiopod miniaturization and its possible causes during the Permian – Triassic crisis in deep water environments , South China. *Palaeogeography, Palaeoclimatology, Palaeoecology*, **252**, 145–163, https://doi.org/10.1016/j.palaeo.2006.11.040.

He, W.-H., Twitchett, R.J., Zhang, Y., Shi, G.R., Feng, Q., Yu, J. & Wu, S. 2010. Controls on body size during the Late Permian mass extinction event. *Geobiology*, **8**, 391–402, https://doi.org/10.1111/j.1472-4669.2010.00248.x.

Johnson, A. 1994. Evolution of European Lower Jurassic Gryphaea (Gryphaea) and contemporaneous bivalves. *Historical Biology*, **7**, 167–186.

Johnson, A., Valentine, A.M., Leng, M.J., Schöne, B.R. & Sloane, H.J. 2019. Life history, environment and extinction of the scallop *Carolinapecten eboreus* (Conrad) in the Plio-Pleistocene of the U.S. Eastern Seaboard. *Palaios*, **34**, 49-70, http://dx.doi.org/10.2110/palo.2018.056.

Jones, D.S. & Quitmyer, I.R. 1996. Marking time with bivalve shells: oxygen isotopes and season of annual increment formation. *Palaios*, **11**, 340-346, http://doi.org/10.2307/3515244.

Keller, G. & Abramovich, S. 2009. Lilliput Effect in late Maastrichtian planktic foraminifera : Response to environmental stress. *Palaeogeography, Palaeoclimatology, Palaeoecology*, **284**, 47–62, https://doi.org/10.1016/j.palaeo.2009.08.029.

Korte, C., Hesselbo, S.P., Jenkyns, H.C., Rickaby, R.E.M. & Spotl, C. 2009. Palaeoenvironmental significance of carbon- and oxygen-isotope stratigraphy of marine Triassic-Jurassic boundary sections in SW Britain. *Journal of the Geological Society*, **166**, 431–445, https://doi.org/10.1144/0016-76492007-177.

Łaska, W., Rodríguez-tovar, F.J. & Uchman, A. 2017. Evaluating macrobenthic response to the Cretaceous-Palaeogene event: A high-resolution ichnological approach at the Agost section (SE Spain). *Cretaceous Research*, **70**, 96–110.

Lockwood, R. 2005. Body size, extinction events, and the early Cenozoic record of veneroid bivalves: a new role for recoveries? *Paleobiology*, **31**, 578–590, https://doi.org/10.1666/04070.1.

Mander, L., Twitchett, R.J. & Benton, M.J. 2008. Palaeoecology of the Late Triassic extinction event in the SW UK. *Journal of the Geological Society*, **165**, 319–332, https://doi.org/10.1144/0016-76492007-029.

Martínez-Díaz, L., Phillips, G.E., Nyborg, T., Espinosa, B., de Araújo Tavora, V., Centeno-garcía, E. & Vega, F.J. 2016. Lilliput Effect in a retroplumid crab (Crustacea: Decapoda) across the K/Pg boundary. *Journal of South American Earth Sciences*, **69**, 11–24, https://doi.org/10.1016/j.jsames.2016.03.007.

McElwain, J.C., Beerling, D.J. & Woodward, F.I. 1999. Fossil plants and global warming at the Triassic-Jurassic boundary. *Science*, **285**, 1386–1391.

Metcalfe, B., Twitchett, R.J. & Price-Lloyd, N. 2011. Changes in size and growth rate of 'Lilliput' animals in the earliest Triassic. *Palaeogeography, Palaeoclimatology, Palaeoecology*, **308**, 171–180, https://doi.org/10.1016/j.palaeo.2010.09.011.

Morten, S.D. & Twitchett, R.J. 2009. Fluctuations in the body size of marine invertebrates through the Pliensbachian-Toarcian extinction event. *Palaeogeography, Palaeoclimatology, Palaeoecology*, **284**, 29–38, https://doi.org/10.1016/j.palaeo.2009.08.023.

Patacci, M. 2016. A high-precision Jacob's staff with improved spatial accuracy and laser sighting capability. *Sedimentary Geology*, **335**, 66–69, https://doi.org/ 10.1016/j.sedgeo.2016.02.001.

Payne, J.L., Summers, M., Rego, B.L., Altiner, D., Wei, J., Yu, M. & Lehrmann, D.J. 2011. Early and Middle Triassic trends in diversity , evenness , and size of foraminifers on a carbonate platform in south China: implications for tempo and mode of biotic recovery from the end-Permian mass extinction. *Paleobiology*, **37**, 409–425.

Posenato, R. 2009. Survival patterns of macrobenthic marine assemblages during the end-Permian mass extinction in the western Tethys (Dolomites, Italy). *Palaeogeography, Palaeoclimatology, Palaeoecology*, **280**, 150–167, https://doi.org/10.1016/j.palaeo.2009.06.009.

Raiswell, R. & Berner, R.A. 1985. Pyrite formation in euxinic and semi-euxinic sediments. *American Journal of Science,* **285**, 710-724, https://doi.org/10.2475/ajs.285.8.710.

Rego, B.L., Wang, S.C., Altiner, D. & Payne, J.L. 2012. Within- and among-genus components of size evolution during mass extinction, recovery, and background intervals: a case study of Late Permian through Late Triassic foraminifera. *Paleobiology*, **38**, 627–643, https://doi.org/10.5061/dryad.3rp1p.

Song, H., Tong, J., Zhang, K., Wang, Q. & Chen, Z.Q. 2007. Foraminiferal survivors from the Permian-Triassic mass extinciton in the Meishan

sections, South China. *Palaeoworld*, **16**, 105-119, https://doi.org/10.1016/j.palwor.2007.05.016

Song, H., Tong, J. & Chen, Z.-Q. 2011. Evolutionary dynamics of the Permian – Triassic foraminifer size : evidence for Lilliput Effect in the end-Permian mass extinction and its aftermath. *Palaeogeography, Palaeoclimatology, Palaeoecology*, **308**, 98–110, https://doi.org/10.1016/j.palaeo.2010.10.036.

Song, H., Wignall, P.B., et al. 2014. Anoxia/high temperature double whammy during the Permian-Triassic marine crisis and its aftermath. *Scientific Reports*, **4**, 1–7, https://doi.org/10.1038/srep04132.

Song, H., Tong, J., et al. 2016. Early Triassic disaster and opportunistic foraminifers in South China. *Geol. Mag.*, **153**, 298–315, https://doi.org/10.1017/S0016756815000497.

Song, H., Wignall, P.B. & Dunhill, A.M. 2018. Decoupled taxonomic and ecological recoveries from the Permo-Triassic extinction. *Science Advances*, **4**, 1–7, https://doi.org/10.1126/sciadv.aat5091.

Steinthorsdottir, M., Jeram, A.J. & McElwain, J.C. 2011. Extremely elevated CO_2 concentrations at the Triassic/Jurassic boundary. *Palaeogeography, Palaeoclimatology, Palaeoecology*, **308**, 418–432, https://doi.org/10.1016/j.palaeo.2011.05.050.

Twitchett, R.J. 2007. The Lilliput Effect in the aftermath of the end-Permian extinction event. *Palaeogeography, Palaeoclimatology, Palaeoecology*, **252**, 132–144, https://doi.org/10.1016/j.palaeo.2006.11.038.

Tyson, R.V. & Pearson, T.H. 1991. Modern and ancient continental shelf anoxia: an overview. *Geological Society Special Publication*, **58**, 1-24.

Urbanek, A. 1993. Biotic crises in the history of Upper Silurian graptoloids: A Palaeobiological model. *Historical Biology*, **7**, 29–50, https://doi.org/10.1080/10292389309380442.

Wang, F., Chen, J., Dai, X. & Song, H. 2017. A new Dienerian (Early Triassic) brachiopod fauna from south China and implications for biotic recovery after the Permian-Triassic extinction. *Papers in Palaeontology*, **3**, 425–439, https://doi.org/10.1002/spp2.1083.

Wiest, L.A., Lukens, W.E., Peppe, D.J., Driese, S.G. & Tubbs, J. 2018. Terrestrial evidence for the Lilliput Effect across the Cretaceous-Paleogene (K-Pg) boundary. *Palaeogeography, Palaeoclimatology, Palaeoecology*, **491**, 161–169, https://doi.org/10.1016/j.palaeo.2017.12.005.

Wignall, P.B. & Hallam, A. 1991. Biofacies, stratigraphic distribution and depositional models of British onshore Jurassic black shales. *Geoogical Society Special Publications*, **58**, 291–309.

Wignall, P.B. & Newton, R.J. 1998. Pyrite framboid diameter as a measure of oxygen deficency in ancient mudrocks. *American Journal of Science*, **298**, 537-552, https//doi.org/10.2475/ajs.298.7.537.

Wilkin, R.T., Barnes, H.L. & Brantley, S.L. 1996. The size distribution of framboidal pyrite in modern sediments: An indicator of redox conditions. *Geochimica et Cosmochimica Acta*, **60**, 3897-3912, https://doi.org/10.1016/0016-7037(96)00209-8.

Wright, P., Cherns, L. & Hodges, P. 2003. Missing molluscs: Field testing

taphonomic loss in the Mesozoic through early large-scale aragonite dissolution. *Geology*, **31**, 211–214, https://doi.org/10.1130/0091-7613(2003)031<0211:MMFTTL>2.0.CO;2.

Zonneveld, J., Beatty, T.W. & Pemberton, S.G. 2007. Lingulide brachiopods and the trace fossil Lingulichnus from the Triassic of western Canada: Implications for faunal recovery after the end-Permian mass extinction. *Palaios*, **22**, 74–97, https://doi.org/10.2110/palo.2005.p05-103r.

Chapter 7: Conclusions and future work

7.1 Conclusions

Post extinction reduction of body size has been documented following the ETE in Britain. Although the Lilliput Effect is often reported following extinction events it was only a minor component here, being only demonstrated unequivocally for two species. The suppression of body size following extinction seems to have resulted more commonly from preferential origination of small species. The subsequent increase of the average body size of a species and communities is caused by a variety of factors. In the Early Jurassic, size increase was caused by within-species size increase among species that originated at small body sizes during the aftermath. This size increase within newly originating species is referred to here as the Brobdingnag Effect, named in honour of a race of giant humans encountered by Gulliver in his second misfortune and a reference to the large size species attain relative to their first appearance. A detailed case study on limid bivalves shows *Plagiostoma giganteum* as the archetypal Brobdingnagian which increased in size by 179% from the earliest Hettangian to the first ammonite zone of the Sinemurian. Expanding the study to include all bivalves up to the latest Pliensbachian showed there were 14 confirmed Brobdingnagians amongst 30 species with statistically useful sample sizes. From growth line analyses these species were shown to be increasing in size due to improved growth rates, increased longevity or a combination of both.

Another major factor in producing a size increase in bivalve assemblages of the Lower Jurassic is the appearance of progressively larger species, some

of which probably represent Cope's Rule. This rule has also shown to be manifest amongst the contemporary ammonite lineages (Hallam 1975; Dommergues *et al.* 2002).

The trend of increasing size is not, however, in-step with other recovery metrics. Ecological tiering is restructured by the upper Pre-*planorbis* Beds (within 0.7 Myr of the extinction) and all sections studied show a marked rise in diversity around the same time, which continues at a lessened rate into the Sinemurian, broadly stabilising from the *turneri* Zone onwards, 6 Myr after the ETE. Within the Sinemurian average body size decreased temporarily, entering a period here referred to as the Sinemurian Small Episode (SSE). The SSE is facilitated by a reduction in size of pre-SSE species and origination of progressively smaller species often in pre-existing genera. Many species ghost range through this interval with only four of them larger than the total Lias average, so this was unlikely to be a significant contributor. The Lilliput Effect is again not significant in this time interval, as those species that exhibit a size decrease into the SSE die out soon after. Body size increase resumed during the Pliensbachian, notably increasing to the *ibex* Zone, and further again at the end of the Stage resulting in an overall increase of 476% relative to those bivalve populations measured in the Westbury Formation.

The underlying causes of the size changes remain elusive, it has been shown that the recovery interval occurred against a background predominantly of oxic-dysoxic conditions but punctuated by periods of anoxia, in shelf locations and yet, unlike the PTME aftermath (Hallam 1991; Dai *et al.* 2018), these conditions did not appear to significantly inhibit recovery. Only during the Pre-*planorbis* interval, when black shales are exceptionally extensive, did diversity decrease, although it promptly rebounded in the subsequent ammonite zone.

Beyond that there is no suggestion that oxygen restriction affected the recovery. The impact of extensive oxygen deficiency on long-term body size trends was minimal. The Blue Lias Formation shows no upward improvement in oxygenation and yet the bivalves in this unit show a long term body size increase. Nonetheless, bivalves from more dysoxic intervals are smaller but there remains a within-lithology and possibly within oxygen regime size increase.

Although the observed size changes most likely reflect improving environments, as suggested by changes in growth lines, no satisfying conclusion could be found. There is no correspondence between size and reconstructed temperatures although data for the latter are often questionable or poorly constrained. As the size patterns are expressed in suspension feeding organisms it is possible that these changes reflect a prolonged interval of improving primary productivity. This is also supported by the lack of size trends seen among deposit feeding bivalves, which are not reliant on suspended food particles.

Recovery from other intervals of extinction (KPg and PTME) require more species level – long-term studies. However those that currently exist suggest that the Brobdingnag Effect is not restricted to the ETE. Other factors, such as decreased prevalence of small disaster forms, may have been more significant in the production of increased average size of communities during recovery.

7.2 Future work

How widespread are the size increases following the ETE?

There is a dearth of stratigraphically well-constrained bivalve measurements from the Lower Jurassic. The limited data available suggest that Lower Jurassic size increase observed here may also have occurred in Germany and France and there is a suggestion that bivalve size increases between the Sinemurian and the Pliensbachian of Argentina (cf. Johnson 1984; Damborenea 1987a; b; 2002). A thorough examination, at the resolution of ammonite zone or finer is required to assess if these putative size trends are global.

Is the Brobdingnag Effect seen in other groups after the ETE?

Gastropods are frequently cited as showing reduced body sizes after mass extinctions. Is this also the case with the ETE? Although no rigorous measurements were taken in this study, the largest gastropods seen during field collections were from *bucklandi*-aged sediments and occurred with the largest *Plagiostoma giganteum* specimens. Other groups that warrant investigation are foraminifera and ostracods. Their high abundances allow for fine resolution and robust size trends to be detected. None of these groups are dependent on suspension feeding and so the apparent absence of any size changes in these groups, alongside the lack of trends seen here in deposit feeding bivalves, would lend support for a primary productivity control on the body size of the bivalves during the Early Jurassic.

How common is the Brobdingnag Effect through geologic time?

Numerous cases are presented here for Brobdingnag size trends during the Early Jurassic, alongside similar reported size changes during the recovery from the PTME. There are of course more extinction events, and many have been associated with the Lilliput Effect. The pace of body size and taxonomic recovery should be investigated for more recovery intervals.

Further growth line analyses

Further analyses of growth line data shown in Chapters 2 and 5 could be undertaken. Data was presented showing how cycles in the spacing of growth increments were recorded in *Plagiostoma giganteum,* however no thorough interpretation of these cycles was given. These data are suitable for Fourier Transform analyses which may allow for detection of lunar or/and annual cycles or growth.

What is the geographic prevalence of the SSE?

The detection of suppressed size during much of the Sinemurian (SSE) requires further investigation, primarily in order to confirm its presence across a wider geographic area and confirm loss of bivalve diversity. Increased sampling from the Dorset, Severn and Hebrides basins across this interval is recommended as well as away from NW Europe.

Constraining Early Jurassic temperature trends

Despite published oxygen isotope curves for much of the British Lias being available, substantial gaps still remain across the extinction interval and records are patchy between the *liasicus* Zone and *semicostatum* Zone. Temperature reconstruction encompassing the Westbury and Lilstock formations is required but, because this interval was deposited in non-marine conditions, oxygen isotopes are an inappropriate proxy, and so an alternative method is required to document this interval, such as Mg/Ca proxies.

References

Dai, X., Song, H., et al. 2018. Rapid biotic rebound during the late Griesbachian indicates heterogeneous recovery patterns after the Permian-Triassic mass extinction. *Geological Society of America Bulletin*, **130**, 2015–2030, https://doi.org/https://doi.org/10.1130/30/B31969.1.

Damborenea, S.E., 1987a. Early Jurassic bivalvia of Argentina. Part 1: stratigraphical introduction and superfamilies Nuculanacea, Arcacea, Mytilacea and Pinnacea. *Palaeontogr. Abteilung A*, **199**, 23–111.

Damborenea, S.E., 1987b. Early Jurassic bivalvia of Argentina. Part 2: superfamilies Pteriacaea, Buchiacea and part of Pectinacea. *Palaeontogr. Abteilung A*, **199**, 113–216.

Damborenea, S.E., 2002. Early Jurassic bivalvia of Argentina. Part 3: superfamilies Monotoidea, Pectinoidea, Plicatuloidea and Dimyoidea. *Palaeontogr. Abteilung A*, **265**, 1–119.

Dommergues, J.-L., Montuire, S. & Neige, P. 2002. Size patterns through time: the case of the Early Jurassic ammonite radiation. *Paleobiology*, **28**, 423–434, https://doi.org/10.1666/0094-8373(2002)028<0423:SPTTTC>2.0.CO;2.

Hallam, A. 1975. Evolutionary size increase and longevity in Jurassic bivalves and ammonites. *Nature*, **258**, 493–496.

Hallam, A. 1991. Why was there a delayed radiation after the end-Palaeozoic extinction? *Historical Biology*, **5**, 257–262, https://doi.org/10.1080/10292389109380405.

Johnson, A., 1984. The palaeobiology of the bivalve families Pectinidae and Propeamussiidae in the Jurassic of Europe. *Zitteliana*, München.

Appendix A

Figures from Chapter 2 rescaled to most recent Hettangian timescale.

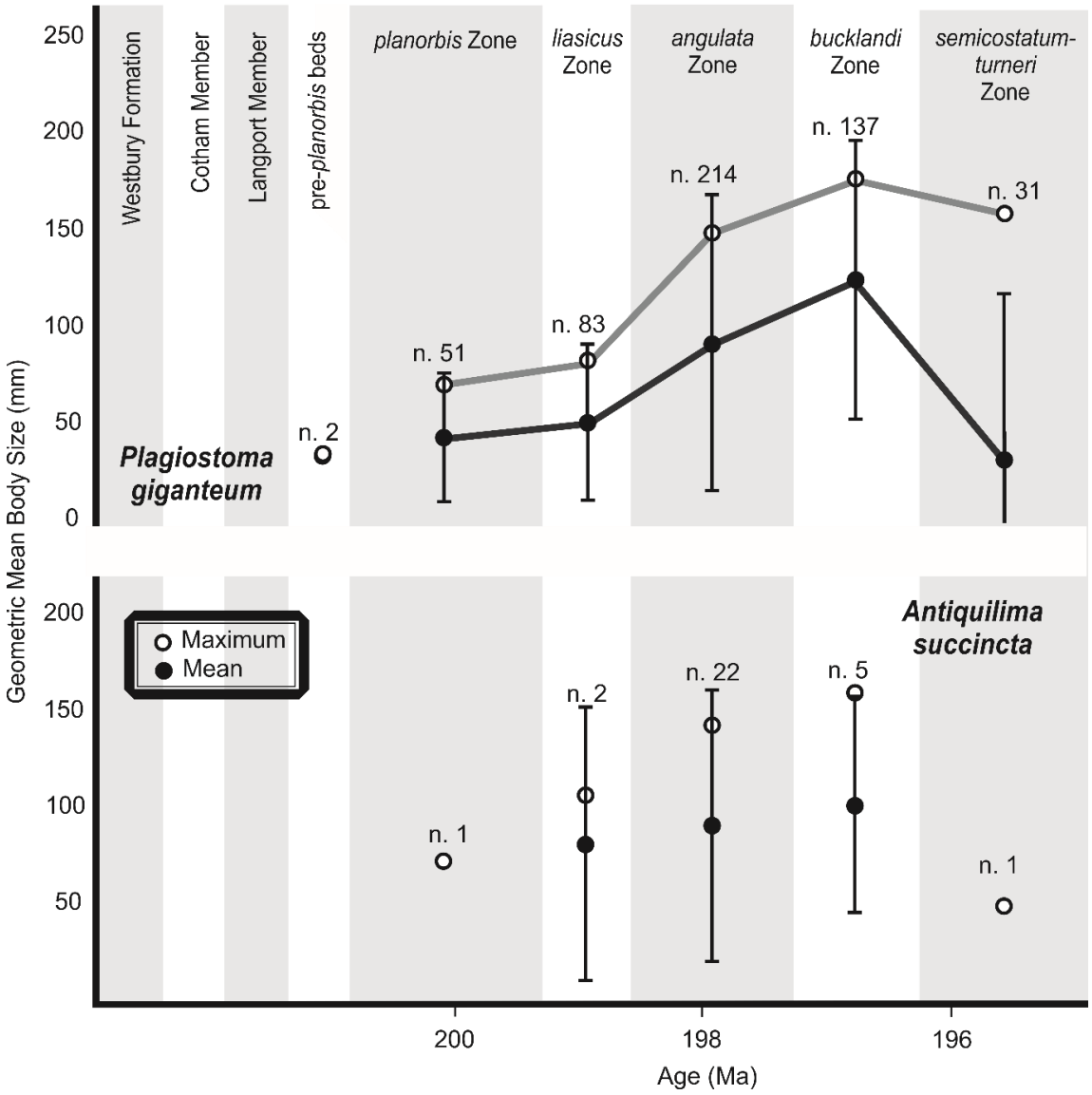

Fig. 2.4 Time-binned variation in the size of *Plagiostoma giganteum* (top) and *Antiquilima succincta* (bottom). Lines connect successive time bins with >10 specimens. Error bars depict 95% confidence intervals. Sample size quoted per time bin.

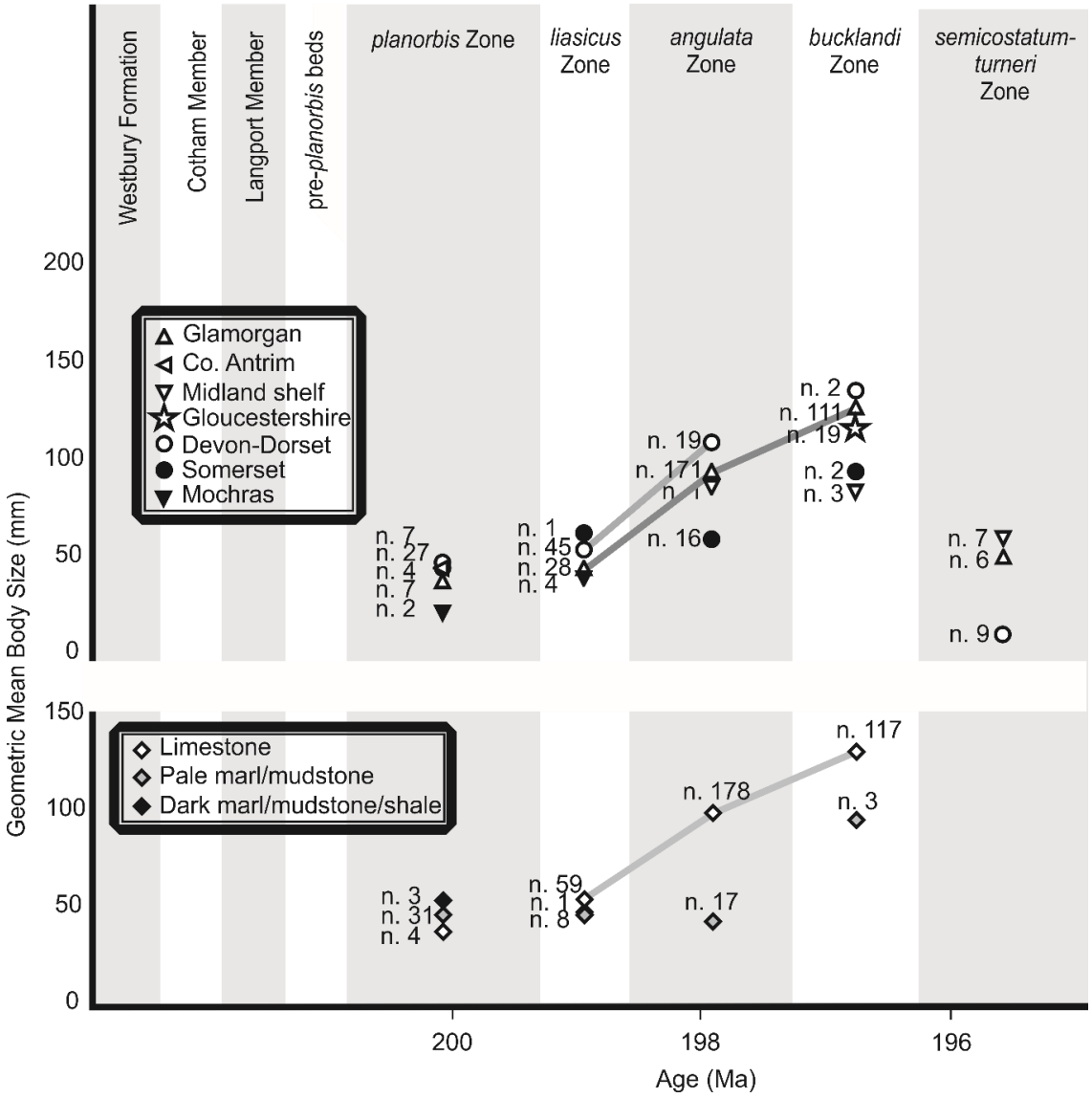

Fig. 2.6 Time-binned variation in the size of *Plagiostoma giganteum* per locality, (top). Variation in size between specimens measured from different oxygenation regimes inferred from host lithology, see methods for details. Lines connect successive time bins with >10 specimens. Sample size quoted per time bin.

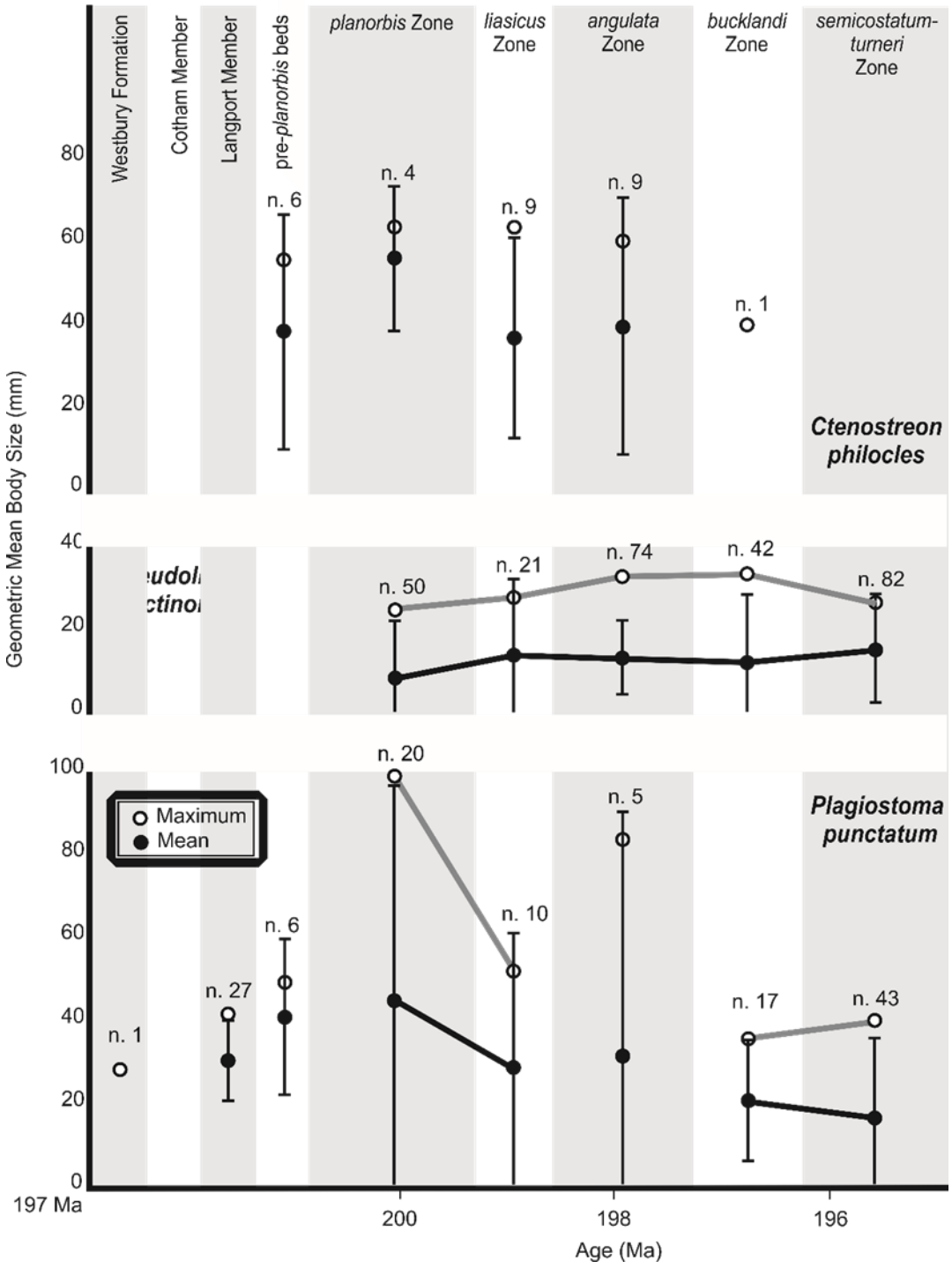

Fig. 2.7. Time-binned variation in the size of *Ctenostreon philocles* (top), *Pseudolimea pectinoides* (middle) and *Plagiostoma punctatum* (bottom). Lines connect successive time bins with >10 specimens. Error bars depict 95% confidence intervals. Sample size quoted per time bin.

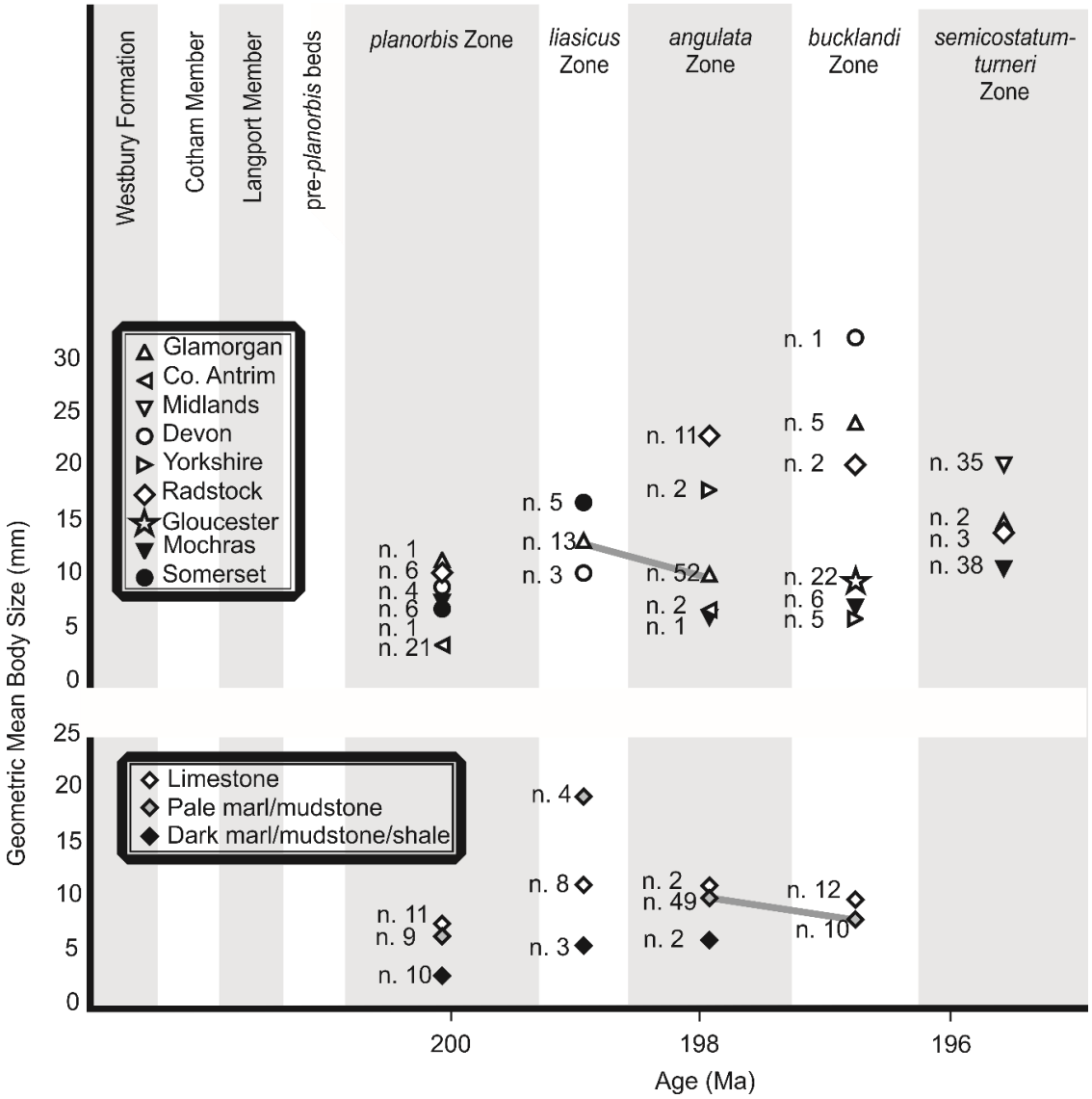

Fig. 2.10. Time-binned variation in the size of *Pseudolimea pectinoides* per locality, (top). Variation in size between specimens from different oxygenation regimes inferred from host lithology, see methods for details. Lines connect successive time bins with >10 specimens. Sample size quoted per time bin.

Appendix B

Bivalve life modes

Species	Ecology	Reference
Entolium lunare	surficial, facultative motile, suspension feeder	Johnson 1984
Pseudopecten equivalvis	surficial, facultative motile, suspension feeder	Ros-Franch et al 2014
Oxytoma (Palmoxytoma) cygnipes	epibyssate, suspension feeder	Ros-Franch et al 2014
'Mytilus'' cloacinus	epibyssate, suspension feeder	Ros-Franch et al 2014
Anningella cf. *faberi*	epibyssate, suspension feeder	Ros-Franch et al 2014
Antiquilima antiquata	epibyssate, suspension feeder	Damborenea and Mancenido, 2005
Antiquilima nodulosa	epibyssate, suspension feeder	Damborenea and Mancenido, 2005
Antiquilima hermanni	epibyssate, suspension feeder	Damborenea and Mancenido, 2005
Antiquilima succincta	epibyssate, suspension feeder	Damborenea and Mancenido, 2005
Camptonectes auritus	epibyssate, suspension feeder	Damborenea and Mancenido, 2005
Camptonectes punctatissimus	epibyssate, suspension feeder	Damborenea and Mancenido, 2005
Camptonectes subulatus	epibyssate, suspension feeder	Damborenea and Mancenido, 2005
Chlamys textoria	epibyssate, suspension feeder	Ros-Franch et al 2014, Johnson 1984
Chlamys valoniensis	epibyssate, suspension feeder	Ros-Franch et al 2014, Johnson 1984
Chlamys lavernockensis	epibyssate, suspension feeder	Ros-Franch et al 2014, Johnson 1984
Chlamys pollux	epibyssate, suspension feeder	Ros-Franch et al 2014, Johnson 1984
Ctenostreon philocles	epibyssate, suspension feeder	Ros-Franch et al 2014
Eopecten angularis	epibyssate, suspension feeder	Ros-Franch et al 2014, also capable of cementation see Hodges 1987
Eopecten velatus	epibyssate, suspension feeder	Ros-Franch et al 2014, also capable of cementation see Hodges 1987
Parainoceramus ventricosus	epibyssate, suspension feeder	Ros-Franch et al 2014
Plagiostoma giganteum	epibyssate, suspension feeder	Ros-Franch et al 2014
Plagiostoma punctatum	epibyssate, suspension feeder	Ros-Franch et al 2014
Pseudolimea acuticostata	epibyssate, suspension feeder	Damborenea and Mancenido, 2005
Pseudolimea dentata	epibyssate, suspension feeder	Damborenea and Mancenido, 2005
Pseudolimea pectinoides	epibyssate, suspension feeder	Damborenea and Mancenido, 2005
Pteria carixensis	epibyssate, suspension feeder	Ros-Franch et al 2014
Rhaetavicula contorta	epibyssate, suspension feeder	Ros-Franch et al 2014
Semuridia dorsetensis	epibyssate, suspension feeder	Ros-Franch et al 2014

Oxytoma fallax	epibyssate, suspension feeder	Ros-Franch et al 2014
Oxytoma inequivalvis	epibyssate, suspension feeder	Ros-Franch et al 2014
Meleagrinella sp.	epibyssate, suspension feeder	Ros-Franch et al 2014
Oxytoma sinemuriensis	epibyssate, suspension feeder	Ros-Franch et al 2014
Grammatodon sp.	epibyssate, suspension feeder	Ros-Franch et al 2014
Grammatodon (Cosemetodon) hettangiensis	epibyssate, suspension feeder	Ros-Franch et al 2014
Grammatodon (Cosmetodon) buckmani	epibyssate, suspension feeder	Ros-Franch et al 2014
Grammatodon (Grammatodon) intermedius	epibyssate, suspension feeder	Ros-Franch et al 2014
Grammatodon (Grammatodon) pullus	epibyssate, suspension feeder	Ros-Franch et al 2014
Parallelodon sp.	epibyssate, suspension feeder	Ros-Franch et al 2014
Catella trapezium	epibyssate, suspension feeder	Ros-Franch et al 2014
Liostrea hisingeri	surficial, cemented, suspension feeder	Ros-Franch et al 2014
Liostrea irregularis	surficial, cemented, suspension feeder	Ros-Franch et al 2014
Actinostreon haidingeriana	surficial, cemented, suspension feeder	Ros-Franch et al 2014
Nanogyra imbricatoradiata	surficial, cemented, suspension feeder	Wignall 1990
Atreta intusstriata	surficial, cemented, suspension feeder	Hodges 1991
Harpax spinosa	surficial, cemented, suspension feeder	Ros-Franch et al 2014
Placunopsis alpina	surficial, cemented, suspension feeder	Ros-Franch et al 2014
Placunopsis sp.	surficial, cemented, suspension feeder	Ros-Franch et al 2014
Plicatula hettangiensis	surficial, cemented, suspension feeder	Damborenea and Mancenido, 2005
Terquemia difformis	surficial, cemented, suspension feeder	Ros-Franch et al 2014
Hippopodium ponderosum	endobyssate, suspension feeder	Ros-Franch et al 2014
Hippopodium tuffleyensis	endobyssate, suspension feeder	Ros-Franch et al 2014
Hippopodium ovale	endobyssate, suspension feeder	Ros-Franch et al 2014
Myoconcha (Modiolina) decorata	endobyssate, suspension feeder	Ros-Franch et al 2014
Myoconcha (Myoconcha) psilonoti	endobyssate, suspension feeder	Ros-Franch et al 2014
'Permophorus' elongatus	endobyssate, suspension feeder	Ros-Franch et al 2014
Cuneigervillia infraliasina	endobyssate, suspension feeder	Ros-Franch et al 2014
Gervillia aerosa	endobyssate, suspension feeder	Ros-Franch et al 2014
Gervillia laevis	endobyssate, suspension feeder	Ros-Franch et al 2014
Gervillia rheinhardti	endobyssate, suspension feeder	Ros-Franch et al 2014
Gervillia hagenowi	endobyssate, suspension feeder	Ros-Franch et al 2014
Gervillella ornata	endobyssate, suspension feeder	Ros-Franch et al 2014
Gervillella praecursor	endobyssate, suspension feeder	Ros-Franch et al 2014
Gervillella sp.	endobyssate, suspension feeder	Ros-Franch et al 2014
Gervillia (Cultriopsis) acuminata	endobyssate, suspension feeder	Ros-Franch et al 2014
Inoperna lilliputensis	endobyssate, suspension feeder	Ros-Franch et al 2014
Inoperna sp.	endobyssate, suspension feeder	Ros-Franch et al 2014
Modiolus hillanus	endobyssate, suspension feeder	Ros-Franch et al 2014
Modiolus bipartus	endobyssate, suspension feeder	Ros-Franch et al 2014

Modiolus cuncata	endobyssate, suspension feeder	Ros-Franch et al 2014
Modiolus minimus	endobyssate, suspension feeder	Ros-Franch et al 2014
Modiolus ornata	endobyssate, suspension feeder	Ros-Franch et al 2014
Modiolus pumila	endobyssate, suspension feeder	Ros-Franch et al 2014
Modiolus scalprum	endobyssate, suspension feeder	Ros-Franch et al 2014
Modiolus sp.	endobyssate, suspension feeder	Ros-Franch et al 2014
Modiolus ventricosus	endobyssate, suspension feeder	Ros-Franch et al 2014
'Modiolus' sodburiensis	endobyssate, suspension feeder	Ros-Franch et al 2014
Modiolus subcancellata	endobyssate, suspension feeder	Ros-Franch et al 2014
Pinna folium	endobyssate, suspension feeder	Ros-Franch et al 2014
Pinna hartmanni	endobyssate, suspension feeder	Ros-Franch et al 2014
Pinna semistriata	endobyssate, suspension feeder	Ros-Franch et al 2014
Pinna similis	endobyssate, suspension feeder	Ros-Franch et al 2014
Pinna sp.	endobyssate, suspension feeder	Ros-Franch et al 2014
Pinna trigonata	endobyssate, suspension feeder	Ros-Franch et al 2014
Isocyprina ewaldi	shallow infaunal, suspension feeder	Ros-Franch et al 2014
Isocyprina (Eotrapezium) concentricum	shallow infaunal, suspension feeder	Ros-Franch et al 2014
Isocyprina (Eotrapezium) depressus	shallow infaunal, suspension feeder	Ros-Franch et al 2014
Isocyprina (Eotrapezium) germari	shallow infaunal, suspension feeder	Ros-Franch et al 2014
Isocyprina (Eotrapezium) cucculatum	shallow infaunal, suspension feeder	Ros-Franch et al 2014
Lyriomyophoria postera	shallow infaunal, suspension feeder	Ros-Franch et al., 2014, see autoecology for *Elegantinia*
Cardinia ovalis	shallow infaunal, suspension feeder	Ros-Franch et al 2014, Hodges 2018
Cardinia concinna	shallow infaunal, suspension feeder	Ros-Franch et al 2014, Hodges 2018
Cardinia listeri	shallow infaunal, suspension feeder	Ros-Franch et al 2014, Hodges 2018
Cardinia nilssoni	shallow infaunal, suspension feeder	Ros-Franch et al 2014, Hodges 2018
Cardinia regularis	shallow infaunal, suspension feeder	Ros-Franch et al 2014, Hodges 2018
Cardinia sp.(SC2)	shallow infaunal, suspension feeder	Ros-Franch et al 2014, Hodges 2018
Ceratomya petricosa	shallow infaunal, suspension feeder	Ros-Franch et al 2014
Idonearca sp.	shallow infaunal, suspension feeder	Ros-Franch et al 2014
Mactromya cardioideum	shallow infaunal, suspension feeder	Delvene 2000
Neocrassina gueuxii	shallow infaunal, suspension feeder	Ros-Franch et al 2014, Hodges 2018
'Astarte' platymorpha	shallow infaunal, suspension feeder	Ros-Franch et al 2014, Hodges 2018
Palaeocardita cf. *austriaca*	shallow infaunal, suspension feeder	Ros-Franch et al 2014
Palaeocardita imbricatoradiata	shallow infaunal, suspension feeder	Ros-Franch et al 2014
Pteromya crowcombeia	shallow infaunal, suspension feeder	Ros-Franch et al 2014
Pteromya langportensis	shallow infaunal, suspension feeder	Ros-Franch et al 2014

Pteromya tatei	shallow infaunal, suspension feeder	Ros-Franch et al 2014
Tutcheria heberti	shallow infaunal, suspension feeder	Ros-Franch et al 2014
Tutcheria cloacina	shallow infaunal, suspension feeder	Ros-Franch et al 2014
Protocardia oxynoti	shallow infaunal, suspension feeder	Ros-Franch et al 2014
Protocardia philippianum	shallow infaunal, suspension feeder	Ros-Franch et al 2014
Protocardia rhaetica	shallow infaunal, suspension feeder	Ros-Franch et al 2014
Protocardia truncata	shallow infaunal, suspension feeder	Ros-Franch et al 2014
Luciniola limbata	shallow infaunal, suspension feeder with chemosymbionts	Ros-Franch et al 2014
Sphaeriola subglobosa	shallow infaunal, suspension feeder with chemosymbionts	Ros-Franch et al 2014
Dacryomya gaveyi	shallow infaunal, deposit feeder	Wignall 1990
Dacryomya heberti	shallow infaunal, deposit feeder	Wignall 1990
Palaeoneilo elliptica	shallow infaunal, deposit feeder	Ros-Franch et al 2014
Palaeoneilo galatea	shallow infaunal, deposit feeder	Ros-Franch et al 2014
Palaeonucula navis	shallow infaunal, deposit feeder	Ros-Franch et al 2014
Rollieria bronni	shallow infaunal, deposit feeder	Ros-Franch et al 2014
Ryderia doris	shallow infaunal, deposit feeder	Ros-Franch et al 2014
Ryderia texturata	shallow infaunal, deposit feeder	Ros-Franch et al 2014
Ryderia titei	shallow infaunal, deposit feeder	Ros-Franch et al 2014
Arcomya arcacea	deep infaunal, suspension feeder	No ref.
Arcomya concinna	deep infaunal, suspension feeder	No ref.
Arcomya sp.	deep infaunal, suspension feeder	No ref.
'Arcomya' vetusta	deep infaunal, suspension feeder	No ref.
Cercomya praecursor	deep infaunal, suspension feeder	Ros-Franch et al 2014
Goniomya hybrida	deep infaunal, suspension feeder	Ros-Franch et al 2014
Goniomya rhombifera	deep infaunal, suspension feeder	Ros-Franch et al 2014
Gresslya galathea	deep infaunal, suspension feeder	Ros-Franch et al 2014
Gresslya intermedia	deep infaunal, suspension feeder	Ros-Franch et al 2014
Gresslya sp.	deep infaunal, suspension feeder	Ros-Franch et al 2014
Homomya ventricosa	deep infaunal, suspension feeder	Ros-Franch et al 2014
Pholadomya 'ovalis'	deep infaunal, suspension feeder	Ros-Franch et al 2014
Pholadomya ambigua	deep infaunal, suspension feeder	Ros-Franch et al 2014
Pholadomya glabra	deep infaunal, suspension feeder	Ros-Franch et al 2014
Platymyoidea morrisi	deep infaunal, suspension feeder	Hodges 1987
Pleuromya ?striato-granulata	deep infaunal, suspension feeder	Ros-Franch et al 2014

Pleuromya costata	deep infaunal, suspension feeder	Ros-Franch et al 2014
Pleuromya crassa	deep infaunal, suspension feeder	Ros-Franch et al 2014
Pleuromya liasina	deep infaunal, suspension feeder	Ros-Franch et al 2014

References

Damborenea, S. & Manceñido, M.O. 2005. Biofacies analysis of Hettangian-Sinemurian bivalve/brachiopod associations from the Neuquén Basin (Argentina). *Geologica Acta*, **3**, 163–178, https://doi.org/10.1344/105.000001405.

Hodges, P. 1987. *Lower Lias (Lower Jurassic) Bivlavia from South Wales and Adjacent Areas*. Unpublished PhD thesis, University College of Swansea, Swansea.

Hodges, P. 1991. The relationship of the Mesozoic bivalve Atreta to the Dimyidae. *Palaeontology*, **34**, 963–970.

Hodges, P. 2000. *The Early Jurassic Bivalvia from the Hettangian and Lower Sinemurian of South-West Britain Part 1*. London, Monograph of the Palaeontographical Society.

Hodges, P. 2018. *The Early Jurassic Bivalvia from the Hettangian and Lower Sinemurian of South-West Britain Part 2*. London, Monograph of the Palaeontographical Society, https://doi.org/10.1080/02693445.2017.11963960.

Johnson, A. 1984. *The Palaeobiology of the Bivalve Families Pectinidae and Propeamussiidae in the Jurassic of Europe*. München, Zitteliana.

Ros-Franch, S., Márquez-aliaga, A. & Damborenea, S.E. 2014. Comprehensive database on Induan (Lower Triassic) to Sinemurian (Lower Jurassic) marine bivalve genera and their paleobiogeographic record. *Paleontological Contributions*, **8**, 1–219, https://doi.org/10.17161/PC.1808.13433.

Wignall, P.B. 1990. Benthic palaeocology of the Late Jurassic Kimmeridge Clay of England. *Special papers in palaeontology*, **43**.

Appendix C

Species abundance counts and summary of framboid analysis per sample horizon

PINHAY BAY (DEVON)											
	Langport	**Pre-planorbis Beds**			***planorbis* Zone**						
Species	**LR1**	**PH15 (H1)**	**PH1a-b**	**PH4**	**PH16**	**LR2**	**PH2**	**LR3**	**PH17SB**	**PH18**	**PH3**
Modiolus minimus	2				5						
Liostrea spp.		5	29	20					2	3	3
Pinna hartmanni							12				5
Chlamys textoria								4		2	
Plagiostoma giganteum							2	1	1	18	2
Chlamys valoniensis									1		
Pseudolimea pectinoides										3	
Cardinia ovalis										1	
Plagiostoma punctatum											
Camptonectes subulatus											
Anningella cf. *faberi*											
Gryphaea arcuata											
Pseudolimea dentata											
Gresslya sp.											
Indeterminate (shallow infaunal) bivalve											
Species richness (n.)	1	1	1	1	1	0	2	2	3	5	3
Mean framboid diameter (µm)		4.52		8.19		4.94	10.45	7.38			12.55
Standard deviation of framboid diameter (µm)		1.54		2.48		1.54	4.13	3.56			5.70
Fossil abundance (shale/mudstones/marls)	2	5			5	0		5	4	27	
Fossil abundance (limestone)			43	20			14				10

PINHAY BAY (DEVON)									
	***liasicus* Zone**								
Species	**PH19**	**PH6**	**PH20**	**PH5**	**PH21**	**LR4**	**PH7**	**PH8**	**PH9**
Modiolus minimus					2				
Liostrea spp.			4	4	2		14	16	
Pinna hartmanni									
Chlamys textoria									
Plagiostoma giganteum	1	7	1	25			9	5	1
Chlamys valoniensis									
Pseudolimea pectinoides			2					1	
Cardinia ovalis									
Plagiostoma punctatum			2						
Camptonectes subulatus									
Anningella cf. *faberi*									
Gryphaea arcuata									
Pseudolimea dentata									
Gresslya sp.									
Indeterminate (shallow infaunal) bivalve									
Species richness (n.)	1	1	4	2	2	0	2	3	1
Mean framboid diameter (µm)				9.09			10.13	10.78	9.26
Standard deviation of framboid diameter (µm)				3.38			5.90	3.31	3.25
Fossil abundance (shale/mudstones/marls)	1		9		4	0			
Fossil abundance (limestone)		7		29			23	22	1

PINHAY BAY (DEVON)												
	***angulata* Zone**								***bucklandi* Zone**			
Species	**PH22**	**PH10**	**PH23**	**PH11**	**PH12**	**PH24**	**LR5**	**PH14**	**LR6**	**PH25**	**PH13**	**LR7**
Modiolus minimus												
Liostrea spp.	11					7						
Pinna hartmanni												
Chlamys textoria												
Plagiostoma giganteum		6		4	4		1	6			2	
Chlamys valoniensis	1											
Pseudolimea pectinoides												
Cardinia ovalis												
Plagiostoma punctatum	1											
Camptonectes subulatus	3					3						
Anningella cf. *faberi*			44									
Gryphaea arcuata								4				
Pseudolimea dentata						1						
Gresslya sp.											1	
Indeterminate (shallow infaunal) bivalve											4	
Species richness (n.)	4	1	1	1	1	3	1	2	0	0	3	0
Mean framboid diameter (µm)				9.54				5.73	5.54		10.97	4.29
Standard deviation of framboid diameter (µm)				2.95				2.01	1.92		5.70	1.29
Fossil abundance (shale/mudstones/marls)	16		44			11	1	10	0	0		0
Fossil abundance (limestone)		6		4	4						7	

ST AUDRIE'S BAY (SOMERSET)									
	Langport	**Pre-*planorbis* Beds**							
Species	**SAB34**	**SAB1/33**	**SAB35**	**SAB58**	**SAB36**	**SAB2**	**SAB3**	**SAB4**	**SAB57**
Modiolus minimus					1	1			
Liostrea spp.		3			6	4	10		
Protocardia philippianum					2				
Anningella cf. *faberi*									
Plagiostoma giganteum									
Chlamys textoria									
Pseudolimea pectinoides									
Rollieria bronni									
Palaeonucula navis									
Cardinia ovalis									
Camptonectes subulatus									
Indeterminate bivalve sp. A				1					
Species richness (n.)	0	1	0	1	3	2	1	0	0
Mean framboid diameter (µm)		6	4.94	7.06	7.06	6.22		5.9	7.62
Standard deviation of framboid diameter (µm)		2.71	2.19	3.55	3.92	3.01		2.73	2.74
Fossil abundance (shale/mudstones/marls)		3	0		9	5	10	0	
Fossil abundance (limestone)				1					0

ST AUDRIE'S BAY (SOMERSET)													
	***planorbis* Zone**												
Species	**SAB5/37**	**SAB56**	**SAB19**	**SAB7**	**SAB12**	**SAB55**	**SAB8**	**SAB54**	**SAB53**	**SAB13/38**	**SAB9**	**SAB14/43**	**SAB52**
Modiolus minimus													
Liostrea spp.													
Protocardia philippianum													
Anningella cf. *faberi*	6		9	13									
Plagiostoma giganteum							1						
Chlamys textoria										1			
Pseudolimea pectinoides												1	
Rollieria bronni													
Palaeonucula navis													
Cardinia ovalis													
Camptonectes subulatus													
Indeterminate bivalve sp. A													
Species richness (n.)	1	0	1	1	0	0	1	0	0	1	0	1	0
Mean framboid diameter (µm)	4.58	9.96	4.27		6.08	6.99	6.77	10.79	6.12	4.61			5.38
Standard deviation of framboid diameter (µm)	1.59	6.05	1.44		2.09	3.12	4.37	4.95	1.83	1.24			1.67
Fossil abundance (shale/mudstones/marls)	6		9	13	0		1			1	0	1	
Fossil abundance (limestone)		0				0		0	0				0

ST AUDRIE'S BAY (SOMERSET)												
	***liasicus* Zone**											
Species	**SAB15/39**	**SAB40/10**	**SAB11**	**SAB16/41**	**SAB6/42**	**SAB17**	**SAB18**	**SAB20**	**SAB21**	**SAB22**	**SAB49**	**SAB23**
Modiolus minimus												
Liostrea spp.												
Protocardia philippianum	1											
Anningella cf. *faberi*			1									8
Plagiostoma giganteum				1								
Chlamys textoria												
Pseudolimea pectinoides												
Rollieria bronni		5										
Palaeonucula navis		1										
Cardinia ovalis				1	5							
Camptonectes subulatus												
Indeterminate bivalve sp. A												
Species richness (n.)	1	2	1	2	1	0	0	0	0	0	0	1
Mean framboid diameter (µm)	8.79	5.93		6.64		4.72		9.86	4.19		4.56	4.13
Standard deviation of framboid diameter (µm)	6.27	2.86		3.23		2.18		7.66	1.49		1.48	1.37
Fossil abundance (shale/mudstones/marls)	1	6	1	2	5	0	0	0	0	0	0	8
Fossil abundance (limestone)												

ST AUDRIE'S BAY (SOMERSET)									
	***liasicus* Zone**								
Species	**SAB27/48**	**SAB25**	**SAB26**	**SAB24/47**	**SAB46**	**SAB51**	**SAB44**	**SAB45**	**SAB50**
Modiolus minimus									
Liostrea spp.									
Protocardia philippianum									
Anningella cf. *faberi*									
Plagiostoma giganteum									
Chlamys textoria									
Pseudolimea pectinoides		1		4					
Rollieria bronni				2					
Palaeonucula navis									
Cardinia ovalis							1		
Camptonectes subulatus							1		
Indeterminate bivalve sp. A									
Species richness (n.)	0	1	0	2	0	0	2	0	0
Mean framboid diameter (µm)	4.63		4.72	6.62	5.94	7.09	8.18		10.88
Standard deviation of framboid diameter (µm)	2.06		1.48	4.37	3.17	2.52	2.49		3.57
Fossil abundance (shale/mudstones/marls)	0	1	0	6	0		2	0	
Fossil abundance (limestone)						0			0

EAST QUANTOXHEAD (SOMERSET)																		
	***angulata* Zone**																	
Species	**Q45**	**Q75**	**Q76**	**Q43**	**Q44**	**Q41**	**Q42**	**Q77**	**Q14**	**Q15**	**Q16**	**Q17/57**	**Q78**	**Q50**	**Q18**	**Q13**	**Q12**	**Q11**
Oxytoma inequivalvis																		
Liostrea spp.					1				1									
Plagiostoma giganteum				3	2				8									
Palaeonucula navis																		
Anningella cf. *faberi*																		
Antiquilima succincta					1													
Cardinia ovalis					2													
Entolium lunare					1													
Cardinia sp.																		
Modiolus minimus	13																	
Pinna similis																		
Gryphaea arcuata																		
Mactromya cardioideum																		
Neocrassina gueuxii																		
Indeterminate bivalve sp. B																		
Juvenile bivalve form C					1													
Juvenile bivalve form A																		
Juvenile bivalve form B																		
Species richness (n.)	1	0	0	1	6	0	0	0	2	0	0	0	0	0	0	0	0	0
Mean framboid diameter (µm)	7.19	12.65	6.08		8.51	4.68	7.51	6.53		5.01	7.5	9.18	8.44	5.26	6.39	13.23		
Standard deviation of framboid diameter (µm)	4.34	5.03	1.97		4.69	1.48	3.03	2.77		2.49	3.36	3.32	3.40	1.85	2.51	14.19		
Fossil abundance (shale/mudstones/marls)	13				8	0	0		9	0	0	0		0	0	0		
Fossil abundance (limestone)		0	0	3				0					0				0	0

EAST QUANTOXHEAD (SOMERSET)													
	***angulata* Zone**												
Species	**Q49**	**Q10**	**Q79/9**	**Q7**	**Q8**	**Q6/47**	**Q3**	**Q4/46**	**Q5**	**Q2**	**Q1/Q80**	**Q53**	**Q39**
Oxytoma inequivalvis											10		
Liostrea spp.		1											
Plagiostoma giganteum													
Palaeonucula navis													
Anningella cf. *faberi*													
Antiquilima succincta													
Cardinia ovalis													
Entolium lunare													
Cardinia sp.													
Modiolus minimus													
Pinna similis													
Gryphaea arcuata			3										
Mactromya cardioideum													
Neocrassina gueuxii													
Indeterminate bivalve sp. B						2							
Juvenile bivalve form C													
Juvenile bivalve form A													
Juvenile bivalve form B													
Species richness (n.)	0	1	1	0	0	1	0	0	0	0	1	0	0
Mean framboid diameter (µm)		3.82	10.1	5.18	5.53			4.67	7		8.76		4.71
Standard deviation of framboid diameter (µm)		1.13	3.63	1.87	2.78			1.61	2.87		3.07		1.57
Fossil abundance (shale/mudstones/marls)	0	1		0	0	2		0	0			0	0
Fossil abundance (limestone)			3				0			0	10		

EAST QUANTOXHEAD (SOMERSET)															
	***bucklandi* Zone**														
Species	**Q40**	**Q81**	**Q20**	**Q38**	**Q19**	**Q52**	**Q37**	**Q36**	**Q34**	**Q54**	**Q35**	**Q82**	**Q55**	**Q33**	**Q29**
Oxytoma inequivalvis															
Liostrea spp.															
Plagiostoma giganteum															
Palaeonucula navis														1	
Anningella cf. *faberi*				3											
Antiquilima succincta															
Cardinia ovalis															
Entolium lunare															
Cardinia sp.															
Modiolus minimus															
Pinna similis		1													
Gryphaea arcuata															
Mactromya cardioideum															
Neocrassina gueuxii															
Indeterminate bivalve sp. B										3					
Juvenile bivalve form C															
Juvenile bivalve form A										1			1		
Juvenile bivalve form B										1					
Species richness (n.)	0	1	0	1	0	0	0	0	0	3	0	0	1	1	0
Mean framboid diameter (µm)		8.99		3.95				5.59			5.76	8.54			
Standard deviation of framboid diameter (µm)		3.97		1.49				2.97			2.04	3.03			
Fossil abundance (shale/mudstones/marls)	0		0	3		0	0	0	0	5	0		1	1	0
Fossil abundance (limestone)		1			0							0			

EAST QUANTOXHEAD (SOMERSET)															
	***bucklandi* Zone**														
Species	**Q28**	**Q30**	**Q31**	**Q32**	**Q83**	**Q56**	**Q27**	**Q21**	**Q24**	**Q25**	**Q23**	**Q57**	**Q58**	**Q59**	**Q84**
Oxytoma inequivalvis															
Liostrea spp.						1							1		
Plagiostoma giganteum															
Palaeonucula navis															
Anningella cf. *faberi*		1				1									
Antiquilima succincta															
Cardinia ovalis															
Entolium lunare															
Cardinia sp.													2		
Modiolus minimus															
Pinna similis															
Gryphaea arcuata						1							1		
Mactromya cardioideum													1		
Neocrassina gueuxii															
Indeterminate bivalve sp. B													1		
Juvenile bivalve form C						4									
Juvenile bivalve form A						5									
Juvenile bivalve form B						5									
Species richness (n.)	0	1	0	0	0	6	0	0	0	0	0	0	5	0	0
Mean framboid diameter (µm)			6.23		8.48						5.62		7.52	4.17	9.6
Standard deviation of framboid diameter (µm)			3.00		3.31						1.57		3.93	1.52	5.15
Fossil abundance (shale/mudstones/marls)	0	1	0	0		17	0		0	0	0		6	0	
Fossil abundance (limestone)					0			0				0			0

EAST QUANTOXHEAD (SOMERSET)															
Species	**Q62**	**Q63**	**Q64**	**Q65**	**Q66**	**Q67**	**Q68**	**Q69**	**Q70**	**Q71**	**Q61**	**Q60**	**Q72**	**Q73**	**Q74**
Oxytoma inequivalvis															
Liostrea spp.															
Plagiostoma giganteum									1						
Palaeonucula navis															
Anningella cf. *faberi*															1
Antiquilima succincta	1														
Cardinia ovalis															
Entolium lunare															1
Cardinia sp.															
Modiolus minimus															
Pinna similis															
Gryphaea arcuata															
Mactromya cardioideum				3											
Neocrassina gueuxii				2											
Indeterminate bivalve sp. B						1		1			1				
Juvenile bivalve form C															
Juvenile bivalve form A	2				3										
Juvenile bivalve form B															
Species richness (n.)	2	0	0	2	1	1	0	1	1	0	1	0	0	0	2
Mean framboid diameter (µm)	5.83	5.26	4.49				4.44	5.78	9.61	6.01			10.4	5.25	
Standard deviation of framboid diameter (µm)	3.27	2.89	1.96				1.67	2.81	5.07	2.16			4.79	2.48	
Fossil abundance (shale/mudstones/marls)	3	0	0	5	3	1	0	1	1	0	1	0	0	0	2
Fossil abundance (limestone)															

LAVERNOCK POINT (GLAMORGAN)								
	Langport Mbr		**Pre-*planorbis* Beds**					
Species	**LP21**	**LP9**	**LP8**	**LP10**	**LP20b**	**LP20a**	**LP11**	**LP7**
Anningella cf. *faberi*								
Camptonectes subulatus								
Atreta intusstriata	7	6						
Modiolus sp. (juvenile)		4						
Cardinia ovalis		1						
Chlamys valoniensis								
Chlamys textoria								
Grammatodon hettangiensis		1						
Liostrea spp.		3	3	1		31		
Modiolus minimus			1					
Modiolus hillanus		11		1				
Modiolus ventricosus								
Plagiostoma giganteum								1
Plagiostoma punctatum								
Myoconcha psilonoti		2						
'Plicatula' hettangiensis		1						
Protocardia philippianum		1						
Indeterminate bivalve sp. A							2	
Pinna similis								
Indeterminate bivalve sp. B								
Species richness (n.)	1	9	2	2	0	1	1	1
Mean framboid diameter (µm)	10.39	11.01	6.68	4.39	8.97	9.18	6.65	7.13
Standard deviation of framboid diameter (µm)	3.83	11.18	3.72	1.34	7.4	4.89	3.86	3.89
Fossil abundance (shale/mudstones/marls)		30	4	2	0		2	1
Fossil abundance (limestone)	7					31		

LAVERNOCK POINT (GLAMORGAN)															
	***planorbis* Zone**														
Species	**LP12**	**LP19**	**LP13**	**LP18b**	**LP18a**	**LP6**	**LP17**	**LP5**	**LP16**	**LP15b**	**LP15a**	**LP4**	**LP14c**	**LP14b**	**LP14a**
Anningella cf. *faberi*	1		1												
Camptonectes subulatus	3														6
Atreta intusstriata															
Modiolus sp. (juvenile)	4		3		17					2					
Cardinia ovalis															
Chlamys valoniensis								2							
Chlamys textoria	1							2							
Grammatodon hettangiensis															
Liostrea spp.					1										
Modiolus minimus	4		4	2		1									
Modiolus hillanus												1			
Modiolus ventricosus												1			
Plagiostoma giganteum								1			2				
Plagiostoma punctatum															
Myoconcha psilonoti															
'Plicatula' hettangiensis															
Protocardia philippianum															
Indeterminate bivalve sp. A	6														
Pinna similis															
Indeterminate bivalve sp. B												1			
Species richness (n.)	6	0	3	1	2	1	0	3	0	1	1	3	0	0	1
Mean framboid diameter (µm)	5.47	9.13	6.61	8.19	7.67	6.46	12.31	5.99	10.87	6.18	6.89	6.66	8.61	8.32	9.31
Standard deviation of framboid diameter (µm)	2.2	4.42	2.97	2.87	3.39	2.8	6.52	2.36	10.21	2.39	2.44	4.83	3.35	3.29	4.06
Fossil abundance (shale/mudstones/marls)	19		8	2	18	1		5		2		3		0	
Fossil abundance (limestone)		0					0		0		2		0		6

LAVERNOCK POINT (GLAMORGAN)			
	***liasicus* Zone**		
Species	**LP3**	**LP2**	**LP1**
Anningella cf*. faberi*			
Camptonectes subulatus			
Atreta intusstriata			
Modiolus sp. (juvenile)			
Cardinia ovalis			
Chlamys valoniensis			
Chlamys textoria		1	
Grammatodon hettangiensis			
Liostrea spp.		2	
Modiolus minimus			
Modiolus hillanus			
Modiolus ventricosus		3	
Plagiostoma giganteum	4	3	
Plagiostoma punctatum		2	
Myoconcha psilonoti			
'Plicatula' hettangiensis			
Protocardia philippianum			
Indeterminate bivalve sp. A			
Pinna similis	1		
Indeterminate bivalve sp. B			
Species richness (n.)	2	5	0
Mean framboid diameter (µm)	8.86	8.06	6.64
Standard deviation of framboid diameter (µm)	10.57	5.04	4.52
Fossil abundance (shale/mudstones/marls)	5	11	0
Fossil abundance (limestone)			

NASH POINT (GLAMORGAN)															
	***angulata* Zone**														
Species	**NP 9**	**NP10**	**NP11**	**NP 7**	**NP12**	**NP13**	**NP14**	**NP15**	**NP16**	**NP17**	**NP 8**	**NP18**	**NP19**	**NP20**	**NP21b**
Gresslya galathea	1		2	1				3				1			
Plagiostoma giganteum		1				4		4	1	30	1	1	28		1
Liostrea spp.			1				1	2		3					3
Camptonectes subulatus			1		1		1		1			2			5
'Plicatula' hettangiensis				1						1					
Pleuromya liasina						1									
Placunopsis sp.							1				1				1
Pseudolimea pectinoides									2				2		1
Entolium lunare									1						
Antiquilima succincta										2		1	1		
Ctenostreon philocles													5		
Pinna similis													3		
Modiolus ventricosus															
Mactromya cardioideum															
Neocrassina gueuxii															
Gryphaea arcuata															
Atreta intusstriata															
Chlamys textoria															
Cardinia ovalis															
Species richness (n.)	1	1	3	2	1	2	3	3	4	4	2	4	5	0	5
Mean framboid diameter (µm)	8.89	10.20	9.02		7.98	7.48	7.73	10.37	6.22	8.70		14.66	6.34	7.98	5.38
Standard deviation of framboid diameter (µm)	2.76	10.01	4.45		3.84	2.12	2.37	7.69	1.61	5.71		5.38	3.85	2.98	1.66
Fossil abundance (shale/mudstones/marls)	1	1	4		1		3	9	5			5	39	0	11
Fossil abundance (limestone)				2		5				36	2				

NASH POINT (GLAMORGAN)														
	***angulata* Zone**													
Species	**NP21a**	**NP21d**	**NP21c**	**NP22**	**NP23**	**NP24**	**NP25**	**NP26**	**NP40**	**NP41**	**NP42**	**NP43**	**NP44**	**NP45**
Gresslya galathea	1							1						
Plagiostoma giganteum		2		29			26					4	8	15
Liostrea spp.	6				2						1		2	
Camptonectes subulatus					2	3								
'Plicatula' hettangiensis														
Pleuromya liasina														
Placunopsis sp.														
Pseudolimea pectinoides		45												
Entolium lunare	1													
Antiquilima succincta				13										
Ctenostreon philocles					2									
Pinna similis		2												
Modiolus ventricosus		5						1						
Mactromya cardioideum							2	1						
Neocrassina gueuxii											1			
Gryphaea arcuata												5	7	
Atreta intusstriata														
Chlamys textoria														
Cardinia ovalis														
Species richness (n.)	3	4	0	2	3	1	2	3	0	0	2	2	3	1
Mean framboid diameter (µm)	7.03	7.28	7.94	7.55	8.76	10.99	8.03	9.63	8.00	9.51	7.59	9.34	7.80	
Standard deviation of framboid diameter (µm)	3.5	4.44	4.94	2.13	2.62	5.12	2.2	7.08	3.01	5.63	3.36	3	3.99	
Fossil abundance (shale/mudstones/marls)		54			6	3		3	0	0	2			
Fossil abundance (limestone)	8		0	42			28					9	17	15

NASH POINT (GLAMORGAN)																
	***bucklandi* Zone**															
Species	**NP46**	**NP47**	**NP39**	**NP38**	**NP37**	**NP36**	**NP34**	**NP35**	**NP32**	**NP33**	**NP31**	**NP30**	**NP29**	**NP28b**	**NP28a**	**NP27**
Gresslya galathea																
Plagiostoma giganteum	1		27			26		3	6		28					4
Liostrea spp.	2		5			14				1					1	
Camptonectes subulatus										1						
'Plicatula' hettangiensis																
Pleuromya liasina																
Placunopsis sp.																
Pseudolimea pectinoides			1													
Entolium lunare			1			1							1			
Antiquilima succincta						1										
Ctenostreon philocles						1										
Pinna similis								9	4		33		30			30
Modiolus ventricosus																
Mactromya cardioideum				1												
Neocrassina gueuxii																
Gryphaea arcuata			10										4			
Atreta intusstriata	1					1										
Chlamys textoria											1					
Cardinia ovalis													1			
Species richness (n.)	3	0	5	1	0	6	0	2	2	2	3	0	4	0	1	2
Mean framboid diameter (µm)	7.87	7.65	8.20	8.16	10.98	7.63	9.90			8.42	8.50	7.78	6.31	8.16	7.97	7.46
Standard deviation of framboid diameter (µm)	3.61	3.28	3.48	3.24	7.06	3.68	5.63			3.11	4.23	4.27	3.02	4.61	3.35	8.58
Fossil abundance (shale/mudstones/marls)		0			0		0			2		0		0	1	
Fossil abundance (limestone)	4		44	1		44		12	10		62		36			34

Appendix D

NMW collection list

Available at: https://doi.org/10.1016/j.palaeo.2019.05.011.

Appendix E

Compendium of bivalve body size data spanning the uppermost Triassic through the Lower Jurassic

Available at: https://data.mendeley.com/datasets/pnfsxzfsb4/draft?a=3aa8cbd1-ca98-4beeb03c-cddd31828b90

Appendix F

Diagnostic features to differentiate species of Lower Jurassic bivalves

A concise series of taxonomic notes in tabulated form are here provided. These describe key morphological features used to distinguish between two or more species belonging to the same genus. In some instances only brief notes are provided for congeneric species to validate the choices made within this work to either synonymise or split taxa. The rest follow widely accepted definitions of the species.

Entolium

E. *liasianum* (Nyst)

E. lunare (Roemer)

E. liasianum	***E. lunare***
Equivalved	As in E. liasianum
Inequilateral (weakly)	Equilateral
suborbicular	subovate
H ~L	H > L juvenile L > H adult
Anterior auricle slightly larger than posterior.	
UA obtuse	UA obtuse, increasing at a decreasing rate.
RV auricles extend dorsally of umbo.	RV auricles extend dorsally of umbo.
LV auricles flush with hinge.	LV auricles meet hinge at obtuse angle, disc at acute.
Anterior margin of anterior auricle slightly convex.	
Posterior margin of posterior auricle straight, meeting hinge at obtuse angle.	RV; posterior meets disc at acute angle, anterior meets disc c. 90°.
Concaved antero-dorsal margin, straight postero-dorsal margin.	Dorsal margins weakly concaved.
Small byssal notch in RV sometimes present.	Small byssal notch in juvenile form.

Hodges (1987) reports *E. liasianum* to occur in the Hettangian and Sinemurian of Britain (Pre-*planorbis-semicostatum, ?jamesoni*), with specimens from the upper Pliensbachian being regarded as a belonging to a different species owing to a larger umbonal angle (UA) and overall larger size compared to those encountered in the Lower Lias. These are typically assigned to *E*. *lunare* (see Johnson 1984; Little 1996), this being because Roemer's type specimen has an UA of 150°, far exceeding that expected for *E. liasianum*. Johnson (1984, 1985) shows that the UA increases with increasing size of the shell, a condition found also during this study. As Pliensbachian specimens of Entolium attain a greater shell size than those of the Hettangian and Sinemurian, a wider UA is to be expected. Further to this all complete specimens measured of *Entolium* occupy the same morphospace on UA:H/L plot (Fig. AF.1). Regarding the species name to assign, *E. lunare* (Roemer 1839) takes precedence over *E. liasianum* (Nyst 1843).

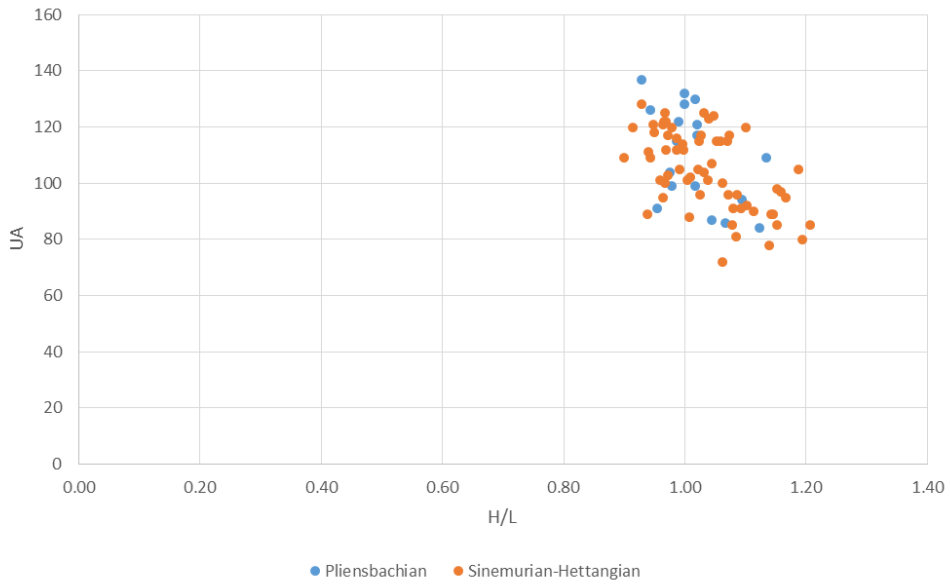

Fig. AF.1 Umbonal angle (UA) in degrees against shell height (H) to length (L) ratios. Hettangian/Sinemurian specimens originally attributed to *Entolium liasianum* and Pliensbachian specimens to *Entolium lunare* showing complete overlap in morphospace.

Camptonectes

C. subulatus (Münster)

C. auritus (Schlotheim)

C. punctatissimus (Quenstedt)

C. jamoignensis (Terquem & Piette)

C. subulatus	*C. auritus*	*C. punctatissimus*
H > L (slightly).	H > L in juveniles, becoming H <L in adults.	H > L (slightly).
Auricles show divaricating and co-marginal striae.	Posterior auricle – divaricating striae Anterior auricle – co-marginal striae.	Radial ribs on anterior auricle of LV.
Anterior auricles meet hinge at c. 90°. Anterior auricle of LV meets disc at acute angles, on RV meets disc at 90° or more.	Anterior auricle of RV meets hinge and disc at c. 90°. Anterior auricle of LV meets disc at acute angle, hinge at obtuse angle.	Anterior auricle RV straight anterior margin, meets hinge at 90°.
Ornament of fine divaricate ribs (c. 40) punctate by intersection of co-marginal striae. Central region of shell smooth.	Ornamented by a variable number of fine divaricate striae, increasing by intercalation and punctate at intersection of co-marginal striae. Across all of valve.	c. 55 slightly irregularly spaced radial ribs, co-marginal punctae occupying interspaces only.

Camptonectes jamoignensis (not shown in table) was considered by Hodges (1987) to occur in the British Lias, this species was regarded a synonym of *C. subulatus* by Johnson (1984). Johnson's classification is here supported as specimens identified in museum collections as *C. jamoignensis* differ from *C. subulatus* by being larger and exhibiting a greater UA. As UA increases with size it is likely that the *C. jamoignensis* are just individuals of *C. subulatus* that survived to a greater age. This is demonstrated by the fact that specimens of *C. jamoignensis* housed within the National Museum of Wales plot as a continuum of GMBS:UA with *C. subulatus* (Fig. AF.2).

C. punctatissimus may also be, as Johnson (1984) suggests, a synonym of *C. subulatus.* The figured type material in Quenstedt (1858) clearly shows ribs with co-marginal punctae occupying the interspaces, this feature is also well shown in Hodges (1987). But Johnson regards this as a mere artefact of preservation. On a similar note, the distinguishing features of *C. auritus* and *C. subulatus*

refer to the restriction of the ornament to the shell margins in the latter species. This was not alluded to in Münster's original description and the type specimen has not been located. It is possible that this feature is also an artefact of preservation. As so few specimens of *Camptonectes* retain their full ornament it is perhaps best to regard assign species with caution, and instead look to generic body size trends.

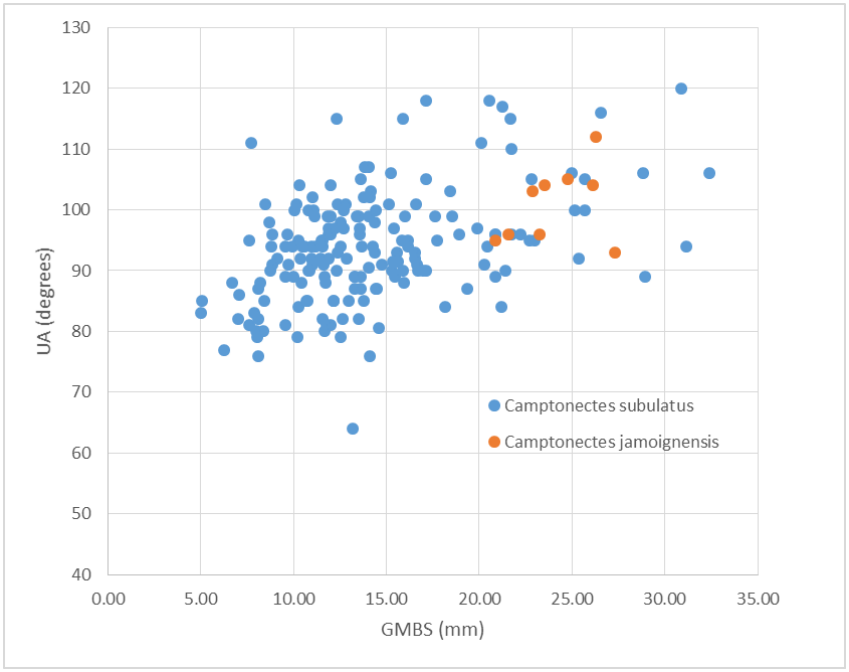

Fig. AF. 2 Changes in umbonal angles (UA) in degrees with body size for *Camptonectes subulatus* and *C. jamoignensis*.

Chlamys

C. valoniensis (Defrance)

C. pollux (d'Orbigny)

C. textoria (Schlotheim)

C. lavernockensis Hodges

C. milvus (Cox)

C. valoniensis	***C. pollux***	***C. textoria***	***C. lavernockensis***	***C. milvus***
RV flattened.	As in *C. valoniensis*.	As in *C. valoniensis.*	Valves of approx. equal inflation.	RV unknown.
H > L (juvenile), L > H (adult).	H ~ L	H > L	H > L (slightly).	
Posterior auricle meets hinge at obtuse, disc at acute.	As in *C. valoniensis.*	As in C. valoniensis.	As in *C. valoniensis*.	Posterior margin of posterior auricle concave, producing pointed auricle.
Anterior margin of anterior auricle convex (RV).	As in *C. valoniensis.*	Anterior auricle anterior margin truncated (RV).	As in C*. textoria.*	Anterior margin of anterior auricle concave, producing pointed sharp auricle.
36-45 radial ribs (for L=20) broadly of two sizes, ribs can also increase via bifurcation.	Lower rib count than *C. valoniensis*, primary ribs develop spines, secondary ribs lack spines (~7 primary, larger ribs).	17-98 radial plicae. Reticulate, ribs can also increase via bifurcation, ribs of variable size (generally 2 orders) crossed by regular sharp commarginal threads.	Each valve bears approx. 70 radial ribs, slightly sinuous, interspaces of variable width, only develop in the lower half of valve. Ribs crossed by regular commarginal threads.	Narrow, widely spaced ribs, lacks concentric threads (except near umbo).

The distinct ornament in *C. lavernockensis* may be the result of preferential abrasion on the oldest region of the shell in *C*. *textoria*, however the smooth region is equally developed on both valves.

Eopecten

E. velatus (Goldfuss)

E. angularis (Tate)

E. velatus	***E. angularis***
Typically, L>H	H>L
UA variable	UA < 90°
Equilateral-inequilateral	Inequilateral
Very large notch with ctenolium	RV similar to Chlamys but with elongated anterior auricle with large byssal notch
All auricles meet hinge at c. 90°	All auricles meet hinge at c. 90°or obtuse
Ornament on LV differentiated into costae and striae in all but the largest specimens	LV bears 100+ sinuous radial ribs increasing by implantation of ribs in the interspaces (rib count includes 1st and 2nd order of ribbing). RV ornament less pronounced
	Auricles bear radial ribs
	Ribs bear small spines (diagnostic)

Plagiostoma

P. giganteum Sowerby

P. punctatum Sowerby

P. giganteum	*P. punctatum*
Posterior auricle more pronounced with depressed lunule	Auricle lengths are equal but anterior slightly smaller, posterior auricle bears radial ribs
Slightly sinuous radial ribs less well developed in centre of shell	c. 100 radial ribs on whole of shell surface and commarginal striae, weathering to form rows of punctae increasing in density towards umbo
Fine fibrous divaricating striae	
Cardinal area subtriangular	Cardinal area curved parallel to dorsal margin

Antiquilima

- *A. antiquata* (J. Sowerby)
- *A. succincta* (Schlotheim)
- *A. hermanni* (Voltz)
- *A. nodulosa* (Terquem)

A. antiquata	*A. succincta*	*A. hermanni*	*A. nodulosa*
Anterior auricle smaller than posterior	Pronounced anterior auricle.	Pronounced anterior auricle.	Anterior auricle smaller than posterior
c. 100 radial ribs. Rounded cross section.	> 65 primary ribs, numerous interspace ribs of various widths.	Juvenile smooth with deeply incised grooves, developing into broad, flat ribs in adults, c. 50 ribs, no interspace ribs	> 70 radial ribs and secondary ribs. Nodes on ribs.

Pseudolimea

P. eryx (d'Orbigny)

P. pectinoides (Sowerby)

P. dentata (Terquem)

P. hettangiensis (Terquem)

P. acuticostata (Münster)

P. eryx	*P. pectinoides*	*P. dentata*	*P. acuticostata*	*P. hettangiensis*
Rounded umbones salient above hinge	Flattened umbones	Median umbones, salient above hinge	As in *P. dentata*	As in *P. eryx*
20 primary ribs, obtuse, sharp crests in cross section	15-20 radial ribs, obtuse, sharp crests in cross section, may appear rounded if specimen is abraded.	20 radial ribs, rounded cross section.	14-15 sharp triangular ribs	16 sharp crested ribs.
Interspaces variable width on individual specimens.	Interspaces variable width with thread like ribs in interspaces.	Evenly spaced interspaces lacking interspace ribs.	Interspaces flat to slightly concave Several fine interspace threads, these thinner ribs cover the anterior and posterior and ears.	Thin, narrow secondary ribs in interspaces.

Distinction between *P. pectinoides*, *P. eryx* and *P. hettangiensis* is quite impractical, Cox (1944) synonymised *P. hettangiensis* into *P. eryx* and remarked how is was often confused with *P. pectinoides.* All three of these species of *Psuedolimea* should be regarded as *P. pectinoides*, with *P. dentata* being distinct owing to the lack of interspaced ribs*. P. acuticostata* may also be a synonym of *P. pectinoides*, however further work is required to test this.

Oxytoma

O. (*O*.) *inequivalvis* (J. Sowerby)

O. (*O*.) *sinemuriensis* (d'Orbigny)

O. (*O*.) *fallax* (Pflücker)

O. (*Palmoxytoma*) *cygnipes* (Young & Bird)

O. (O.) inequivalvis	***O. (O.) sinemuriensis***	***O. (O.) fallax***	***O. (P.) cygnipes***
Posterior auricle flattened, elongate and pointed.	Posterior auricle flattened obtusely angled at hinge line, not pointed.	Posterior auricle flattened.	Same as in *O*. *inequivalvis.*
Posterior auricle bears pronounced auricle sinus.	Lacks pronounced auricle sinus.	Posterior auricle not separated by sinus.	Posterior auricle bears pronounced sinus.
c. 12 primary ribs, curving away from umbo.	c. 24 primary ribs, less pronounced than in *O. inequivalvis.*	24-26 radial riblets.	4-8 primary radial ribs extent beyond margin of shell, divaricate slightly, ribs bear 2-3 commarginal rows of spines, primary rib count increases with size.
Secondary ribs originate some way from umbo	Numerous fine interspace striae.	Appears to lack secondary ribs.	Fine radial thread in interspaces.
RV smaller, flattened, suborbicular, umbones small, not salient above hinge.	RV unknown.	RV Less convex than LV.	RV condition same as for *O. inequivalvis.*

Grammatodon (Grammatodon)

G. (G.) insons Melville

G. (G.) intermedius (Simpson)

G. (G.) pullus (Terquem)

G. (G.) insons	*G. (G.) intermedius*	*G. (G.) pullus*
Sub-quadrate - ovoid	Same as for *G. insons*	Trapezoidal, oblique, H = 60% L
Moderately inflated	Same as for *G. insons*	Well inflated
Faint radial ribs, most pronounced on anterior margin, concentric growth lines	Same as for *G. insons*	>30 radial fine ribs and co-marginal striae.
Posterior margin rounded and extends ventrally beyond hinge plate	Same as for *G. insons*	Posterior margin straight, meets dorsal margin at oblique angle, anterior margin rounded meeting dorsal at c. 90°, ventral straight-weakly curved
No sulcus	Same as for *G. insons*	Median sulcus running from centre of umbo to ventral margin in each valve.

Melville (1956) distinguished his species of *Grammatodon* from *G. intermedius* on the basis of the latter being smaller, shorter and more quadrate in outline, as well as bearing stronger and more regular growth lines, and radial ribs of a more consistent strength. Additionally Melville remarked that *G. intermedius* has shorter and more oblique anterior hinge teeth than seen in *G. insons*. These distinctions are minimal and separation of the two species in juveniles may be difficult.

Grammatodon (Cosmetodon)

G. (*C.*) *hettangiensis* (Terquem)

G. (*C.*) *buckmanni* (Richardson)

G. (C.) hettangiensis	*G. (C.) buckmanni*
Posterior margin rounded.	Posterior margin pointed.
Posterior meets hinge at 110°.	Posterior meets hinge at 130°.
Ornament or radial ribs appears more pronounced than in *G. (C.) buckmanni*.	Numerous faint radial ribs.

Terquem's type is identical to *G.* (*C.*) *buckmanni* with the exception of those points outlined above.

Liostrea

L. hisingeri (Nilsson)

L. irregularis (Münster)

L. hisingeri	*L. irregularis*
Both valves flat.	LV greater inflation than RV.
Often comma-shaped outline.	Irregular outline.
Often free-lying/cemented to substrate.	Usually attached to other shells.

Considerable morphological overlap between the two species. *L. hisingeri* is the primary faunal component of the Ostrea Beds of the Pre-*planorbis* beds.

Plicatula

P. spinosa (J. Sowerby)

P. hettangiensis (Terquem)

P. spinosa	*P. hettangiensis*
Sub-elliptical, slightly elongated, H > L	Irregularly triangular
Medium attachment area relative to shell size	Small attachment area relative to shell size
Both valves bear irregular, partly interrupted radial ribs. Commarginal ornament at irregular intervals, scale-like.	Small spines at intersection of roughly commarginal growth halts and radial rugosities
	Spines increase in size towards margin becoming tabular
	Secondary rugosities may be present between primary ones

Damborenea (2002) provides argument for placement of *P. spinosa* into the genus *Harpax* based on details in the hinge and convexity of the right valve (attached valve), which in *Harpax* the RV is less convex than the LV, a condition reversed in *Plicatula.* Terquem (1885) described *P. hettangiensis* as “la valve supérieure est plane” the upper valve is flat, this suggests this may remain in *Plicatula*.

Hippopodium

H. tuffleyensis Palmer

H. ovale Moore

H. ponderosum J. Sowerby

H. tuffleyensis	*H. ovale*	*H. ponderosum*
H/L = c. 0.65	H/L = c. 50	H/L = c. 0.70
Antero-dorsal margin slopes steeply down from umbo.	Dorsal margin seems more-or-less flat.	Similar to *H. ovale*.
Antero-ventral lobe extends anteriorly of beaks.	As in *H. tuffleyensis*	Antero-ventral lobe does not project beyond beaks, producing a fairly straight antero-dorsal margin

Myoconcha

M. (*Myoconcha*) *psilonoti* Quenstedt

M. (*Modiolina*) *decorata* (Münster)

M. (Myoconcha) psilonoti	***M. (Modiolina) decorate***
Posterior-ventral margin gently convex	Dorsal and ventral margins parallel
Small terminal beaks, slightly incurved	Small beaks, not terminal
12 weak radial ribs cover much of shell (bar the antero-ventral region) and commarginal growth halts	8 radial ribs in dorsal region only.
Internally LV short but curved tooth below beaks	Thin curved tooth near anterior margin
Anterior adductor scar subtrigonal behind myomorphic buttress	Suboval adductor, pronounced myomorphic buttress

M. (Modiolina) decorata is differentiated from *M*. (*Myoconcha*) *psilonoti* by the lower rib count, greater inflation, and straighter valves. Ribs are also developed over a narrower region. Appears similar to *Inoperna* but has more ribs and lacks commarginal folds.

Modiolus

M. minimus (J. Sowerby)

M. hillanus (J. Sowerby)

M. ventricosus (Roemer)

M. scalprum (J. Sowerby)

M. minimus	*M. hillanus*	*M. ventricosus*	*M. scalprum*
Inequilateral, oblique.	As in *M. minimus.*	Extremely inequilateral.	As in *M. ventricosus.*
Sharpest curvature for length of shell.	Lower curvature for length.	Still lower curvature for length.	Almost straight, lowest curvature of the four species.
Pronounced growth halts.	Pronounced growth halts.	Numerous fine concentric ridges, no pronounced growth halts.	Numerous fine concentric ridges, some specimens feature pronounced growth halts.
		Anterior well rounded, umbones nearly terminal, not distinct.	Anterior less rounded antero-dorsal margin concaved umbones more distinct.

Main distinction between the four key species of *Modiolus* encountered is decreasing curvature of shell from *M. minimus* to *M. scalprum*, as measured by an increasing L to oblique length (l) and decreased H/L (Fig. AF 3). This evolutionary trend is perhaps an example of neotony, as shell curvature increases during growth of the individual. Additional species encountered are: *M. bipartitus*, *M. cuncata*, *M. ornata*, *M. pumila*, *and M. subcancellata* however in most instances insufficient material was examined to permit a detailed assessment of their taxonomy.

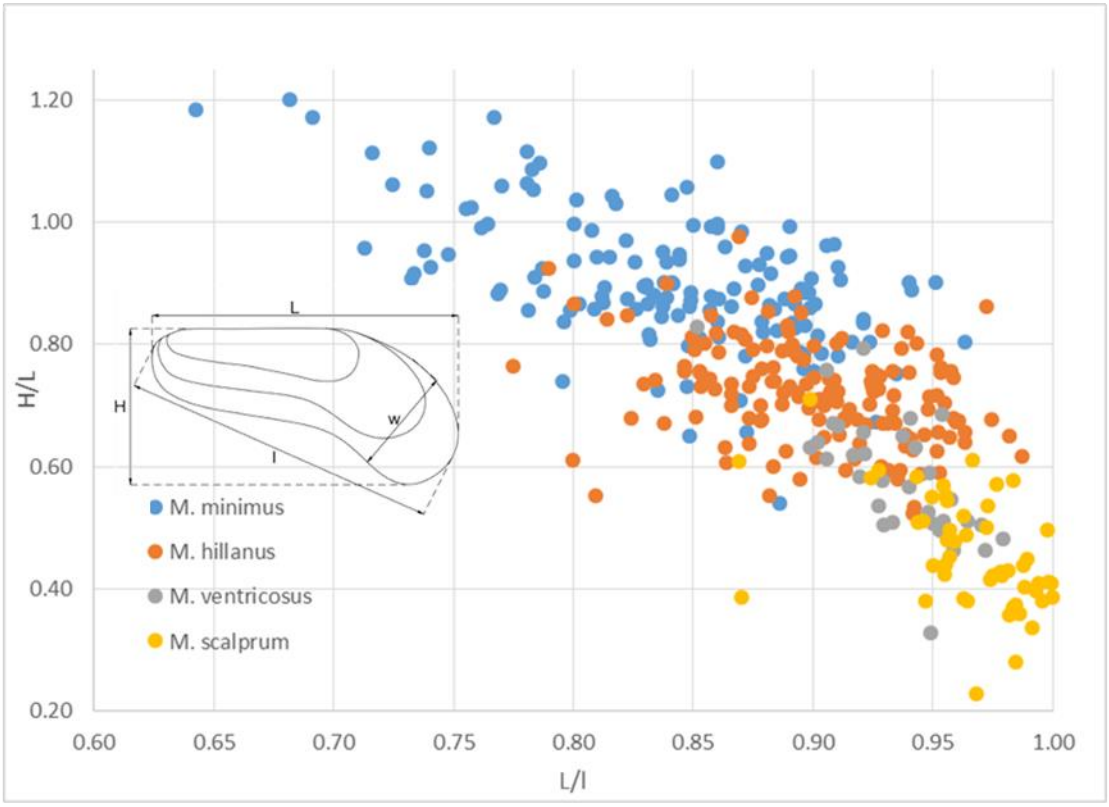

Fig. AF.3 Morphospace plot for species of *Modiolus*, showing variation in curvature of shell as measured by H/L and L/l (oblique length, see inset).

Gervillia

G. hagenowi (Dunker)

G. laevis Buckman

G. aerosa (Simpson)

G. rheinhardti (Terquem & Piette)

These four species were recorded erroneously in Appendix E as belonging to the genus *Cunigervillia.* Only *C. infraliasina* (Quenstedt) of the bakevelliidae specimens herein measured can be assigned to that genus.

Distinction between these is not clear and further work is required to refine their taxonomy, as such no table of distinguishing features is herein presented. In the current standing *G. hagenowi* is the most reclined, more elongate with greater obliquity. *G. aerosa* and *G. rheinhardti* are similar in that they are less reclined, having a greater H:L ratio. Distinction of *G. rheinhardti* from *G. aerosa* appears difficult although a slight anterior rounded projection (not a wing) may prove useful for discrimination. *G. laevis* appears as an intermediate form between the very elongate *G. hagenowi* and the shorter *G. aerosa.*

Gervillella

G. praecursor (Quenstedt)

G. ornata (Moore)

G. praecursor	*G. ornata*
Ornamented by commarginal growth lines and undulations.	c. 7 prominent radial ribs crossed by commarginal growth lines and undulations.

The genus of species *praecursor* seems in question, Marquez-Aliaga *et al*. (2010) placed this into the sub-genus *bakevelloides* of the genus *Bakevillia*. Equally generic assignment for *G. ornata* is questionable (Ivimey-Cook *et a*l. 1999).

'Permophorus'

P. elongatus (Moore)

P. angulatus (Moore)

P. elongatus	*P. angulatus*
Two poorly to moderately well-developed lines extending from umbones to posterior-ventral margin, may divide shell into 3 elongate triangular sections.	Three acute, slightly curved ribs extending from umbo to posterior margin

Pinna

P. hartmanni Zeiten

P. similis Chapuis & Dewalque

P. trigonata Martin

P. folium Young & Bird

P. semistriata Terquem

P. similis	*P. trigonata*	*P. folium*	*P. hartmanni*	*P. semistriata*
UA 34-40°	UA 60-70°	UA 20-30°		UA c. 30°
Ventral: 7 or more weak radial ribs, strong commarginal folds sweeping towards anterior.	Ventral: Irregularly spaced commarginal folds sweep towards ventral margin.	Ventral: Half of ventral surface covered by fine straight to slightly sinuous ribs, ventral-most half only bears commarginal undulations, more pronounced than commarginal ribs on dorsal surface.	Ventral: Symmetrical arrangement of commarginal folds and radial ribs.	Appears to lack radial ornament, bearing only concentric folds.
Dorsal: 10 or more strong radial ribs, weaker commarginal ornament.	Dorsal: Faint radial ribs near dorsal sometimes visible.	Dorsal: Fine, straight to slightly sinuous radial ribs across dorsal, rib count increases with size, commarginal ribs across whole of shell.	Dorsal: See above.	
Cross-section diamond shaped	As in *P. similis*?	As in *P. similis*.	Cross-section, two convex valves, not diamond.	As in *P. similis*.

Isocyprina (Eotrapezium)

I. (*E*.) *cucullatum* (Goldfuss)

I. (*E*.) *concentricum* (Moore)

I. (*E*.) *ewaldi* (Bornemann)

I. (*E*.) *depressum* (Moore)

I. (*E*.) *germari* (Dunker)

I. (E.) cucullatum	*I. (E.) concentricum*	*I. (E.) ewaldi*	*I. (E.) depressum*	*I. (E.) germari*
L>H	As in *I*. (*E*.) *cucullatum.*	Higher H/L ratio than *I*. (*E*.) *concentricum.*	L>H	As in *I.* (*E*.) *depressum*.
Posterior truncated, Posterior margin more-or-less straight.	Posterior appears truncated.	As in *I*. (*E*.) *concentricum.*	Posterior sloped but not as truncated in appearance.	Posterior rounded, not truncated.
Strong carina.	Moderately developed carina.	Strong carina.	Carina weakly developed.	No distinct carina.
Umbo 1/3 shell length from anterior.	Variable positioning of the umbo, typically around 1/3 from anterior.	As in *I*. (*E*.) *concentricum.*	Umbones slightly anterior of mid-length of valve.	Beaks placed near anterior.
Antero-dorsal and postero-dorsal margins concaved.	Antero-dorsal region concaved.	As in *I*. (*E*.) *concentricum.*	Antero-dorsal region concaved, postero-dorsal convex.	Sloped postero-dorsal margin, anterior well rounded, antero-dorsal concaved sharply.
Smooth or concentric striations.	Strong concentric ornament, meets posterior margin at c. 90°.	Smooth with only fine commarginal striae, growth lines curve back towards umbo.	Concentric ornamentation.	Concentric ornamentation.
Triangular.	Triangular to elongate.	Triangular.	Elongate-ovoid.	Elongate, almost triangular.

I. (*E*.) *concentricum*, *I*. (*E*.) *ewaldi*, *I*. (*E*.) *depressum*, *I*. (*E*.) *germari* are mostly specimens from Westbury Formation with no internal features known, all of these species are dubious but as no new information is gained no change is supposed.

Cardinia

C. listeri (J. Sowerby)

C. ovalis (Stutchbury)

C. nilssoni (Koch & Dunker)

C. regularis (Terquem)

C. concinna (J. Sowerby)

C. listeri	*C. ovalis*	*C. nilssoni*	*C. regularis*	*C. concinna*
Deltoid.	Sub-circular to sub ovate.	Cuneiform to elongate oval.	Ovoid.	Oblong-ovate.
H < L	H < L	2H ~ L	H < L	3H ~ L
Posterior margin wedge-shaped.	Posterior margin rounded.	Posterior margin tending towards wedge-shape.	Posterior rounded.	Posterior margin tending towards wedge-shape.
Postero-dorsal margin gently arched.		Postero-dorsal area often slightly flattened.		Postero-dorsal gently curved.
Umbones at ~1/4 L anteriorly.	Umbones in anterior 1/3.	Small umbones, placed ~1/5 L from anterior.	Umbones in anterior 1/3.	Umbones in anterior 1/6.
Strong commarginal imbrications appearing as growth halts.	Commarginal imbrications with finer commarginal striae in interspaces.	Well defined commarginal imbrications, less well-defined commarginal striae in interspaces.	Strong commarginal imbrications appearing as growth halts.	Commarginal imbrications less well developed.
	Cardinal area much narrower than in *C. listeri.*			

C. regularis may be a juvenile synonym for *C. ovalis*, these two being inseparable in appearance, differing only in the former being typically smaller in size. The morphology of *C. ovalis* is highly variable however grades into *C. listeri*, with various transitionary forms from the upper *angulata* Zone (Hodges 2018).

Tutcheria

T. cloacina (Quenstedt)

T. heberti (Terquem)

T. cloacina	*T. heberti*
Sub-orbicular, inflated	Sub-ovate, inflated
c. 30 broad rounded or flat-topped radial ribs, reduced interspaces.	35 radial ribs with rounded cross section, no interspaces.

It is somewhat unclear on how to distinguish between these two species. Specimens of *Tutcheria* from the Westbury Formation are typically assigned to *T. cloacina*, whereas those from the Sinemurian to *T. heberti*. Brauns (1871) considered them to be the same species, however insufficient well-preserved material was here examined to determine if this is so.

Pteromya

P. langportensis (Richardson & Tutcher)

P. tatei (Richardson & Tutcher)

P. crowcombeia Moore

P. crowcombeia	*P. tatei*	*P. langportensis*
Elongate, oval.	As in *P. crowcombeia.*	Not very elongate, greater relative height of the three species.
Posterior ridge present in LV, not present in RV.	Wide umbonal carina.	No posterior ridge on internal mould nor distinct postero-dorsal angle.
Area posterior to ridge is flattened appearing as an obtuse wedge on posterior of shell.	Postero-dorsal region lacks commarginal ribs.	
Variable strength of commarginal ribs.	Commarginal ribs fade in strength towards ventral margin.	Internal moulds suggest commarginal ornament.

Protocardia

P. rhaetica (Merian)

P. truncata (J. de C. Sowerby)

P. philippanum (Dunker)

P. oxynoti (Quenstedt)

P. truncata	***P. philippianum***	***P. rhaetica***	***P. oxynoti***
Radial ribs extend anteriorly of carina, 4-6 of the ribs are anterior of the ridge, about half of the total. Radial ribs become weaker towards posterior, narrow interspaces.	Radial ribs confined to region posterior to carina, 5-7 ribs.	10-15 ribs on posterior.	2-3 ribs situated anterior of the ridge.
Moderately inflated	Moderately inflated	Less inflated	Moderately inflated
Umbonal ridge extends from umbo to postero-ventral corner.	Weak umbonal ridge	Lacks carina	Weaker umbonal ridge than in *P. truncata.*
Posterior margin straight to weakly convex.	Posterior weakly convex, not as truncate as in *P. truncata*.	Posterior and anterior rounded.	Posterior margin straight to weakly convex.

Ryderia

R. doris (d'Orbigny)

R. texturata (Terqeum & Piette)

R. titei (Moore)

R. doris	***R. texturata***
Fine commarginal striae only.	Commarginal ornament on anterior part of shell disappears posteriorly giving way to an undulose vertical ornament extending along the rostrum.

R. titei, ornament consists of commarginal striae, suggesting this is a synonym of *R. doris* (see Ivimey-Cool *et al*. 1999).

Palaeoneilo

P. elliptica (Goldfuss)

P. galatea (d'Orbigny)

P. elliptica	***P. galatea***
Pointed posterior margin.	Blunt rounded posterior margin.
Postero-dorsal margin sloped.	Postero-dorsal margin almost straight, weakly concaved.
Ventral margin convex.	Ventral margin weakly convex.

Dacryomya

D. heberti (Martin)

D. gaveyi (Cox)

D. heberti	***D. gaveyi***
Anterior teeth larger than posterior teeth	Posterior teeth larger than anterior teeth
Beaks placed posteriorly	Beaks placed anteriorly

D. heberti grades into the larger *D. gaveyi* with a transition in the position of the beaks. Hodges (2000), remarks on a 60% size increase above the *oxynotum* zone.

Arcomya

A. arcacea Seebach

A. concinna Tate & Blake

A. vetusta (Phillips)

A. concinna	*A. vetusta*
Elongate ovoid.	Sub-rectangular to elongate trapezoidal.
Ventral margin convex.	Ventral margin straight to weakly convex.
Rounded posterior margin.	Posterior margin appears truncated.

Distinction of the three species herein measured is tenuous, Tate & Blake 1875 distinguish A. *acracea* from *A. concinna* by less inflated umbones, and a lack of posterior keel. However, the type material and description could not be located for *A. arcacea*.

Goniomya

G. hybrida (Münster)

G. rhombifera (Goldfuss)

G. hybrida	*G. rhombifera*
V-shaped ornament on valves.	Base of V-shaped ornament is truncated.

Gresslya

G. galathea (Agassiz)

G. intermedia (Simpson)

G. galathea	*G. intermedia*
Equivalved to sub-equivalved.	Inequivalved.
Elongate ovate – cuneiform.	Elongate sub-trapezoid.
Umbones placed 1/4 L from anterior.	Umbones placed 1/3 L from anterior.
Anterior projects forwards of umbones. Narrower than posterior.	Anterior projects forwards of umbones. Approximately equal height to posterior.
Ventral margin straight to weakly convex.	Ventral margin convex.

Pholadomya

P. ambigua J. Sowerby

P. glabra Agassiz

P. glabra	***P. ambigua***
Sub-elliptical	Sub-rectangular
Up to 12 radial ribs, sometimes faint.	5-9 ribs, typically 7 strongly developed.
Strong commarginal folds.	Strong commarginal folds.
Posterio-dorsal margin weakly concave.	Posterio-dorsal margin strongly concaved.
Anterior pronounced and posterior rounded, not truncated	Short rounded anterior, less pronounced.

An additional comment regarding the distinction of the two species (*P. glabra* and *P. ambigua*) is that *P. ambigua* has a more spherical form overall, both H/L and length/inflation (L/I) are closer to 1 than seen in most specimens of *P. glabra* (Fig. AF.4). A single specimen assigned to *P. "ovalis"* was measured from WARMS collections, this is distinct from *P. ambigua* by the weak radial ornament and from *P. glabra* by the short rounded anterior and extremely inflated valves.

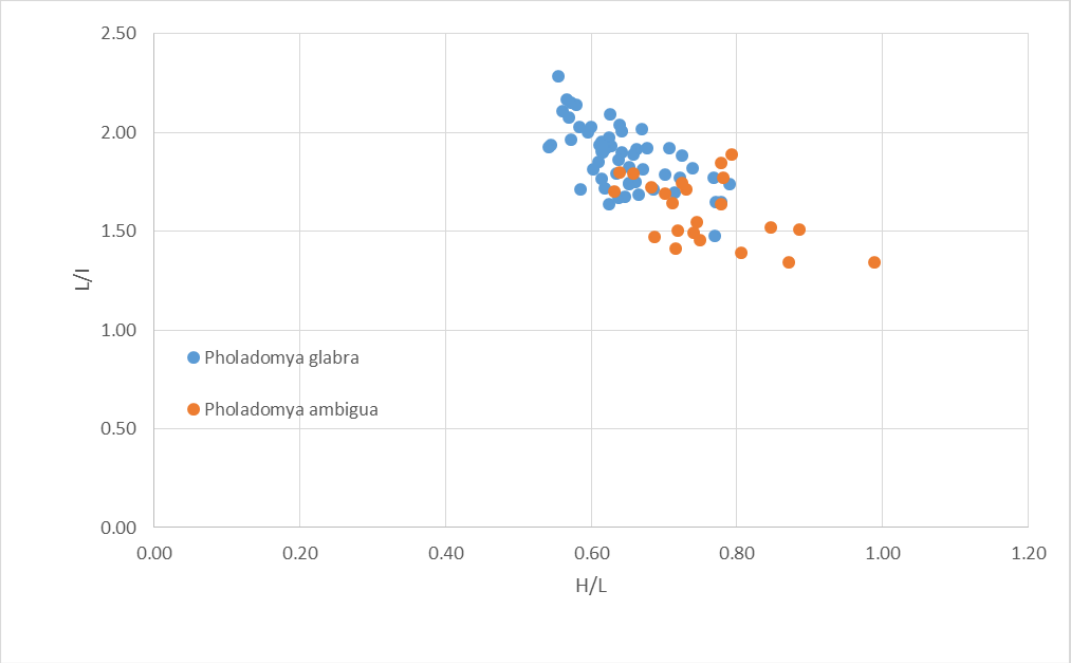

Fig. AF.4 Morphospace plot for species of *Pholadomya*.

Pleuromya

P. crassa Agassiz

P. liasina (Zeiten)

P. costata (Young & Bird)

P. crassa	*P. liasina*	*P. costata*
Suboval	Sub-elliptical	Sub-trigonal, elongate (truncated anterior relative to *P. liasina*)
Orthogyrate beaks not prominent	As in *P. crassa.*	prosogyrate
Commarginal growth halts.	As in *P. crassa.*	Regular rounded commarginal ribs, approx. same width as interspaces, well developed

P. liasina has subsequently been reassigned to *P. striatula* Agassiz by Hodges (2019). A single specimen housed in BRLSI was assigned to *P. striato-granulata* (Moore) this bears find rows of pustules most notable towards the ventral margins.

References

Brauns, D. 1871. *Der untere Jura im nordwestlichen Deutchland*.

Cox, L.R. 1944. On Pseudolimea Arkell. *Proceedings of the Malacological Society*, London, **26**, 74–88.

Damborenea, S.E. 2002. Early Jurassic bivalvia of Argentina. Part 3: superfamilies Monotoidea, Pectinoidea, Plicatuloidea and Dimyoidea. *Palaeontographica Abteilung A*, **265**, 1–119.

Hodges, P. 1987. *Lower Lias (Lower Jurassic) Bivlavia from South Wales and Adjacent Areas*. Unpublished PhD thesis, University College of Swansea, Swansea.

Hodges, P. 2000. *The Early Jurassic Bivalvia from the Hettangian and Lower Sinemurian of South-West Britain Part 1*. London, Monograph of the Palaeontographical Society.

Hodges, P. 2018. *The Early Jurassic Bivalvia from the Hettangian and Lower Sinemurian of South-West Britain Part 2*. London, Monograph of the Palaeontographical Society, https://doi.org/10.1080/02693445.2017.11963960.

Hodges 2019 *The Early Jurassic Bivalvia from the Hettangian and Lower Sinemurian of South-West Britain Part 3*. London, Monograph of the Palaeontographical Society, https://doi.org/10.1080/02693445.2019.1620993.

Ivimey-Cook, H.C., Hodges, P., Swift, A. & Radley, J.D. 1999. Bivalves. *In*: Swift, A. & Martill, D. M. (eds) *Fossils of the Rhaetian Penarth Group*. London, The Palaeontological Association, 83–127.

Johnson, A. 1984. *The Palaeobiology of the Bivalve Families Pectinidae and Propeamussiidae in the Jurassic of Europe*. München, Zitteliana.

Johnson, A., 1985. The rate of evolutionary change in European Jurassic scallops. Special Papers in Palaeontology, **33**, 91-102

Little, C.T.S., 1996. The Pliensbachian-Toarcian (Lower Jurassic) extinction event. Geological Society of America Special Papers. **307**, 505–512. https://doi.org/10.1130/0-8137-2307-8.505

Marquez-Aliaga, A., Damborenea, S., Gómez, J.J. & Goy, A. 2010. Bivalve from the Triassic-Jurassic transition in northern Spain (Asturias and western Basque-Cantabrian Basin). *Ameghiniana,* **47**, 185-205, http://doi.org/10.5710/AMGH.v47i2.3.

Melville, R.V. 1956. The stratigraphical palaeontology, ammonites excluded, of the Stowell Park borehole. *Bulletin of the Geological Survey of Great Britain,* **11**, 67-139.

Nyst, P.H. 1843. *Description des Coquilles et des Polypiers Fossiles des Terrains Tertiaires de la Belgique.* Brussels.

Quenstedt, F.A. 1858. *Der Jura.* Tübingen.

Roemer, F.A. 1839. *Die Versteinerungen des Norddeutschen Oolithen-gebirges.* Hannover.

Tate, R. & Blake, J.F. 1876. *The Yorkshire Lias.* London.

Terquem, O. 1885. *Paleontologie de l'étage inférieur de la formation Liasique de la province de Luxembourg, Grand-Duche (Hollande) et de Hettange, du département de la Moselle.* Mém. Soc. G*éol. Fr.*